Stress- and Strain-Based Reliability Assessment of Pipelines Subjected to Internal Pressure and Permanent Ground Movement

by

Qian Zheng

A thesis submitted in partial fulfillment of the requirements for the degree of

Doctor of Philosophy

in

STRUCTURAL ENGINEERING

Department of Civil and Environmental Engineering
University of Alberta

ABSTRACT

As a critical member of infrastructural lifeline, pipelines fulfill a vital role in energy delivery across long distances from source to market. Pipelines at service can be exposed to a wide variety of loads depending on the environment and the area of application. Internal pressure and ground movements, which are two typical loads respectively controlled by force and displacement, are of great concern in pipeline integrity. Internal pressure is the primary load exerted on the pipe wall for the duration of operation; ground movements induced by geohazards are significant threats to long-distance transmission pipelines. This research carries on the reliability-based analysis of pipes subjected to internal pressure and ground movements regarding the respective industry concerns.

For pipes subjected to internal pressure, a comprehensive reliability assessment is performed towards intact and defected pipes based on the CSA Z662:19. Various limit states related to the pipe design, pre-commission hydrostatic testing, and operation are studied. Specifically, both corrosion and crack defects are considered for pipeline integrity assessment based on different defect scenarios. The probabilities of failure (PoFs), are reported with respect to design factors, hydrostatic test pressure factors, and safety factors, which can be used in designing new pipes, determining the applied pressure in hydrostatic tests, and operation pressure control of defected pipes, respectively. The effects of pipe grade, pipe dimensions (i.e., diameter and wall thickness), corrosion or crack defect sizes (e.g., length and depth), and internal pressure on PoFs for different limit states are also investigated.

In light of the limitations that existing models are not applicable for reliability calculation, a novel model is developed to predict the pipe response to ground movements based on the finite difference method (FDM-based model). The pipe is modeled as an Euler-Bernoulli beam with

large deformations, and the governing differential equations are formulated as functions of displacements of the deformed pipe in the axial and lateral directions at each grid node. The nonlinearities arising from the pipe material and the pipe-soil interaction are accommodated within the finite difference formulation. The initial thermal axial strains and biaxial state of stress due to internal pressure can be appropriately incorporated into the stress-strain relationship of the material based on the flow rule of plasticity. Results of the FDM-based model are in good agreement with those derived from the finite element method (FEM).

The strain-based limit state function is established where the FDM-based model is used to calculate the results of strain demands. The PoFs of pipes at a given magnitude of ground movements are calculated using the Monte Carlo Simulation (MCS). The calculation code is equipped with computational optimization functions to enhance computational efficiency. At last, calculator-like tools are established respectively for assessment of the integrity of pipelines subjected to ground movements, using the developed codes of the FDM-based model and the related reliability calculation. Furthermore, considering the probability of ground movement initiation, the formula of calculating the cumulative PoFs of pipes is developed for decision-making on the maintenance plan for pipes buried across landslide-prone zones.

PREFACE

This thesis is an original work by Qian Zheng. Six papers have been published/in preparation for publication on the basis of this thesis. The details of the corresponding chapters are summarized below:

A version of Chapter 2 has been published as ***Q. Zheng, A. K. Abdelmoety, Y. Li, M. Kainat, N. Yoosef-Ghodsi, S. Adeeb, 2021. Reliability analysis of intact and defected pipes for internal pressure related limit states specified in CSA Z622: 19, Int. J. Press. Vessels Pip. 192, 104411.*** International Journal of Pressure Vessels and Piping, 192, 104411. For the consistency and coherence of this thesis, contents have been modified, removed, or added from the submitted paper. Qian Zheng was responsible for conceptualization, methodology development, numerical model development, analysis implementation, and paper composition. Samer Adeeb and Yong Li was in charge of conceptualization, supervision, funding acquisition, and paper revision. All other authors provided extensive and resourceful technical input for methodology formulation and result validation.

A version of Chapter 3 has been published as ***Q. Zheng, L. Graf-Alexiou, Y. Li, N. Yoosef-Ghodsi, M. Fowler, M. Kainat, S. Adeeb, Strain demand of elastic pipes subjected to permanent ground displacements using the finite difference method, J. Pipeline. Sci. Eng. 1 (2021) 176-186.*** For the consistency and coherence of this thesis, contents have been modified, removed, or added from the submitted paper. Qian Zheng was responsible for conceptualization, methodology development, numerical model development, analysis implementation, and paper composition. Samer Adeeb and Yong Li was in charge of conceptualization, supervision, funding acquisition, and paper revision. All other authors provided extensive and resourceful technical input for methodology formulation and result validation.

A version of Chapter 4 has been published as ***Q. Zheng, Y. Li, N. Yoosef-Ghodsi, M. Fowler, M. Kainat, S. Adeeb, 2022. A finite difference-based approach for strain demand prediction of inelastic pipes subjected to permanent ground displacements, Eng. Struct. 273, 115072.*** For the consistency and coherence of this thesis, contents have been modified, removed, or added from the submitted paper. Qian Zheng was responsible for conceptualization, methodology development, numerical model development, analysis implementation, and paper composition. Samer Adeeb and Yong Li was in charge of conceptualization, supervision, funding acquisition,

and paper revision. All other authors provided extensive and resourceful technical input for methodology formulation and result validation.

A version of Chapter 5 has been presented in a conference proceeding as ***Q. Zheng, W. Qiu, Y. Li, N. Yoosef-Ghodsi, M. Fowler, M. Kainat, S. Adeeb, Reliability assessment of pipes subjected to ground displacements based on a novel methodology for strain demand predictions, in: Technology for Future and Ageing Pipelines, Great Southern Press, Gent, 2022.*** For the consistency and coherence of this thesis, contents have been modified, removed, or added from the submitted paper. Qian Zheng was responsible for conceptualization, methodology development, numerical model development, analysis implementation, and paper composition. Samer Adeeb and Yong Li was in charge of conceptualization, supervision, funding acquisition, and paper revision. All other authors provided extensive and resourceful technical input for methodology formulation and result validation.

A version of Chapter 6 has been presented in a conference proceeding as ***Q. Zheng, W. Qiu, N. Ergezinger, Y. Li, N. Yoosef-Ghodsi, M. Fowler, S. Adeeb, Development of an online calculation tool for safety evaluation of pipes subjected to ground movements, in: International Pipeline Conference (IPC2022), American Society of Mechanical Engineers (ASME), Calgary, 2022, pp. V001T06A004.*** For the consistency and coherence of this thesis, contents have been modified, removed, or added from the submitted paper. Qian Zheng was responsible for conceptualization, methodology development, numerical model development, analysis implementation, and paper composition. Samer Adeeb and Yong Li was in charge of conceptualization, supervision, funding acquisition, and paper revision. All other authors provided extensive and resourceful technical input for methodology formulation and result validation.

A version of Chapter 7 is in preparation as ***Q. Zheng, I. Allouche, W. Qiu, Y. Li, N. Yoosef-Ghodsi, M. Fowler, S. Adeeb, Probabilistic analysis of pipelines buried through geohazard-prone zones based on a novel approach, Journal of Pipeline Systems Engineering and Practice.*** For the consistency and coherence of this thesis, contents have been modified, removed, or added from the submitted paper. Qian Zheng was responsible for conceptualization, methodology development, numerical model development, analysis implementation, and paper composition. Samer Adeeb and Yong Li was in charge of conceptualization, supervision, funding acquisition,

and paper revision. All other authors provided extensive and resourceful technical input for methodology formulation and result validation.

DEDICATION

To my loving family

ACKNOWLEGMENTS

Foremost, I would like to express my deepest gratitude to my supervisors, Dr. Samer Adeeb and Dr. Yong Li, for their invaluable guidance and encouragements over the course of my Ph.D. studies, from inception to completion. Their brilliant insights guided me through my research and trained me to be an independent researcher. This dissertation would not have been possible without their overwhelming support and mentorship.

My sincere appreciation also goes to every member of my examination committee, Dr. Carlos 'Lobo' Cruz Noguez, Dr. Ali Imanpour, and Dr. Ron Wong for their intelligent direction, and for graciously encouraging me towards producing a better version of this research work. I am also grateful to the chair of my defense exam, Dr. Qipei (Gavin) Mei, for his investment of time and effort into making this research endeavour a success.

Many thanks also go to the industrial partners, Nader Yoosef-Ghodsi, Matt Fowler, and Muntaseer Kainat, from Enbridge Liquids Pipelines (Edmonton) for their technical instructions and constructive comments for the thesis, which are important supports for the success of the thesis.

Further thanks go to my primary funding support from China Scholarship Council (CSC) and additional funding obtained through scholarships from the University of Alberta, Mitacs, and Alberta Innovates.

And last but not the least, I want to thank my family members and my friends, for all their endless supports and encouragements in the special journey of my life.

TABLE OF CONTENTS

LIST OF TABLES

LIST OF FIGURES

CHAPTER 1: INTRODUCTION

1.1 Background

As a critical member of infrastructural lifeline, pipelines fulfill a vital role in energy delivery; networks of large transmission pipelines are akin to energy highways. Pipelines are generally constructed underground and extend over vast distances transmitting major crude oil and natural gas from often-remote locations to the populated areas where the products are needed. Compared to ship, truck or train, pipeline transport is safer, more efficient, and creates fewer greenhouse gas emissions. However, damages of pipelines may lead to major catastrophic consequences including environmental effects and disruptions to essential services for human needs.

For the design of pipelines, two criteria, stress-based design and strain-based design, can be used dependent on the load type. In conventional stress-based design, the equivalent resultant stress is not allowed to be greater than the permissible stress (usually the product of design factor and yield stress) essentially restraining the pipe to operate within the elastic limit [1]. Stress-based design is primarily used in the case of force-controlled loads, such as internal pressure, thermal expansion and contraction. On the other hand, strain-based design recognizes that a pipe retains a large portion of its structural capacity even after being deformed beyond its elastic limit. In strain-based design, the amount of strain occurring under the load (referred to as strain demand) is limited by the level of strain that would lead to a severe failure such as rupture (referred to as strain capacity). Strain-based design is most appropriate in the case of displacement-controlled load which can easily cause stresses exceeding the yield strength of the pipe material without fear of loss of containment [2][3].

The most common and prominent force-controlled pipeline loading is the internal pressure of the contained fluid. As described in the code for oil and gas pipeline systems published by the Canadian Standard Association (referred to as CSA Z662:19 hereafter), internal pressure plays a significant role in the lifecycle of pipelines. In the design and integrity assessment stages, internal pressure can serve as an independent or a companion load in various limit states, and several limit states are internal pressure-related [4]. On the other hand, ground movement, usually induced by

geohazards, epitomizes displacement-controlled loading that a buried pipe may encounter during its operational life. In the route selection, avoiding these geohazard areas would be the safest way for pipeline alignment, but this option may not be practically possible especially for long-distance pipelines. Particularly in Canada, the common geologic processes that could potentially affect pipeline systems include landslides, slow slope movement in mountain areas, frost heave, and thaw settlement seasonally occurring in permafrost regions in the North of Canada [5][6]. Landslides can be initiated in slopes when forces acting down-slope (mainly due to gravity) exceed the strength of the earth materials that compose the slope due to some natural factors or human activities. In the summer season, thawing of permafrost would occur due to global warming at the higher latitudes. Melting of the ice-rich soil layers can reduce ice volume and cause the settlement of the ground. When the winter season comes, the metled water is froszen in the soil and heave up the ground [7]. Those geotechnical activities are predisposed to cause significant deformation-induced strains on the pipe, which could result in possible local buckling and rupture of the pipe wall. Field observations have highlighted the deleterious consequences of geotechnical movement of the surrounding soil medium on the structural integrity of buried pipelines. According to the statistical data in Pipeline Industry Performance Report 2016 by Canadian Energy Pipeline Association (CEPA), geohazard-induced damage accounted for 7.4% of the causes of pipeline incidents in the years from 2011 to 2015 [8]. While geotechnical threats are not the leading cause reflected in the survey, they deserve adequate attention due to the associated high consequence.

Pipeline structural safety is traditionally assessed by comparing the stress or strain-based demand with the respective capacity. To account for uncertainties relevant to loads, materials, and used models, traditional design involves a deterministic approach relying on the use of a reasonable global safety factor that provides a lower bound to the ratio of the actual strength to the required strength. However, due to the high uncertainties associated with loads, materials, and measurements, a deterministic approach is considered oversimplified; it cannot appropriately consider the effect of the individual parameters' variability on the design safety [9]. On the other hand, reliability-based analysis developed based on a probability concept is able to account for pertinent uncertainties, while offering a precise estimate of the probability of failure (PoF, i.e., the occurrence of undesired events) to the problem. Developments in design codes based on reliability-

based analysis are actively occurring in various parts of the world today. Some well-known international standards associations, e.g., the American Society of Mechanical Engineers (ASME), the American Society of Civil Engineers (ASCE), the Canadian Standards Association, the Det Norske Veritas (DNV), and the International Organization for Standardization (ISO), have incorporated reliability-based analysis in the design and assessment of engineering structures. Especially for the pipeline industry, some recognized codes, i.e., ISO 16708 and CSA Z662 (Annex O), are widely accepted by Europe and North America respectively among peers.

This doctoral research is in the pursuit of two objectives concerning the current demands in the pipeline industry particularly in North America: (1) in the case of internal pressure, to investigate the inherent connection between the factor of safety (utilized in the deterministic assessment) and reliability (or PoF, used in the probabilistic evaluation) along with every stage in the lifecycle of the pipeline, which aims to provide a direct reference to safety control for design office and engineers in the field; (2) as for the pipeline subjected to ground movements, to develop a practical method for calculating the reliability of pipes at given magnitudes of ground movement. The method is expected to provide a fast and accurate result for screening and assessing steel pipelines subjected to a variety of geohazard conditions, and to be used in the overall maintenance plan based on reliability assessment of pipes buried through geohazards zones which possess the potential to induce ground movements.

1.2 Literature review

1.2.1 Pipes subjected to internal pressure

1.2.1.1 Failure pressure of intact pipes

When subjected to internal pressure loading, pipelines' failure pressure is the paramount and necessary parameter for establishing various limit state functions. Pipe material failure is generally associated with the steel yield or ultimate stresses which respectively denote the forthcoming of plastic deformation and plastic collapse. Yielding occurs when the yield strength (σ_y) is exceeded by the corresponding equivalent stress. Plastic collapse is pertinent to the impossibility of the remaining wall thickness to resist the ultimate strength, i.e., pipe burst due to the operating

pressure. The limit state of yielding is considered during the pipeline design for the determination of design pressure (P_d) which is calculated based on Barlow's formula with consideration of the materials and locations (characterized as a design factor (F)) (see Eq. (1-1)) [10].

$$P_d = \frac{2t \bullet}{D} \quad \bullet \tag{1-1}$$

where D and t are the pipe diameter and wall thickness respectively. Considering the ultimate strength of pipes, Jiao et al. [11] proposed the concept of flow stress which is defined as a portion of the tensile strength (σ_t) to replace σ_y in Eq. (1-1) to estimate the burst pressure, which has been adopted to present the stress capacity in the burst limit state in CSA Z662 [4].

1.2.1.2 Failure pressure of pipes with corrosion or crack

Reliability studies on purely flawless pipes are scarce. Extensive research has been conducted on estimating the burst pressure of pipes with corrosion or crack defects. Corrosion is a common threat causing metal loss due to environmental exposure; cracks in a pipeline can have various origins such as manufacturing defects, welding defects, and external damage. The development of failure pressure models requires idealizing the flaws into primarily regular shapes as depicted in Figure 1-1.

Existing burst pressure models of corroded pipes consider the material property, the pipe dimension, and the defect size and shape. These models can be generally categorized into three types: NG-18 equation and its derivations, semi-regression models based on finite element results, and other models defined specifically which are not in the format of the former two.

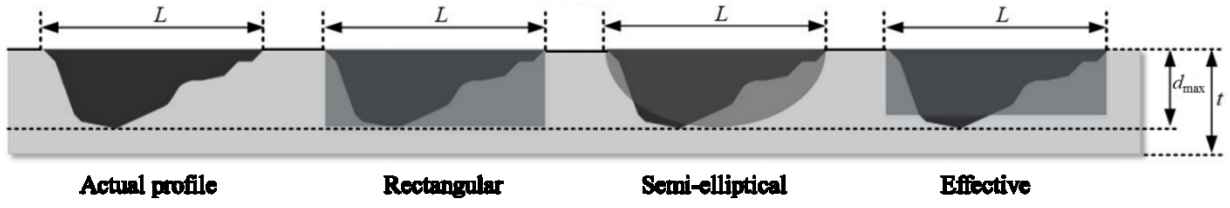

Figure 1-1: Schematic view of corrosion profiles with shape idealization on the pipe wall

NG-18 equation assumes that failure occurs due to a stress-dependent mechanism, and it is derived from the expression of the hoop stress for intact pipes with considerations of the dimensions of the corrosion defect. The expression for the NG-18 equation contains a term, referred to as a bulging factor or Folias factor [12], representing the correction due to the expected difference in the stress distribution between a cracked plate and a cylindrical vessel. The NG-18 equation and NG-18-based equations to calculate the burst pressure (P_b) can be generalized as a function of pipe geometry ($f_{geometry}$), material property (σ_{flow}), corrosion shape idealization (f_{shape}), and Folias factor (M) (see Eq. (1-2)). These models are summarized in Table A-1 in APPENDIX A.

$$P_b = f_{geometry} \bullet \left(1 - f_{shape} \bullet \left(\frac{1}{1 - f_{shape} \bullet \left(\frac{1}{M} \right)} \right) \right) \tag{1-2}$$

Semi-regression models are basically developed based on the Barlow equation with a modifier representing the effect of corrosion flaws. This type of model can be generalized as Eq. (1-3) where the regression factor ($f_{regression}$) is a fitted function of corrosion dimensions and pipe geometries. Usually, the training data for regression is obtained from finite element models. Some published semi-regression models are listed in Table A-2 in APPENDIX A.

$$P_b = f_{geometry} \bullet \left(\quad \right) \bullet \left(\quad \right) \tag{1-3}$$

CSA Z662 model [4] and CPS model [13] are two exceptions from the conventional format of Eqs. (1-2) and (1-3). The CSA criterion [4] incorporates the model errors to describe the pressure necessary to reach a plastic collapse with respect to high-grade steels and low-grade steels; the model error factors (e_1, e_2, e_3, e_4) were obtained by calibration against burst tests. Corroded Pipe Strength (CPS) model [13] uses interpolation between the burst pressures derived from a plain pipe (P_{PP} , upper limit) and a pipe with a longitudinal groove (P_{LG} , lower limit) using a geometric parameter (g). The calculation flow of the two methods is stated in APPENDIX A.

Failure pressure models of cracked pipes are developed based on the criteria of plastic collapse and fracture toughness. The interaction between the two failure modes is taken into

account in the failure assessment diagram (FAD), which is constructed by the brittle fracture parameter (K_r) and plastic collapse parameter (L_r) as shown in Figure 1-2. The pipe is supposed to be safe if the state point lies below the FAD envelope. The failure pressure is the pressure leading to the assessment point falling on the cut-off line. This method is suggested by BS7910 [14], API 579 [15], and R6 [16]. Equations of the NG-18 model (also known as the Battelle model) [17] and the algorithm built-in CorLAS application [18] consider the two failure criteria simultaneously but independently. The calculation procedure of the two models is given in APPENDIX A.

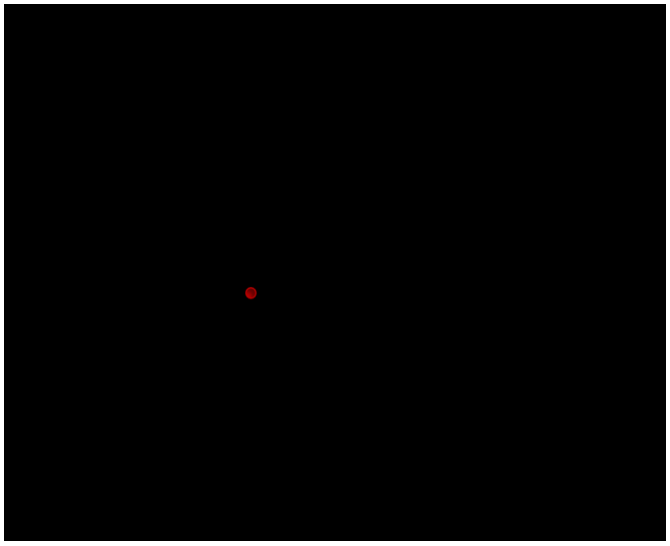

Figure 1-2: Illustration of the FAD model

Considerable studies have been conducted on the reliability assessment of pipelines based on the developed failure pressure models. Rafael et al. [19] conducted a thorough comparison of the failure criteria, metal loss acceptability, failure probability, mean time to failure, and prediction errors of available burst pressure prediction models of corroded pipes from academic publications and recognized codes. Teixeira et al. [20] developed the limit state function of burst for intact and corroded pipes based on experimental and numerical results conducted by Netto et al. [21], and a sensitivity analysis was performed with the conclusion that corrosion depth and internal pressure are the most important variables for the burst of pipes. Using the Monte Carlo Simulation (MSC),

the study offered a set of simple reliability-based evaluation tools for pipeline safety assessment. Hasan et al. [22][23] examined a number of code/standard-based models predicting the burst pressure for corroded pipes. The study found the PoF of burst models suggested by codes/standards significantly varies for the same defect size, and comprehensive suggestions were accordingly offered for industrial use.

Bai et al. [24] proposed a fracture reliability model of dented pipes with cracks considering the uncertainty of random variables and model error, then the safety factor was calibrated based on the probabilistic study by MCS. Lee et al. [25] formulated the limit state function based on the stress intensity factor, and the PoF was assessed based on an X65 pipe with an external semi-elliptical crack. Guillal et al. [26] analyzed the effect of the shape factor (the ratio between crack depth and length) on the reliability, in which the limit state function was established based on fracture toughness. The massive and comprehensive study on burst capacity of defected pipes contributes to the model error evaluation on well-known failure pressure prediction equations, such as the study on corroded pipes by Zhou et al. [27] and cracked pipes by Yan et al. [28]. The comparison demonstrated that RSTRENG and CorLAS are of the highest accuracy for corroded pipes and cracked pipes, respectively.

Though a large amount of reliability research towards corroded and cracked pipes exists in the literature, the majority of studies neglected to investigate the reliability of pipelines during the design operation stages. To be specific, the relationship between the reliability of pipes and the factor indicating safety needs to be developed. These relationships would guide pipeline designers and operators for crucial field-related decision making.

1.2.2 Pipes buried through geohazard zones related to ground movements

Onshore pipelines are generally required to be constructed over considerably long distances. In many instances, pipe segments are inevitably installed through geotechnically unstable environments which are typically associated with unfavorable geological actions. Some specific geohazards, such as landslides, mining-induced subsidence, liquefaction-induced lateral spreading, and fault displacement, can generate permanent ground displacement (PGD), typically

represent credible threats to pipeline integrity [29] and are the focus of this research. ("geohazard(s)" hereafter denote(s) those possessing potential to induce ground movements).

Current probabilistic studies on pipes buried across geohazard zones are mostly related to risk analysis. Risk is generally defined as the product of the probability of occurrence of an event (P_{event})and the consequences of the event (C_{event}) (see Eq. (1-4)). For a particular case where a pipeline is buried across ground movement-related geohazard zones, the risk equation is often subdivided to incorporate several more terms. Usually, the probability of pipe failure due to geohazard is related to the annual probability of the geohazard occurring ($P_{geohazard}$), a conditional probability to assess the likelihood frequency of the geohazard impacting the pipeline in space ($S_{impact\ pipe}$), and a vulnerability factor to assess the likelihood of the pipeline fail once the geohazard has touched the pipeline (V_{pipe}). Thus, the risk associated with pipeline failure from a geohazard can be represented by Eq. (1-5) [30].

$$Risk = P_{event} \bullet \tag{1-4}$$

$$Risk = P_{geohazard} \bullet \quad \bullet \quad \bullet \tag{1-5}$$

Vulnerability factor (V_{pipe}) is the likelihood of pipeline failure given that ground movement occurs and induces a strain on the pipeline. Estimation of the vulnerability factor in the risk analysis is frequently processed in a simplified manner based on expert judgement supported by statistics or empirical probabilities [29][30][31][32]. However, the results are subjected to substantial uncertainties and are less rigorous than the physical modelling method. The likelihood of pipe failure given the specific ground movement condition, which can be understood as the PoF of the pipe subjected to given magnitudes of ground movement, can be estimated more accurately through reliability-based analysis by considering the uncertainties of the influencing factors of both the pipe resistance and demand. To conduct the reliability assessment, the strain demand caused by ground movements is essential for developing the limit state function. To date, three major approaches have been developed to estimate the behavior of pipes subjected to ground movements.

1.2.2.1 Analytical method

Based on cable theory, Newmark and Hall [33] pioneered the study of pipes subjected to ground movements by introducing an analytical method to solve the pipe's response to a tectonic fault. The soil slip friction on the pipe was directly related to the earth pressure, and the passive soil resistance was not considered. The pipeline elongation was investigated through the small deflection theory. This study was further refined by Kennedy et al. [34] where the uniform passive soil pressure was considered and the large deflection theory was applied to the pipe segment immediately adjacent to the fault. This model was developed for pipes subjected to large fault displacement in which the pipe section was entirely yielded so it behaved essentially like a flexible cable deforming into a single constant curvature approaching asymptotically to the undeformed portion of the pipeline as shown in Figure 1-3. At the point of inflection B, the axial tensile force was only considered for equilibrium. Wang and Yeh [35][36] proposed a beam-based model where the pipe was partitioned into four segments as depicted in Figure 1-4: two in the high curvature zone on both sides of the fault trace (AB and AD) which were assumed as circular arcs; and another two at some distance away from the fault zone (BC and DE) which were modeled as beams-on-elastic-foundation. The flexural rigidity (bending stiffness), omitted in Kennedy et al. [34], was taken into account in equilibrium equations, which enables the model to be applicable to compression-dominated strike-slip faults.

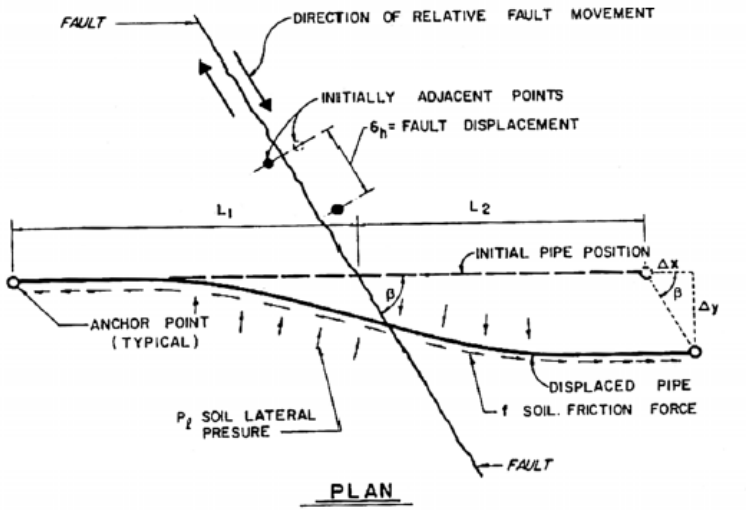

Figure 1-3: Schematic diagram of deformation of the buried pipe subjected to fault displacement in Kennedy et al. [34]

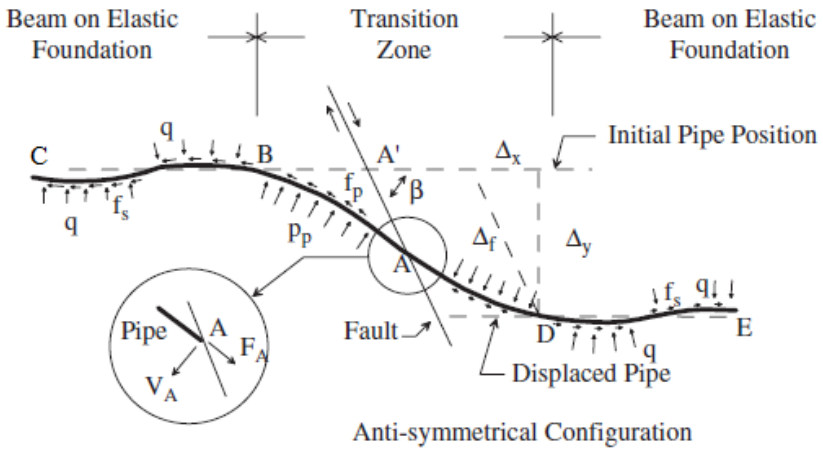

Figure 1-4: Schematic diagram of deformation of the buried pipe subjected to strike-slip fault displacement in Wang and Yeh [35][36]

Analytical studies in recent decades is devoted to improving the model accuracy on the basis of the developed models. Based on the existing analytical methods [34][35][36], Karamitros et al [37][38] introduced a number of refinements, i.e., analyzing the curved segment with the aid of elastic-beam theory to locate the critical combination of axial and bending strains, considering the actual stress distribution on the pipe cross-section to account for the effect of curvature on axial strains. This model was demonstrated to possess fair accuracy for a wide range of applications in practice after comparison with a series of finite element models. Subsequent studies, Trifonov and Cherniy [39][40], optimized the calculation to different extents based on the refinement of the pipe modeling, inspection of the longitudinal deformation effects, and consideration of the pressure and temperature variation. More recently, Vazouras et al. [41] and Sarvanis et al [42] proposed a closed-form solution to pipes' strain subjected to ground movements based on assuming the shape function for the deformed pipeline shape.

Literature review manifests that most of the published analytical models are established based on the tectonic fault movements, that is, the observation on the pipe is around the intersection between the pipe and the fault trace, where two pipe segments are simulated and the two ends are

anchored. As for some other geohazards, typically such like landslides which are one of the most geohazard concerns in North America [31][32] and two ground discontinuities should be considered, three pipe segments are required for the analysis thus the analytical algorithm designed for tectonic faults cannot be employed.

O'Rourke [43] developed an analytical procedure to approximate the adequacy of the pipe restricted to transverse ground movement induced by landslides. The magnitude of PGD (δ) and the length of PGD area (W) were key geotechnical parameters for pipes' response (see Figure 1-5). With a larger length of PGD area, the pipeline was characterized as a cable, called flexure pipe, where the pipe displacement closely followed the ground movement. Otherwise, the pipeline was modelled as a fixed-fixed beam, named stiff pipe, where the soil would flow over and under the pipeline. The critical length of PGD of the two pipe models was investigated according to the local buckling failure. The critical length of PGD area for flexible pipe (pipe moves with the landslide) and stiff pipe (soil flows over and under the pipe) were discriminated based upon local buckling stress capacity. Taking after the bending prediction model from O'Rourke [43], Liu et al. [44] developed an analytical model to study the elastic pipe response to transverse PGD in which the resistance of pipe due to flexural (beam-like) and axial (cable-like) behaviors was considered in parallel.

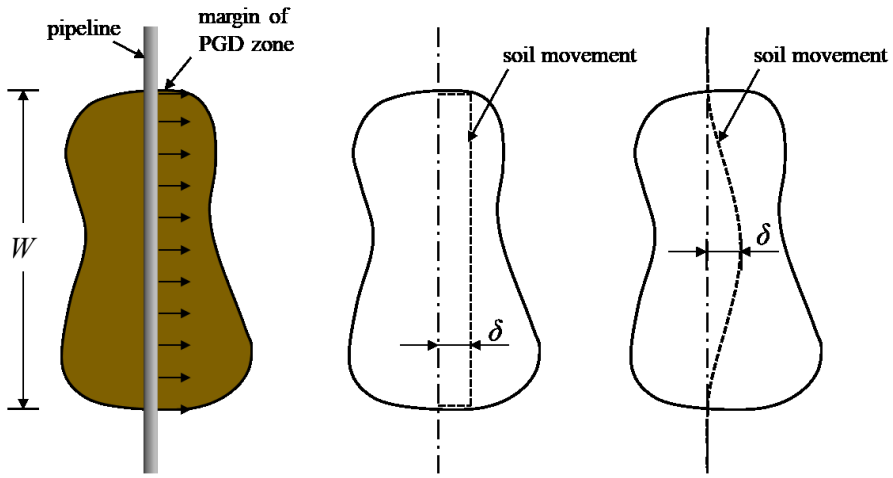

(a) Pipeline (b) Abrupt ground movement (c) Distributed ground movement

Figure 1-5: Pipeline subject to transverse ground movement

Similarly, the idea in [43] was employed to investigate the response of steel pipes subjected to longitudinal ground movements induced by landslides [45]. Two modes, i.e., PGD length control and PGD displacement control, were respectively studied according to the interaction between the magnitude of PGD (δ) and the length of PGD margin (W). With a small length of PGD margin, the pipe displacement was substantially smaller than the magnitude of PGD, which caused the "noncompliant pipe" that behaved more or less like a beam subject to soil-structure interaction forces due to soil flow. Otherwise, the pipe displacement was essentially identical to the magnitude of PGD, that is, the pipe conformed to the imposed soil deformation, which was called the "compliant pipe".

Based on the assumption of Euler-Bernoulli beam, Yoosef-Ghodsi et al. [46] proposed an analytical method for estimating the pipes' response to longitudinal ground movements induced by slope in which the effects of internal pressure and temperature change were concerned. The stress-strain relationship of the pipe material was considered bilinear, and the inelastic pipe behavior was approximated based on the flow rule in plasticity. Recently, Zahid et al. [47] developed a simplified analytical formulation for axial strain calculation of pipes withstanding the longitudinal ground movements, whereas it only focused on the elastic behavior of the pipe.

The existing analytical models provide simplified methodical design approaches for solving the pipes' response to methods under landslides. However, the substantial assumptions sacrificed the accuracy of predictions and confined the methods to a tight applicable range. The ignorance of inelasticity of the pipe material in the most current analytical methods would lead to unconservative strain demands. Besides, in most engineering practice, the ground movement does not always happen parallel to the pipe or perpendicular to the pipe, which restraints the application of the models in practice.

1.2.2.2 Numerical method

With the rapid advancement of computational technologies, the finite element method (FEM) has been a widely adopted numerical tool for pipeline analysis, e.g., using the general-

purpose commercial finite element software Abaqus and Ansys. Numerical modelling of the pipe's performance under the ground movement has experienced a spike in recent decades. In the simulation of a pipe subjected to ground displacements, three critical issues arise: element selection for the pipe, constitutive modeling of soil, and representation of pipe-soil interactions. For instance, Takada et al. [48] used shell elements to simulate the pipe segment near the fault plane for accurately capturing the flexural behavior under fault displacement, while they used beam elements to model the pipe segment to obtain the axial elongation. This model is sketched in Figure 1-6 and the fault displacement was applied as a static loading at the pipe-fault crossing point in the direction of the fault (no consideration of the pipe-soil interaction). Similarly, Liu et al. [49] proposed the pipe-elbow hybrid model to simulate pipes' behavior under compression and bending at strike-slip faults. Pipe elements were used to model the pipe segment far away from the fault trace; elbow elements, essentially shell elements capable of accounting for the ovality of the pipe cross-section, were employed to simulate the pipe segment near the fault trace. The pipe-soil interaction was simulated by soil springs and the fault displacement was exerted on the soil nodes on the right side of the model as illustrated in Figure 1-7. Liu et al. [50][51] modified Takada's model by replacing the beam element with an equivalent boundary condition which was essentially a bilinear soil spring element as shown in Figure 1-8. The property of the equivalent boundary condition (soil spring) was developed based on the assumption that the pipe segment far away from the fault trace was elastic. Vazouras et al. [52] dealt with the soil by using continuous solid elements and the pipe-soil interaction was modelled by the contact surface approach. The pipe was simulated by shell elements as shown in Figure 1-9.

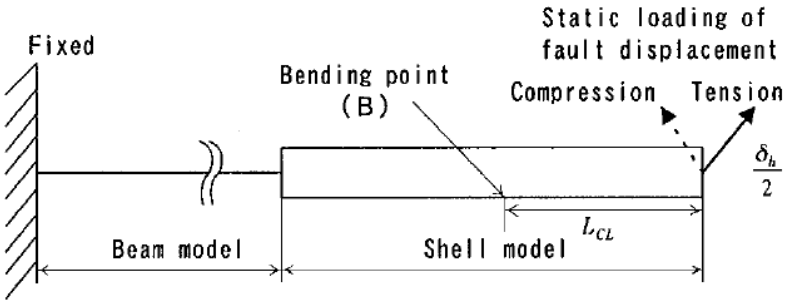

Figure 1-6: Beam-shell hybrid finite element model used in Takada et al. [48]

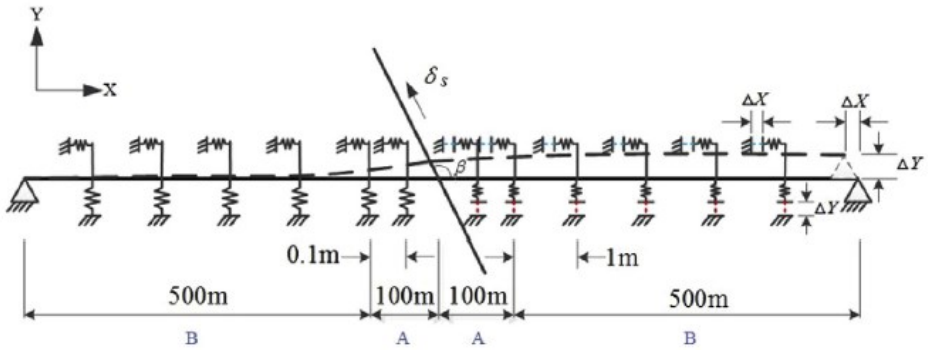

Figure 1-7: Pipe-elbow hybrid model subjected to a compression-dominated strike-slip fault in Liu et al. [49]

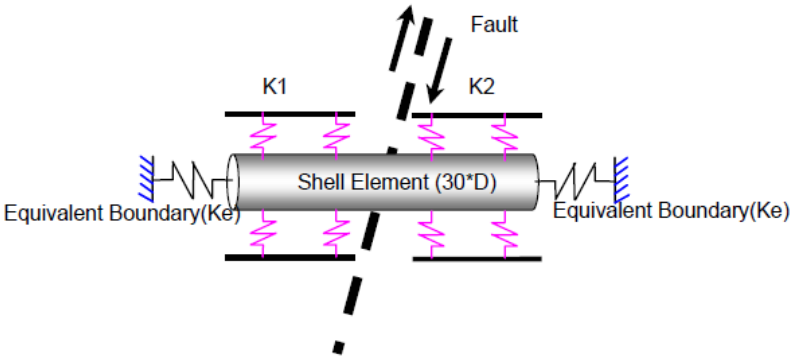

Figure 1-8: Shell element model with equilibrium boundary conditions in Liu et al. [50][51]

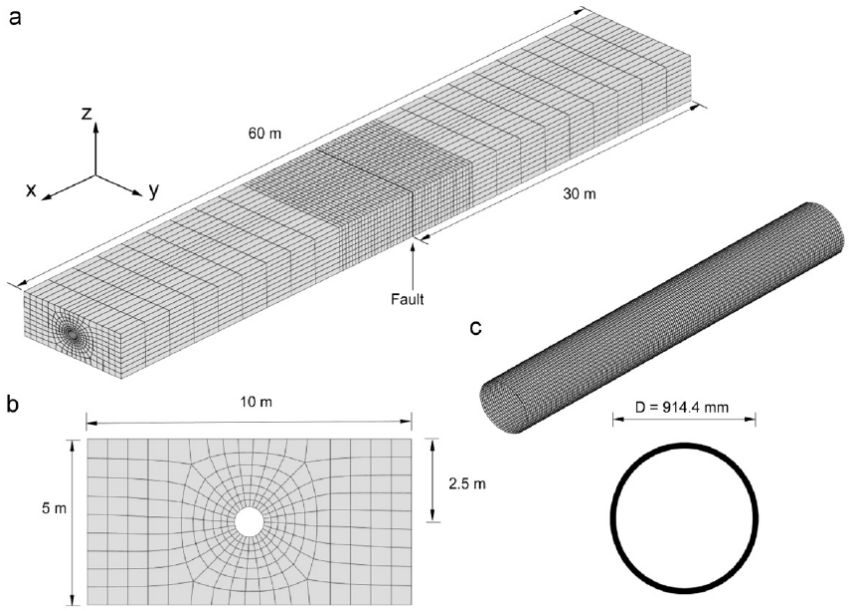

Figure 1-9: Finite element model of the (a) soil formulation, (b) soil cross-section, and (c) steel pipe in Vazouras et al. [52]

Karamanos et al. [53] generalized the existing finite element models into two levels from the perspective of accuracy for engineering practice: level 1 denoted to the one-dimensional beam (pipe)-type finite element models, and the pipe-soil interaction was represented by soil recommended by ALA guideline [54], which was adequate for regular design purposes; level 2 was the three-dimensional shell-type finite element models, and the surrounding soil was modeled by solid elements, which offered a rigorous numerical tool but requires more computational expertise. Vasseghi et al. [55] conducted the failure analysis of a natural gas pipeline undergoing the ground movements induced by landslides based on the practice of level 1 model using Ansys. For a more accurate inspection of pipeline-soil interaction behavior, Liu et al. [56] examined the mechanism of the natural gas pipeline under the deflection due to mud-rock flow using the level 2 model.

Some new prediction models have been established based on FEM-derived results in recent years. Shokouhi et al. [57] proposed a FEM-ANN hybrid approach for the seismic strain of high-density polyethylene pipelines subjected to an active fault. The artificial neural network (ANN) trained by FEM-based strain gave a fairly good prediction, which made the strain prediction much

easier. Liu et al. [49] developed a regression equation to estimate the strain demand of X80 pipes under fault displacements based on finite element results. For the sake of extending the predictive investigation, Liu et al. [58] further proposed a comprehensive model using the ANN in which the training database was collected based on systematic parametric calculations in Abaqus. Similarly, Xie et al. [59] made use of the Support Vector Machine (SVM) to surrogate the ANN in Liu et al. [58], which demonstrated a great agreement with the actual results.

The finite element model is a powerful way to achieve accurate pipes' reaction to ground movements by using the shell element to simulate the pipe segment under large deformation. While it is a challenge of time when the pipeline is long and fine mesh is required. This makes the reliability calculation prohibitively expensive by employing MCS in which a large number of simulations is required. Efficiency of the strain prediction model is a significant consideration for reliability assessment.

1.2.2.3 Experimental method

Notable experimental research studies on the effects of ground movements on buried pipes have been reported in the literature. However, compared with the above-mentioned approaches, experimental verification of the predicted behavior of buried pipelines subjected to ground movements is, at best, sparse. It is unrealistic to employ experimental approaches in reliability calculation. Instead, the test data is the most effective proof to benchmark or validate the applicability of analytical and numerical assumptions.

O'Rourke et al. [60] firstly conducted a small-scale experiment using the centrifuge machine at Rensselaer Polytechnic Institute. The axial strain and bending strain along the pipe at different fault offsets were collected. Ha et al. [61][62] extended this experiment by using an upgraded split-box container (used to simulate the fault displacement) to examine the differences in behavior of buried high-density polyethylene pipelines subjected to normal and strike-slip faults. The experimental equipment is shown in Figure 1-10. Demofonti et al. [63] proposed an elaborate procedure for testing the strain of pipes under horizontal ground-induced deformation based on a full-scale experiment system in Perdasdefogu (Sadinia, Italy) as shown in Figure 1-11, which

provided a better understanding of pipe-soil interaction and calibration of the numerical models. Feng et al. [64] conducted a field experiment (full-scaled model) to monitor the stress and strain on the pipeline against the landslide deformation. The model test followed practical pipeline operations, actual deformation, and failure of the landslide. The full view of the model is displayed in Figure 1-12.

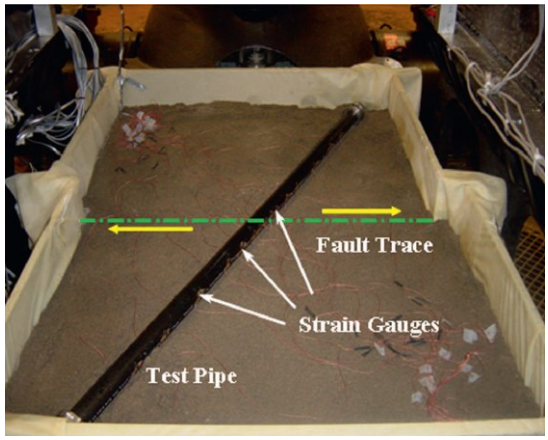

Figure 1-10: Experimental equipment in Ha et al. [62]

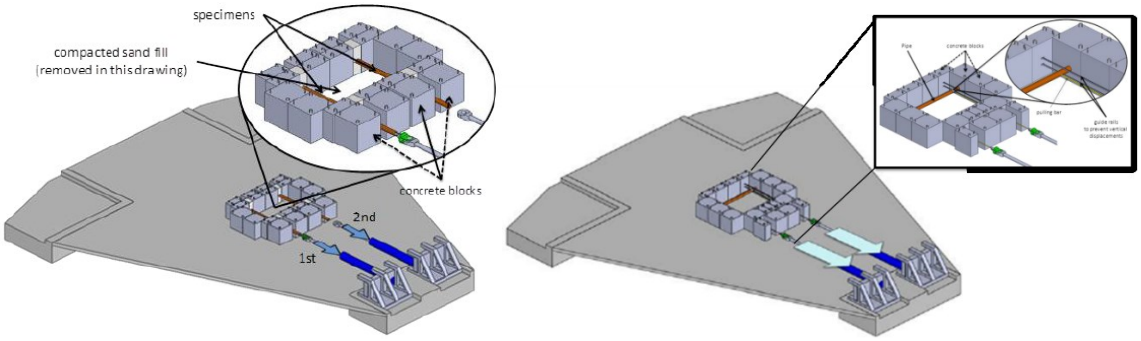

(a) Axial pull-out test (b) Transverse pipe-soil interaction test

Figure 1-11: Full-scale test facility in Demofonti et al. [63]

Figure 1-12: Full view of the landslide and pipeline model in Feng et al. [64]

Reliability assessment on pipes subjected to ground movements is limited. Zhou [65] analyzed the pressurized pipes under the ground displacement induced by slope instability, and the strain demand is estimated based on the model proposed by Yoosef-Ghodsi et al. [46] which was only applicable to pipes deforming in the longitudinal direction. And the analytical model [46] was also employed in the semi-quantitative method proposed by Sen et al. [66] for assessing the reliability of the pipes buried under slope areas with the potential of generating ground movement. Zheng et al. [67] assessed the reliability of the pipeline buried across Bo-A fault in China where the strain demand in the limit state function was represented by the trained BP neural network as developed by Liu et al. [58]. Nevertheless, the collection of strain demand datasets was time-consuming based on a large number of calculations by Abaqus.

1.3 Statement of the Problem

Internal pressure and ground movements are two significant representatives of force-controlled and displacement-controlled pipeline loadings respectively. In the case of pipes under internal pressure, the literature review presents a lack of systematic reliability evaluation of pipelines in the span of lifecycle, starting from the pipe design, pre-commission hydrostatic tests, to operation management (e.g., defect scenario-based integrity assessment). Furthermore, existing studies rarely link the PoF to all these factors (e.g., design factors, hydrostatic test pressure factors, safety factors) used in the design code. In addition, MCS has been mostly used but it is inefficient or inaccurate when the PoF is significantly low. Another widely used method, the first-order

reliability method (FORM), is efficient but the accuracy highly depends on the problems. A more advanced reliability calculation technique should be applied in practice in pipeline engineering, e.g., the method proposed by Rashki [68].

With regards to pipes subjected to ground movements induced by geohazards, extensive research effort has been made on deterministic analysis by strain prediction modelling; relevant probabilistic analysis is not commonly available. To the author's knowledge, there is currently a gap in pipeline integrity literature in terms of available methods for reliability assessment which are applicable to field practice for pipes withstanding ground displacements. For the reliability-based assessment, a brand-new strain demand prediction model is required as the two conventional approaches, analytical method and FEM-based numerical simulation, are unsuitable for reliability analysis due to the inherent restrictive assumptions of the analytical solutions and the inefficient computation of finite element models.

1.4 Research objectives and methodologies

The overall objective of this research is to conduct a comprehensive reliability investigation of pipes subjected to internal pressure (force-controlled loading) and ground movements (displacement-controlled loading), which aims to fill the gap in the research and provide a practical reference to the pipeline industry. To this end, the research work is mainly coordinated with the following two sub-objectives.

Objective 1: To investigate the PoF of pipes subjected to internal pressure in the stage of design, hydrostatic test, and operation based on CSA Z662:19.

a) Investigate the relationship between the design factor and the corresponding PoF of intact pipes under internal pressure for use in the design stage.
b) Evaluate the PoF at different values of hydrostatic test pressure factor based upon intact pipes for use in the pre-commissioning stage (hydrostatic test).
c) Investigate the relationship between the safety factor and the corresponding PoF of defected pipes under internal pressure for use in the operation stage.

Objective 2: To develop a reliability assessment method for pipes buried across geohazard zones prone to ground movements.

a) Establish a model based on moderate deformation coupled Euler-Bernoulli beam for predicting the strain demand of pipelines subjected to ground movement via the finite difference method.
b) Propose a highly efficient calculation scheme for the reliability assessment of pipelines subjected to a given ground movement.
c) Develop an online platform for response analysis and reliability calculation for industry use.
d) Propose a method to estimate the cumulative PoF of pipelines buried across the geohazard-prone zones considering the probability of ground movement initiation.

1.5 Organization of Thesis

Details of this research have been thoroughly documented in the form of this thesis, consisting of eight chapters as briefly outlined as follows.

Chapter 1 provides the background of this research and highlights the research gaps through an overall literature review. Potential difficulties of the research are presented, and the corresponding objective and methodologies are outlined.

Chapter 2 reveals the relationship between the design factor (or safety factor) used in the deterministic method and PoFs adopted in reliability-based analysis for intact pipes in the design and hydrostatic stages, as well as the defected pipes in operation. Limit state functions are established based on the instruction in CSA Z662:19. An advanced reliability method is practiced for obtaining the PoFs.

Chapter 3 proposes a novel model to estimate the strain demand of the pipe under ground movements based on the finite difference method. This chapter restrains the attention on elastic behavior of pipes under ground movements. Comparison between the results derived by the proposed method and the benchmark FEM is conducted.

Chapter 4 extends the method in Chapter 3 by considering the inelastic behavior of the pipe. The mechanical property of the material is idealized as bilinear curves, and the explicit formulas

of axial force and bending moment, which are required for the finite difference method, are deducted. The proposed method is also applied to predict the pipes response to tectonic faults. Comparisons among the existing analytical models, finite element models, and the developed finite difference model are performed.

Chapter 5 implements the reliability-based calculation based on the established model in Chapter 4. Some computational optimization methods are utilized to equip the code to improve the calculation efficiency. The reliability results are calculated based on MCS and the advanced reliability method.

Chapter 6 establishes two calculation tools for assessing the integrity of pipe under ground movements respectively in deterministic and probabilistic ways based on a website. The programs developed in Chapter 4 and Chapter 5 are employed for developing the tools. Workability of the tools is tested using study cases.

Chapter 7 further develops the predictive model in Chapter 4 by considering the effects of internal pressure and temperature change into the finite difference model. The formula of calculating cumulative PoFs of pipes buried across geohazard-prone zones are proposed by taking into consideration the probability of ground movement initiation.

Chapter 8 summarizes the research work and states the conclusions, contributions, and highlights. The limitations of the current work and recommendations for future work are provided.

References

[1] M.S. Okyere, Stress-based design of pipelines, in: R.W. Revie (Eds.), Oil and Gas Pipelines, John Wiley & Sons Inc., Hoboken, 2015, pp. 49-66.

[2] B. Liu, X.J. Liu, H. Zhang, Strain-based design criteria of pipelines, J. Loss Prev. Process Ind., 22 (2009) 884-888.

[3] N. Yoosef-Ghodsi, Strain-based design of pipelines, in: R.W. Revie (Eds.), Oil and Gas Pipelines, John Wiley & Sons Inc., Hoboken, 2015, pp. 37-48

[4] CSA. Oil and gas pipeline system, CSA standard Z662:19. Mississauga, Ontario, Canada: Canadian Standard Association; 2019.

[5] Pipeline Research Council International (PRCI). Guidelines for Constructing Natural Gas and Liquid Hydrocarbon Pipelines Through Areas Prone to Landslide and Subsidence Hazards, Technical Toolboxes, Inc., 2009.

[6] J.M. Oswell, Pipelines in permafrost: geotechnical issues and lessons, Can. Geotech. J. 48 (2011), 1412-1431.

[7] Y.Y. Wang, D. West, D. Dewar, J. Hart, A. McKenzie-Johnson, D. Gray, Management of Ground Movement Hazards for Pipelines, CRES project No. CRES-2012-M03-01, 2016.

[8] Canadian Energy Pipeline Association, Pipeline Industry Performance Report. https://cepa.com/en/performance-report/, 2016 (accessed 20 September 2021).

[9] J.J. Muhammed, Deterministic and probabilistic approaches in the analysis of the bearing capacity of a bridge foundation on undrained clay soil, Slovak J. Civ. Eng. 27 (2019) 44-51.

[10] ASME B31.8, Gas transmission and distribution piping systems, American Society of Mechanical Engineers, New York, 2018.

[11] G. Jiao, T. Sotberg, R. Igland, SUPERB 2M Project: Wall Thickness Sizing: Limit-States Based Design for Offshore Pipelines, SUPERB project report, 1995.

[12] J.F. Kiefner, P.H. Vieth, A modified criterion for evaluating the remaining strength of corroded pipe (No. PR-3-805), Battelle Columbus Div., Ohio, 1989.

[13] D.S. Cronin, R.J. Pick, Prediction of the failure pressure for complex corrosion defects, Int. J. Press. Vessels Pip. 79 (2002), 279-287.

[14] BS 7910, Guide to methods for assessing the acceptability of flaws in metallic structures. London, UK: British Standards Institution, 2005.

[15] API 579, Fitness for Service Assessments, American Society of Mechanical Engineers, New York, 2007.

[16] Amendment 10 R6, revision 4, Assessment of the integrity of the structures containing defects, Gloucester: EDF Energy, 2013.

[17] J. Kiefner, W. Maxey, R. Eiber, A. Duffy, Failure stress levels of flaws in pressurized cylinders, in: Progress in flaw growth and fracture toughness testing, ASTM International, 1973.

[18] C.E. Jaske, J.A. Beavers, Development and evaluation of improved model for engineering critical assessment of pipelines, in: International Pipeline Conference (IPC2002), American Society of Mechanical Engineers (ASME), Calgary, 2002, pp. 1459-1466.

[19] R. Amaya-Gómez, M. Sánchez-Silva, E. Bastidas-Arteaga, F. Schoefs, F. Munoz, Reliability assessments of corroded pipelines based on internal pressure–A review, Eng. Fail. Anal. 98 (2019) 190-214.

[20] A.P. Teixeira, C. Guedes Soares, T.A. Netto, S.F. Estefen, Reliability of pipelines with corrosion defects, Int. J. Press. Vessel. Pip. 85.4 (2008) 228-237.

[21] T.A. Netto, U.S. Ferraz, S.F. Estefen, The effect of corrosion defects on the burst pressure of pipelines, J. Constr. Steel Res. 61 (2005) 1185–204.

[22] M. Hasan, F. Khan, S. Kenny, Identification of the cause of variability of probability of failure for burst models recommended by Codes/Standards, J. Press. Vessel Technol. 133 (2011) 041101.

[23] S. Hasan, F. Khan, S. Kenny, Probability assessment of burst limit state due to internal corrosion, Int. J. Press. Vessel. Pip. 89 (2012) 48–58.

[24] Y. Bai, R. Song, Fracture assessment of dented pipes with cracks and reliability-based calibration of safety factor, Int. J. Press. Vessel. Pip. 74.3 (1997) 221-229.

[25] O.S. Lee, H.M. Kim, D.H. Kim, H.B. Choi, Reliability Estimation of a Natural Gas Pipeline with Surface Crack, in: Proceedings of the ASME 2009 Pressure Vessels and Piping Conference (PVP2009), New York, 2009, pp. 459-466.

[26] A. Guillal, N. Abdelbaki, M.E.A. Bensghier, M. Betayeb, Effect of shape factor on structural reliability analysis of a surface cracked pipeline-parametric study, Frat. ed Integrita. Strutt. 13 (2019): 341-349.

[27] W. Zhou, G.X. Huang, Model error assessments of burst capacity models for corroded pipelines, Int. J. Press. Vessel. Pip. 99 (2012) 1–8.

[28] Z. Yan, S. Zhang, W. Zhou, Model error assessment of burst capacity models for energy pipelines containing surface cracks, Int. J. Press. Vessel. Pip. 120 (2014) 80-92.

[29] R.R. Read, M. Rizkalla, Bridging the gap between qualitative, semi-quantitative and quantitative risk assessment of pipeline geohazards: the role of engineering judgment, in:

ASME International Pipeline Geotechnical Conference (IPG2015), American Society of Mechanical Engineers (ASME), Bogota, 2015, pp. V001T02A004.

[30] A. Baumgard, M. Beaupre, M. Leir, Implementing a quantitative geohazard frequency analysis framework as a component of risk assessment of new pipelines, in: 2016 11th International Pipeline Conference (IPC2016), American Society of Mechanical Engineers (ASME), Calgary, 2016, pp. V002T07A020.

[31] R. Guthrie, E. Reid, Estimating landslide induced probability of failure to pipelines using a structured reductionist approach, in: 2018 12th International Pipeline Conference (IPC2018), American Society of Mechanical Engineers (ASME), Calgary, 2018, pp. V002T07A004.

[32] M. Porter, J. Van Hove, P. Barlow, Analysis of dynamic system risks where pipelines cross slow-moving landslides, in: 2022 14th International Pipeline Conference (IPC2022), American Society of Mechanical Engineers (ASME), Calgary, 2022, pp. V001T07A007.

[33] N.M. Newmark, W.J. Hall, Pipeline design to resist large fault displacement, in: Proceedings of U.S. National Conference on Earthquake Engineering, Earthquake Engineering Research Institute, Michigan, 1975, pp. 416-425.

[34] R.P. Kennedy, A.W. Chow, R.A. Williamson, Fault movement effects on buried oil pipeline, ASCE J. Transport. Eng. 103 (1977) 617-633.

[35] L.R.L. Wang, Y.A. Yeh, A refined seismic analysis and design of buried pipeline for fault movement, Earthq. Eng. Struct. Dyn. 13 (1985) 75-96.

[36] L.R.L. Wang, Y.A. Yeh, Seismic design of buried pipeline for fault movement effects, J. Press. Vessel. Technol. 108 (1986) 202-208.

[37] D.K. Karamitros, G.D. Bouckovalas, G.P. Kouretzis, Stress analysis of buried steel pipelines at strike-slip fault crossings, Soil. Dyn. Earthq. Eng. 27 (2007) 200-211.

[38] D.K. Karamitros, G.D. Bouckovalas, G.P. Kouretzis, An analytical method for strength verification of buried steel pipelines at normal fault crossings, Soil Dyn. Earthq. Eng. 31(2011) 1452-1464.

[39] O.V. Trifonov, V.P. Cherniy, A semi-analytical approach to a nonlinear stress–strain analysis of buried steel pipelines crossing active faults, Soil Dyn. Earthq. Eng. 30 (2010) 1298-1308.

[40] O.V. Trifonov, V.P. Cherniy, Elastoplastic stress strain analysis of buried steel pipelines subjected to fault displacements with account for service loads, Soil Dyn. Earthq. Eng. 33 (2012) 54-62.

[41] P. Vazouras, P. Dakoulas, S.A. Karamanos, Pipe–soil interaction and pipeline performance under strike-slip fault movements, Soil Dyn. Earthq. Eng. 72 (2015) 48-65.

[42] G.C. Sarvanis, S.A. Karamanos, Analytical model for the strain analysis of continuous buried pipelines in geohazard areas, Eng. Struct. 152 (2017) 57-69.

[43] M.J. O'Rourke, Approximate analysis procedures for permanent ground deformation effects on buried pipelines, in: Proceedings from the Second U.S.-Japan workshop on liquefaction, large ground deformation and their effects on lifelines, National Center for Earthquake Engineering Research, New York, 1989, pp. 336-347.

[44] X. Liu, M.J. O'Rourke, Behaviour of continuous pipeline subject to transverse PGD, Earthq. Eng. Struct. Dyn. 26 (1998) 989-1003.

[45] M.J. O'Rourke, X. Liu, R. Flores-Berrones, Steel pipe wrinkling due to longitudinal permanent ground deformation, J. Civ. Eng. 121 (1995) 443-451.

[46] N. Yoosef-Ghodsi, J. Zhou, D.W. Murray, A simplified model for evaluating strain demand in a pipeline subjected to longitudinal ground movement, in: 2008 7th International Pipeline Conference (IPC2008), American Society of Mechanical Engineers (ASME), Calgary, 2009, pp. 657-664.

[47] U. Zahid, A. Godio, S. Mauro, 2020. An analytical procedure for modelling pipeline-landslide interaction in gas pipelines, J. Nat. Gas Eng. 81, 103474.

[48] S. Takada, N. Hassani, K. Fukuda, A new proposal for simplified design of buried steel pipes crossing active faults, Earthquake Eng. Struct. Dyn. 30 (2001) 1243-1257.

[49] X. Liu, H. Zhang, Y. Han, M. Xia, W. Zheng. A semi-empirical model for peak strain prediction of buried X80 steel pipelines under compression and bending at strike-slip fault crossings, J. Nat. Gas Eng. 32 (2016) 465-475.

[50] A. Liu, Y. Hu, F. Zhao, X. Li, S. Takada, L. Zhao, An equivalent-boundary method for the shell analysis of buried pipelines under fault movement, Acta. Seismol. Sin. 1 (2004) 150-156.

[51] A. Liu, S. Takada, Y. Hu, A shell model with an equivalent boundary for buried pipelines under the fault movement, in: 13th World Conference on Earthquake Engineering, Vancouver, 2004, pp. 613.

[52] P. Vazouras, S.A. Karamanos, P. Dakoulas, Finite element analysis of buried steel pipelines under strike-slip fault displacements, Soil Dyn. Earthq. Eng. 30 (2010) 1361-1376.

[53] S. A. Karamanos, B. Keil, R. J. Card, (2014). Seismic design of buried steel water pipelines, in: Pipelines 2014: From Underground to the Forefront of Innovation and Sustainability, ASCE, pp. 1005-1019.

[54] American Lifelines Alliance (ALA), Guidelines for the Design of Buried Steel Pipe, American Society of Civil Engineers, 2001.

[55] A. Vasseghi, E. Haghshenas, A. Soroushian, A., M. Rakhshandeh, M., 2021. Failure analysis of a natural gas pipeline subjected to landslide, Eng. Fail. Anal. 119, 105009.

[56] P. Liu, J. Zheng, B. Zhang, P. Shi, Failure analysis of natural gas buried X65 steel pipeline under deflection load using finite element method, Mater. Des. 31 (2010) 1384-1391.

[57] S.K.S Shokouhi, A. Dolatshah, E. Ghobakhloo, Seismic strain analysis of buried pipelines in a fault zone using hybrid FEM-ANN approach, Earthq. Struct. 5 (2013) 417-438.

[58] X. Liu, Q. Zheng, K. Wu, Y. Yang, Z. Zhao, H. Zhang, 2020. Development of a novel approach for strain demand prediction of pipes at fault crossings on the basis of multi-layer neural network driven by strain data, Eng. Struct. 214, 110685.

[59] J. Xie, L. Zhang, Q. Zheng, X. Liu, S. Dubljevic, H. Zhang. Strain demand prediction of buried steel pipeline at strike-slip fault crossings: a surrogate model approach, Earthq. Struct. 20 (2021) 109-122.

[60] M.J. O'Rourke, V. Gadicherla, T.H. Abdoun, Centrifuge modeling of PGD response of buried pipe, Earthq. Eng. 4 (2005) 69-73.

[61] D. Ha, T.H Abdoun, M.J. O'Rourke, M.D. Symans, T.D. O'Rourke, M.C. Palmer, H.E. Stewart, Buried high-density polyethylene pipelines subjected to normal and strike-slip faulting-a centrifuge investigation, Can. Geotech. J. 45 (2008) 1733-1742.

[62] D. Ha, T.H. Abdoun, M.J. O'Rourke, M.D. Symans, T.D. O'Rourke, M.C. Palmer, H.E. Stewart, Centrifuge modeling of earthquake effects on buried high-density polyethylene (HDPE) pipelines crossing fault zones, J. Geotech. 134 (2008) 1501-1515.

[63] G. Demofonti, J. Ferino, S.A. Karamanos, P. Vazouras, P. Dakoulas, An integrated experimental-numerical approach to predict strain demand for buried steel pipelines in geo-hazardous areas, in: Rio Pipeline Conference and Exposition, 2013.

[64] W. Feng, R. Huang, J. Liu, X. Xu, M. Luo, Large-scale field trial to explore landslide and pipeline interaction, Soils Found. 55 (2015) 1466-1473.

[65] W. Zhou, Reliability of pressurised pipelines subjected to longitudinal ground movement, Struct. Infrastruct. Eng. 12 (2012) 1123-1135.

[66] M. Sen, S. Hassanien, On estimating pipelines reliability at slope crossings, in: Proceedings of The Asset Integrity Management-Pipeline Integrity Management Under Geohazard Conditions, American Society of Mechanical Engineers (ASME), New York, 2019, pp. 81-92.

[67] Q. Zheng, X. Liu, H. Zhang, X. Gu, M. Fang, L. Wang, S. Adeeb, 2021. Reliability evaluation method for pipes buried in fault areas based on the probabilistic fault displacement hazard analysis, J. Nat. Gas Eng. 85, 103698.

[68] M. Rashki, M. Miri, M.A. Moghaddam, A new efficient simulation method to approximate the probability of failure and most probable point, Struct. Saf. 39 (2012) 22-29.

CHAPTER 2: RELIABILITY ANALYSIS OF INTACT AND DEFECTED PIPES FOR INTERNAL PRESSURE RELATED LIMIT STATES SPECIFIED IN CSA Z622:19

This chapter is derived from the published paper:

Q. Zheng, A. K. Abdelmoety, Y. Li, M. Kainat, N. Yoosef-Ghodsi, S. Adeeb, 2021. Reliability analysis of intact and defected pipes for internal pressure related limit states specified in CSA Z622: 19, Int. J. Press. Vessels Pip. 192, 104411.

Abstract

The importance of reliability-based design and assessment has been widely recognized by the pipeline industry. Thus, this paper aims at providing comprehensive reliability assessment of intact and defected pipes subjected to internal pressure based on the CSA Z662:19. Various limit states related the pipe design, pre-commission hydrostatic testing, and operation are studied. Specifically, both corrosion and crack defects are considered for pipeline integrity assessment based on different defect scenarios. Reliability results, or probabilities of failure, are reported with respect to design factors, hydrostatic test pressure factors, and safety factors, which can be used in designing new pipes, determining the applied pressure in hydrostatic tests, and operation pressure control of defected pipes, respectively. The effects of pipe grade, pipe dimensions (i.e., diameter and wall thickness), corrosion or crack defect sizes (e.g., length and depth), and internal pressure on PoFs for different limit states are also investigated.

Keywords: intact pipe; crack; corrosion; internal pressure; reliability analysis; CSA Z662:19

List of Symbols

A = Average defect depth in CorLas

A_{eff} = Effective flaw area

A_0 = Reference area

D = Pipe diameter

D_n = Nominal dimeter

E = Young's modulus

F = Design factor

F_{sf} = Free surface factor

F_3 = Shih-Hutchinson solution

I = Failure indicating function

J_c = Critical J-integral

K = Hydrostatic test pressure factor

L = Defect total length

M = Folias (bulging) factor

N = Total number of samples in Monte Carlo Simulation

P = Internal pressure

P_{bi} = Burst pressure of intact pipes

P_i = Calculated pressure resistance in Kiefner & Shannon model

P_i = Calculated pressure resistance of intact pipes in Kiefner & Shannon model

$P_{f(corrosion)}$ = Failure pressure of corroded pipes

$P_{f(flow)}$ = Failure pressure based on flow stress in CorLas

$P_{f(toughness)}$ = Failure pressure based on toughness in CorLas

P_r = Pressure resistance

Q_f = Shape factor

R_D = Dimensionless variable of diameter

R_p = Dimensionless variable of internal pressure

R_t = Dimensionless variable of wall thickness

$R_{\sigma t}$ = Dimensionless variable of tensile strength

$R_{\sigma y}$ = Dimensionless variable of yield strength

W_i = Weight of the ith sample vector

$\boldsymbol{X}$ = Basic random variable vector in Weighted Monte Carlo Simulation

$\boldsymbol{X_i}$ = Vector composed by the generated basic random variable X_i

$\boldsymbol{X_l}$ = The vector composed by lower bounds of each basic random variable

$\boldsymbol{X_u}$ = The vector composed by upper bounds of each basic random variable

X_j = The jth basic random variable in Weighted Monte Carlo Simulation

X_{jl} = The lower bound of variable X_j in Weighted Monte Carlo Simulation

X_{ju} = The upper bound of variable X_j in Weighted Monte Carlo Simulation

c = Model error factor accounting for flow stress definition in burst of intact pipes

d = Defect depth

e_1, e_2, e_3, e_4 = Model error factors

f_{ij} = The value of probability density function for random variable x_{ij}

f_j = The value of probability density function for random variable X_j

g_1 = Limit state function of yielding of defect-free pipes

$g_2^{operation}$ = Limit state function of burst of defect-free pipes during operation

$g_2^{hydrotest}$ = Limit state function of burst of defect-free pipes during hydrostatic test

g_3 = Limit state function of defected pipes

$g_3^{corrosion}$ = Limit state function of burst of corroded pipes

g_3^{crack} = Limit state function of burst of cracked pipes

n = Total number of basic random variables

n_e = Strain hardening exponent

n_f = Number of samples fall into the failure domain in sampling method

t = Wall thickness of the pipe

t_n = Nominal wall thickness

$\boldsymbol{x}$ = Random vector of random variables

x_i = Component of vector $\boldsymbol{x}$, the ith random variable in a general format

x_{ij} = The jth component in the random vector $\boldsymbol{X_i}$

y = Indicator of $D/2t$

σ = Solved stress in the equation of critical J-integra

σ_f = Failure stress

σ_h = Hoop stress

σ_{fl} = Flow stress

σ_n = Failure normal stress

σ_t = Tensile strength

σ_y = Yield strength

Glossary of Terms

CoV = Coefficient of Variation

CSA = Canadian Standard Association

CVN = Charpy Impact Energy

FORM = First-Order Reliability Method

LLS = Leakage Limit State

MCS = Monte Carlo Simulation

MAP = Maximum Annual Pressure

MOP = Maximum Operating Pressure

PDF = Probability Density Function

PoF = Probability of Failure

SF = Safety Factor

SLS = Serviceability Limit State

SMYS = Specified Minimum Yield Strength

SMTS = Specified Minimum Tensile Strength

ULS = Ultimate Limit State

WMCS = Weighted Monte Carlo Simulation

2.1 Introduction

Pipelines are the most widely used means for transmitting oil and gas due to low cost and high efficiency. However, the safety and integrity of pipelines have received increasing attention in recent years. Among numerous threats that affect the safety of pipelines, internal pressure is the most common and prominent one in the pipeline operational lifespan [1]. As described in the code for oil and gas pipeline system published by the Canadian Standard Association (referred to as

CSA Z662:19 hereafter), internal pressure plays a significant role in the lifecycle of pipelines. In the design and integrity assessment stages, internal pressure can serve as an independent or a companion load in various limit states, and several limit states are internal pressure-related. For example, in the design of new pipes, the maximum operating pressure (MOP) is determined based on pipes' yielding strength and a design factor, which aims to achieve a certain safety margin. Before putting pipes into commission, a hydrostatic test needs to be performed for checking the strength and leakage with the intended minimum pressure defined based on a specific factor K multiplied by the MOP. Similarly, in integrity assessment during the operational period of in-service pipes, safety factors are utilized to adjust the operating pressure to accommodate the reduced capacity due to defects in pipes. All these decision-making processes involve certain levels of conservatism or risk due to the use of various factors in a deterministic format to implicitly account for various sources of uncertainties.

In contrast to deterministic analysis, reliability assessment is a probabilistic approach for safety and integrity evaluation of structures. It explicitly accounts for uncertainties inherent the real-world problems, so that rational decision-making can be achieved based on an estimate of the probability of failure (i.e., the occurrence of undesired events). As such, in the CSA Z662:19, reliability-based design and assessment is included as an informative appendix (Annex O). In the literature, extensive endeavors have been devoted to the probabilistic analysis of pipelines. Rafael et al. [2] conducted a thorough comparison on the reliability of corroded pipes based on available models from academic publications and recognized codes, and the sensitivity of each model with the corrosion defect was evaluated. Teixeira et al. [3] developed the limit state function of burst for intact and corroded pipes based on experimental and numerical results conducted by Netto et al. [4], and the sensitivity analysis was performed with the conclusion that corrosion depth and internal pressure are the most important variables for the burst of pipes. Similarly, based on the burst pressure formulation proposed by Netto et al. [4], Wang et al. [5] established the burst pressure prediction model of corroded pipes by regression analysis on the finite element-based results and experimental data. Using the Monte Carlo Simulation (MSC), the study offered a set of simple reliability-based evaluation tools for pipeline safety assessment. Hasan et al. [6][7] examined a number of code/standard-based models predicting the burst pressure for corroded

pipes. The study found the probability of failure (PoF) of burst models suggested by codes/standards significantly varies for the same defect size, and comprehensive suggestions were accordingly offered for industrial use.

As for cracked pipes, Bai et al. [8] proposed a fracture reliability model of dented pipes with cracks considering the uncertainty of random variables and model error, then the safety factor was calibrated based on probabilistic study by MCS. Lee et al. [9] formulated the limit state function based on the stress intensity factor, and the PoF was assessed based on an X65 pipe with an external semi-elliptical crack. Guillal et al. [10] conducted the analysis on the effect of the shape factor (the ratio between crack depth and length) on the reliability, in which the limit state function was established based on fracture toughness. The massive and comprehensive study on burst capacity of defected pipes contributes to the model error evaluation on well-known failure pressure prediction equations, such as the study on corroded pipes by Zhou. et al. [11] and cracked pipes by Yan et al. [12]. The comparison demonstrated that RSTRENG and CorLAS are of highest accuracy for corroded pipes and cracked pipes, respectively.

Although these studies contributed to the development of reliability-based assessment of pipelines to various degrees, there is a lack of a comprehensive reliability evaluation of pipelines from the perspective of pipeline lifecycle, starting from the pipe design, pre-commission hydrostatic tests, to operation management (e.g., defect scenario-based integrity assessment). Furthermore, existing studies rarely link the probability of failure to all these factors (e.g., design factors, hydrostatic test pressure factors, safety factors) used in the design code. Note that in these studies [2][3][4][5][6][7][9][10], Monte Carlo Simulation (MCS) was mostly used for its simplicity but it is inefficient or inaccurate when the probability of failure is significantly low. Another widely used method, the first order reliability method (FORM) [3][4][6][7][9][10], is efficient but the accuracy highly depends on the problems.

Recognizing the importance of reliability assessment, this study aims to provide a comprehensive reliability analysis for pipelines focusing on internal pressure related limit states as specified by CSA Z662:19, covering the pipe design, hydrostatic testing, and defect scenario-based integrity assessment. Reliability results, or probabilities of failure, are presented with respect to design factors, hydrostatic test pressure factors, and safety factors used in designing new pipes,

pre-commission test, and operation pressure control of defected pipes, respectively. Results of this paper can be directly referred to for safety control of pipelines during its life cycle, which is of significant value for industrial use. It is worth noting that an innovative reliability method, Weighted Monte Carlo Simulation (WMCS), is utilized to facilitate reliability calculation for its high efficiency particularly for reliable estimate of low probabilities of failure. The workability of WMCS can be tested by the engineering practice in this study, and its simplicity and robustness make it worth to be applied by industry.

2.2 Weighted Monte Carlo Simulation (WMCS)

Generally, PoF can be calculated by various reliability methods, including the approximate analytical method (e.g., FORM) and stochastic sampling methods (e.g., MCS) with different levels of sophistication. However, results based on FORM can be inaccurate when the limit state function is nonlinear or when the distribution is significantly different from Gaussian. MCS can give sufficiently accurate results by sampling the design space based on the full probabilistic characterization of random variables. However, this method is inefficient when it comes to low PoF problems since a large number of samples are required to achieve a relatively accurate estimate of the PoF. This is because the PoF is estimated as the ratio between the number of samples in the failure domain (n_f) and the total number of samples (N) in MCS as shown in Eq. (2-1).

$$\mathrm{PoF} = \frac{n_f}{N} \tag{2-1}$$

To ensure reliable estimation of the probability of failure for pipes, this paper chose a readily used and efficient reliability method instead. This method, denoted as WMCS hereafter, was inspired by the traditional MCS. It was proposed by introducing weight indices to each sample and validated well through various benchmark problems [13]. The main idea behind WMCS is to replace the number of simulations in the MCS (see Eq. (2-1)) by a weighted sum, as expressed in Eq. (2-2).

$$\text{PoF} = \frac{\sum_{i=1}^{m} I(\boldsymbol{x}_i)\bullet}{\sum_{i=1}^{m} W_i(\boldsymbol{x}_i)} \tag{2-2}$$

where the weight of the i^{th} sample $\boldsymbol{x}_i$ (i = 1, 2, …, m and m is the sample size) (W_i) is defined as the product of probabilities density function (PDFs) evaluated at the sampled value for each random variable; the indicator function ($I(\boldsymbol{x}_i)$) is equal to 1 if $\boldsymbol{x}_i$ falls in the failure domain characterized by $g(\boldsymbol{x}_i) \le 0$, and 0 otherwise. The theoretical aspect of WMCS was detailed in [13], but the procedure utilized in this paper is presented as follows.

Step 1: stipulating an appropriate range of each basic random variable

MSC can be employed to simply get an appropriate range for basic variables. The minimum and maximum values for each variable X_j (j = 1, 2, …, n where n is the number of basic random variables) are regarded as the appropriate lower bound X_{jl} and upper bound X_{ju}. Thus, the range of basic variable vector $\boldsymbol{X}$ can be expressed as $\boldsymbol{X} \in [\boldsymbol{X}_l, \boldsymbol{X}_u]$, where $\boldsymbol{X}_l = [X_{1l}, X_{2l}, \cdots$ and $\boldsymbol{X}_u = [X_{1u}, X_{2u}, \cdots$.

Step 2: generating samples of basic random variables

Within the range obtained in ***Step 1***, random samples for each basic variable (e.g., X_j) are generated through a uniform random variable generator.

Step 3: assigning weights to the generated samples

For each sample of the random vector, $\boldsymbol{X}_i = (x_{i1}, x_{i2}, \cdots$, the value of the PDF for random variable X_j , $f_j(j = 1, 2, \cdots$ is evaluated at $x_{ij}(j = 1, 2, \cdots$, yielding $f_{ij} = f_j(x_{ij}), (j = 1, 2, \cdots$. The weight of the sample $\boldsymbol{X}_i$ can then be calculated as the product of $f_{ij}(j = 1, 2, \cdots$, see Eq. (2-3).

$$W_i = \prod_{j=1}^{n} f_{ij},\ i = 1, 2, \cdots \qquad \cdots \tag{2-3}$$

Step 4: identifying samples in safety or failure domains

Plugging every sample $\boldsymbol{X}_i = \left(x_{i1}, x_{i2}, \cdots\right.$ into the limit state function, Eq. (2-4) can be used to evaluate the indicator function: 1 for samples located in the failure domain and 0 for those that fall in the safe domain ($g > 0$).

$$I\left(\boldsymbol{X}_i\right) = \begin{cases} 1, & g\left(\boldsymbol{X}_i\right) \le 0 \\ 0, & g\left(\boldsymbol{X}_i\right) > 0 \end{cases} \tag{2-4}$$

***Step 5: computing* PoF**

PoF can be obtained based on Eq. (2-2).

2.3 Internal pressure-related limit states for pipelines in CSA Z662:19

Limit states, which are used to define the undesirable events, shall be classified into ultimate (ULS), leakage (LLS), and serviceability (SLS) limit states for pipes, depending on the loss of containment as per CSA Z662:19. The ULS refers to a loss of containment that represents a safety hazard; the LLS is associated with limited loss of containment that results in a limited potential for safety or environmental consequences; and finally, the SLS is related to a deviation of the design or service requirements of the pipeline without producing any loss of containment.

In the case of internal pressure, the yielding (belonging to SLS) and burst (belonging to ULS) are two main limit states of primary concerns for design and integrity assessment of pipelines. The yielding limit state is the criterion for new pipeline design. The burst limit state is used as a criterion in pipes' hydrostatic test for newly designed pipes and integrity assessment for defected pipes with a given defect scenario. The burst limit state is frequently considered in the operation for integrity management, which suggests that the operating pressure should be temporarily turned down in compliance with the pressure capacity decreased by defects to provide an additional safety margin [1][14]. As such, all these limit states will be considered in this paper by relating the PoFs with various deterministic factors as mentioned earlier.

2.4 Reliability analysis of intact pipes

In this paper, different pipe grades are considered, including low-strength types (X42, X52), mid-strength types (X60, X65), and high-strength types (X70, X80). Their corresponding material properties, such as specified minimum yield strength (SMYS), specified minimum tensile strength (SMTS), and the yield-to-tensile ratio (Y/T = SMYS/SMTS), are provided in Table 2-1 as per prescribed values in API 5L-2018 [15].

Table 2-1: Specified material properties for each steel grade for pipes

Pipe grade		**SMYS (MPa)**	**SMTS (MPa)**	**Y/T**
Low-strength	X42	290	414	0.700
	X52	359	455	0.788
Mid-strength	X60	414	517	0.800
	X65	448	531	0.844
High-strength	X70	483	565	0.854
	X80	552	621	0.899

2.4.1 Serviceability limit state (SLS): yielding

Stress-based pipe design for serviceability is achieved by limiting the circumferential stress, or hoop stress (σ_h) induced by internal pressure (Figure 2-1), to be less than the pipe yield strength stress (σ_y). Thus, the limit state function (g_1) can be formulated based on Barlow's equation as Eq. (2-5).

$$g_1 = \frac{2t\bullet}{D} \quad (2\text{-}5)$$

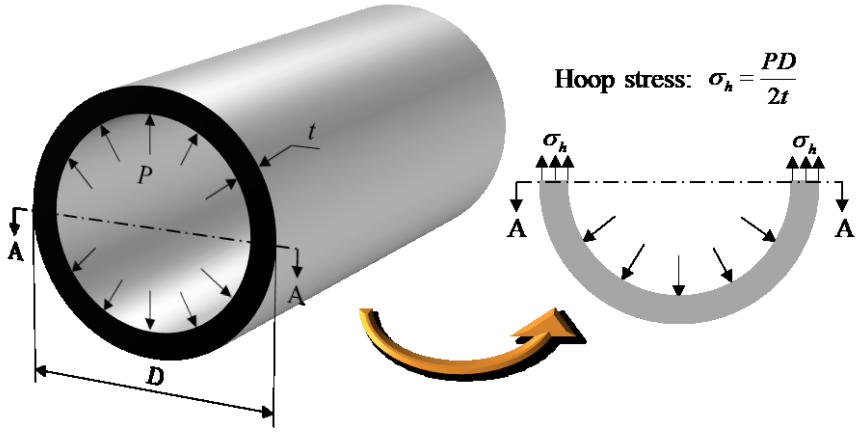

Figure 2-1: Hoop stress for intact pipes due to internal pressure

The internal pressure (P) is considered as the maximum annual pressure (MAP) in this paper. In reliability analysis presented later to determine the probability of yielding, the uncertainty in σ_y, D, t, and P are characterized by dimensionless random variables R_{σ_y}, R_D, R_t, and R_p, respectively (see Table 2-2). As stipulated by CSA Z662:19, the MOP can be calculated based on the nominal values of pipe diameter (D_n) and wall thickness (t_n), SMYS, and the design factor (F), according to Eq. (2-6).

$$\text{MOP} = \frac{2 \cdot}{D_n} \cdot \cdot \tag{2-6}$$

The aforementioned random variables are probabilistically characterized with the distribution type, the mean value, the coefficient of variation (CoV) as summarized in Table 2-2. Note that all random variables are assumed to be statistically independent and their statistics are primarily based on the guideline from CSA Z662:19.

Table 2-2: Probabilistic characteristics for pipe geometry, material properties, and internal pressure

Variable	Description	Distribution	Mean	CoV	Source

R_D	Dimensionless of pipe diameter, D/D_n	Normal	1.00	0.0006	Zimmerman et al. [16]
R_t	Dimensionless of wall thickness, t/t_n	Normal	1.01	0.01	Zimmerman et al. [16]
R_{σ_y}	Dimensionless of yield strength, σ_y/SMYS	Normal	1.10	0.036	Jiao et al. [17]
R_{σ_t}	Dimensionless of tensile strength, σ_t/SMTS	Normal	1.12	0.035	Jiao et al. [17]
R_p	Dimensionless of internal pressure, MAP/MOP	Gumbel	1.07	0.02	Jiao et al. [17]

Using the dimensionless random variables introduced, the limit state function expressed in Eq. (2-5) can be rewritten readily as Eq. (2-7).

$$g_1 = \frac{2R_t \bullet}{R_D} - 2R \bullet \tag{2-7}$$

As observed in Eq. (2-7), the limit state function is independent of the nominal or specified values for yield strength, internal pressure, pipe diameter, and wall thickness. By contrast, only the dimensionless variables are involved, which implies risk-consistent design since the reliability level achieved in the design will be independent of the pipe grade and pipe dimensions. As such, the safety level is determined by the design factor (*F*), which is used in the design of new pipes. The safety margin is well controlled by design factors, and a larger design factor leads to a narrower safety margin due to higher MOP according to Eq. (2-7).

PoFs with respect to various design factors are presented in Figure 2-2. The PoF increases exponentially with the increase of (*F*). For example, the PoF (i.e., probability of yielding) is 2.81×10^{-7} at *F*=0.8 and 1.13×10^{-11} for *F*=0.72. Note these two design factors are used in class location 1 for division 1 and 2, respectively, as per CSA Z662:19.

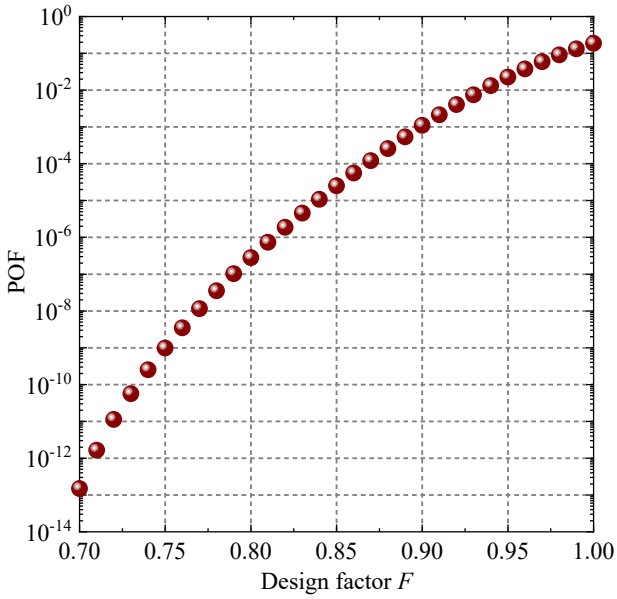

Figure 2-2: PoFs for the yielding limit state of intact pipes designed using different design factors

2.4.2 Ultimate limit state (ULS): burst

For safety concerns, an ULS, such as plastic collapse, needs to be checked to prevent overpressure. As per CSA Z662, plastic collapse is the event of the internal pressure reaching the pressure capacity or burst pressure of the intact pipe (P_{bi}). It can occur during the operation of pipes and a hydrostatic test, which is required by different codes of practice before a pipe is put into operation. In such a test, a predetermined pressure higher than MOP is applied to the pipe, and thus the hoop stress can be beyond the yield strength and possibly exceed the ultimate tensile strength of the pipe. To perform reliability assessment for the burst pressure limit state during operation and a hydrostatic test, two limit state functions are given in Eqs. (2-8) and (2-9), respectively.

$$g_2^{operation} = P_{bi} - \mathrm{MAP} \tag{2-8}$$

$$g_2^{hydrotest} = P_{bi} - K\bullet \tag{2-9}$$

The hydrostatic test pressure factor (*K*) prescribed in CSA Z662:19 is different based on the test purpose (e.g., strength or leak) and location class. Note that the uncertainty of internal pressure is not considered since the testing pressure is predefined and controlled by the operators during the hydrostatic test. As recommended by CSA Z662:19, the resistance P_{bi} is determined based on the "flow stress" (σ_{fl}) as shown in Eq. (2-10).

$$P_{bi} = 2c\sigma_{fl}\, t/D \tag{2-10}$$

It is important to note that the "flow stress", as the name implies, is a measure of the stress at which the metallic material yields or flows. The "flow stress" is typically taken as a value between the yield strength and the ultimate strength of the metallic material. Jiao et al. [18] suggested a flow stress $0.953\sigma_t$ (σ_t is the tensile strength) with a model error coefficient (c) accounting for uncertainty regarding the definition of the flow stress, which follows a normal distribution with a mean of 1.0 and a CoV of 4%. Similar to the yielding SLS, the limit state functions as expressed in Eqs. (2-8) and (2-9) can be rearranged as equivalent limit state functions shown in Eqs. (2-11) and (2-12) for pipes in operation and a hydrostatic test, respectively.

$$g_2^{operation} = 1.906c\sigma_t t - \mathrm{MAP}\bullet \qquad \bullet \bullet \bullet \tag{2-11}$$

$$g_2^{hydrotest} = 1.906c\sigma_t t - K\bullet \qquad \bullet \qquad \bullet \bullet \tag{2-12}$$

where the uncertainty in σ_t is characterized by a dimensionless random variable R_{σ_t} (see Table 2-2) whose statistics are included in Table 2-2. In addition to the design factor (*F*) and the hydrostatic test pressure factor (*K*), the reliability of intact pipes against burst failure is affected by the pipe grades since the yield-to-tensile ratio (Y/T) in the limit state function varies for different pipe grades. This factor is less than 1.0 and known to increase with pipe grades as shown in Table 2-1. Note that the two limit state functions are independent of the nominal values for pipe diameter and wall thickness; thus, the reliability level against burst failure is independent of the pipe design dimensions.

PoFs for the burst limit state (i.e., the probability of burst) of pipes in operation and in the hydrostatic test are respectively depicted in Figure 2-3 (a) and (b). As shown in Figure 2-3 (a), the

PoFs increase with design factors resulted from the reduction in the safety margin due to higher MOP (see Eq. (2-8)). Higher-grade pipes show higher PoFs (i.e., burst probabilities) because of higher Y/T ratios, which implies that higher pipe grades are more vulnerable to burst if the same design factor is used. For a risk-consistent design aiming at a constant PoF across different pipe grades, lower design factors should be used for higher-grade pipes. For comparison, the PoF curve for the yielding limit state is also included in Figure 2-3 (a). As observed, PoFs for the yielding limit state (SLS) are generally higher than those for the burst limit state (ULS), except when the design factor is lower than 0.72 for the X80 pipes. This is mainly due to the increasing Y/T ratios for high-grade steel in the limit state function shown in Eq. (2-11). In CSA Z662:19, the permissible PoF for SLS is 10^{-1} per km-year. The target PoF for ULS is a function of population density, pipe diameter, and internal pressure. For example, for class location 1 where the design factor 0.80 and 0.72 should be employed, the target PoF is estimated between 10^{-4} and 10^{-3}. Hence, PoFs in Figure 2-3 (a) are satisfying the prescribed requirements. The burst probability for pipes during a hydrostatic test is shown in Figure 2-3 (b) as a function of *KF*, which is the product of the design factor (*F*) and the hydrostatic test pressure factor (*K*). A similar trend is observed: the PoF increases with the increase of the *KF* factor, and the PoF associated with a given *KF* factor is higher for a higher pipe grade.

Note that in these two burst limit state functions for pipes in operation and a hydrostatic test, the uncertain burst pressure is the same, but the applied pressure considered is different. Specifically, in $g_2^{operation}$ for pipe in operation, the random applied pressure ($\mathrm{MAP} = R_p \bullet$) is considered, while in $g_2^{hydrotest}$ for the hydrostatic test, the deterministic applied pressured ($K \bullet$) is considered. Consequently, when $K = 1$, F is equal to KF but they lead to different PoF values. Taking X65 for an example, $F = 0.9$ is associated with PoF = 4.56×10^{-6} for pipes in operation while $KF = 0.9$ is associated with PoF =1.07×10^{-9} for pipes during a hydrostatic test. On the other hand, the same PoF corresponds to different values for F and KF. For example, PoF = 10^{-9} for X65 is associated with a design factor $F = 0.80$ for pipes in operation; by contrast, PoF = 10^{-9} is associated with $KF = 0.9$. This implies that a factor of $K = 0.9/0.80$ can be used for the hydrostatic test to ensure the same PoF as the design.

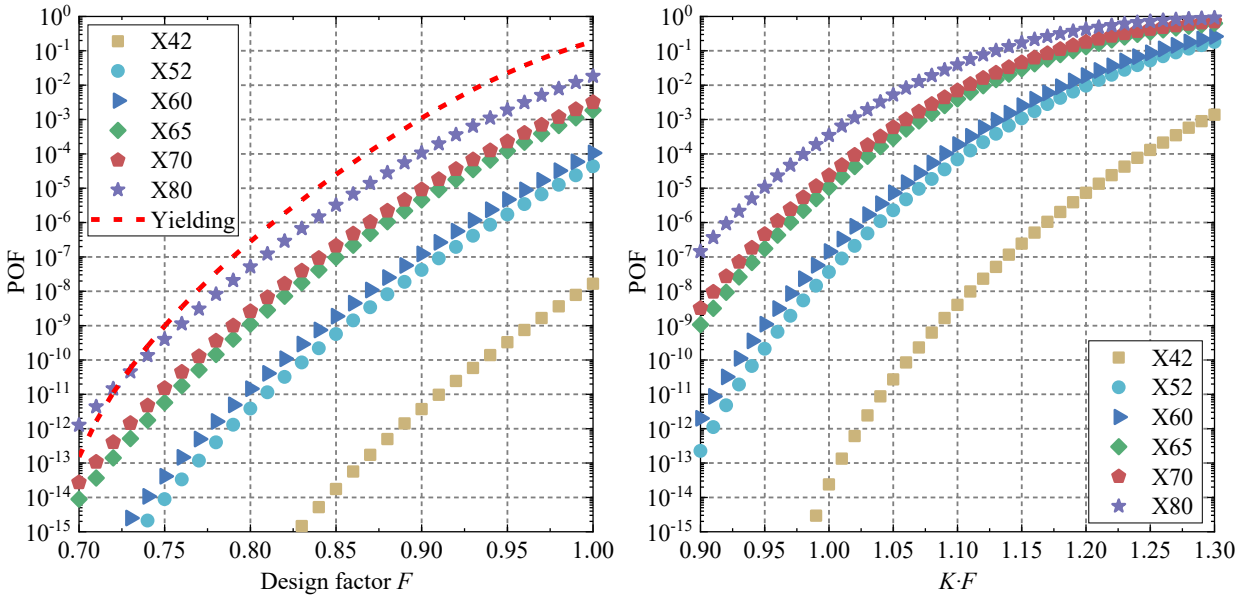

Figure 2-3: PoFs for burst limit state of intact pipes under internal pressure: (a) PoFs versus design factors F for design; and (b) PoFs versus KF for a hydrostatic test

2.5 Reliability assessment of defected pipes

Integrity assessment of in-service pipes is of significant value for the pipeline industry, as defects in pipes, such as cracks and corrosions, make pipelines more susceptible to failure under internal pressure. As illustrated in Figure 2-4, irregular crack-like and corrosion defects are typically idealized to regular shapes such as rectangles or semi-ellipses for failure pressure prediction and further integrity assessment [2]. For corroded pipes, only wall reduction-typed defects are considered, and pit corrosion or interactive defect is beyond the research scope of this study. However, the probabilistic approach taken here can also be applied to pipes with pitting corrosion or interactive defects.

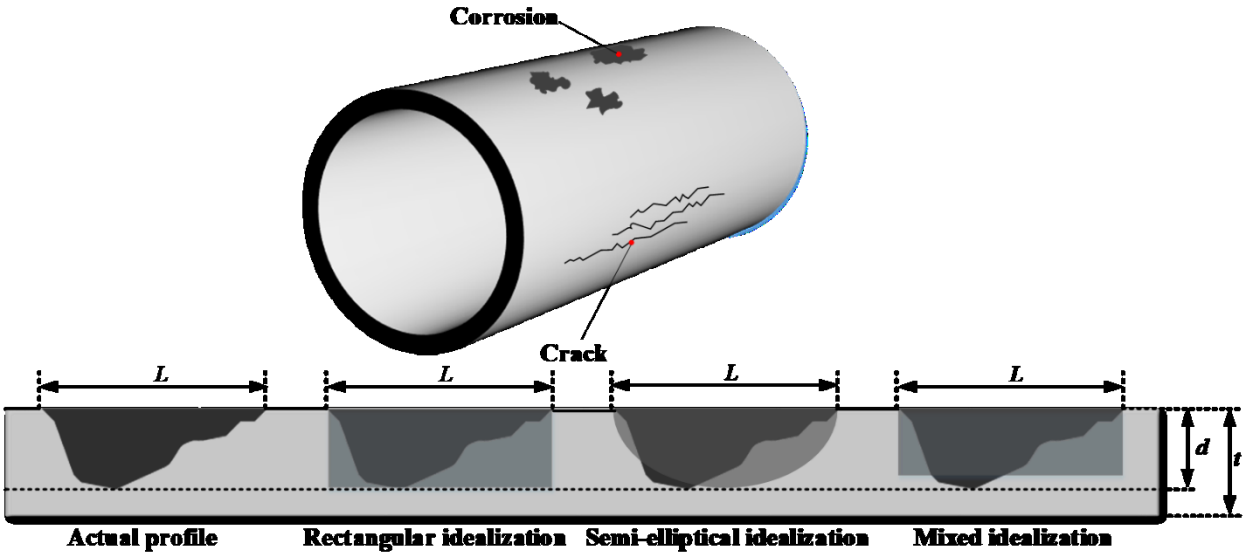

Figure 2-4: Schematic view of crack and corrosion profiles with shape idealization on a pipe

With the predicted failure pressure, or pressure resistance of defected pipes (P_r), the pipe failure under internal pressure can be mathematically expressed using the limit state function g_3 as displayed in Eq. (2-13).

$$g_3 = P_r - \text{MAP} \tag{2-13}$$

In the presence of injurious defects of a given scenario (e.g., defect length (L) and depth (d)), the reduction of operating pressure is expected to provide an additional margin of safety. Similar to the design factor (F) used in the design of new pipes as discussed in the section 2.4, the safety factor (SF) can be used to control the pressure reduction by using SF >1, where SF is defined as the ratio of the pressure resistance (P_r) to the MAP (Eq. (2-14)).

$$\text{SF} = \frac{P_r}{\text{MAP}} \tag{2-14}$$

2.5.1 Burst of cracked pipes (ULS)

The burst pressure of cracked pipes can be predicted using CorLAS which was developed to assess the integrity of pipes with crack-like defects. The built-in algorithm has demonstrated great

accuracy on burst pressure estimation [12] comparing with other peer models. Therefore, it is employed as the pressure resistance term in the burst limit state for cracked pipes. This methodology is based on two evaluation criteria: flow strength, and fracture toughness, which are briefly summarized as follows [19].

- ***Flow strength-based failure pressure***

The flow strength-based failure pressure ($P_{f(flow)}$) is computed according to Eq. (2-15).

$$P_{f(flow)} = \frac{\sigma_f}{\frac{D}{2t} - y} \tag{2-15}$$

where the pipe geometry indicator (y) is defined by Eq. (2-16).

$$y = \begin{cases} 0.4, & \text{when } D/2t \le 10 \\ 0, & \text{when } D/2t > 10 \end{cases} \tag{2-16}$$

Burst stress (σ_f) is defined as the flow stress (σ_{fl}) multiplied by a magnification factor that accounts for the tendency of the crack area to bulge outwards under the effect of internal pressure, as shown in Eq. (2-17).

$$\sigma_f = \sigma_{fl} \left(\frac{1 - \frac{A_{eff}}{A_0}}{1 - \frac{A_{eff}}{MA_0}} \right) \tag{2-17}$$

where the reference area $A_0 = L\bullet$; the flow stress (σ_{fl}) is defined as Eq. (2-18); the effective flaw area (A_{eff}) can be calculated by Eq. (2-19); and the Folias factor (M) is expressed as Eq. (2-20).

$$\sigma_{fl} = \begin{cases} \sigma_y + 68.94 \text{ (in MPa)}, & \text{for pipe grade} < \text{X70} \\ \frac{\sigma_y + \sigma_t}{2}, & \text{for pipe grade} \ge \text{X70} \end{cases} \tag{2-18}$$

$$A_{eff} = \begin{cases} Ld, & \text{for rectangular flaw} \\ \frac{\pi Ld}{4}, & \text{for semi-elliptical flaw} \end{cases} \tag{2-19}$$

$$M = \begin{cases} \sqrt{1 + 0.6275\left(\frac{L^2}{Dt}\right) - 0.003375\left(\frac{L^2}{Dt}\right)^2}, & \frac{L^2}{Dt} \le 50 \\ 3.3 + 0.032\left(\frac{L^2}{Dt}\right), & \frac{L^2}{Dt} > 50 \end{cases} \quad (2\text{-}20)$$

- ***Fracture toughness-dependent failure pressure***

Fracture toughness-dependent failure pressure ($P_{f(toughness)}$) can be computed by Eq. (2-21) for both internal and external flaws.

$$P_{f(toughness)} = \begin{cases} \frac{\sigma_n t}{\frac{\pi A}{4} + 0.5D}, & \text{for internal flaw} \\ \frac{2\sigma_n t}{D}, & \text{for external flaw} \end{cases} \quad (2\text{-}21)$$

where the average defect depth (A) is defined in Eq. (2-22) depending on defect shapes.

$$A = \begin{cases} d, & \text{for rectangualr flaw} \\ \frac{4A_{eff}}{\pi L}, & \text{for elliptical flaw} \end{cases} \quad (2\text{-}22)$$

The failure normal stress (σ_n) is obtained per Eq. (2-23).

$$\sigma_n = \sigma \frac{1 - \frac{A_{eff}}{A_0}}{1 - \frac{A_{eff}}{M \bullet}} \quad (2\text{-}23)$$

where σ is the stress solved for in Eq. (2-24) using an iterative procedure such as Newton-Raphson.

$$J_c = Q_f F_{sf} A \left[\frac{\sigma^2 \pi}{E} + F_3 \left(\frac{0.005 - \frac{\sigma_y}{E}}{\sigma_y^{\frac{1}{n_e}}} \right) \sigma^{\frac{1+n_e}{n_e}} \right] \quad (2\text{-}24)$$

Here, the critical J-integral (J_c) is related to Charpy impact energy (CVN) as shown in Eq. (2-25); the shape factor (Q_f) can be calculated based on a fitted equation Eq. (2-26); the free surface

factor (F_{sf}) depends on the crack depth, which is given in Eq. (2-27); the strain hardening exponent (n_e) is offered as Eq. (2-28); and the Shih-Hutchinson solution (F_3) can be estimated based on Eq. (2-29).

$$J_c = \frac{12\text{CVN}}{0.124} \tag{2-25}$$

$$Q_f = 1.2581 - 0.20589z - 11.493z^2 + 29.586z^3 - 23.584z^4$$

$$z = \begin{cases} 0.5, \text{ for } \dfrac{A}{L} > 0.5 \\ \dfrac{A}{L}, \text{ for } 0 < \dfrac{A}{L} \le 0.5 \end{cases} \tag{2-26}$$

$$F_{sf} = \begin{cases} \dfrac{2t}{\pi A}\tan\left(\dfrac{\pi A}{2t}\right)(1-2z) + 2z, & \text{for } \dfrac{A}{t} \le 0.95 \\ \left(8.515 + \left(\dfrac{A}{t} - 0.95\right)\dfrac{162}{t}\right)(1-2z) + 2z, & \text{for } \dfrac{A}{t} > 0.95 \end{cases} \tag{2-27}$$

$$n_e = -0.00546 + 0.556\frac{\sigma_y}{\sigma_t} - 0.547\left(\frac{\sigma_y}{\sigma_t}\right)^2 \tag{2-28}$$

$$F_3 = \left[3.85(1-n_e)\sqrt{\frac{1}{n_e}} + \pi n_e\right](1+n_e) \tag{2-29}$$

After determining $P_{f(flow)}$ and $P_{f(toughness)}$, the failure pressure is taken as the smaller one per Eq. (2-30).

$$P_{f(crack)} = \min\left(P_{f(flow)},\ P_{f(toughness)}\right) \tag{2-30}$$

As such, burst limit state function for cracked pipes under internal pressure can be written as Eq. (2-31).

$$g_3^{crack} = P_{f(crack)} - \text{MAP} \tag{2-31}$$

With the limit state function defined above, a wide spectrum of defected pipes is assessed to quantify the PoFs with respect to the safety factors. Table 2-3 summarizes the defected pipe cases considered in this study, including pipes with different grades, pipe dimensions (i.e., in terms of

diameter and wall thickness), and defect sizes (i.e., in terms of defect depth-to-wall thickness ratio and defect length-to-depth ratio). To minimize the number of cases considered here, all these configuration parameters are varied one at a time compared to the reference defected pipe (i.e., grade = X42, D_n= 711 mm, t_n = 8.74 mm, d/t= 0.5, and L/d = 20). The same statistical data provided in the section 2.4 is used together with the statistical data for CVN provided in Table 2-4. Note that the minimum CVN prescribed in API 5L-2018 is adopted as the mean of CVN, and a CoV of 14% is assumed based on the range given by CSA Z662:19 for all pipes. Additionally, the Young's modulus (E), as suggested by Sotberg et al. [22], yields a normal distribution with a mean of 2.10×10^5 MPa and a CoV of 0.04. For the cases considered, the deterministic allowable operational pressure is calculated based on the deterministic burst pressure estimated considering different safety factors. Thus, the safety margin is expected to be greater when adopting a higher safety factor as revealed later in the reliability analysis results.

Table 2-3: Defected pipe cases used in the reliability assessment

Configuration parameters	**Unit**	**Range**
Pipe grade	-	X42; X52; X60; X65; X70; X80
Diameter (D_n)	mm	711; 813; 914; 1016
Wall thickness (t_n)	mm	8.74; 11.91; 17.48; 25.40
Defect depth-to-wall thickness ratio, d/t	-	0.1; 0.3; 0.5; 0.7
Defect length-to-depth ratio, L/d	-	10; 15; 20; 25

Table 2-4: Probabilistic characteristics of Charpy impact energy

Diameter (mm)	**Distribution**	**Mean (unit: J)**						**CoV**
		X42	**X52**	**X60**	**X65**	**X70**	**X80**	
$D \leq 508$	Lognormal	41	41	41	41	56	80	14%
$508 \leq D \leq 610$	Lognormal	41	41	41	45	60	84	14%
$610 \leq D \leq 711$	Lognormal	41	41	43	49	65	94	14%
$711 \leq D \leq 813$	Lognormal	41	41	47	52	68	102	14%

$813 \le D \le 610$	Lognormal	41	41	49	56	73	110	14%
$610 \le D \le 1016$	Lognormal	41	42	52	58	77	118	14%
$1016 \le D \le 1118$	Lognormal	41	43	54	61	81	125	14%
$1118 \le D \le 1219$	Lognormal	41	46	56	64	84	133	14%
$1219 \le D \le 1422$	Lognormal	42	49	61	69	91	148	14%

Reliability analyses are performed for cracked pipes considered and the PoFs with respect to safety factors are presented in Figure 2-5. Overall, the PoFs decrease with safety factors because of greater pressure reduction applied for defected pipes. It is important to note that pipe grades, pipe dimensions, and crack sizes considered here have negligible influence on reliability when the operating pressure is adjusted based on the defected pipe configuration using a certain safety factor. This implies very small variability in the reliability levels of cracked pipes with different pipe or defect configurations, if a certain safety factor is adopted.

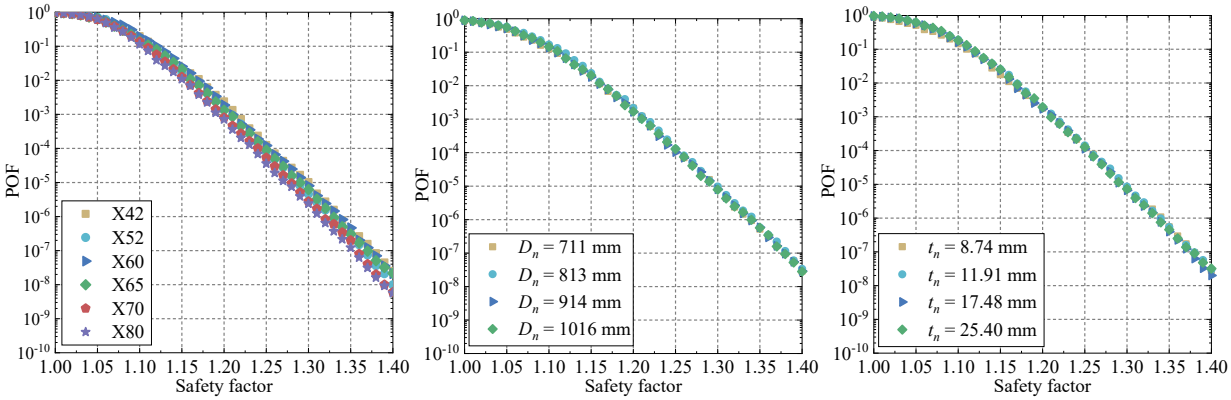

(a) (b) (c)

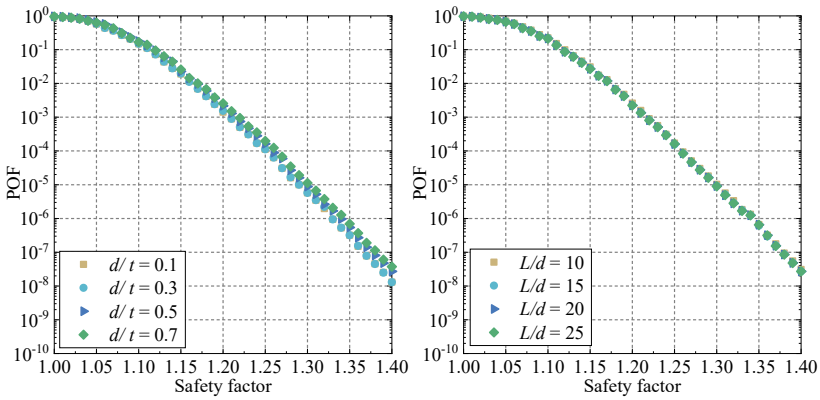

(d) (e)

Figure 2-5: PoFs for the burst limit state of cracked pipes with respect to safety factors under internal pressure considering different (a) pipe grades; (b) diameters; (c) wall thicknesses; (d) crack depth-to-wall thickness ratios; and (e) crack length-to-depth ratios

Based on CSA Z662:19, model errors should be considered in developing limit state functions (e.g., for corroded pipes as presented later), but no such information is provided or recommended in CSA Z662:19. As such, the CorLAS model error factors studied by Yan et al. [12], i.e., test-to-prediction ratio $R_{tp(\mathrm{CorLAS})}$ following a normal distribution with a mean of 0.96 and CoV of 22.8%, is used here for a case study using pipes (grade = X80, D_n = 711 mm, t_n = 8.74 mm, d/t= 0.5, and L/d = 20). Figure 2-6 shows the relationship between the PoFs and the design factors using the CorLAS with and without considering the model error. It shows that the PoFs are increased significantly, and this is attributed to the large model error (i.e., CoV = 22.8%). The authors believe that the accuracy of the CorLAS model is worthy of further investigation or more accurate models are needed.

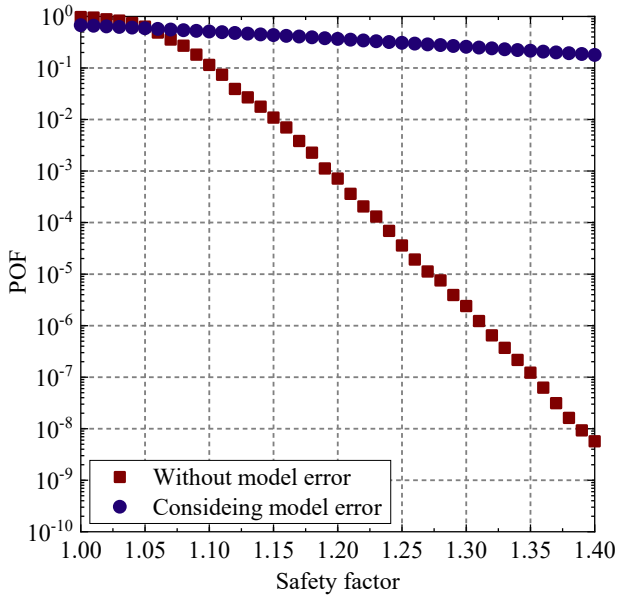

Figure 2-6: The PoFs versus safety factors with and without considering the model error proposed by Zijian Yan et al. [12]

2.5.2 Burst of corroded pipes (ULS)

The adopted pressure resistance model for corroded pipes [20] by CSA Z662:19 is used in this study. The model developed was calibrated with burst tests of corroded pipe segments removed from service [21], and the model error factors were obtained based on 25 burst test data points for high-grade steels and 38 points for low-grade steels. The estimated failure pressure of burst ($P_{f(corrosion)}$) including model error is defined in Eq. (2-32)[1].

$$P_{f(corrosion)} = \begin{cases} e_1 P_c + (1-e_1) P_i - e_2 \sigma_t, & \text{SMYS} > 241 \text{ MPa} \\ e_3 P_c + (1-e_3) P_i - e_4 \sigma_y, & \text{SMYS} \le 241 \text{ MPa} \end{cases} \quad (2\text{-}32)$$

where the model error factors e_1 = 1.04 and e_3 = 1.17 are deterministic multiplicative model error terms, while e_2 and e_4 are additive model error terms yielding the normal distribution. The mean and standard deviation of e_2 are respectively -0.00056 and 0.001469, the two stochastic properties for e_4 are -0.007655 and 0.006506; P_c denotes the calculated pressure of intact pipes using Eq. (2-33) and P_i represents pressure capacity of intact pipes calculated by Eq. (2-34).

$$P_c = P_i \left(\frac{1 - \frac{d}{t}}{1 - \frac{d}{tM}} \right) \tag{2-33}$$

$$P_i = \begin{cases} \dfrac{2t\bullet}{D}, & \text{SMYS} > 241 \text{ MPa} \\ \dfrac{2t\bullet}{D}, & \text{SMYS} \le 241 \text{ MPa} \end{cases} \tag{2-34}$$

Hence, the limit state function ($g_3^{corrosion}$) for burst failure of pipes with corrosion defects can be written as Eq. (2-35).

$$g_3^{corrosion} = P_{f(corrosion)} - \text{MAP} \tag{2-35}$$

Using this limit state function, the same group of defected pipes (i.e., with the same corrosion defect size as the crack defect size considered earlier) are assessed through reliability analysis to quantify the PoF with respect to the safety factors (see in Figure 2-7). Pipe grade shows no impact on the curve of PoF versus safety factors, which is similar to the situation in cracked pipes. However, pipe dimensions (i.e., diameter and wall thickness) and corrosion defect sizes (defect depth and length) influence PoFs more than cracked pipes. Corroded pipes with larger diameters and smaller thicknesses lead to higher PoFs, which means corroded pipes with larger diameter-to-wall thickness ratios (D_n/t_n) will be less safe by reducing pressure using a specific safety factor. In addition, pipes with the deeper and longer corrosion defects show relatively higher PoF values. This implies that, for risk-consistent decision-making on integrity management of corroded pipes, different safety factors should be recommended for different pipes with different corrosion defects.

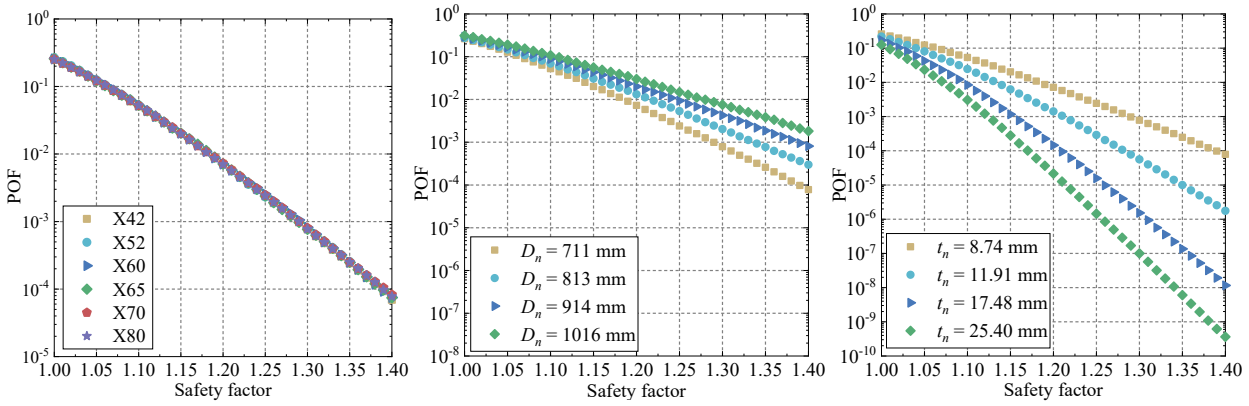

(a) (b) (c)

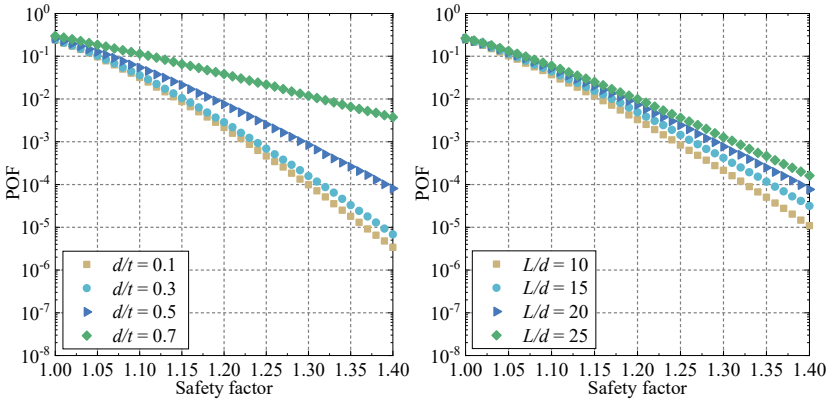

(d) (e)

Figure 2-7: PoFs for the burst limit state of corroded pipes with respect to safety factors under internal pressure considering different (a) pipe grades; (b) diameters; (c) wall thicknesses; (d) corrosion depth-to-wall thickness ratios; and (e) corrosion length-to-depth ratios

2.6 Chapter conclusions

This paper assessed the reliability levels of intact and defected pipes (cracked and corroded) under internal pressure designed and operated according to CSA Z662:19. Using the Weighted Monte Carlo Simulation, the probabilities of failure for yielding (serviceability limit state) and burst (ultimate limit state) of intact pipes can be efficiently calculated with respect to design factors used in the design of new pipes. Similarly, probabilities of failure for burst failure are also reported for the pipes considering different hydrostatic test pressure factors during the hydrostatic tests. For defected pipes with cracks and corrosions, probabilities of burst are studied with respect to safety factors to provide guidance in pressure control in operation of defected pipes. This study presents the significance of CSA Z662:19 in the reliability-based assessment on pipes, and in particular, the obtained results when model uncertainty is considered, can be employed in engineering for safety control for higher level of confidence.

The reliability assessment of intact pipes shows probabilities of failure for yielding limit state are independent of yield strength, internal pressure, pipe diameter, and wall thickness. The probability of failure exponentially increases with the increase of design factor. Specifically, for

design factors 0.80 (division 1) and 0.72 (division 2) used in class location 1, probabilities of failure for yielding limit state are 2.81×10^{-7} and 1.13×10^{-11} respectively. Probabilities of failure for burst limit state (ultimate limit state) are generally lower than those for yielding limit state (serviceability limit state). Study on the probability of failure for burst limit state of pipes during hydrostatic tests can assist determining the applied pressure reliably based on the hydrostatic test factor and intended maximum operating pressure. It is found that higher-grade pipes are more vulnerable to burst as their higher yield-to-tensile ratios lower the capacity.

Higher safety factor corresponds to a higher reliability level (lower probabilities of failure) based on the investigation on defected pipes. For cracked pipes, grade, dimensions (i.e., diameter and wall thickness), and crack sizes (i.e., crack length and depth) have negligible influence on probabilities of failure for burst limit state when adjusting operating pressure based on a particular safety factor, when no model error is considered. The published model error of CorLAS is so large leading to a considerable increase in the associated probabilities of failure and thus reliable burst pressure predictions models are needed for cracked pipes. As for corroded pipes, grade shows no impact on the curve of probability of failure versus safety factors. However, pipe dimensions and corrosion defect sizes influence probabilities of failure more than cracked pipes. Besides, pipes with the deeper and longer corrosion defects show relatively higher probabilities of failure.

References

[1] CSA. Oil and gas pipeline system, CSA standard Z662:19. Mississauga, Ontario, Canada: Canadian Standard Association; 2019.

[2] R. Amaya-Gómez, M. Sánchez-Silva, E. Bastidas-Arteaga, F. Schoefs, F. Muñoz, Reliability assessments of corroded pipelines based on internal pressure–A review, Eng. Fail. Anal. 98 (2019) 190-214.

[3] A.P. Teixeira, C. Guedes Soares, T.A. Netto, S.F. Estefen, Reliability of pipelines with corrosion defects, Int. J. Press. Vessel. Pip. 85.4 (2008) 228-237.

[4] T.A. Netto, U.S. Ferraz, S.F. Estefen, The effect of corrosion defects on the burst pressure of pipelines, J. Constr. Steel Res. 61 (2005) 1185–204.

[5] N. Wang, M.S. Zarghamee, Evaluating Fitness-for-Service of Corroded Metal Pipelines: Structural Reliability Bases, J. Pipeline Syst. Eng. 5 (1) (2014) 04013012.

[6] M. Hasan, F. Khan, S. Kenny, Identification of the cause of variability of probability of failure for burst models recommended by Codes/Standards, J. Press. Vessel Technol. 133 (2011) 041101.

[7] S. Hasan, F. Khan, S. Kenny, Probability assessment of burst limit state due to internal corrosion, Int. J. Press. Vessel. Pip. 89 (2012) 48–58.

[8] Y. Bai, R. Song, Fracture assessment of dented pipes with cracks and reliability-based calibration of safety factor, Int. J. Press. Vessel. Pip. 74.3 (1997) 221-229.

[9] O.S. Lee, H.M. Kim, D.H. Kim, H.B. Choi, Reliability Estimation of a Natural Gas Pipeline with Surface Crack, in: Proceedings of the ASME 2009 Pressure Vessels and Piping Conference (PVP2009), New York, 2009, pp. 459-466.

[10] A. Guillal, N. Abdelbaki, M.E.A. Bensghier, M. Betayeb, Effect of shape factor on structural reliability analysis of a surface cracked pipeline-parametric study, Frat. ed Integrita. Strutt. 13 (2019): 341-349.

[11] W. Zhou, G.X. Huang, Model error assessments of burst capacity models for corroded pipelines, Int. J. Press. Vessel. Pip. 99 (2012) 1–8.

[12] Z. Yan, S. Zhang, W. Zhou, Model error assessment of burst capacity models for energy pipelines containing surface cracks, Int. J. Press. Vessel. Pip. 120 (2014) 80-92.

[13] M. Rashki, M. Mahmoud, M.A. Moghaddam, A new efficient simulation method to approximate the probability of failure and most probable point, Struct. Saf. 39 (2012) 22-29.

[14] ASME, ASME B31.8S-2001: Managing System Integrity of Gas Pipelines, American Society of Mechanical Engineers, 2001.

[15] API, API Specification 5L: Line pipe, American Petroleum Institute, 2018.

[16] T.J.E. Zimmerman, A. Cosham, P. Hopkins, N. Sanderson, Can limit states design be used to design a pipeline above 80% SMYS?, in: 17th International Conference on Offshore Mechanics and Arctic Engineering (OMAE 1998), Lisbon, 1998.

[17] G. Jiao, T. Sotberg, R. Igland, SUPERB 2M statistical data-basic uncertainty measures for reliability analysis of offshore pipelines, SUPERB project report, No. STF70 F95212, 1995.

[18] G. Jiao, T. Sotberg, R. Igland, SUPERB 2M Project: Wall thickness sizing: limit-states based design for offshore pipelines, SUPERB project report, 1995.

[19] S.J. Polasik, C.E. Jaske, T.A. Bubenik, Review of Engineering Fracture Mechanics Model for Pipeline Applications, in: International Pipeline Conference (IPC2016), American Society of Mechanical Engineers (ASME), Calgary, 2016, pp. V001T03A038.

[20] M. Brown, M. Nessim, H. Greaves, Pipeline defect assessment: deterministic and probabilistic considerations, Second International Conference on Pipeline Technology, Ostend, Belgium, September. 1995.

[21] J.F. Kiefner, P.H. Vieth, A modified criterion for evaluating the remaining strength of corroded pipe, A Report for the Pipeline Corrosion Supervisory Committee of the Pipeline Research Committee of the American Gas Association, Battelle Columbus Div., Ohio, Unit State, 1989 (No. PR-3-805).

[22] T. Sotberg, B.J. Leira, Reliability-based pipeline design and code calibration, Proceedings of the 13th International Conference on Offshore Mechanics and Arctic Engineering, New York, Unit State, 1994 (No. 940230).

CHAPTER 3: STRAIN DEMAND OF ELASTIC PIPES SUBJECTED TO PERMANENT GROUND DISPLACEMENTS USING THE FINITE DIFFERENCE METHOD

This chapter is derived from the published paper:

Q. Zheng, L. Graf-Alexiou, Y. Li, N. Yoosef-Ghodsi, M. Fowler, M. Kainat, S. Adeeb, Strain demand of elastic pipes subjected to permanent ground displacements using the finite difference method, J. Pipeline. Sci. Eng. 1 (2021) 176-186.

Abstract

Long-distance pipelines are one of the primary means of oil and gas transportation. During the construction process, long-distance pipelines are inevitably buried across geohazard zones, which potentially generate permanent ground displacements. These ground displacements can potentially induce excessive strains in the pipe posing a great threat to the pipe's safety and integrity. In this study, a new numerical methodology for the response analysis of pipes subjected to ground displacements is proposed based on the finite difference method. Simulating the pipeline as a large deformation Euler-Bernoulli beam, the finite difference method is used to solve the two interacting nonlinear differential equations of equilibrium in the longitudinal and lateral directions considering the nonlinear pipe-soil interaction induced by the ground displacement. Implemented using the nonlinear equation solver of FindRoot by Mathematica for solving nonlinear equations, the longitudinal strain along the pipeline can be subsequently derived, and the tensile and compressive strain demands can be therefore determined for engineering reference. Finally, the applicability of this method is validated based on two hypothetical study cases involving symmetric and non-symmetric soil resistance on the lateral direction of the pipe. Comparing the

results with the finite element analysis solver Abaqus, we demonstrate that this present methodology has excellent predictive capabilities. Our study is carried out for elastic response calculation, but the proposed method shows a great promise for further development involving material nonlinearity, which is appropriate for the preliminary safety evaluation for the design of new pipelines or for risk pre-screening of existing pipelines.

Keywords: strain demand; buried pipes; permanent ground displacement; finite difference method; elastic response

3.1 Introduction

Pipelines are the most commonly used means for transporting oil and gas from the sources to the end users. Generally, pipelines constructed underground traverse long distances and inevitably pass through a wide variety of soils, geological zones, and regions of varying seismicity, which have the potential to cause surficial soil cracks and offsets, namely, permanent ground displacements. Large ground displacement is considered as one of the most important extreme events for buried pipes inducing considerably high strain levels as a result of excessive bending and axial elongation. Excessive strain demand can lead to leakage of the oil and gas, which in turn can cause secondary damage to the surroundings. Therefore, calculating the strain demand of the pipe subjected to ground displacements is of great importance to the design and maintenance of pipelines.

Damage to pipelines due to permanent ground displacement is the subject of extensive research. In their pioneering work, Newmark and Hall [1] studied pipes' response subjected to seismic faults in 1975, in which simplified analytical techniques were developed based on cable theory. Kennedy et al. [2] extended the cable-based method proposed by Newmark and Hall by incorporating the bending of the pipeline near the pipe-fault intersection point considering lateral soil forces. Wang and Yeh [3] subsequently proposed a refined model to predict the elongation of the pipeline buried across strike-slip faults and reverse faults. Takada et al. [4] developed a simplified model for calculating the strain demand in steel pipes buried at fault crossings

considering the cross-sectional deformation of the pipe. A variety of analytical and semi-analytical methods were also developed by Karamitros et al. [5] and Trifonov et al. [6][7]. Yoosef-Ghodsi et al. [8] proposed a simplified model to predict strain demands of pipes undergoing uniform longitudinal slides with consideration of internal pressure and temperature changes. More recently, Sarvanis and Karamanos [9] proposed a systematic approach for strain analysis of continuous pipelines buried in geohazard areas, including seismic fault movement, slope instability, liquefaction-induced lateral spreading, and soil subsidence. This work enhanced the analytical approach proposed by Vazouras et al. [10], which was only applicable to the case of symmetric soil resistance and neglected the zero-curvature condition at the two ends of the deformed pipe segment. Liu et al. [11] developed an enhanced analytical approach to calculate the longitudinal strain of buried pipe under strike-slip faults with intersection angle less than 90°, in which an equivalent modulus model was proposed to account for the decreased pipe stiffness due to material nonlinearity. These analytical methods adopt a bilinear stress-strain relationship for pipe material, which introduces errors to outcomes. In addition, a solid structural background is needed to implement a relatively accurate analytical model such as the systematic work by Sarvanis and Karamanos [9] which cannot be easily implemented by pipeline practitioners and researchers.

With the rapid advancement of computational technologies, the finite element method has been a widely adopted numerical tool for pipeline analysis (e.g., using the general-purpose commercial finite element software Abaqus and Ansys). In the simulation of a pipe subjected to ground displacements, three critical issues arise: element selection for the pipe, constitutive modeling of soil, and representation of pipe-soil interactions. For example, Takada et al. [4] used shell elements to simulate the pipe segment near the fault plane for accurately capturing the flexural behavior under fault displacement, while they used beam elements to model the pipe segment to obtain the axial elongation. This beam-shell hybrid model has higher computational efficiency and accuracy compared with some other peer models, such as the pipe-element model, fixed boundary shell-element model, and equivalent-spring-boundary model [12]. Similarly, the pipe-elbow hybrid model, in which the pipe segment near the fault plane is modelled by elbow elements, was developed to obtain the combined effect of compression and bending on the pipe [13][14][15]. Liu et al. [16][17] modified Takada's model by applying equivalent boundary

conditions to the far end of the pipe, which can represent the effect of imposed boundary conditions. Based on this type of model, Liu et al. [18] analyzed the effects of the yield strength and the strain hardening parameter on the buckling behavior of high-strength pipes. As for the model of soil and pipe-soil interaction, solid elements were utilized to simulate the soil in some publications [10][19][20], together with contact defined for the pipe-soil interface. For the sake of simplification, soil springs are recommended by ALA Guidelines [21] instead of modeling the soil domain and the pipe-soil interface explicitly. Properties of the interaction between the pipe and soil are characterized by a bilinear relationship of resistance against displacement based on properties of the soil, burial depth, pipe diameter and coating. These relationships are widely used in the response analysis on pipes withstanding displacement-based loads [13][14][15][16][17][18]. However, the issue of computational efficiency arises with the finer mesh, longer model of pipe, and greater loading of ground displacement. Besides, the acquisition of the commercial software brings about a higher cost to the engineering project.

In addition to analytical methods and numerical simulation mentioned above, a number of experimental investigations, e.g. small-scale experiments based on the shaking table [21] and centrifuge machines [22][23], and full-scale tests with soil boxes [24] and field model [25], were conducted in order to obtain the actual response of pipes subjected to ground displacement. Those achievements in analytical, numerical and experimental studies all contribute to the development of performance analysis of buried pipes subjected to ground movements.

For practical use in the pipeline industry, a simple model is preferred for engineers to determine the strain demand of steel pipes subjected to ground movements. A substantial amount of research has been conducted to assist pipeline design by offering application tools based on empirical fitting formulas for strain demand. However, a simplified numerical model based on mechanics is equally attractive to engineers. This paper presents a novel and simple numerical model in which the finite difference method is used to predict strain demands of pipelines subjected to general ground movement. To this end, a system of finite difference equations is constructed based on the governing equations for a large deformation Euler-Bernoulli beam considering the nonlinearity in the pipe-soil interaction. To reduce the complexity of the systems of equations, we only restrict our work to the elastic response. The resulting set of nonlinear finite difference

equations can be solved iteratively by the built-in nonlinear solver in Mathematica (the code is provided as supplementary material). Two hypothetical cases are studied to test the accuracy and efficiency of this model, by comparing the results derived from the proposed model and the counterparts from the finite element model developed using beam elements in Abaqus [26]. This study offers a valuable tool for response analysis of pipes buried across geohazard zones, which can be used for preliminary design of pipelines or safety pre-screening of existing pipelines.

3.2 Proposed methodology

The problem under consideration can be graphically described in Figure 3-1. The graph only depicts the pipe's deformation in the horizontal plane (x - y plane) due to a prescribed geohazard which could represent a slope, landslide, and liquefaction-induced lateral spreading, but can be extended to the situation with vertical deformations in the vertical plane (x - z plane) triggered by geohazards in the form of ground heave and soil subsidence. For the sake of simplicity, the ground discontinuity induced by all the above-mentioned geohazards is referred to hereafter as "ground displacement" or "ground movement".

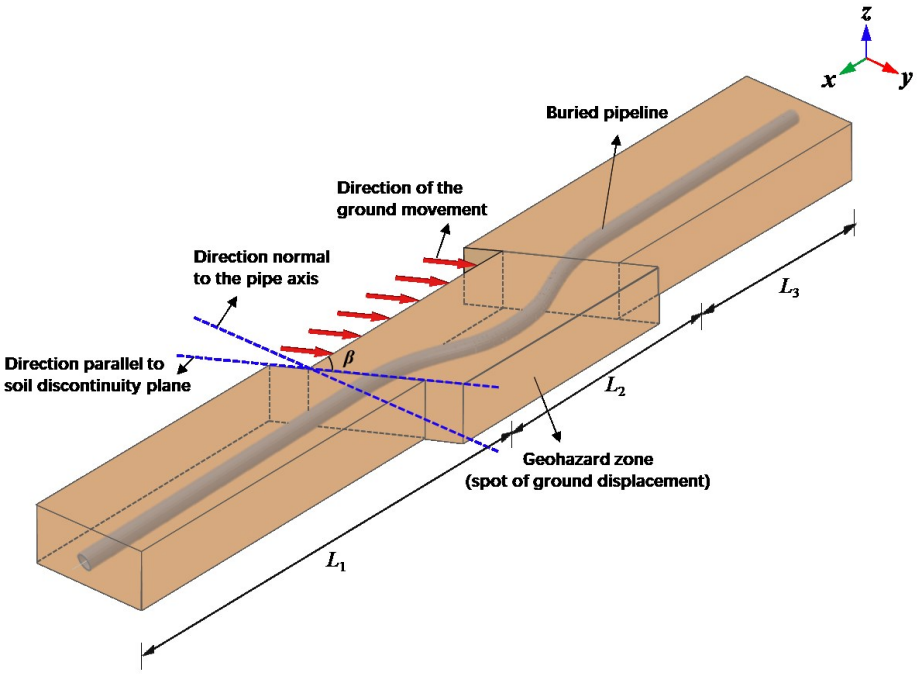

Figure 3-1: Graphical representation of the pipe subjected to ground displacements induced by geohazards

3.2.1 Governing equations

The pipeline is modeled as a large deformation Euler-Bernoulli beam. Due to the differential ground displacement, a large rotation will occur on the discontinuity plane. Therefore, the Euler-Bernoulli beam equations involving moderately large rotations are adopted to account for the deformation behavior of the pipe undergoing ground displacements. The deformed shape of the Euler-Bernoulli beam induced by the axial load $f(u)$ and lateral load $q(v)$ is depicted in Figure 3-2, and the governing equations are shown in Eq. (3-1) [13].

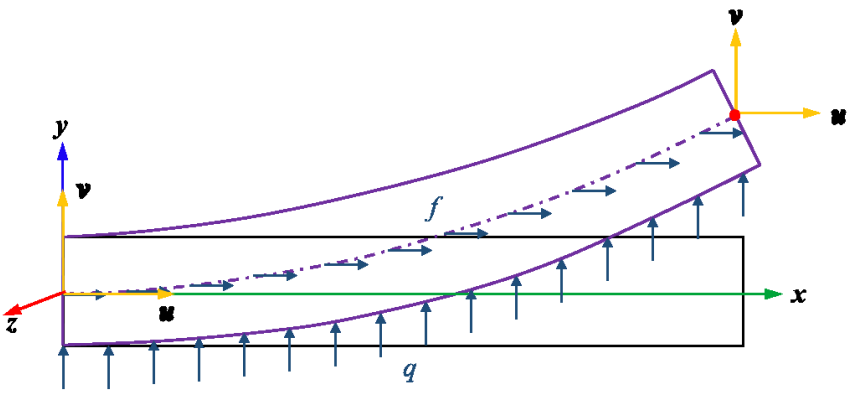

Figure 3-2: Euler-Bernoulli beam under large deformation

$$\begin{cases} \dfrac{dN}{dx} + f\left(U_g - u\right) = 0 \\ \dfrac{d^2M}{dx^2} - \dfrac{d}{dx}\left(N\dfrac{dv}{dx}\right) - q\left(V_g - v\right) = 0 \end{cases} \tag{3-1}$$

where N and M are the axial internal force and internal bending moment on the cross-section of the beam respectively; u and v represent the axial deformation and lateral deformation of the pipe. As indicated, f and q are externally distributed loads in the longitudinal and lateral directions, which are represented by the nonlinear soil stiffness-displacement relationships of soil springs in the respective directions. U_g and V_g are respectively the ground movements in the longitudinal and lateral directions.

3.2.2 Brief introduction to the finite difference method

The finite difference method is a numerical tool to solve differential equations by approximating derivatives with finite differences. Compared with the finite element method which is based on the integral form or weak formulation, the finite difference method mainly works for structured spatial difference and is based on the differential form of the governing equations. In the finite difference method, a regular mesh is typically defined and the continuum representation of each node in space can be expressed by a set of discrete equations, named finite difference equations. Together with boundary (or initial) conditions, the large algebraic system of equations is to be solved in place of the differential equation [27]. Commonly, for the problem with a regular-

shaped body and boundary conditions, the finite difference method is quite easy to implement and gives very efficient and high-quality results, which inspired the development of this study involving the line-shaped pipeline object.

From a geometric perspective, the first-order derivative of the function at the point x_i is the slope of the tangent to the function at that point. As for a smooth curve, this derivative can be expressed in three ways as shown in Figure 3-3. Where, the $f'_-(x_i)$ and $f'_+(x_i)$ are one-sided approximations to $f'(x_i)$, called the backward finite difference and the forward finite difference respectively. Another possibility is using the values on both sides of $f(x_i)$ to estimate the derivative, which can provide a better estimation at the specific point, called the central finite differences. It is simply the average of the one-sided results when $x_{i+1} - x_i = x_i - x_{i-1}$. These approximations will be accurate enough when $h \to 0$. Naturally, the principle for the first derivative can be extended accordingly to higher-order derivatives.

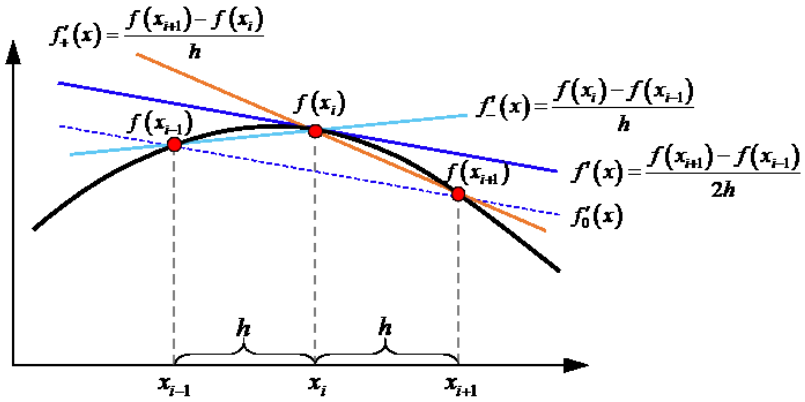

Figure 3-3: Various approximations to $f'(x)$ interpreted as the slope of secant lines

3.2.3 Consideration of finite differences towards governing equations

The derivatives in Eq. (3-1), e.g., $\frac{dN}{dx}$, $\frac{d^2M}{dx^2}$, and $\frac{d}{dx}(N\frac{dv}{dx})$, can be represented based on finite differences as stated in section 3.2.2. In order to calculate the strains, the finite difference equation set should be constructed based on the deformation functions *u* and *v*. To do this, the axial

internal force N and bending moment M in Eq. (3-1) should be expressed by u and v. By restricting the treatment in this work to elastic deformation, the general distribution of the longitudinal strain and stress in the cross-section of pipes is sketched in Figure 3-4 on account of the assumption of "plane sections remain plane".

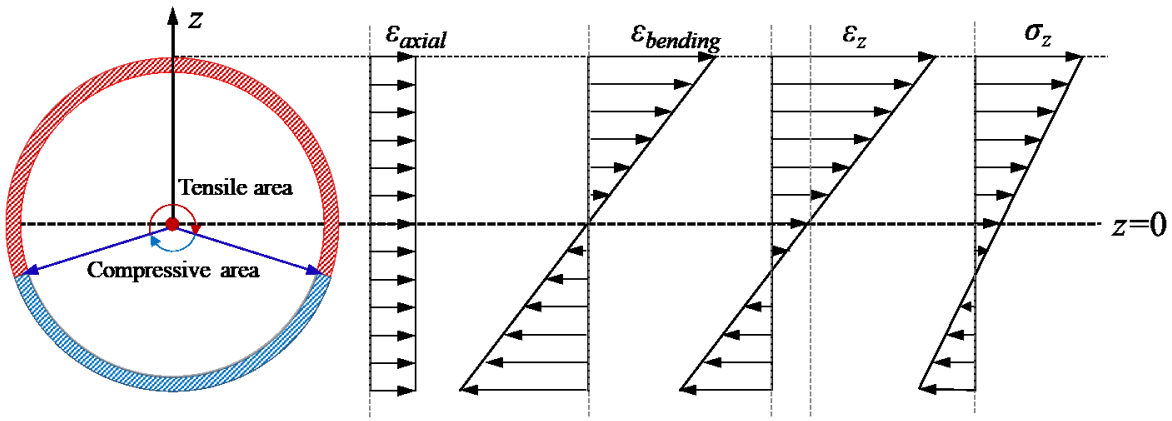

Figure 3-4: Strain and stress distribution on the pipe's cross-section

As illustrated in Figure 3-4, the axial strain ε_{axial} induced by stretching and the bending strain $\varepsilon_{bending}$ under the flexural behavior contribute to the longitudinal strain ε_l (the subscript z denotes the vertical position on the cross-section). Based on the large deformation theory, pipe's deformation in the x-direction u_x, in the y-direction u_y, and in the z-direction u_z can be written as Eqs. (3-2) to (3-4) (see Figure 3-2).

$$u_x = u - zv' \tag{3-2}$$

$$u_y = 0 \tag{3-3}$$

$$u_z = v \tag{3-4}$$

Using the definition of the Lagrangian Green strain, the longitudinal strain ε_l for the beam that is valid for large rotations but small strains can be derived as Eq. (3-5).

$$\varepsilon_l = \varepsilon_{xx} = \nabla u_{xx} + \frac{1}{2}\left(\nabla {u_{xx}}^2 + \nabla {u_{yx}}^2 + \nabla {u_{zx}}^2\right) \tag{3-5}$$

Plugging the derivatives of u_x, u_y, and u_z as shown in Eqs. (3-6) to (3-8) to Eq. (3-5) and ignoring the higher-order derivatives, the formulation of longitudinal strain ε_l can be simplified as Eq. (3-9).

$$\nabla u_{xx} = \frac{\partial u_x}{\partial x} = u' - zv'' \tag{3-6}$$

$$\nabla u_{yx} = \frac{\partial u_y}{\partial x} = 0 \tag{3-7}$$

$$\nabla u_{zx} = \frac{\partial u_z}{\partial x} = v' \tag{3-8}$$

$$\varepsilon_l = u' - zv'' + \frac{1}{2}\left[\left(u' - zv''\right)^2 + v'^2\right] = u' + \frac{1}{2}v'^2 + zv'' \tag{3-9}$$

Hence, the expression of ε_{axial} and $\varepsilon_{bending}$ can be written as Eqs. (3-10) and (3-11).

$$\varepsilon_{axial} = u' + \frac{v'^2}{2} \tag{3-10}$$

$$\varepsilon_{bending} = v''\bullet \tag{3-11}$$

Under the assumption of elastic deformation, the longitudinal stress σ_l is linearly distributed in the cross-section and accordingly the tensile and compressive areas can be obviously distinguished. According to the definition of axial internal force and bending moment, *N* and *M* can be expressed using Eqs. (3-12) and (3-13) respectively. The integrand term of $\varepsilon_{bending}$ and ε_{axial} to the area in the expression of *N* and *M* are cancelled based on the principle of odd function integration in a symmetric interval.

$$N = \int_A \sigma_l dA = \int_A E\varepsilon_l dA = E\int_A \left(\varepsilon_{axial} + \varepsilon_{bending}\right) dA = E\int_A \varepsilon_{axial} dA \tag{3-12}$$

$$M = \int_A \sigma_l z dA = \int_A E\varepsilon_l z dA = E\int_A \left(\varepsilon_{axial} + \varepsilon_{bending}\right) z dA = E\int_A \varepsilon_{bending} z dA \tag{3-13}$$

where *z* is the vertical coordinate of the concerned point in the pipe's cross-section as depicted in Figure 3-4; *A* is the cross-sectional area of the pipe; *E* is Young's modulus of the pipe steel.

Substituting the Eqs. (3-10) and (3-11) into Eqs. (3-12) and (3-13), the formulation of N and M can be rearranged as Eqs. (3-14) and (3-15) as functions of u and v.

$$N = E\int_A \varepsilon_{axial} dA = EA\left(u' + \frac{1}{2}v'^2\right) \tag{3-14}$$

$$M = E\int_A \varepsilon_{bending} z dA = EIv'' \tag{3-15}$$

where I is the area moment of inertia. Therefore, the governing equations Eq. (3-1) can be modified as Eq. (3-16) by plugging Eqs. (3-14) and (3-15) into the original version Eq. (3-1).

$$\begin{cases} EA\left(u'' + v'v''\right) + f(U_g - u) = 0 \\ EIv'''' - EA\left(u'' + v'v''\right)v' - EA\left(u' + \frac{1}{2}v'^2\right)v'' - q(V_g - v) = 0 \end{cases} \tag{3-16}$$

3.2.4 Representative of the pipe-soil interaction

This paper considers the soil as distributed nonlinear springs as recommended by ALA Guidelines [21]. As stated in ALA Guidelines, the soil spring property can be characterized as a bilinear curve of soil force on pipe against the displacement, which is plotted as the dashed lines in Figure 3-5, where T_u, P_u, Q_u, and Q_d represent the soil resistance in the axial, lateral, vertical upward (uplift) and vertical downward (bearing) directions, in N/m. Δt, Δp, Δq_u, and Δq_d are the corresponding displacements with the unit of m. The values for these parameters depend on the properties of the surrounding soil, pipe diameter, burial depth, and coating of the pipe.

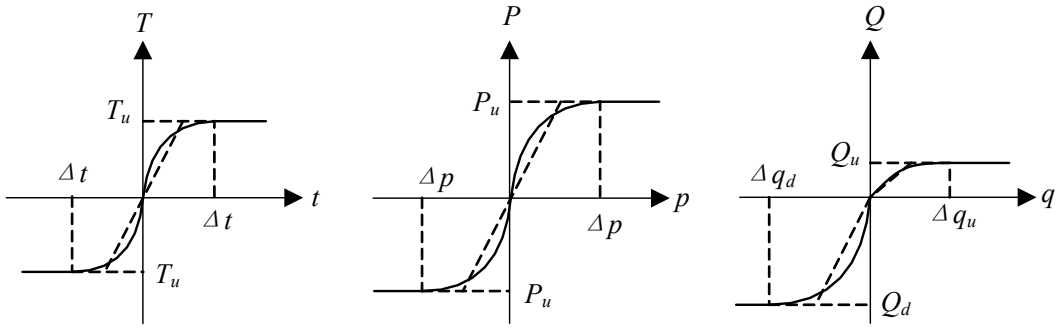

(a) Axial (b) Lateral (c) Vertical

Figure 3-5: Soil spring properties in each direction

The pipe-soil interaction is considered as the external force term in the governing equation Eq. (3-16). Consider the case that the middle segment of a pipe is subjected to a ground displacement of magnitudes U_g and V_g in the longitudinal and lateral directions respectively. The external distributed force $f(u)$ and $q(v)$ can be respectively represented by the soil spring properties in axial and lateral directions, which are shown as Eqs. (3-17) and (3-18) respectively.

$$f = \begin{cases} T_u & , \quad u < U_g - \Delta t \\ T_u / \Delta t \bullet & , \quad U_g - \Delta t \le u \le U_g + \Delta t \\ -T_u & , \quad u > U_g + \Delta t \end{cases} \tag{3-17}$$

$$q = \begin{cases} P_u & , \quad v < V_g - \Delta p \\ P_u / \Delta p \bullet & , \quad V_g - \Delta p \le v \le V_g + \Delta p \\ -P_u & , \quad v > V_g + \Delta p \end{cases} \tag{3-18}$$

For the middle section as depicted in Figure 3-1, the ground axial and lateral displacements induced by the geohazards are denoted by U_g and V_g respectively. As the external force acting on the pipe is a function of the relative displacement between the ground and the pipe, the governing equations in the middle section can be written as Eq. (3-19) where u and v respectively denote the pipe deformation in the axial and lateral directions. For the pipe segments connected to both ends of the middle pipe, and where the ground displacements are assumed to be equal to zero, the governing equations are represented by Eq. (3-20).

$$\begin{cases} EA\left(u'' + v'v''\right) + f(U_g - u) = 0 \\ EIv'''' - EA\left(u'' + v'v''\right)v' - EA\left(u' + \frac{1}{2}v'^2\right)v'' - q(V_g - v) = 0 \end{cases} \tag{3-19}$$

$$\begin{cases} EA\left(u'' + v'v''\right) - f(u) = 0 \\ EIv'''' - EA\left(u'' + v'v''\right)v' - EA\left(u' + \frac{1}{2}v'^2\right)v'' + q(v) = 0 \end{cases} \tag{3-20}$$

3.2.5 Implementation procedure of the proposed methodology

The implementation of the finite difference method is described using the following steps. An auxiliary picture corresponding to the pipe deformation in Figure 3-1 is offered for each step to facilitate the understanding for readers.

Step 1: pipeline mesh.

In this step, each segment of the pipeline is meshed with the node IDs shown in the figure below. Generally, those nodes are equally spaced along each segment. The numbers of nodes for each segment, denoted as L_l, L_m and L_r, are respectively n_l, n_m, and n_r including the boundary points, which are in blue (the subscripts l, m, and r respectively indicate the right, middle, and right pipe segments).

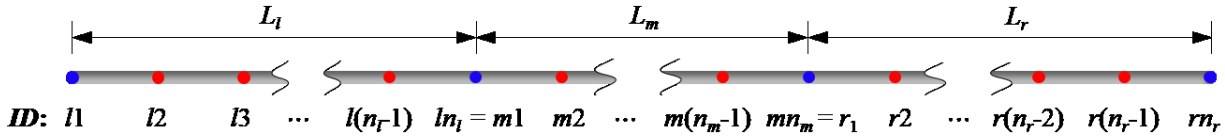

Step 2: derivatives calculation.

The unknown u_i and w_i, respectively denote axial and lateral deformations for the i^{th} node. u'_i, u''_i, v'_i, v''_i, v'''_i, and v''''_i at each node (as shown in the figure below) represent the derivatives of u_i and v_i, which can be evaluated based on the finite difference method explained in section 3.2.2. Note that the central finite difference is employed for the internal nodes. One-sided finite difference, either forward or backward finite difference depending on their respective location, is adopted for the boundary nodes. For example, the derivatives for left boundary node $l1$ of segment L_l should be represented based on forward finite differences. In contrast, the derivatives for the right boundary node ln_l of segment L_l should be calculated by backward finite differences.

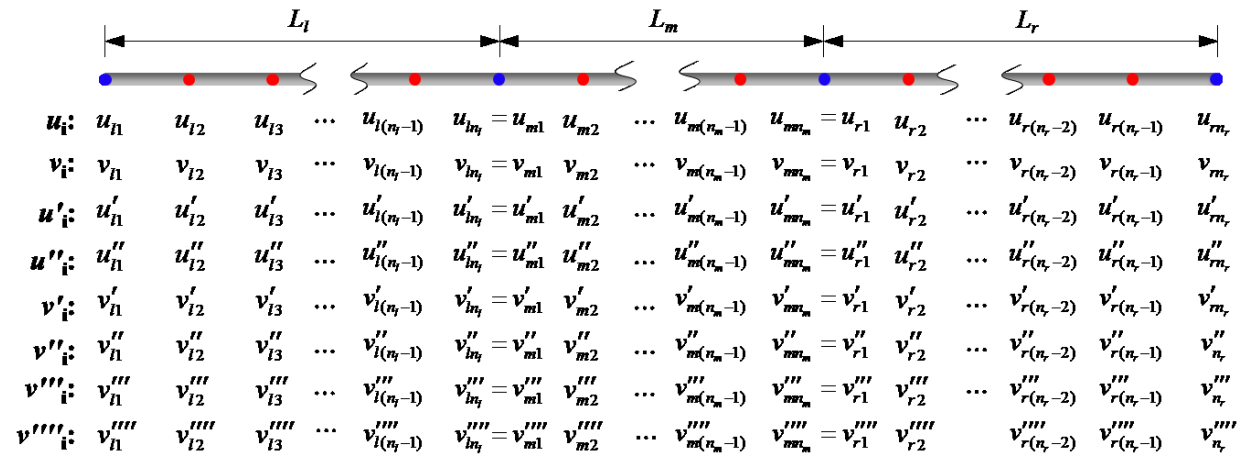

Step 3: governing equations in the finite-difference form.

Step 3 aims at constructing the governing equations at each internal node (the red node) based on Eq. (3-19) for segment L_m and Eq. (3-20) for segments L_l and L_r, where the derivative terms are evaluated by the finite differences defined in ***Step 2***. For instance, the governing equations at node $l3$ in segment L_l, denoted as Eq_{l3}, can be written as Eq. (3-21).

$$\begin{cases} EA\left(u''_{l3}+v'_{l3}v''_{l3}\right)-f(u_{l3})=0 \\ EIv''''_{l3}-EA\left(u''_{l3}+v'_{l3}v''_{l3}\right)v'_{l3}-EA\left(u'_{l3}+\dfrac{1}{2}v'^{2}_{l3}\right)v''_{l3}+q(v_{l3})=0 \end{cases} \tag{3-21}$$

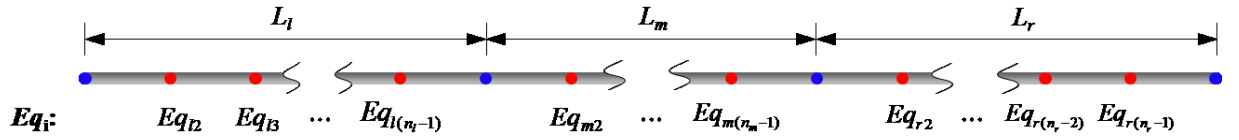

Step 4: boundary conditions in the finite-difference form.

For the boundary nodes (the blue nodes), boundary conditions are imposed in terms of the finite difference equations. Both ends of the pipeline are fixed, and the pipeline is continuous. For example, the fixed boundary conditions for node $l1$ can be expressed as Eq. (3-22). The continuity conditions for the nodes ln_l and m_1 which connects segment L_l and L_m can be defined as Eq. (3-23). Similarly, the boundary conditions in Eqs. (3-22) and (3-23) can be respectively applied to node ln_l and mn_m (r_1) due to symmetry.

$$\begin{cases} u_{l1} = 0 \\ v_{l1} = 0 \\ v'_{l1} = 0 \end{cases} \tag{3-22}$$

$$\begin{cases} u_{ln_l} = u_{m1} \\ u'_{ln_l} = u'_{m1} \\ v_{ln_l} = v_{m1} \\ v'_{ln_l} = v'_{m1} \\ v''_{ln_l} = v''_{m1} \\ v'''_{ln_l} = v'''_{m1} \end{cases} \tag{3-23}$$

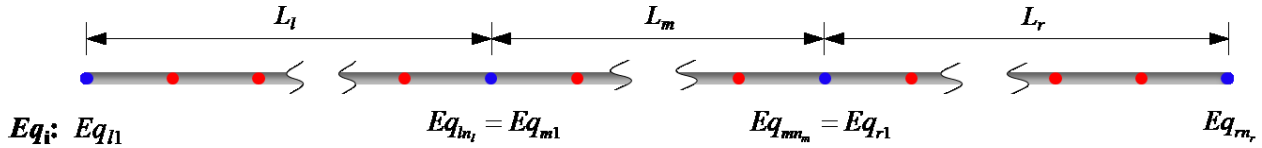

Step 5: solving nonlinear finite difference equations.

Gathering the functions established in ***Step 3*** and ***Step 4***, a set of simultaneous nonlinear finite difference equations can be built with the unknowns being the axial deformation u_i and lateral deformation v_i for each node, as illustrated in the figure below. Using a nonlinear solver, the unknown u_i and v_i can be found. Note that no specialized nonlinear solver is required, e.g., FindRoot in Mathematica, root or fslove in the optimize library of Python, fsolve or lsqnonlin in Matlab can all be used. For these nonlinear solvers, the initial guess of the unknown u_i and v_i should be provided as required.

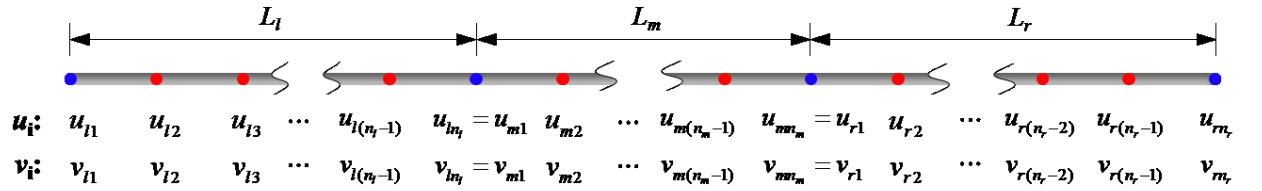

$$\{Eq_i\} = \begin{Bmatrix} Eq_{l1}, Eq_{l2}, \cdots, Eq_{l(n_l-1)}, Eq_{ln_l}, \\ Eq_{m1}, Eq_{m2}, \cdots, Eq_{m(n_m-1)}, Eq_{mn_m}, \\ Eq_{r1}, Eq_{r2}, \cdots, Eq_{r(n_r-1)}, Eq_{rn_r} \end{Bmatrix} \Leftrightarrow f \begin{pmatrix} u_{l1}, u_{l2}, \cdots, u_{lu_l}, v_{l1}, v_{l2}, \cdots, v_{lu_l}, \\ u_{m1}, u_{m2}, \cdots, u_{mu_m}, v_{m1}, v_{m2}, \cdots, v_{mu_m}, \\ u_{r1}, u_{r2}, \cdots, u_{ru_r}, v_{r1}, v_{r2}, \cdots, v_{ru_r} \end{pmatrix} = 0$$

Step 6: strain demand calculation.

Step 6 calculates the longitudinal strains at the pipe top and bottom at each node based on Eq. (3-9). The tensile strain demand and compressive strain demand are respectively defined as the maximum value (a positive value) and minimum value (a negative value) of the obtained longitudinal strains along the pipe.

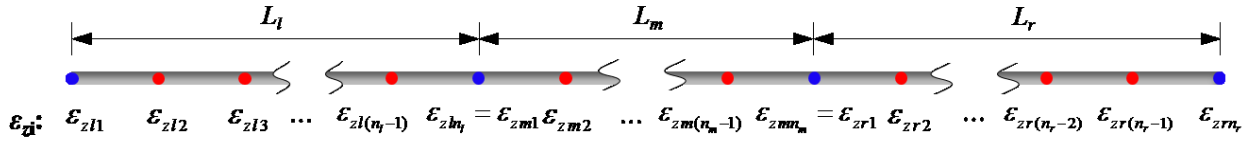

Based on the above-elaborate procedure, the proposed methodology can be carried out based on any kind of programming language. In this study, the authors use Mathematica for the study cases in the section 3.3.

3.3 Validation of the proposed methodology against finite element solutions

The proposed methodology is validated comparing with results obtained using the finite element model described in section 3.3.1 based on two hypothetical study cases. One case with horizontal ground movements and the pipe subjected to symmetric pipe-soil interaction, which can be representative of geohazards like landslides in flat terrains and liquefaction-induced lateral spreading. The other investigates the applicability in vertical ground displacements and hence the non-symmetric soil loading applied on the pipe, which represents the circumstances like frost heave and ground subsidence. Due to the preliminary assumption of linear pipe material, the elastic responses arising from the present methodology (implemented based on Mathematica) and Abaqus are compared to validate the accuracy of the approach.

3.3.1 Description of the beam-type finite element model

The finite element solutions are utilized to validate our proposed methodology. The beam-type finite element model, also referred to as “pipe element”, is a special-purpose beam element which has been widely utilized in the practice of preliminary design or pre-screening of pipes against geohazards. In the validation example, the pipe is simulated by PIPE32 elements (3-node

quadratic pipe in space). The interaction between the pipe and the surrounding soil is modelled using soil springs which are attached to the nodes of the pipe in three principal directions (see Figure 3-6). The PSI36 elements (3-dimensional 6-node pipe-soil interaction element) are employed to represent the action exerted by the ground to the pipe. As required in Abaqus, the nonlinear soil spring follows a bilinear law representing the load-deformation behavior of the pipe-soil interaction, which was described in section 3.2.4. The pipe is meshed to have the same number of nodes as the counterpart implemented in the proposed methodology.

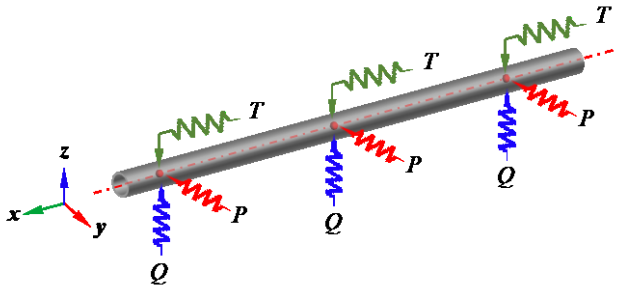

Figure 3-6: Pipe finite elements and attached soil springs in three principal directions

3.3.2 Case study

This paper considers two study cases to illustrate and verify the proposed methodology. Case 1 deals with an elastic pipeline crossing the ground movement, which happens in the horizontal plane (*x*-*y* plane) where the soil resistance is symmetric. Case 2 considers an elastic pipeline withstanding the ground heave occurring in the vertical plane (*x*-*z* plane) where the soil resistance is non-symmetric, i.e., resistances connected to the pipe top and pipe bottom are not equal. The prospective deformations of the pipe in case 1 and case 2 are depicted in Figure 3-7.

The study cases tackle a 457-mm-diameter pipe with a wall thickness of 7.92 mm. Young's modulus for the pipe material is taken as 199 GPa. Assuming the distance from the ground surface to the pipe centerline is 1.8 m, the pipe is backfilled with cohesionless sand having an internal friction angle of 34° and unit weight 1760 kg/m^3. The axial friction factor is set as 0.6 [21]. Hence,

the required parameters of the soil springs can then be estimated based on the recommendations in ALA Guidelines [21] as listed in Table 3-1.

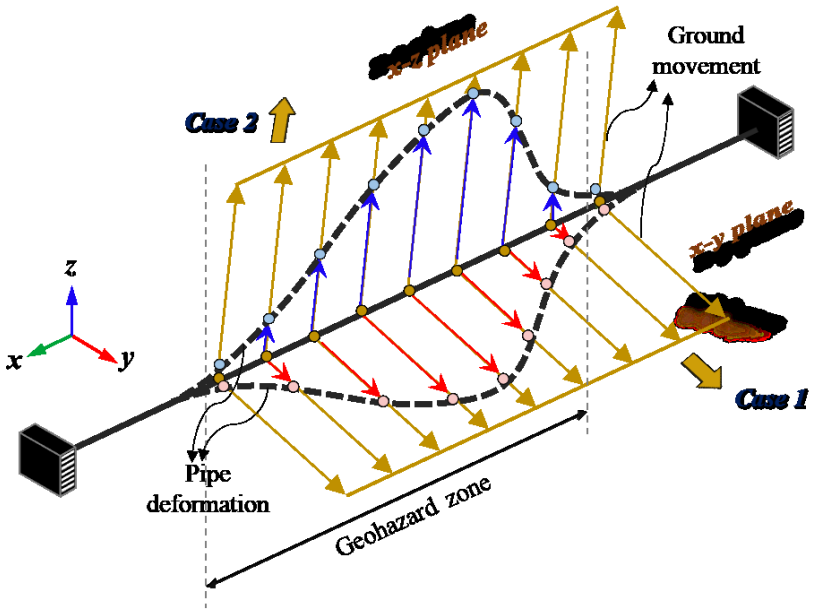

Figure 3-7: Schematic representation of pipe's deformation in case 1 and case 2

Table 3-1: Soil spring parameters for case 1 and case 2

Variable	**Case 1**	**Case 2**
Coefficient of pressure at rest, K_0	0.44	0.44
Axial soil spring resistance T_u (kN/m)	13	13
T_u yield displacement Δt (mm)	5	5
Horizontal bearing capacity factor, N_{qh}	12.5	12.5
Lateral soil spring resistance P_u (kN/m)	200	-
P_u yield displacement Δp (mm)	69	-
Vertical uplift factor, N_{qv}	3.4	3.4
Uplift soil spring resistance Q_u (kN/m)	-	55
Q_u yield displacement Δq_u (mm)	-	30
Bearing capacity factor, N_c	42.2	42.2

Bearing capacity factor, N_q	29.4	29.4
Bearing capacity factor, N_γ	37.3	37.3
Bearing soil spring resistance Q_d (kN/m)	-	538
Q_d yield displacement Δq_d (mm)	-	46

The middle span, representing the segment involved in the ground movements, is assumed as L_m = 10 m. The pipe span in the non-geohazard region is set as $L_l = L_r$ = 100 m, which is long enough to eliminate the fixed boundary effect as verified using initial calculations with different L_l and L_r lengths. In case 1, the middle segment bears the load from the ground happening in the horizontal plane (*x*-*y* plane). As for case 2, segment L_m is subjected to the vertical ground heave. The middle pipe segment is evenly meshed by 41 nodes, and the two end segments are meshed with 101 nodes for each (the boundary nodes are counted in). Considering the different combinations of ground displacements d (up to 3 m) and ground-pipe intersection angle β (the angle between the direction of ground movement and pipe axis, considered as 30°, 60°, and 90°), a parametric comparison is conducted to examine the validity of this methodology in the case of symmetric soil resistance (case 1) and non-symmetric soil resistance (case 2).

Figure 3-8 presents the investigated pipe's strain demand in tension and compression arising from the proposed method (referred to as PM) and finite element method (referred to as FEM) at different ground-pipe intersection angles, 30°, 60° and 90°, for case 1 and case 2. Note that large movement is considered here for the hypothetical case studies to show the applicability of the proposed method to problems with large ground movement or deformations. For the sake of simplicity, the soil forces and deformations in the horizontal plane (*x*-*y* plane) in case 1 and in the vertical plane (*x*-*z* plane) in case 2 are generally referred to as lateral soil forces and lateral deformation. The comparison shows a very good agreement between the proposed methodology and the finite element method, which indicates that the proposed methodology has a great predictive capability to simulate the pipes' response to different ground movements under the symmetric soil resistance conditions and non-symmetric soil resistance situations. As for case 1, the strain demand linearly increases with the ground displacement to its extreme value, e.g., 0.91% for the tensile strain demand and -0.75% for the compressive strain demand due to the yielding of

soil springs. In addition, compared with the results obtained based on smaller intersection angles, the strain demand (before the yielding of soil springs) is greater with larger intersection angles where the component of ground movements in the lateral direction increases, which indicates that the lateral soil springs have a more pronounced effect on the pipe's response. Case 2 adopts different soil forces. In the concerned range of ground displacement, the extreme value of strain demand is not reached. Comparing the strain demand in a small ground movement (before the yielding of soil springs in case 1), the strain demand in case 2 is slightly smaller than that in case 1, which demonstrated that the uplift soil springs acting on the non-geohazard pipe sections don't give enough constraint as the lateral soil springs in case 1.

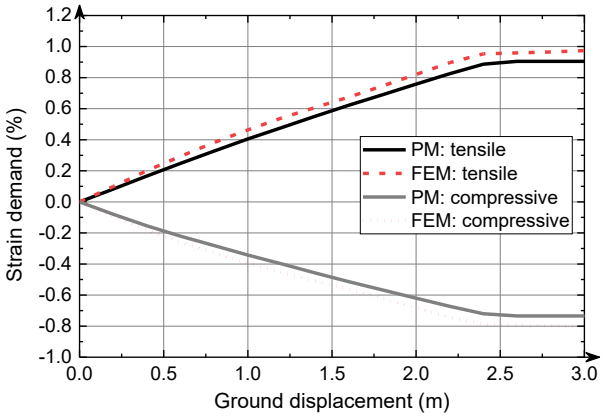

(a) Case 1: β=30°

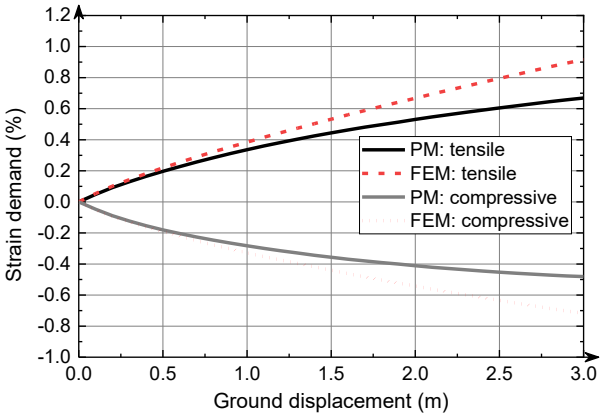

(b) Case 2: β=30°

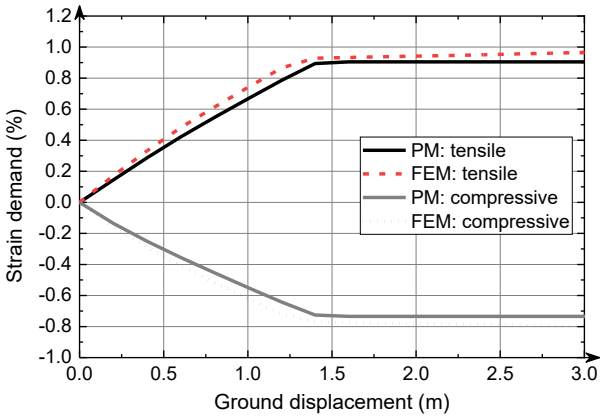

(c) Case 1: β=60°

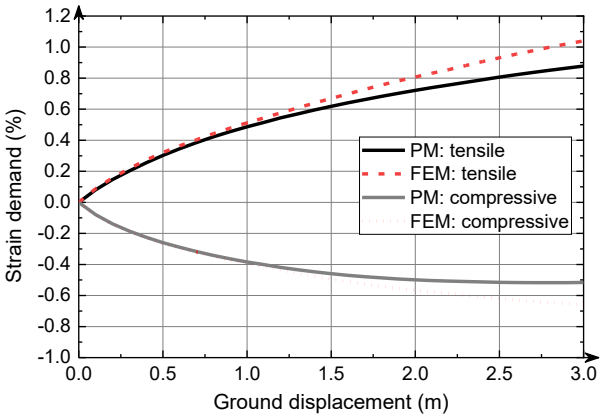

(d) Case 2: β=60°

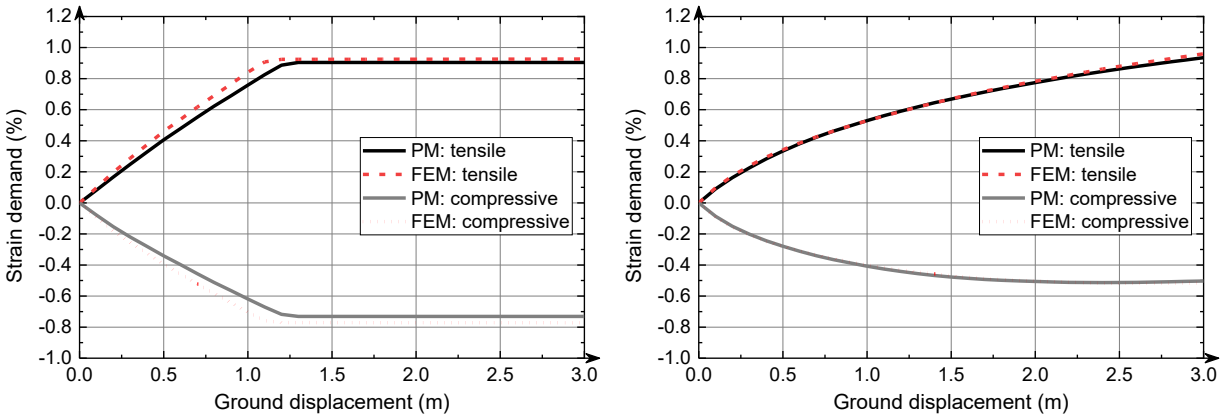

(e) Case 1: β=90° (f) Case 2: β=90°

Figure 3-8: Comparison on strain demand between proposed methodology and FEM results for case 1 and case 2

The pipe's deformations calculated using the proposed method, including the axial displacement u and lateral deflection v at the ground movement of 1.0 m for both cases, are compared with those results obtained with the finite element method, see Figure 3-9 and Figure 3-10. The location of tensile and compressive strain demands is respectively indicated by red and blue points, which aim to display the critical spots corresponding to the locations of the highest derivatives of the displacements. They are found to occur around the same location using the proposed method and finite element method. The predicted deformations of the pipe compare exceptionally well with the results from the finite element model. As observed, the extreme axial deformations happen around the boundary of the geohazard-involved segment, e.g., near the ends of segment L_m. On the contrary, the maximum lateral displacements occur at the middle location of segment L_m. In addition, the lateral deformations grow with the increase of the intersection angle, which demonstrates the observation that higher intersection angles lead to greater strain demands.

The axial deformations in case 1 and case 2 are almost the same, and they are negligibly small as the force from axial soil springs is weak. While the lateral deformations in case 2 are higher than those in case 1. The discrepancy is induced by the different soil spring scenarios used in case 1 and case 2. In case 2, the bearing soil springs on the middle segment L_m are much stiffer than the uplift soil springs in segments L_l and L_r, which indicates a lesser constraint on segment L_l

and L_r thus the effect from soil springs on segment L_m is more pronounced (a greater lateral deformation in case 2).

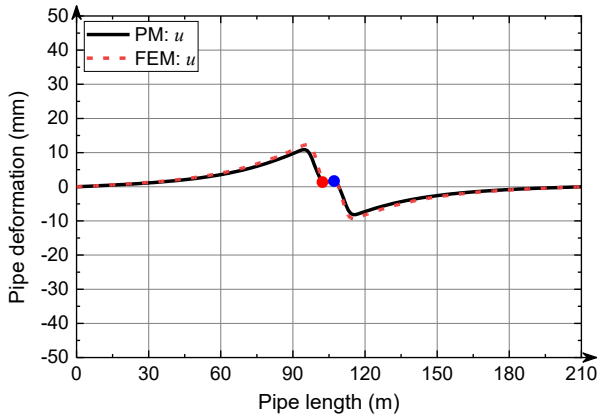

(a) Case 1: β=30°

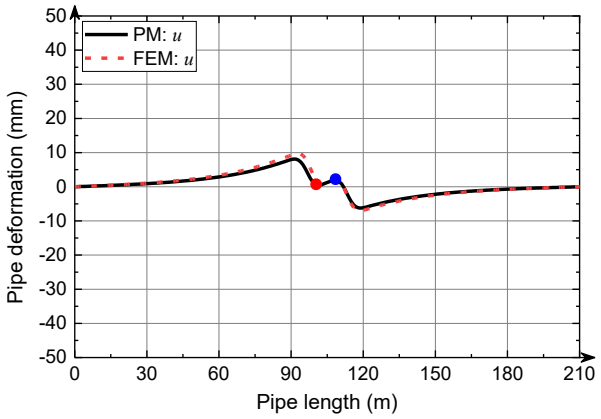

(b) Case 2: β=30°

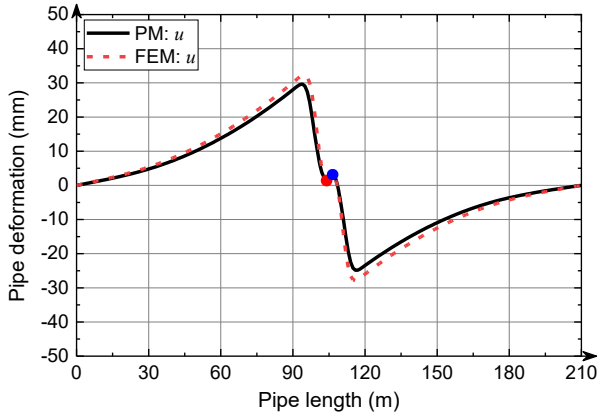

(c) Case 1: β=60°

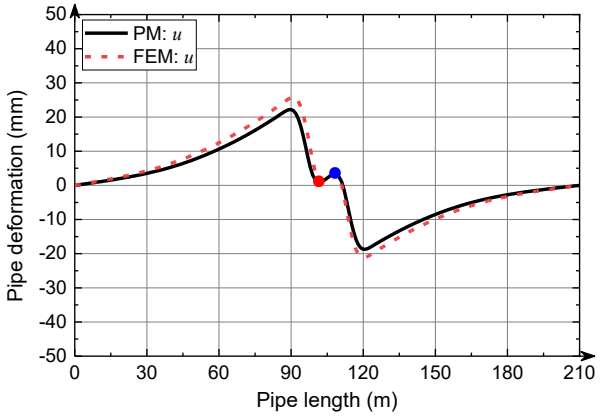

(d) Case 2: β=60°

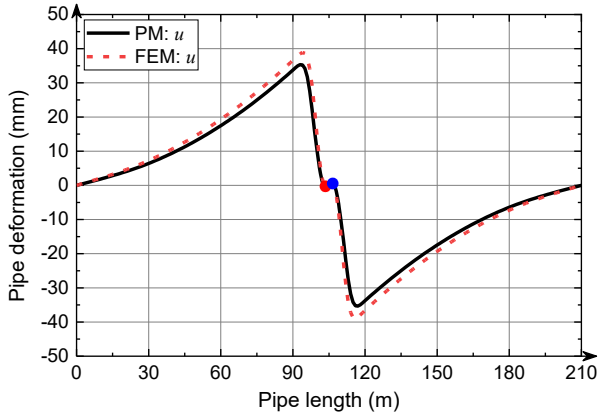

(e) Case 1: β=90°

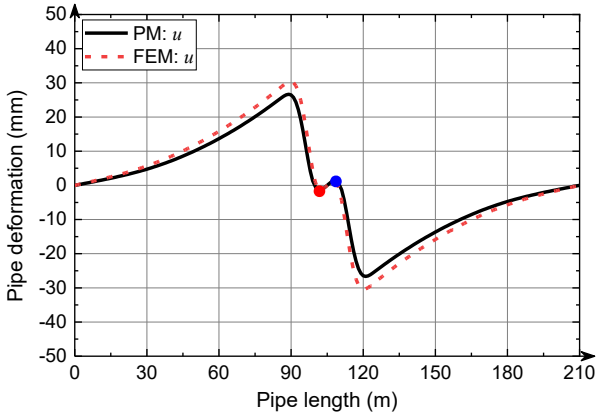

(f) Case 2: β=90°

Figure 3-9: Comparison on axial deformation of the pipe between the proposed methodology and FEM results for case 1 and case 2 (ground movement is 1.0 m)

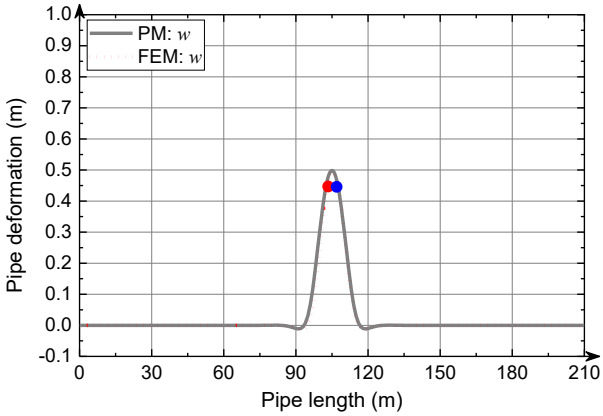

(a) Case 1: β=30°

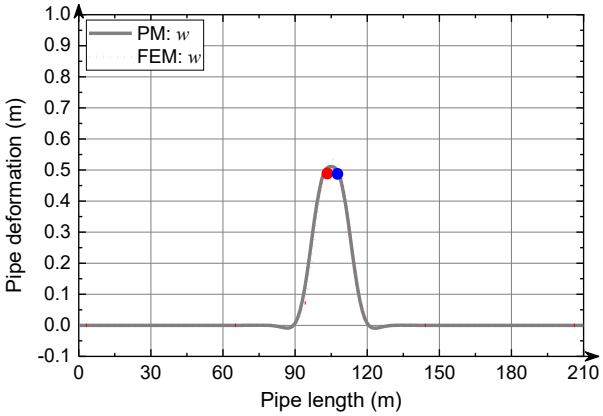

(b) Case 2: β=30°

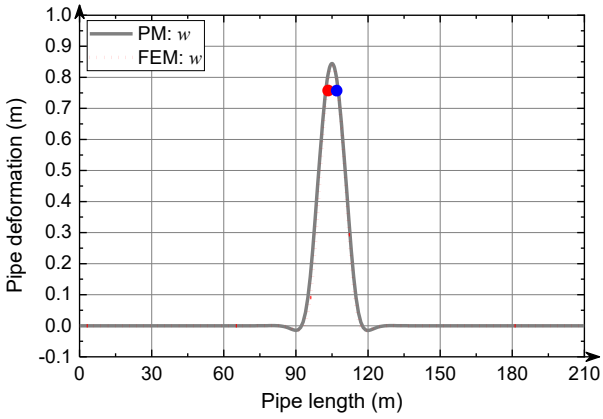

(c) Case 1: β=60°

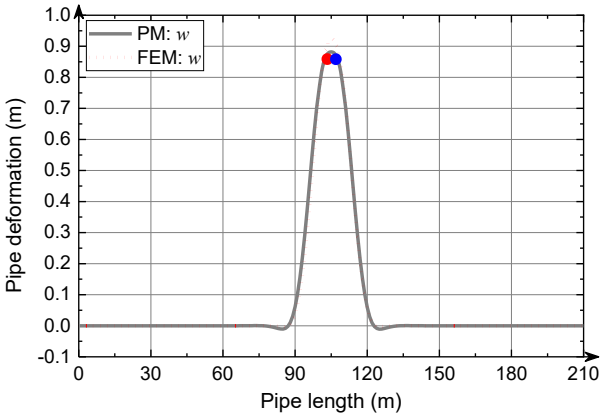

(d) Case 2: β=60°

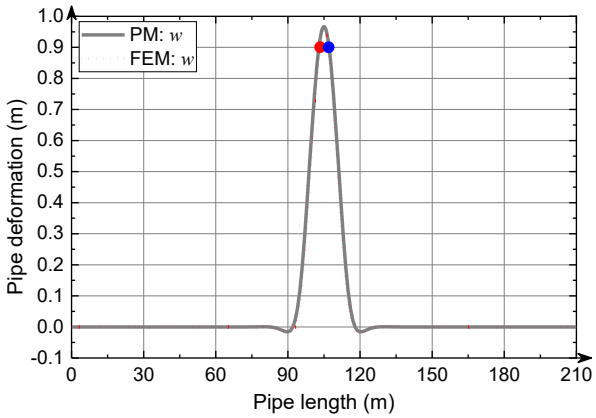

(e) Case 1: β=90°

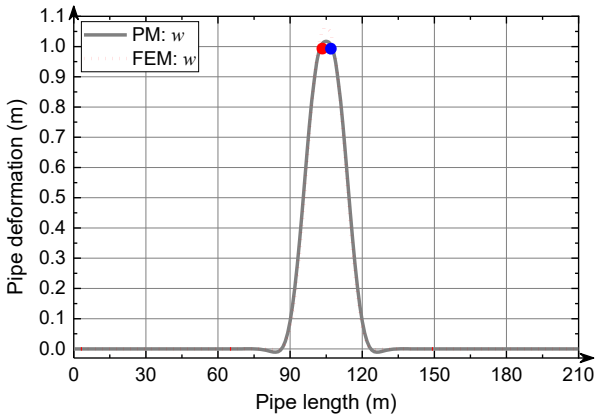

(f) Case 2: β=90°

Figure 3-10: Comparison on lateral deformation of the pipe between the proposed methodology and FEM results for case 1 and case 2 (ground movement is 1.0 m)

Based on the results of the above two study cases, the accuracy of the proposed methodology is demonstrated, which is quite excellent for this preliminary study on the application of the finite difference method to the response analysis of pipes subjected to large displacement-based ground loads. Moreover, this study lays a promising foundation for a future study involving the pipe elastic-plastic material nonlinearity.

3.4 Chapter conclusions

A new methodology is developed for predicting the pipe's response to the ground movement triggered by geohazards based on the finite difference method. To do this, the pipeline is considered as an Euler-Bernoulli beam with large deformations, and the governing differential equations of the elastic response of the pipe are formulated as functions of the deformation variables u and v at each node. The loading, represented within the pipe-soil interaction, is considered as soil springs with a bilinear load-displacement property. A large set of nonlinear finite difference equations can be therefore established together with boundary conditions and the solution can be achieved based on the nonlinear equation solver in the programming language that the reader prefers. Here, we use the nonlinear equation solver of FindRoot in Mathematica.

Subsequently, the strain at each node can be derived and the tensile and compressive strain demands can be obtained. Finally, two study cases that the pipe is subjected to symmetric and non-symmetric lateral soil stiffness respectively are introduced to test the workability of the present methodology. Our work shows that the proposed methodology is of great accuracy compared with the finite element method using Abaqus. The present work contributes a new methodology in this research field. However, further development involving material nonlinearity is required to enrich the existing prediction models for engineering practice.

Reference

[1] N.M. Newmark, W.J. Hall, Pipeline design to resist large fault displacement, in: Proceedings of US national conference on earthquake engineering, Michigan, 1975, pp. 416-425.

[2] R.P. Kennedy, R.A. Williamson, A.M. Chow, Fault movement effects on buried oil pipeline, J. Transp. Eng. Part A Syst. 103.5 (1977) 617-633.

[3] L.R.L Wang, Y.H. Yeh, A refined seismic analysis and design of buried pipeline for fault movement, Earthq. Eng. Struct. Dyn. 13.1 (1985) 75-96.

[4] S. Takada, N. Hassani, K. Fukuda, A new proposal for simplified design of buried steel pipes crossing active faults, Earthq. Eng. Struct. Dyn. 30.8 (2001) 1243-1257.

[5] D.K. Karamitros, G.D. Bouckovalas, G.P. Kouretzis, Stress analysis of buried steel pipelines at strike-slip fault crossings, Soil. Dyn. Earthq. Eng. 27.3 (2007) 200-211.

[6] O.V. Trifonov, V.P. Cherniy, A semi-analytical approach to a nonlinear stress–strain analysis of buried steel pipelines crossing active faults, Soil. Dyn. Earthq. Eng. 30.11 (2010) 1298-1308.

[7] O.V. Trifonov, V.P. Cherniy, Elastoplastic stress–strain analysis of buried steel pipelines subjected to fault displacements with account for service loads, Soil. Dyn. Earthq. Eng. 33 (2012) 54-62.

[8] N. Yoosef-Ghodsi, J. Zhou, D.W. Murray, A simplified model for evaluating strain demand in a pipeline subjected to longitudinal ground movement, in: International Pipeline Conference (IPC2008), American Society of Mechanical Engineers (ASME), Calgary, 2008, pp. 657-64

[9] G.C. Sarvanis, S.A. Karamanos, Analytical model for the strain analysis of continuous buried pipelines in geohazard areas, Eng. Struct. 152 (2017) 57-69.

[10] P. Vazouras, P. Dakoulas, S.A. Karamanos, Pipe–soil interaction and pipeline performance under strike–slip fault movements, Soil. Dyn. Earthq. Eng. 72 (2015) 48-65.

[11] X. Liu, H. Zhang, M. Xia, J. Liu, Q. Zheng, An improved analytical strain analysis method for buried steel pipelines subjected to abrupt permanent ground displacement, in: International Pipeline Conference (IPC2020), American Society of Mechanical Engineers (ASME), Calgary, 2020, pp. V002T06A012.

[12] W. Zheng, H. Zhang, X. Liu, J. Chen, Comparative study on the FEM models of buried pipeline under fault movement, China Pet. Mach. 43.12 (2015) 109-113.

[13] X. Liu, H. Zhang, Y. Han, M. Xia, W. Zheng, A semi-empirical model for peak strain prediction of buried X80 steel pipelines under compression and bending at strike-slip fault crossings, J. Nat. Gas Eng. 32 (2016) 465-475.

[14] X. Liu, S.P. Sun, Strain based design of buried pipelines crossing faults, Spec. Struct. 22.2 (2005) 81-85.

[15] X. Gu, H. Zhang, Research on aseismatic measures of gas pipeline crossing a fault for strain-based design, in: ASME Pressure Vessels and Piping Conference (PVP2009), American Society of Mechanical Engineers (ASME), New York, 2009, pp. 571-580.

[16] A. Liu, Y. Hu, F. Zhao, X. Li, S. Takada, L. Zhao, An equivalent-boundary method for the shell analysis of buried pipelines under fault movement, Acta. Seismol. Sin. 17.1 (2004) 150-156.

[17] A. Liu, S. Takada, Y. Hu, A shell model with an equivalent boundary for buried pipelines under the fault movement, in: 13th World Conference on Earthquake Engineering, Vancouver, 2004.

[18] X. Liu, H. Zhang, M. Li, M. Xia, W. Zheng, K. Wu, Y. Han, Effects of steel properties on the local buckling response of high strength pipelines subjected to reverse faulting, J. Nat. Gas Eng. 33 (2016) 378-387.

[19] G.C. Sarvanis, S.A. Karamanos, P. Vazouras, E. Mecozzi, A. Lucci, P. Dakoulas, Permanent earthquake‐induced actions in buried pipelines: Numerical modeling and experimental verification, Earthq. Eng. Struct. Dyn., 47.4 (2018) 966-987.

[20] P. Vazouras, S.A. Karamanos, P. Dakoulas, Finite element analysis of buried steel pipelines under strike-slip fault displacements, Soil Dyn. Earthq. Eng. 30.11 (2010) 1361-1376.

[21] American Lifelines Alliance (ALA), Guidelines for the Design of Buried Steel Pipe, American Society of Civil Engineers, 2001

[22] M. O'Rourke, V. Gadicherla, T. Abdoun, Centrifuge modeling of PGD response of buried pipe, Earthq. Eng. Eng. Vib. 4.1 (2005) 69-73.

[23] D. Ha, T. Abdoun, M. O'Rourke, Buried high-density polyethylene pipelines subjected to normal and strike-slip faulting-a centrifuge investigation, Can. Geotech. J. 45.12 (2008) 1733-1742.

[24] G. Demofonti, J. Ferino, S.A. Karamanos, P. Vazouras, P. Dakoulas, An integrated experimental-numerical approach to predict strain demand for buried steel pipelines in geo-hazardous areas, in: Rio Pipeline Conference and Exposition, 2013, IBP1441_13.

[25] W. Feng, R. Huang, J. Liu, X. Xu, M. Luo, Large-scale field trial to explore landslide and pipeline interaction, Soils and Found. 55.6 (2015) 1466-1473.

[26] Dassault Systems Simulia Corporation, Abaqus, 2017.

[27] A. Ghali, A.M. Neville, T.G. Brown, Structural Analysis: A unified classical and matrix approach, sixth ed., Spon Press, London and New York, 2009.

CHAPTER 4: A FINITE DIFFERENCE-BASED APPROACH FOR STRAIN DEMAND PREDICTION OF INELASTIC PIPES SUBJECTED TO PERMANENT GROUND DISPLACEMENTS

This chapter is derived from the published paper:

Q. Zheng, Y. Li, N. Yoosef-Ghodsi, M. Fowler, M. Kainat, S. Adeeb, 2022. A finite difference-based approach for strain demand prediction of inelastic pipes subjected to permanent ground displacements, Eng. Struct. 273, 115072.

Abstract

Permanent ground displacement triggered by geohazards constitutes a major threat to the integrity of long-distance pipelines. In this study, a novel and simple method is proposed to evaluate inelastic pipes' behavior under ground movements considering soil-pipe interaction based on the finite difference method. The existing finite difference-based method previously proposed by the authors for strain analysis of buried pipelines subjected to ground movements excludes material nonlinearity in pipes, which limits its applicability in engineering practice. To remedy this situation, the method presented herein maintains the well-established concepts of the existing finite-difference-based method but also introduces the scheme to consider the inelastic material behavior of steel pipes. More specifically, the expressions of internal axial force and bending moment, required in the finite difference equations, are explicitly derived based on the actual stress distribution on the pipe cross-section. The proposed method is validated against the finite element method (one-dimensional beam model) in terms of the strain and deformation demands using two indicative case studies, referred to as symmetric and non-symmetric soil resistance conditions, respectively. The comparison between finite element analysis and the proposed method indicates

good agreement. Additionally, the proposed method is compared with four existing analytical methods for pipes subjected to strike-slip fault displacement. The proposed method is a simple but general technique to analyze pipes' response under a wide range of geohazards, and thus can be potentially used as an alternative method for preliminary design, safety pre-screening, and reliability-based assessment of pipes against geohazards.

Keywords: strain demand; inelastic pipe; soil-pipe interaction; permanent ground displacement; finite difference method

4.1 Introduction

As an essential component of energy infrastructure, pipelines serve to transport oil and gas from production areas to target consumers. Onshore pipelines are generally constructed over considerably long distances. In many instances, pipe segments are inevitably installed through geotechnically unstable environment, which is typically associated with unfavorable geological actions such as landslides, discontinuous permafrost (frost heave and thaw settlement), slope failures, ground subsidence, tectonic shifting, etc. Such activities can cause significant deformation-induced strains in pipes, which in turn result in local buckling and rupture of the pipe wall [1][2]. Field observations have highlighted the deleterious effects that soil movements have on the structural integrity of buried pipelines [3]. Thus, it is imperative to study response prediction of pipes subjected to geohazard-induced ground movements.

Research on pipes' behavior in response to ground movements can date back to the 1960s and 1970s when underground infrastructures were damaged by earthquakes, e.g., the Tokachi-Oki earthquake (Japan, 1968), the San Fernando earthquake (the USA, 1971), and the Managua earthquake (Nicaragua, 1972). Subsequently, analytical and finite element methods have been mainly developed to calculate pipes' response to ground movements. In recent years, physical experimental studies, including small- and full-scale tests [4][5][6][7], have been conducted to validate the applicability of analytical procedures and finite element models, which also reveals the growing attention to buried pipelines subjected to geohazard-induced ground movements.

However, experimental tests are time-consuming and budget-demanding. Simple and efficient analysis techniques for pipe response prediction remains highly demanded for research and engineering practice.

Newmark and Hall [8] pioneered the study of pipelines subjected to ground movements by introducing an analytical method to solve pipes' response to a tectonic fault based on the small deflection assumption. Kennedy et al. [9] extended that analytical method considering large deflection of pipes, which were assumed to have a single constant curvature near the fault plane. In the two methods mentioned above, however, only the axial tensile force in the pipe at the inflection point was considered, i.e., without accounting for the flexural behavior. Based on the model proposed by Kennedy et al [9], Wang and Yeh [10][11] further examined pipes' performance considering pipes' bending rigidity, the shear force at the inflection point, and the boundary condition of a semi-infinite beam on an elastic foundation, which yielded more rational results. After the refinements in Kennedy et al. [9] and Wang and Yeh [10][11], Karamitros et al. [12] improved the analytical method further by appropriately considering the effect of axial tension on the pipeline bending stiffness. This method was later extended to normal fault crossings [13]. Additionally, following the work done by Wang and Yeh [10][11] and Karamitros et al. [12], Trifonov and Cherniy [14] took into account the effect of internal pressure and temperature variation within the elastoplastic model using the plastic flow rule, and the method was subsequently extended to involve different soil conditions along the pipeline [15]. In light of the limitation in the abovementioned studies that axial force was not properly considered, Talebi and Kiyono [16][17] improved the analytical solution by incorporating the axial pipe-soil interaction and axial forces owing to geometrical nonlinearity into the governing differential equation; however, this method can only be applicable for elastic pipes. Furthermore, Sarvanis and Karamanos [18] presented a closed-form analytical formulation according to the assumed-shape of deformed pipes. Nevertheless, the formulation didn't provide a clear explanation of the characterization of plastic material behavior; plus, the formulation can only be employed for geohazards including one ground discontinuity. More recently, based on the assumption of partitioning the pipeline into four segments in [10][11], Hu et al. [19] divided the largely-deformed pipe section (near the fault trace) into a finite number of segments and applied equilibrium

equations to each segment to estimate the internal force and moment on the cross-section; the required moment-strain relationship in the iterative calculation process was derived on the specific pipe case and material property.

The majority of existing analytical approaches, as discussed above, were established regarding tectonic faults where only one ground discontinuity was considered. For some geotechnical hazards, such as landslides, liquefaction-induced lateral spreading, ground settlement, and heave due to seasonal temperature change in permafrost zones, the length of geohazard zone significantly affects the pipeline behavior [20]. As such, it is necessary to analyze the pipeline bearing two ground discontinuities, as shown in Yoosef-Ghodsi et al. [21] and Zahid et al. [22], whereas ground displacement was only considered in the longitudinal direction. Note that the method in [22] had treated well pipe self-weight and service loads, elastoplastic behavior of pipes was not properly described like [21] where the plastic flow rule was adopted to account for the portion after the onset of yielding. Acknowledging the fact that existing analytical approaches for buried pipeline response to tectonic faults (one ground discontinuity) appear adequate, researchers should devote more efforts to the study of pipeline response subjected to landslide-like geohazards (two ground discontinuities).

In contrast to analytical methods, which are usually associated with various assumptions and the restriction on the geohazard condition, numerical modeling allows explicit consideration of nonlinearity in the problem. With several commercial software packages available, analysis of pipes subjected to ground movements currently relies heavily on numerical approaches (e.g., finite element simulation). A review of finite element models in the literature indicates that various models have been developed with different considerations of elements used for pipe modeling, interaction between the pipe and surrounding soils, and the boundary conditions per different purposes. The accuracy of finite element models is typically calibrated with available experimental data. Modeling the pipe body completely using shell elements for its entire length requires considerable computational resources and time. To mitigate the issue, Takada et al. [23] utilized beam elements to simulate pipe segments far away from the fault trace, namely beam-shell hybrid model. The beam-shell hybrid approach was used by Hu et al. [24] where the backfill was represented by soil spring elements, and analytically-derived nonlinear pipe-soil interaction

springs were added to model the boundary conditions representing the pipe further away from the fault trace, which shortened the length of pipe explicitly modeled without sacrificing the accuracy. Regarding soil modeling, Trifonov [25] represented the surrounding soil, including the trench backfill and native soil, by solid elements with appropriate constitutive models. The developed finite element models were commonly used for parametric analysis to offer suggestions for alleviating damage on pipes, or for data generation to develop empirical or surrogate models. For example, Liu et al. [26][27][28] developed a regression equation and an artificial neural network to estimate the strain demand of pipes under fault displacements based on data generated from finite element simulations.

Endeavors towards these two classical approaches, i.e., analytical and finite element, have greatly contributed to the response analysis of pipes subjected to displacement-controlled loads in engineering practice. Specifically, the analytical methods proposed by Newmark and Hall [8] and Kennedy et al. [9] have been incorporated into guidelines for seismic design of oil and gas pipelines for the sake of their simplicity [29][30]. But both methods use the stress in the extreme fiber of pipe cross-sections for the axial force approximation, and the actual stress distribution on the pipe cross-section is ignored where the inelasticity of the pipe material is not considered properly. To account for the pipe material inelasticity, most refined analytical models [10][11][12][13] approximated the bending moment using a secant modulus, that is, the slope corresponding to the inelastic stress to the original point. Although substantial refinements have been made to attain higher prediction accuracy, applicability of those analytical methods is still limited. Finite element-based numerical simulations are much handier and more robust to find accurate solutions regardless of pipe behavior (i.e., elastic or inelastic). Nevertheless, they require familiarity with model development specific to commercial software and considerable computational resources. Moreover, high dependency on commercial software packages makes them less flexible, which can cause great inconvenience to extended studies, such as Monte Carlo simulation in reliability-based assessment where a large number of simulations is required.

For common practice, it is desirable to use straightforward methods allowing reasonably accurate predictions of pipeline response. As such, this study presents a new approach using the finite difference method to analyze the strain demands of pipelines subjected to ground

movements. Some pilot studies, i.e., Al-Khafaji and Jacobs [31] and Zheng et al. [32], reported the feasibility of the finite difference method to solve the deformation of the beams/pipes under arbitrary force loadings or ground-induced displacement loadings assuming the elastic behavior of the pipe. However, under large ground movements, buried steel pipes can experience material nonlinearity. The assumption of elastic material in pipes causes a major limitation for their use in engineering practice. It is worth noting that considering material nonlinearity in pipes is non-trivial in the finite difference-based approach due to the interaction or coupling between the axial and bending behavior. Specifically, in Zheng et al. [32], the governing equation accounting for the elastic range can be explicitly derived in a finite-difference format, which is not true when concerning the material nonlinearity.

To this end, this study extends the method developed by Zheng et al. [32] to take into account the material nonlinearity in pipes. Based on the bilinear stress-strain relationship assumed for steel material, the axial force and bending moment are derived respectively for straight segments (without flexure deformation) and curved segments (with flexure deformation). The obtained axial force and bending moment, as functions of the unknowns of the axial and lateral deformations, are incorporated into the governing equations of pipelines subjected to soil movements. The strain demands and pipe displacements derived from the proposed method are compared with the results of simplified finite element models based on two hypothetical study cases, referred to as symmetric and non-symmetric soil force conditions, respectively. Additionally, the proposed method is compared with four existing analytical methods for another case study of pipelines subjected to strike-slip fault displacements.

4.2 Development of the proposed method

The method proposed in this paper aims to solve the pipe response under ground movements in a horizontal or vertical plane as illustrated in Figure 4-1. Examples of such engineering problems are a buried pipeline subjected to a geohazard in which the soil moves either in the horizontal plane due to landslides (see Figure 4-1 (a)) or strike-slip seismic fault (see Figure 4-1 (c-1)), or in the vertical plane due to the uplifting force triggered by the frost heave (see Figure 4-1 (b)) or normal fault (see Figure 4-1 (c-2)). The proposed method is established based on the finite difference

approach to solve the underlying governing equations (i.e., coupled nonlinear partial differential equations) for the problems considered here. To the end, both the axial and flexural deformation fields along the pipe are obtained, and then the strain demand can be further derived.

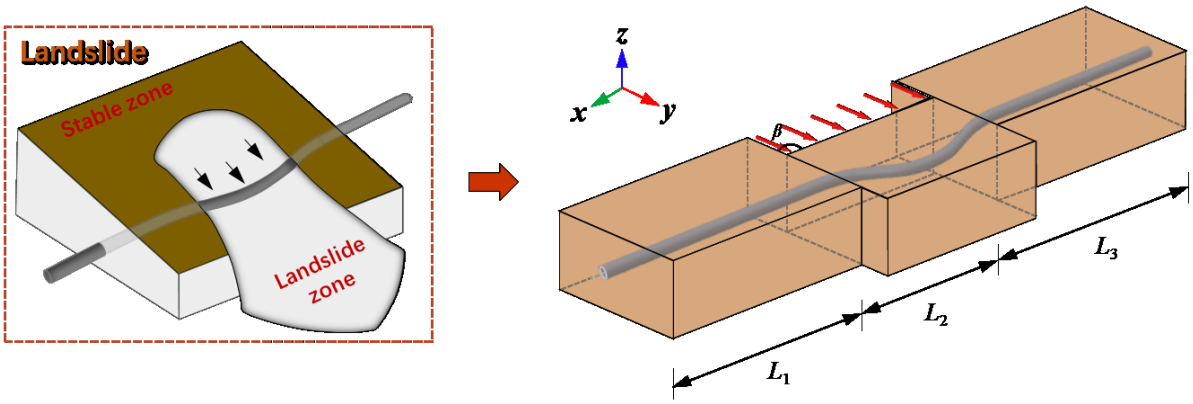

(a) Pipe's deformation due to the landslide

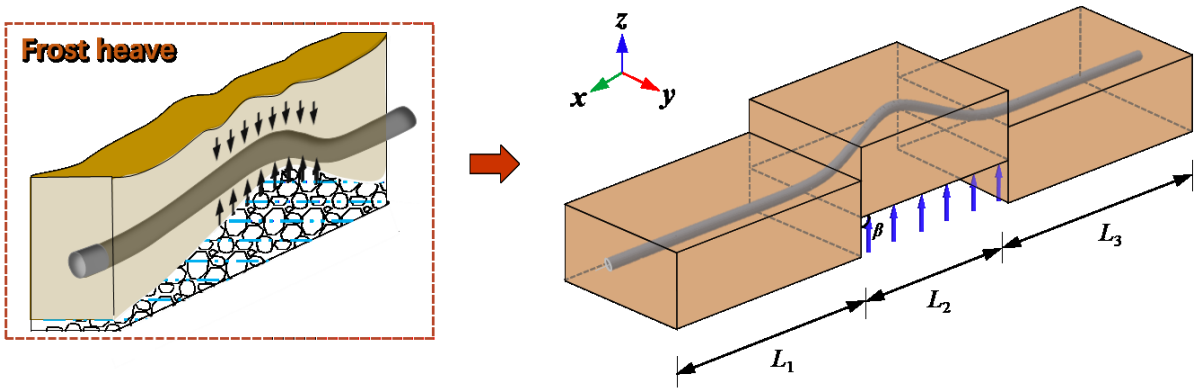

(b) Pipe's deformation due to the frost heave

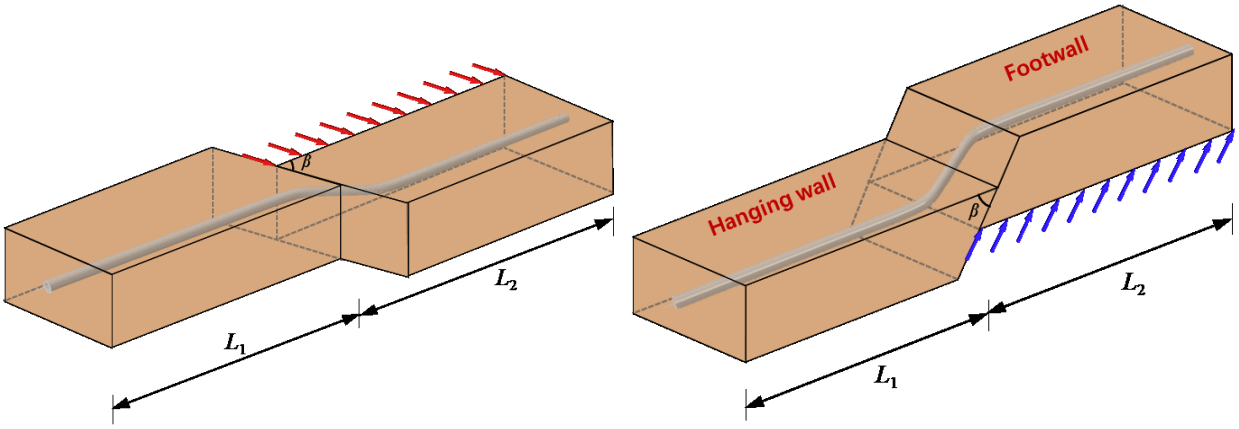

(c-1) Strike-slip fault (c-2) Normal fault

(c) Pipe's deformation due to tectonic faults

Figure 4-1: Graphical representation of ground-induced deformations in a pipeline

4.2.1 Governing equations

The deformation of a pipeline under large ground movement can be considered as an Euler-Bernoulli beam subjected to distributed loads induced by soil, as depicted in Figure 4-2. The distributed loads applied to the pipe consist of the exerted axial load density f and the lateral load density q, which depend on the difference between the axial displacement of pipe $u(x)$ and the corresponding soil movement $U_g(x)$ along the pipe, and the difference between the lateral displacement of the pipe $v(x)$ and the corresponding soil movement $V_g(x)$, respectively, as shown in Figure 4-2. As such, the governing equations of the pipe considering large deformation can be derived based on the equilibrium, as shown by Eq. (4-1).

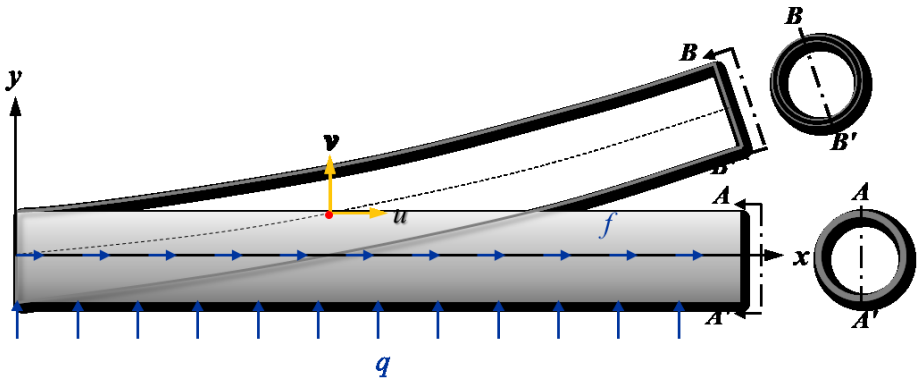

Figure 4-2: Euler-Bernoulli beam under large deformation

$$\begin{cases} \dfrac{dN(x)}{dx} + f\left(U_g(x) - u(x)\right) = 0 \\ \dfrac{d^2M(x)}{dx^2} - \dfrac{d}{dx}\left(N(x)\dfrac{dv(x)}{dx}\right) - q\left(V_g(x) - v(x)\right) = 0 \end{cases} \tag{4-1}$$

where $N(x)$ and $M(x)$ are the internal axial force and internal bending moment on the cross-section, respectively.

4.2.2 Calculation procedure for elastic pipes

The application of the finite difference method to solve elastic pipe's deformation has been reported by Zheng et al. [32]. To facilitate the discussion of the proposed method for inelastic pipes, the general idea of the elastic pipe analysis using the finite difference method is briefly summarized as follows.

- *Derivation of the axial force and bending moment*

  According to the linear relationship between the stress and strain, the axial force N and bending moment M in the governing equation are derived based on the integration of the stress over the pipe cross-section. The obtained axial force and bending moment are functions of the axial and lateral displacements, i.e., $u(x)$ and $v(x)$, which are the unknowns in the governing equations (see Eq. (4-1)).

- *Formulation of the finite-difference equations*

Incorporating the derived expressions of axial force and bending moment into the governing equations, the governing equations can be cast to equations with unknowns of pipe displacements (u and v), derivatives of the displacements (u' and v'), second derivatives of the displacements (u'' and v''), and fourth derivatives of the lateral displacements (v''''). Based on the finite difference method, these derivatives are represented by the unknowns of displacements (u and v) at finite difference grid points, and thus the governing equations can be rearranged into the finite-difference format, a system of nonlinear equations.

- *Definition of the pipe-soil interactions*

  The axial load density f and lateral load density q are used to represent the pipe-soil interactions, which are described using elastic-perfectly plastic relationships between the pipe deformation and the soil force. In the finite difference equations, they are equivalently characterized with mechanical properties of discrete nonlinear soil springs connecting to the pipe in three principal directions. The ultimate soil spring resistance (per unit length) and the yield displacement are calculated based on the empirical equations in ALA Guideline Appendix B [33].

- *Calculation of the displacements and strains*

  A large set of simultaneous finite-difference equations together with boundary conditions can be solved for the unknowns of axial and lateral deformations (u and v) at predefined grid points along the pipe using a nonlinear equation solver. Based on the calculated u and v at grid points, the longitudinal strain along the pipe can also be obtained.

4.2.3 Derivations of $N(x)$ and $M(x)$ considering pipe material inelasticity

With respect to the analysis procedure summarized in section 4.2.2 [32], this paper mainly focuses on its extension to inelastic pipes. Thus, this section aims to find the expressions of axial force $N(x)$ and bending moment $M(x)$, which can be explicitly expressed functions of $u(x)$ and $v(x)$ using the bilinear stress-strain relationship assumed for pipe steel.

Based on the assumption of "plane sections remain plane", the axial strain and bending strain (i.e., the normal strain caused by bending) $\varepsilon_{bending}$ can be assumed to have three distribution patterns in the pipe cross-section for each as illustrated in Figure 4-3. It is noted that the pipe cross-section is assumed to maintain the original circular hollow shape during deformation. Hence, the longitudinal strain ε_l, as the summation of the axial strain and bending strain (see Eq. (4-2)) [32], can end up in eight major scenarios (excluding the combination of no axial strain and no bending strain).

$$\varepsilon_l = \varepsilon_{axial} + \varepsilon_{bending} = \left(u' + \frac{v'^2}{2} \right) - v'' \bullet \tag{4-2}$$

where z is the position along the axis of z as shown in Figure 4-3.

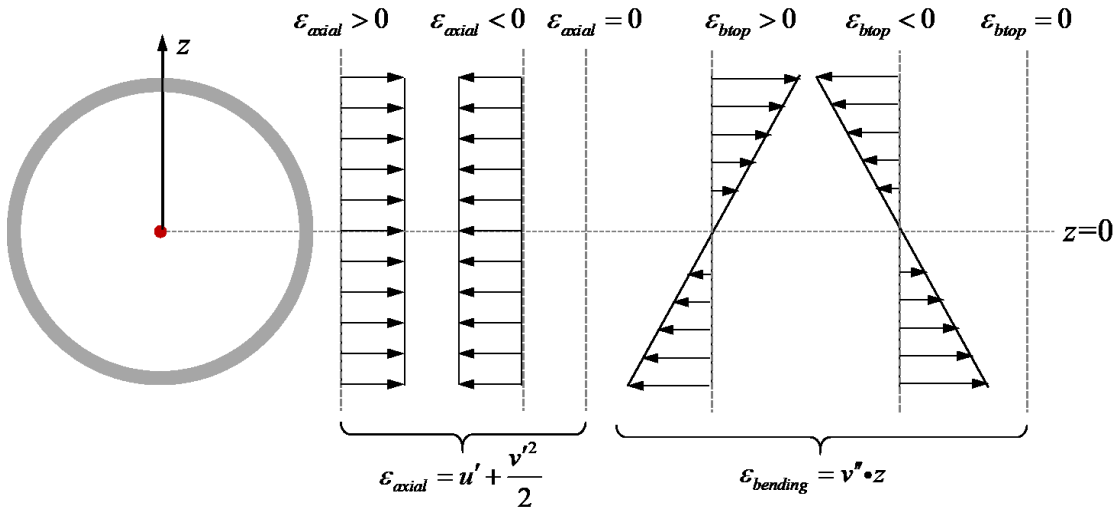

Figure 4-3: Axial strain and bending strain distribution on the pipe cross-section

To simplify the derivation, this study groups the 8 scenarios into two cases: longitudinal strain without and with bending strain.

4.2.3.1 Longitudinal strain pattern without bending strain

For the scenarios when the bending action does not exist (where $v'' = 0$ thus $M = 0$), the strain and stress distributions on the pipe cross-section can be illustrated by the two cases as depicted in Figure 4-4. The bilinear stress-strain relationship is employed to formulate the constitutive expression. Let σ_y and ε_y be the yield stress and strain, E and E_p the modulus of elastic and plastic regions, respectively. The formulation of the internal axial force N can be derived as follows:

(1) When the pipe cross-section is elastic: $-\varepsilon_y \le \varepsilon_l = \varepsilon_{axial} \le \varepsilon_y$

$$N = \int_A \sigma_l dA = E\varepsilon_l A = E\varepsilon_{axial} A = E\left(u' + \frac{v'^2}{2}\right)A \tag{4-3}$$

where A is the area of the pipe cross-section.

(2) When the pipe cross-section is fully plastic

For case 1 in Figure 4-4, $\varepsilon_l = \varepsilon_{axial} > \varepsilon_y$

$$N = \int_A \sigma_l dA = \left(E\varepsilon_y + E_p\left(u' + \frac{v'^2}{2} - \varepsilon_y\right)\right)A \tag{4-4}$$

For case 2 in Figure 4-4: $\varepsilon_l = \varepsilon_{axial} < -\varepsilon_y$

$$N = \int_A \sigma_l dA = \left(-E\varepsilon_y + E_p\left(u' + \frac{v'^2}{2} + \varepsilon_y\right)\right)A \tag{4-5}$$

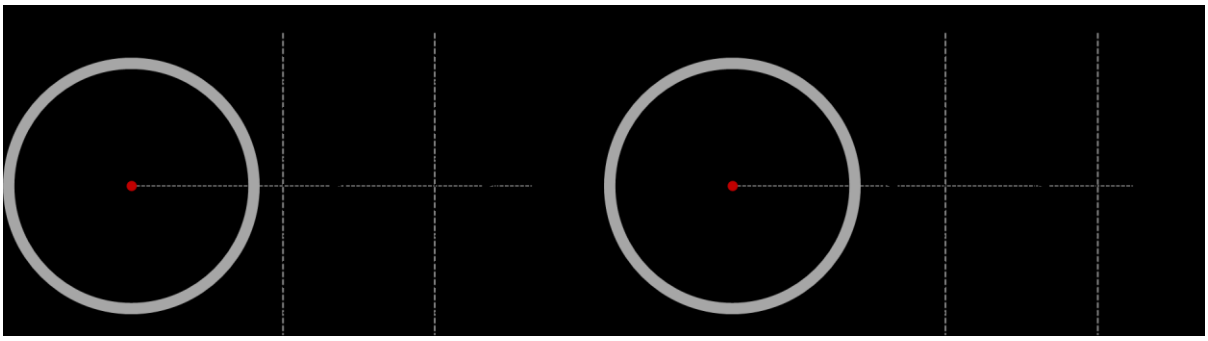

(a) Case 1 (b) Case 2

Figure 4-4: Longitudinal strain distribution without bending in the pipe cross-section

4.2.3.2 Longitudinal strain pattern with bending strain

The strain and stress distributions on the pipe cross-section with consideration of bending can be generalized as two significant situations as pictured in Figure 4-5, where the partially plastic pattern is shown. The difference between these two situations is the position of tensile and compressive actions: the pipe "top" is subjected to tension in case 1 and compression in case 2. Other potential patterns, which are not shown in Figure 4-5, will be considered within the derivation below.

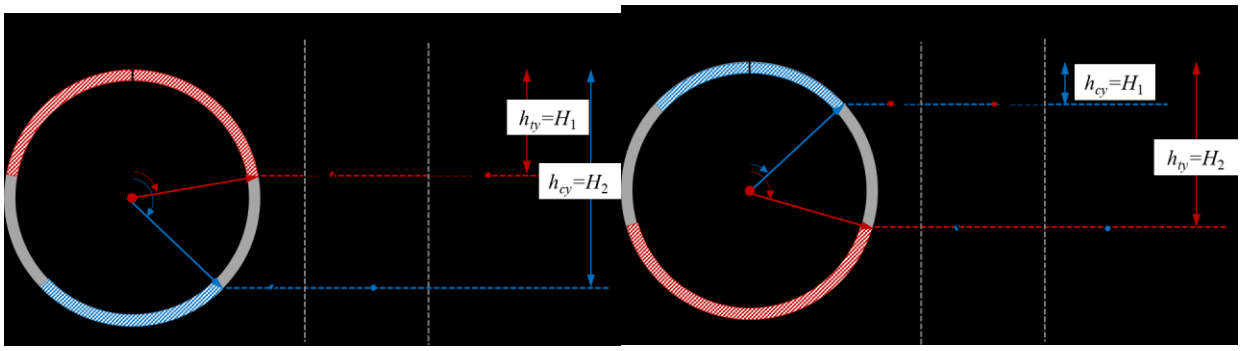

(a) Situation 1 (b) Situation 2

Figure 4-5: Longitudinal strain distribution with bending in the pipe cross-section

Based on Eq. (4-2), the longitudinal strain on the pipe top ε_{top} and bottom ε_{bot} can be rearranged as Eqs. (4-6) and (4-7), respectively.

$$\varepsilon_{top} = u' + \frac{v'^2}{2} - v''\left(\frac{D}{2}\right) \tag{4-6}$$

$$\varepsilon_{bot} = u' + \frac{v'^2}{2} + v''\left(\frac{D}{2}\right) \tag{4-7}$$

where D is the outer diameter of the pipe.

Note that the positions of the yield points are used as the boundary between the elastic and plastic fields in the later calculation. The vertical coordinate (the origin is the pipe top, and the positive side points to the below) from the pipe top to the tensile yield point h_{ty} and compressive yield point h_{cy} can be derived on the geometric basis as shown in Eqs. (4-8) and (4-9) respectively.

$$h_{ty} = \frac{\varepsilon_{top} - \varepsilon_y}{\varepsilon_{top} - \varepsilon_{bot}} D = \frac{2u' + v'^2 + v''\bullet}{-2v''} \tag{4-8}$$

$$h_{cy} = \frac{\varepsilon_{top} + \varepsilon_y}{\varepsilon_{top} - \varepsilon_{bot}} D = \frac{2u' + v'^2 + v''\bullet}{-2v''} \tag{4-9}$$

where the yield strain ε_y is mathematically positive.

To distinguish the two situations of stress distributions shown in Figure 4-5, two auxiliary variables H_1 and H_2, representing the lower and the greater of h_{ty} and h_{cy} respectively, are introduced to facilitate the derivation of *N* and *M*. In addition, the corresponding intersection angles to h_{ty} and h_{cy}, namely φ_1 and φ_2 as shown in Figure 4-5 ($\varphi_1 < \varphi_2$ due to the relationship of $H_1 < H_2$), can be defined as Eq. (4-10), which includes all the possible stress distribution patterns. For instance, when $H_1 = h_{ty} < 0$ and $0 < H_2 = h_{cy} < D$, the corresponding stress pattern should be fully elastic of the pipe top subjected to tension and partially plastic of the pipe bottom subjected to compression.

$$\varphi_i = \begin{cases} 0 & , \quad H_i \le 0 \\ \arccos\left(\dfrac{D - 2H_i}{D}\right) & , \quad 0 < H_i < D \quad (i = 1, 2) \\ \pi & , \quad H_i \ge D \end{cases} \tag{4-10}$$

In the cylinder coordinate system, the longitudinal strain ε_l (in rectangular coordinate) can be expressed as ε_θ (based on the cylinder coordinate, see Eq. (4-11)). The variation of strains in the radial direction can be neglected due to the thin-wall pipeline structure.

$$\varepsilon_\theta = u' + \frac{v'^2}{2} - v'' \bullet \left(\frac{D}{2}\right) \bullet \cos\theta \tag{4-11}$$

where θ is the intersection angle between the axis z and the position vector corresponding to the material fiber position, ranging from 0 to π. The stress distribution can be therefore written as Eq. (4-12) based on the bilinear property of the stress-strain relationship.

$$\sigma_\theta = \begin{cases} sign\left(h_{cy} - h_{ty}\right) E\varepsilon_y + E_p\left(\varepsilon_\theta - sign\left(h_{cy} - h_{ty}\right)\varepsilon_y\right) & , \quad 0 \le \theta \le \varphi_1 \\ E\varepsilon_\theta & , \quad \varphi_1 < \theta < \varphi_2 \\ -sign\left(h_{cy} - h_{ty}\right) E\varepsilon_y + E_p\left(\varepsilon_\theta + sign\left(h_{cy} - h_{ty}\right)\varepsilon_y\right) & , \quad \varphi_2 \le \theta \le \pi \end{cases} \tag{4-12}$$

where the sign function $sign\left(h_{cy} - h_{ty}\right)$ is to indicate the relative position between the tensile yield point and the compressive yield point.

Based on the definition of the internal axial force and bending moment, the expressions of N and M are respectively derived as Eqs. (4-13) and (4-14).

$$\begin{aligned} N &= 2\int_0^\pi \sigma_\theta \left(\frac{D-t}{2}\right) t d\theta \\ &= (D-t)t \begin{pmatrix} \left(u' + \frac{v'^2}{2}\right)\left(E_p\left(\pi + \varphi_1 - \varphi_2\right) - E\left(\varphi_1 - \varphi_2\right)\right) \\ + sign\left(h_{cy} - h_{ty}\right)\varepsilon_y\left(E - E_p\right)\left(\varphi_1 + \varphi_2 - \pi\right) \\ + \frac{D}{2}v''\left(E - E_p\right)\left(\sin\varphi_1 - \sin\varphi_2\right) \end{pmatrix} \end{aligned} \tag{4-13}$$

$$\begin{aligned} M &= 2\int_0^\pi \sigma_\theta \left(\frac{D-t}{2}\right)^2 t\cos\theta d\theta \\ &= \frac{1}{4}(D-t)^2 t \begin{pmatrix} -\frac{D}{2}v''\left(E_p\left(\pi + \varphi_1 - \varphi_2\right) - E\left(\varphi_1 - \varphi_2\right)\right) + \left(E - E_p\right) \\ \left(-\left(2\left(u' + \frac{w'^2}{2} - sign\left(h_{cy} - h_{ty}\right)\varepsilon_y\right) - \frac{D}{2}v''\cos\varphi_1\right)\sin\varphi_1 \right. \\ \left. + \left(2\left(u' + \frac{w'^2}{2} + sign\left(h_{cy} - h_{ty}\right)\varepsilon_y\right) - \frac{D}{2}v''\cos\varphi_2\right)\sin\varphi_2\right) \end{pmatrix} \end{aligned} \tag{4-14}$$

where t is the wall thickness of the pipe.

4.2.4 Implementation procedure

Considering the buried pipe subjected to a horizontal landslide as shown in Figure 4-1 (a), the governing equations for the interior grid points in the middle segment L_2, which is in the soil movement zone, can be written as Eq. (4-15) based on the central finite difference method. Similarly, the finite difference equations for the pipe outside the soil movement zone, i.e., segments L_1 and L_3, can be written as Eq. (4-16). The grid points are equally-spaced in each segment in this study. λ is the interval distance of grid points, and the subscripts 1, 2, and 3 indicate the corresponding pipe segment.

$$\begin{cases} \dfrac{1}{2\lambda_2}\left(N_{i+1}-N_{i-1}\right)+f\left(U-u_i\right)=0 \\ \dfrac{1}{\lambda_2^{\,2}}\begin{bmatrix} \left(M_{i+1}-2M_i+M_{i-1}\right) \\ -\dfrac{1}{4}\left(N_{i+1}-N_{i-1}\right)\bullet \\ -N_i\left(v_{i+1}-2v_i+v_{i-1}\right) \end{bmatrix}-q\left(V-v_i\right)=0 \end{cases} \tag{4-15}$$

$$\begin{cases} \dfrac{1}{2\lambda_{1,3}}\left(N_{i+1}-N_{i-1}\right)-f\left(u_i\right)=0 \\ \dfrac{1}{\lambda_{1,3}^{2}}\begin{bmatrix} \left(M_{i+1}-2M_i+M_{i-1}\right) \\ -\dfrac{1}{4}\left(N_{i+1}-N_{i-1}\right)\bullet \\ -N_i\left(v_{i+1}-2v_i+v_{i-1}\right) \end{bmatrix}+q\left(v_i\right)=0 \end{cases} \tag{4-16}$$

where i is the index denoting the ID of a grid point. Note that the block pattern of ground displacement is considered here, where U and V are the magnitude of the axial and lateral components, respectively, of the ground movement for the middle segment L_2; no ground displacement for the two end segments. Implementation of the proposed method to get the unknown displacements at all grid points along the pipe is elaborated as follows.

Step 1 : meshing the pipe.

Meshing the pipe with equally-spaced grid points along the axial direction for each segment. The number of grid points for each pipe segment is n_1, n_2, and n_3 including boundary nodes (pictured as solid points in Figure 4-6).

Step 2 : approximating the derivative terms using finite difference.

Writing the first-order derivatives of the axial displacement u' and the lateral displacement v', and the second-order derivatives of the lateral displacement v'' based on finite-difference(see Figure 4-6 (b)). The central finite difference is employed for interior grid points (hollow points in Figure 4-6), while the one-sided finite difference is employed for boundary grid points.

Step 3 : calculating the axial force and bending moment.

Computing internal axial forces N and internal bending moments M at interior grid points (see Figure 4-6 (c)). The formulation of N and M are expressed as functions of u', v', and v'' as calculated in ***Step 2***.

Step 4 : constructing the governing equation for each interior grid point.

Establishing the equations for interior grid points in segment L_2, and segments L_1 and L_3 based on Eqs. (4-15) and (4-16), respectively. For the case in which the pipe is subjected to a horizontal landslide, the symmetric lateral soil resistance is assumed. Hence, in those equations, the external axial and lateral soil loads applied to pipes can be expressed as Eqs. (4-17) and (4-18), respectively, according to the elastic-perfectly plastic soil force described.

$$f(\Delta u) = \begin{cases} T_u & , \quad \Delta u > \Delta t \\ T_u / \Delta t \bullet & \quad \cdot \Delta t \le \Delta u \le \Delta t \\ -T_u & , \quad \Delta u < -\Delta t \end{cases} \tag{4-17}$$

$$q(\Delta v) = \begin{cases} P_u & , \quad \Delta v > \Delta p \\ P_u / \Delta p \bullet & \quad \Delta p \le \Delta v \le \Delta p \\ -P_u & , \quad \Delta v < -\Delta p \end{cases} \tag{4-18}$$

where Δu and Δv are the relative displacement between the soil and pipe respectively in the axial and lateral directions.

Step 5 : imposing boundary conditions for each boundary grid point.

The three pipe segments are consecutive, and both ends of the pipe are assumed fixed. These boundary conditions are imposed in the finite difference equations. The simultaneous finite difference equations are finally established on each grid point as seen in Figure 4-6 (d), which is a large system of equations with unknown deformations along the pipe at all grid points.

Step 6 : solving the simultaneous nonlinear equations.

Using a nonlinear equation solver to solve for the unknowns in the finite difference equation set established in ***0***. Subsequently, the longitudinal strain along the pipe can be evaluated according to Eq. (4-2) in section 4.2.3. The maximum (and minimum) strain along the pipe and its corresponding location, referred to as the tensile (and compressive) strain demand and the critical spot in this paper respectively, can be then obtained. It is noteworthy that the loss of axial stiffness of pipe due to large strains is not considered within the method. Furthermore, the present method does not account for the effects of local buckling and section deformation.

(a) Displacements at each grid point

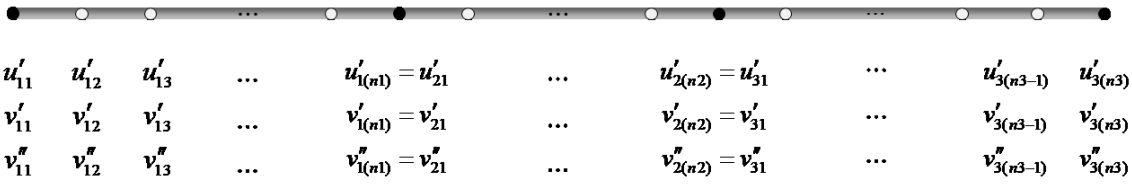

(b) Derivatives of the displacements at each grid point

(c) Internal bending moment and axial force at each grid point

(d) Equations for each grid point

Figure 4-6: Schematic view for the calculation procedure of the proposed method

4.3 Validation of the proposed method

The proposed method is validated using two study cases against the benchmark finite element model. These two study cases involve three pipe segments, and the middle segment is subjected to ground movements of block pattern, as illustrated in Figure 4-1. It should be noted that in Case 1, the pipe is subjected to symmetric soil forces in the horizontal plane as a result of horizontal landslide actions; in Case 2, the pipe is under non-symmetric soil forces in the vertical plane as a result of ground heave.

4.3.1 Case 1

The study case concerns a 559-mm-diameter X52 steel pipe with a wall thickness of 7.14 mm. The properties of the pipe material include Young's modulus E = 210 MPa, yield strength σ_y = 359 MPa (hence yield strain ε_y = 0.17%), ultimate strength σ_u = 455 MPa, and ultimate strain ε_u = 3%.

The buried depth, defined as the distance from the ground surface to the pipe centerline, is assumed as 1.5 m, and backfill soil is silt sand having an internal friction angle of 34° and unit weight of 1410 kg/m^3. The coating dependent factor relating the internal friction angle of the soil to the friction angle at the pipe-soil interface is set as 0.6 which is used for calculating the yield force of axial soil springs. Based on the recommendations in ALA Guidelines [33], the parameters of bilinear soil springs are estimated as listed in Table 4-1. Note that the pipe considered in Case 1 is subjected to horizontal ground movement and thus transverse horizontal soil springs are used to describe the lateral soil forces applied to the pipe.

Table 4-1: Parameters of soil springs

Variable	Value
Axial yield force per unit length T_u (kN/m)	12
Axial yield displacement Δ_t (mm)	3
Transverse horizontal yield force per unit length P_u (kN/m)	153
Transverse horizontal yield displacement Δ_p (mm)	70
Uplift soil spring resistance Q_u (kN/m)	34
Q_u yield displacement Δ_{qu} (mm)	20
Bearing soil spring resistance Q_d (kN/m)	485
Q_d yield displacement Δ_{qd} (mm)	60

In Case 1, the action of the ground movement on the pipe is graphically illustrated in Figure 4-1 (a). The middle segment in the soil movement zone is assumed as L_2 = 10 m. The end segments connected to the middle span are $L_1 = L_3$ = 40 m. Different combinations of ground displacements δ (from 0 up to 2.5 m) and the intersection angle (the angle between the pipe axis and the direction of ground movement) β (= 0°, 30°, 60° and 90°) are considered.

In the proposed method, the middle segment and the end segments are discretized to 20 and 40 intervals, respectively. In the finite element method using the commercial software ABAQUS [34], the pipe is modeled with beam-type elements, namely PIPE32 (3-node quadratic pipe in space). The nonlinear soil springs are employed to simulate the pipe-soil interaction using PSI36 elements (3-dimensional 6-node pipe-soil interaction element). The parameters of the soil spring properties (see Table 4-1) are calculated based on ALA-2001 Guidelines (Appendix B) [33], as summarized in Table 4-1. For a fair comparison, the same discretization is adopted for the pipe and soil springs in both the proposed method and the finite element method.

Figure 4-7 presents the pipe's strain demand and displacement predicted using the proposed method (referred to as PM) and finite element method (referred to as FEM) at different intersection angles, 0°, 30°, 60° and 90°, for Case 1. Note that for each intersection angle, both the transverse lateral and axial pipe displacements are reported for a specific ground displacement level. Particularly, at the intersection angle of 0° where the pipe only withstands axial soil force, a finer

interval of ground movement is applied. As observed from Figure 4-7 (a), the strain demand due to the axial soil force is tiny and the pipe stays elastic. The strain demand linearly increases with growth of the ground movement to its extreme value, i.e., 0.0023% for the tensile strain demand and -0.0023% for the compressive strain demand due to the yielding of axial soil springs. The induced pipe displacements are shown in Figure 4-7 (b), which indicates that the maximum displacement happens in the middle of the pipe and no lateral displacement is generated. The comparison indicates a very good agreement between the proposed method and the finite element method in terms of strain demands and pipe displacements.

When the intersection angle is higher than 0° where the pipe is under the combined effect of axial and lateral soil forces, at small ground movements, the pipe is in the elastic stage in which the strain demand is smaller than the yield strain ε_y, and the results derived from the proposed method are of great agreement with the results calculated by the simplified finite element model using one-dimensional beam elements. With the development of the ground movement, the pipe shows elastic-plastic behavior and the strain demand increases accordingly. In this stage, the strain demand and the displacement (e.g., at the ground movement of 1 m) predicted by the proposed method are in good agreement with finite element results, which indicates that the consideration of inelasticity in this study is correct and applicable in the proposed method. As the ground movement further grows, the soil spring proceeds to yield and the strain demand of the pipe reaches a constant level of around 2.5% for tension and 0.8% for compression. In addition, the effect of lateral soil springs is more prominent than that of axial soil springs since lateral soil springs impose greater force. The extreme value of strain demand occurs earlier with the increase of intersection angle, which implies that the pipe becomes more vulnerable at a greater intersection angle. At the same time, axial displacements are much lower than lateral displacements (see Figure 4-7 (d), (f), and (h)). To make a clear comparison, the pipe's axial displacements are scaled up to 10 times in the plots. Generally, the comparison with FEM-based results indicates that the proposed method has a good predictive capability to capture the pipe's response to the ground movement.

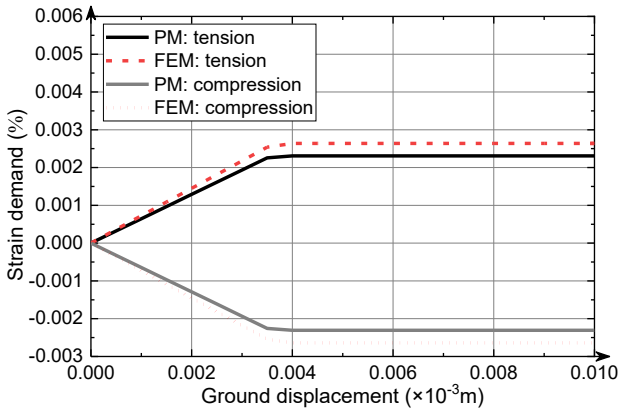

(a) Strain demand (β=0°)

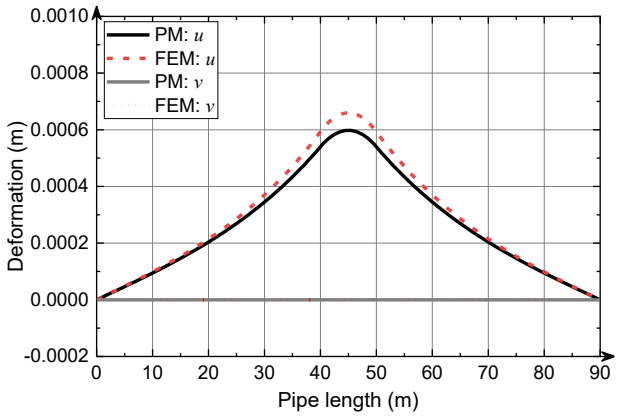

(b) Displacements (β=0°, δ = 0.01 m)

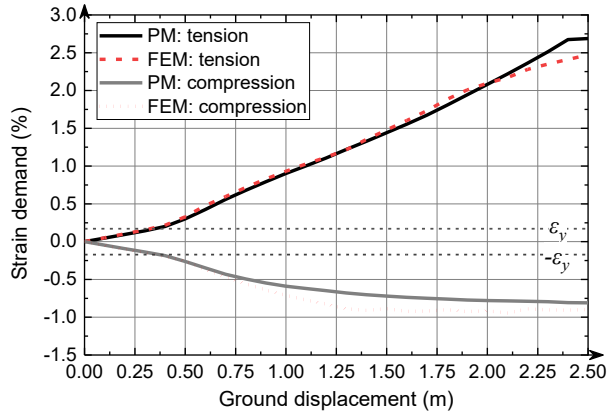

(c) Strain demand (β=30°)

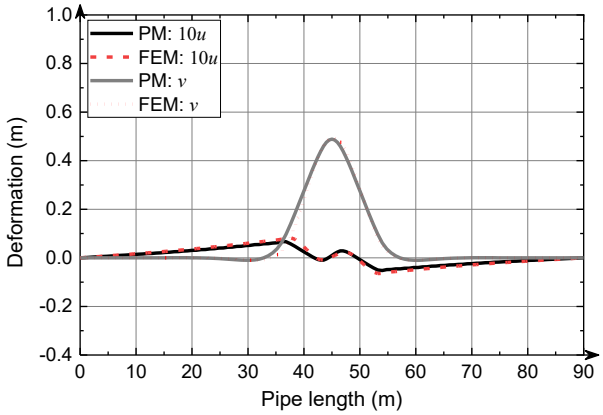

(d) Displacement (β=30°, δ = 1 m)

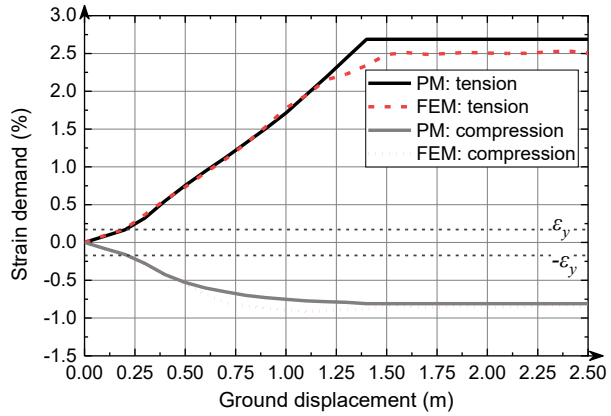

(e) Strain demand (β=60°)

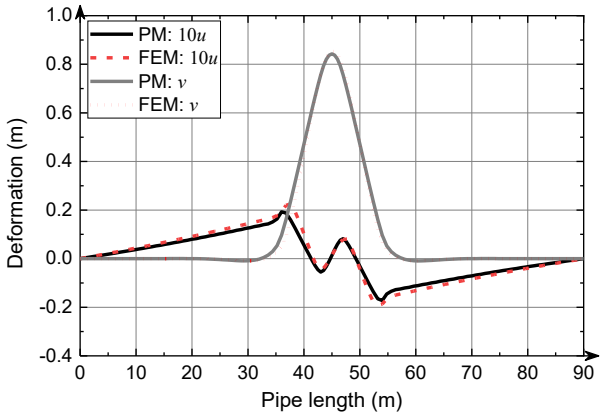

(f) Displacement (β=60°, δ = 1 m)

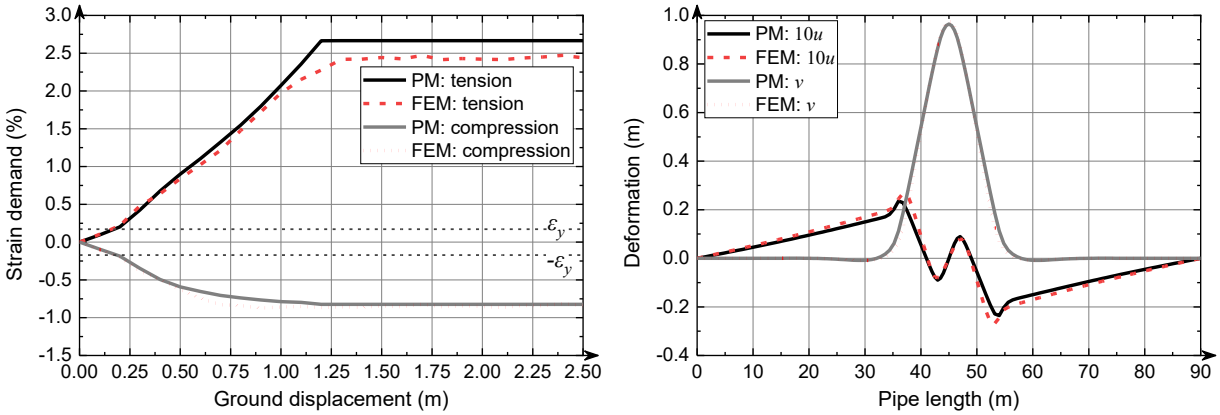

(g) Strain demand (β=90°) (h) Displacement (β=90°, δ = 1 m)

Figure 4-7: Comparison between the proposed method and finite element method in terms of strain demand and pipe deformations for Case 1

4.3.2 Case 2

The same pipe considered as in Case 1 is studied in Case 2, but subjected to ground movement in the vertical plane. Specifically, for the transverse force, the ground movement is applied to the middle segment L_2 in the vertical upward direction. The loads are characterized by the non-symmetric lateral soil forces from uplift soil springs and bearing soil springs (see properties summarized in Table 4-1). Other than different soil spring properties used here in Case 2, the same finite difference models and finite element models as in Case 1 are developed to determine the strain demand and pipe displacement fields.

The comparison of the results obtained using the proposed method and FEM for Case 2 are presented in Figure 4-8. The comparison demonstrates a fairly good agreement between the predications from the proposed method and finite element results. When the ground movement is not perpendicular to the pipe axis, with the increase of ground movement, the difference in the strain demand can be observed due to the two different algorithms of finite element method and finite difference method. In the finite element model, the load is applied incrementally and strains are calculated based on the deformed shape. Meanwhile, the ground displacement is exerted as a one-time load and strains are evaluated based on the undeformed pipes. When the ground movement is large, at the location near the connections of pipe segments where strain demands

occur, the pipe doesn't deform as much as it does in the finite element model, which leads to a conservative strain demand. Under the non-symmetric soil forces in Case 2, the pipe reflects larger lateral displacements in the middle segment and its adjacent areas since the uplift soil force cannot present an equivalent strong force to resist the pipe displacement. The larger lateral pipe displacement causes greater stretch along the pipe, which leads to a larger axial pipe displacement.

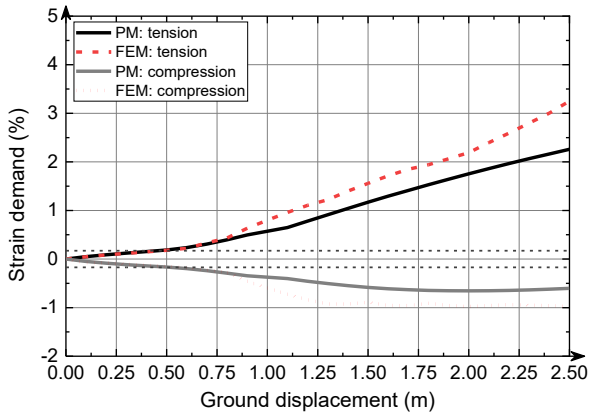

(a) Strain demand ($\beta = 30°$)

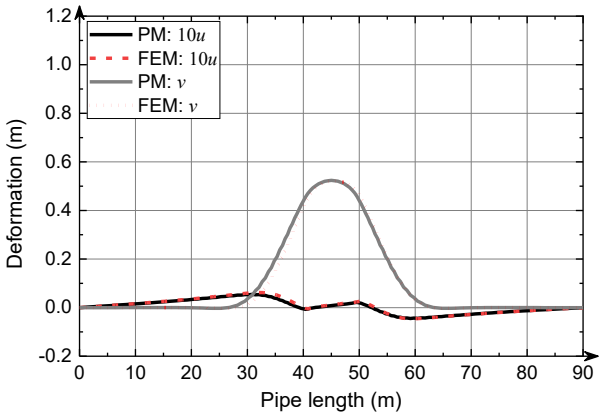

(b) Displacement ($\beta = 30°$, $\delta = 1.0$ m)

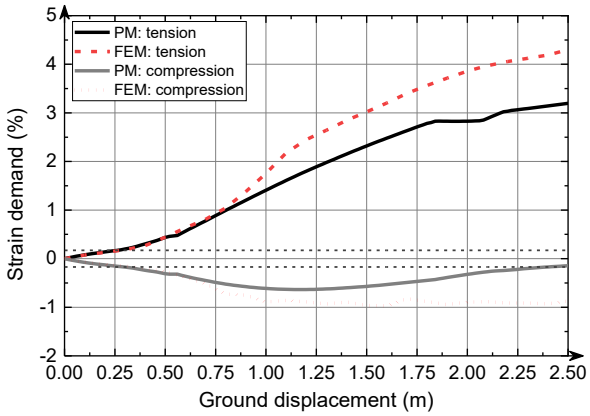

(c) Strain demand ($\beta = 60°$)

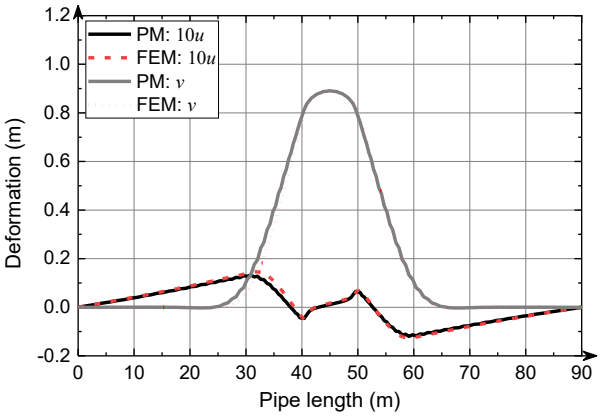

(d) Displacement ($\beta = 60°$, $\delta = 1.0$ m)

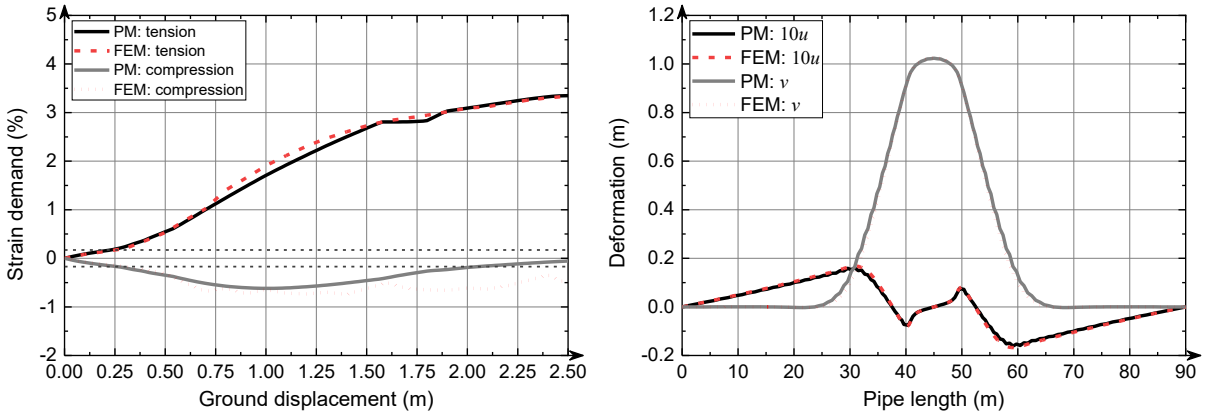

(e) Strain demand ($\beta = 90°$) (f) Displacement ($\beta = 90°$, $\delta = 1.0$ m)

Figure 4-8: Comparison between the proposed method and finite element method in terms of strain demand and pipe deformations for Case 2

To compare the computational efficiency of the proposed method and the finite element model in ABAQUS, computational time of each task in both Case 1 and Case 2 is recorded. Tasks are processed sequentially in both the proposed method and the finite element method in ABAQUS, and both calculations are conducted in a computer configurated by an Intel® Core™ i5-6500 CPU @3.20GHz and a memory of RAM 16 GB. Figure 4-9 shows the comparative results on the average calculation time with respect to different intersection angles in Case 1 and Case 2. It can be seen that the proposed method takes much less time than the corresponding finite element method in every task, which demonstrates that the proposed method outperforms the finite element method in efficiency for solving the one-dimensional beam problems. In addition, efficiency of the proposed method can be highly improved after employing the compiler in Numba library for Python, i.e., the average calculation time is around 0.5 second.

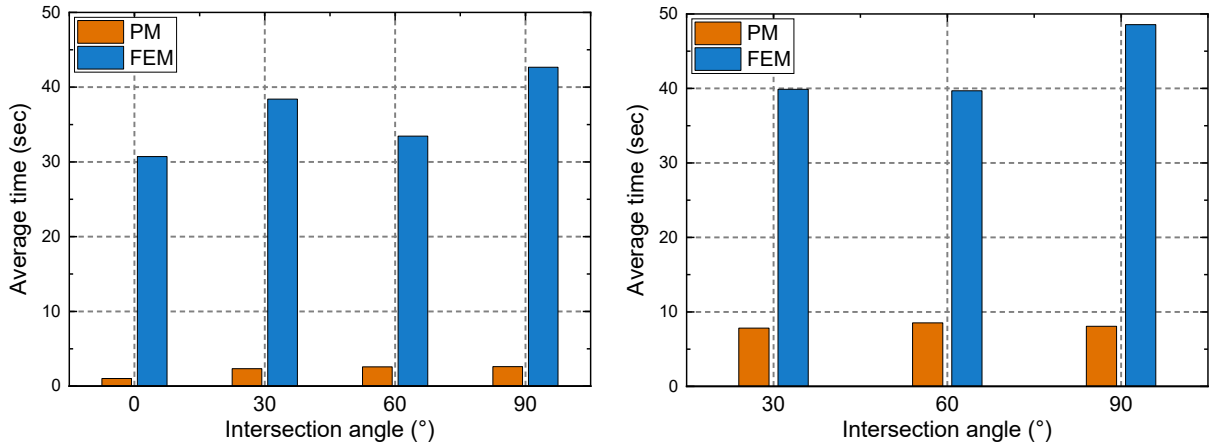

(a) Case 1 (b) Case 2

Figure 4-9: Comparison between the proposed method and finite element method in terms of computational time for Case 1 and Case 2

4.4 Comparison of the proposed method with existing analytical methods

This section presents a case study of the classical problem of a pipe subjected to strike-slip faults, for which four existing analytical methods exist: the ones developed by Newmark and Hall [8] and Kennedy et al. [9] as written in the design guideline [29][30], the refined analytical method proposed by Karamitros et al. [12], and the closed-form solution developed by Sarvanis and Karamanos [18]. This allows to evaluate the applicability of the proposed method with comparison to those analytical methods; the finite element results are also presented as a reference. For this purpose, the pipe and the soil properties in Case 1 are considered. The total length of the pipe considered is 1,000 m, i.e., 500 m for the left and 500 m for the right segment. The tectonic fault movement is only exerted to the right pipe segment. The end node of the left pipe segment is fixed; for reasons of simplicity, the axial and lateral components decomposed by the fault displacement are applied as translations to the end node of the right pipe segment without rotation. The discretization size of the pipe in both the proposed method and the finite element model is 1 m. Note that the pipe is assumed to be subjected to the strike-slip fault where the ground movement is in the horizontal plane and thus the lateral soil resistance is symmetric.

In this case study, three different strike-slip faults with pipe-fault intersection angles of β = 30°, 60°, and 90° are considered, with different fault-related ground displacements (i.e., δ = 3 m

at maximum). Note that the model of Kennedy et al. [9] made use of Ramberg-Osgood stress-strain curve where the strain ε and corresponding stress σ can be seen in Eq. (4-19). The fitted coefficients of X52 steel are α = 9 and r = 10. The difference from the bilinear elastoplastic behavior assumed in the proposed method is negligible.

$$\varepsilon = \frac{\sigma}{E}\left[1+\left(\frac{\alpha}{r+1}\right)\left(\frac{|\sigma|}{\sigma_y}\right)\right] \tag{4-19}$$

The pipe is supposed to withstand the tension-dominated loading when the pipe-fault intersection angle is less than 90° [9]. Hence, the tensile strain demand, as the basis of pipeline design against this situation, is used for the evaluation of the proposed method and other different methods as illustrated in Figure 4-10.

As observed, due to the assumptions associated with different analytical methods, their applicability ranges are different. Among the tested methods, a good overall agreement can be seen only between the predictions of the proposed method and finite element results. Additionally, by investigating the portion exceeding the pipe yield strain of ε_y = 0.17%, it demonstrates that the proposed method is capable of predicting the inelastic behavior of the pipe. The ultimate state of the entire pipe-soil system due to the yielding of soil springs can be observed in Figure 4-10 (c) where the maximum strain demand stabilizes at about 2.4% when the fault displacement exceeds 2 m.

In contrast, the Newmark-Hall method shows the most conservative results. In the analysis of Newmark-Hall method, only the axial pipe-soil interaction is considered and the pipe near the fault zone deforms as a straight cable; neglection of the lateral pipe-soil interaction leads to conservative strain demands. The Newmark-Hall method gradually loses its workability with the increase of pipe-fault intersection angles where the bending effect gradually is pronounced. As seen from Figure 4-10 (c), the strain demand calculated by the Newmark-Hall method approaches zero.

The Kennedy et al. method was developed to analyze the pipe's behavior subjected to large fault displacement by assuming the pipe deforming like a flexible cable near the fault trace. This method seriously over-predicts the strain demand in the pipe for small fault displacements. The

trend of strain demand is reversed at intermediate levels of fault displacements. As expected, the Kennedy et al. method provides relatively accurate results in the region of large fault displacement which is the applicable range claimed in Kennedy et al. [9].

The refined model proposed by Karamitros et al. [12] introduces a number of improvements based upon the assumptions established in the existing analytical methods, which aims to achieve a wider range of applications. The comparative results in Figure 4-10 demonstrate that the Karamitros et al. method possesses the best predictability among the four analytical methods. However, it overestimates the strain demand at the larger fault displacements when the fault trace is perpendicular to the pipe (see Figure 4-10 (c)). The axial strain is neglected since the geometrical elongation of the pipe is zero in Karamitros et al. method so the bending strain is solely considered in the strain demand calculation. The obtained maximum bending strain almost linearly grows with the increase of the fault displacement.

The closed-form expression in Sarvanis and Karamanos [18] was derived according to the assumed-shape function for pipe deformation under symmetric and non-symmetric soil resistance. The comparative results in Figure 4-10 demonstrate that the predicted strain demands calculated by this closed-form solution increase in a fairly linear manner with increasing fault displacements in all pipe-fault intersection angle cases. The calculated strain demand using the closed-form solution matches fairly well with the FEM results up to a certain critical displacement (around 1 m). A similar phenomenon was observed for Case 2 as reported in [18] when the ground displacement is less than a critical fault value (i.e., 1.5 times the pipe diameter). When the fault displacement exceeds the critical value, results calculated by the closed-form solution show noticeable discrepancies from FEM results, which indicates that Sarvanis-Karamanos method is incapable of capturing the coupling effect due to the nonlinearities in pipe materials and soil springs.

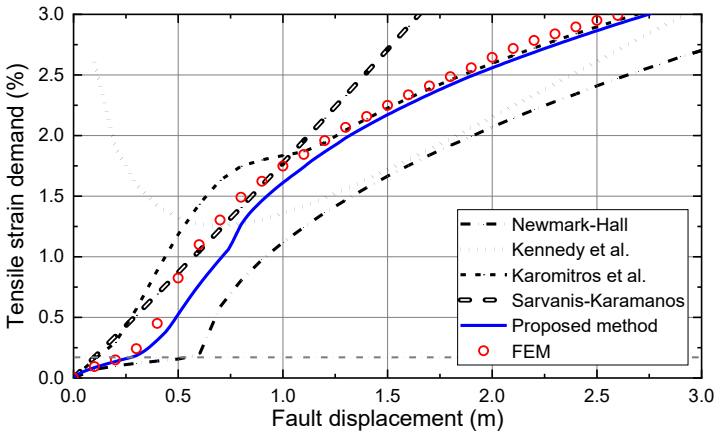

(a) Pipe-fault intersection angle of 30°

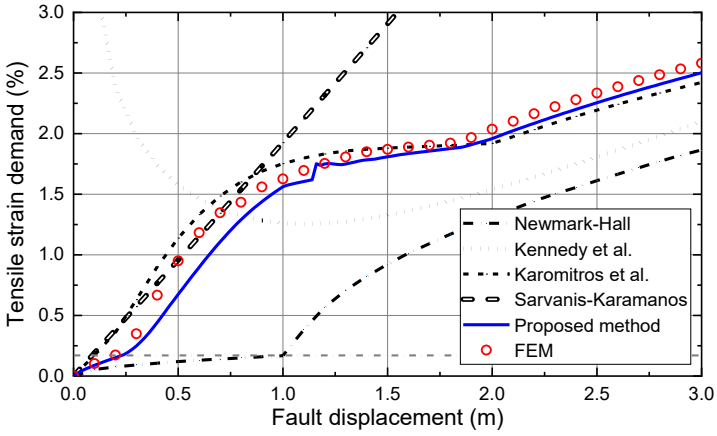

(b) Pipe-fault intersection angle of 60°

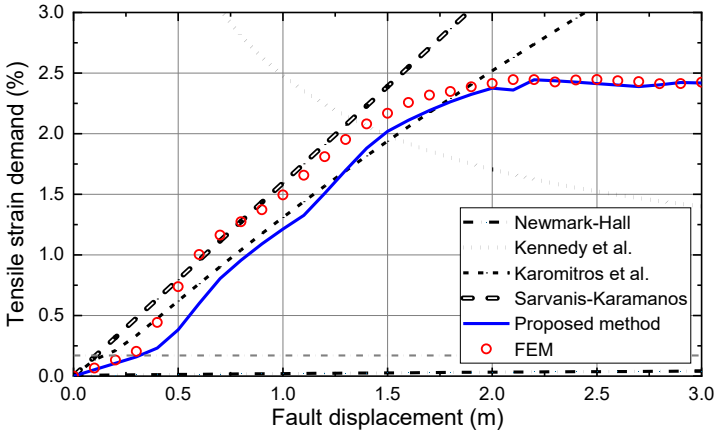

(c) Pipe-fault intersection angle of 90°

Figure 4-10: Comparison of the proposed method and four existing analytical methods as well as the finite element method in terms of tensile strain demand in a pipe subjected to strike-slip fault with different ground movement levels at different pipe-fault intersection angles

4.5 Chapter conclusions

A new method is developed to analyze pipes' strain demand under permanent ground movements using the finite difference method, by extending the method proposed in Zheng et al. [32] to account for the inelastic behavior of the pipe material. To this end, the axial force and the bending moment in a pipe, as required in the finite difference equations, are derived as explicit functions of the deformations at each node after considering the stress distribution of the pipe cross-section based on the bilinear property of the stress-strain behavior and different strain distributions. Two indicative case studies of geohazards, including ground movement in the horizontal and vertical planes, respectively, are utilized to validate the proposed method against the finite element method. The comparison with finite element results has demonstrated that the proposed method has a great predictive capability for pipes' strain demand and displacement fields when pipes are subjected to ground movements. Furthermore, based on the tensile strain demand prediction of pipes subjected to strike-slip fault displacements, the proposed method is compared with four existing analytical methods as well as the finite element method. It is demonstrated that the proposed method is applicable to a wider range of applications compared with the four analytical methods. The proposed method provides a unified approach to evaluate the pipe's response to ground movements triggered by geohazards, such as landslides, ground heave and subsidence, tectonic fault, etc. The algorithm for the proposed method is straightforward and can be implemented in programming software packages without requiring solid expertise in structural mechanics. This method provides an alternative practical approach, which is acceptable for preliminary design, safety pre-screening, and extended studies such as reliability-based assessment.

Note that the proposed method and the validation finite element model are on the basis of the one-dimension beam model, which cannot be applicable for solving the complex spatial

behavior of the pipe cross-section like local buckling. Detailed finite element analysis, i.e., full 3D models, is still necessary to investigate the pipe strength required for comprehensive analysis.

Reference

[1] J.A. Mason, T.D. O'Rourke, Tensile behavior of steel pipelines with welded slip joints, in: Proceedings of the 2009 TCLEE Conference, Lifeline Earthquake Engineering in a Multihazard Environment, American Society of Civil Engineers (ASCE), Reston, 2009, pp. 831-841.

[2] J.A. Mason, T.D. O'Rourke, Compressive behavior of steel pipelines with welded slip joints, in: Proceedings of the 2009 TCLEE Conference, Lifeline Earthquake Engineering in a Multihazard Environment, American Society of Civil Engineers (ASCE), Reston, 2009, pp. 811-822.

[3] M.J. O'Rourke, X. Liu, Seismic design of buried and offshore pipelines, Buffalo, MCEER; 2012.

[4] D. Ha, T.H Abdoun, M.J. O'Rourke, M.D. Symans, T.D. O'Rourke, M.C. Palmer, H.E. Stewart, Buried high-density polyethylene pipelines subjected to normal and strike-slip faulting-a centrifuge investigation, Can. Geotech. J. 45 (2008) 1733-1742.

[5] M.J. O'Rourke, V. Gadicherla, T.H. Abdoun, Centrifuge modeling of PGD response of buried pipe, Earthq. Eng. 4 (2005) 69-73.

[6] F.R. Rofooei, H.H. Jalali, N.K. Attari, M. Alavi, Full-scale laboratory testing of buried pipelines subjected to permanent ground displacement caused by reverse faulting, in: Proceedings of the 15th World Conference on Earthquake Engineering, Lisboa, 2012, pp. 24-28.

[7] W. Feng, R. Huang, J. Liu, X. Xu, M. Luo, Large-scale field trial to explore landslide and pipeline interaction, Soils Found. 55 (2015) 1466-1473.

[8] N.M. Newmark, W.J. Hall, Pipeline design to resist large fault displacement, in: Proceedings of U.S. national conference on earthquake engineering, 1975. pp. 416-425.

[9] R.P. Kennedy, A.W. Chow, R.A. Williamson, Fault movement effects on buried oil pipeline, ASCE J. Transport. Eng. 103 (1977) 617-633.

[10] L.R.L. Wang, Y.A. Yeh, A refined seismic analysis and design of buried pipeline for fault movement, Earthq. Eng. Struct. Dyn. 13 (1985) 75-96.

[11] L.R.L. Wang, Y.A. Yeh, Seismic design of buried pipeline for fault movement effects, J. Press. Vessel. Technol. 108 (1986) 202-208.

[12] D.K. Karamitros, G.D. Bouckovalas, G.P. Kouretzis, Stress analysis of buried steel pipelines at strike-slip fault crossings, Soil Dyn. Earthq. Eng. 27 (2007) 200-211.

[13] D.K. Karamitros, G.D. Bouckovalas, G.P. Kouretzis, An analytical method for strength verification of buried steel pipelines at normal fault crossings, Soil Dyn. Earthq. Eng. 31(2011) 1452-1464.

[14] O.V. Trifonov, V.P. Cherniy, Elastoplastic stress strain analysis of buried steel pipelines subjected to fault displacements with account for service loads, Soil Dyn. Earthq. Eng. 33 (2012) 54-62.

[15] O.V. Trifonov, The effect of variation of soil conditions along the pipeline in the fault crossing zone, Soil Dyn. Earthq. Eng. 104 (2018) 437-448.

[16] F. Talebi, J. Kiyono, 2020. Introduction of the axial force terms to governing equation for buried pipeline subjected to strike-slip fault movements, Soil Dyn. Earthq. Eng. 133 106125.

[17] F. Talebi, J. Kiyono, A refined nonlinear analytical method for buried pipelines crossing strike‐slip faults. Earthquake Eng. Struct. Dyn. 50 (2021) 2915-2938.

[18] G.C. Sarvanis, S.A. Karamanos, Analytical model for the strain analysis of continuous buried pipelines in geohazard areas, Eng. Struct. 152 (2017) 57-69.

[19] Z. Hu, X. Ren, Q. Wang, R. Wang, R. Pan, Analytical method for the mechanical response of buried pipeline under the action of strike-slip faulting, Undergr. Space 7 (2022) 268-277.

[20] M.J. O'Rourke, X. Liu, R. Flores-Berrones, Steel pipe wrinkling due to longitudinal permanent ground deformation, KSCE J. Civ. Eng. 121 (1995) 443-451.

[21] N. Yoosef-Ghodsi, J. Zhou, D.W. Murray, A simplified model for evaluating strain demand in a pipeline subjected to longitudinal ground movement, in: International Pipeline Conference (IPC2008), American Society of Mechanical Engineers (ASME), Calgary, 2008, pp. 657-664

[22] U. Zahid, A. Godio, S. Mauro, 2020. An analytical procedure for modelling pipeline-landslide interaction in gas pipelines, J. Nat. Gas. Sci. Eng. 81, 103474.

[23]S. Takada, N. Hassani, K. Fukuda, A new proposal for simplified design of buried steel pipes crossing active faults, Earthquake Eng. Struct. Dyn. 30 (2001) 1243-1257.

[24] A. Liu, Y. Hu, F. Zhao, X. Li, S. Takada, L. Zhao, An equivalent-boundary method for the shell analysis of buried pipelines under fault movement, Acta. Seismol. Sin. 1 (2004) 150-156.

[25] O.V. Trifonov, 2015. Numerical stress-strain analysis of buried steel pipelines crossing active strike-slip faults with an emphasis on fault modeling aspects, J. Pipeline Syst. Eng. 6, 04014008.

[26] X. Liu, H. Zhang, Y. Han, M. Xia, W. Zheng. A semi-empirical model for peak strain prediction of buried X80 steel pipelines under compression and bending at strike-slip fault crossings, J. Nat. Gas Eng. 32 (2016) 465-475.

[27] X. Liu, H. Zhang, X. Gu, Y. Chen, M. Xia, K. Wu, Strain demand prediction method for buried X80 steel pipelines crossing oblique-reverse faults, Earthq. Struct. 12 (2017) 321-332.

[28] X. Liu, Q. Zheng, K. Wu, Y. Yang, Z. Zhao, H. Zhang, 2020. Development of a novel approach for strain demand prediction of pipes at fault crossings on the basis of multi-layer neural network driven by strain data, Eng. Struct. 214, 110685.

[29] SY/T 0450, 2004. Code for seismic design of oil and gas steel pipeline. The National Development and Reform Commission, Beijing, China.

[30] S.R. Dash, S.K. Jain, Guidelines for seismic design of buried pipelines, IITK-GSDMA Codes. 2007.

[31] A.W. Al-Khafaji, R. Jacobs, Excel Based Settlement of beams on elastic foundations with free-ends and arbitrary loading, in: E. Pellicer, J.M. Adam, V. Yepes, and S. Yazdani, editors, Resilient Structures and Sustainable Construction, Fargo: ISEC Press, 2017.

[32] Q. Zheng, L. Graf-Alexiou, Y. Li, N. Yoosef-Ghodsi, M. Fowler, M. Kainat, S. Adeeb, Strain demand of elastic pipes subjected to permanent ground displacements using the finite difference method, J. Pipeline. Sci. Eng. 1 (2021) 176-186.

[33] American Lifelines Alliance (ALA), Guidelines for the Design of Buried Steel Pipe, American Society of Civil Engineers, 2001.

[34] Dassault Systems Simulia Corporation, Abaqus, 2017.

CHAPTER 5: RELIABILITY ASSESSMENT OF PIPES SUBJECTED TO GROUND DISPLACEMENTS BASED ON A NOVEL METHODOLOGY FOR STRAIN DEMAND PREDICTIONS

This chapter is derived from the paper presented in a conference:

Q. Zheng, W. Qiu, Y. Li, N. Yoosef-Ghodsi, M. Fowler, M. Kainat, S. Adeeb, Reliability assessment of pipes subjected to ground displacements based on a novel methodology for strain demand predictions, in: Technology for Future and Ageing Pipelines, Great Southern Press, Gent, 2022.

Abstract

Long-distance pipelines are inevitably buried across geological zones potentially inducing permanent ground displacements. Under the effect of permanent ground displacements, the pipe material could potentially be subjected to large deleterious plastic strains that could precipitate failure. This paper aims to present a structural safety reliability assessment methodology for pipes subjected to ground displacements. To do this, a novel and comprehensive model for predicting the pipeline strain demand induced by ground displacements is proposed based on the finite difference method. A large set of nonlinear finite difference equations is established based on the nonlinear governing differential equations of the Euler-Bernoulli beam under the large deflections considering nonlinearities arising from geometrics, material response, and soil stiffness. The longitudinal strains along the pipe are then obtained solving the nonlinear equations. Subsequently, the strain-based limit state function can be established where the proposed model is built-in as the function for strain demand. For the sake of efficiency, the Weighted Monte Carlo simulation is employed to implement the reliability calculation, and the program is optimized by a

parallelization technique. The accuracy of the obtained probability of failure is validated comparing with the Monte Carlo simulation. The study indicates that the prediction model is a good alternative to calculate the pipes' response to ground-induced movements for a rough estimation. Plus, the proposed reliability calculation method is reliable and efficient, which is appropriate for the preliminary safety evaluation for the design of new pipelines or for risk pre-screening of existing pipelines.

5.1 Introduction

As a member in the lifeline infrastructure systems, pipelines play a vital role in the transmission of various gas and fluid substances. Generally, pipes are constructed underground to avoid the severe weather conditions, natural calamities, and several other forces that pipes may be exposed to when installed above ground. However, geohazards, e.g., geotechnical hazards including processes such as landslides, ground settlement and subsidence, and soil heave, and tectonic hazards like ground rupture and displacement, soil liquefaction, and lateral spreading, can potentially result in severe damage to underground structures. In general, the pipe is deformed due to the force exerted by the surrounding soils induced by ground displacements in geohazards. Therefore, investigations of the integrity and safety of pipelines buried in geohazard zones have witnessed growing interest among pipeline researchers and operators.

There have been countless studies on pipes' mechanical response to ground displacements since the pioneering study by Newmark and Hall [1] where an analytical model was introduced for calculating strains within a pipeline buried across a tectonic fault. This work [1] has been continued by various modifications [2][3] which aim to improve the applicability of the developed analytical models. Some published models [4][5][6][7][8] have been shown to be capable of predicting the pipes' response with high accuracy. The rapid development of computer engineering, however, inspires alternate numerical approaches such as the finite element approach, which is the most commonly-used way to attain pipes' response to external loads. A plethora of papers has appeared dealing with response analysis on buried pipes withstanding the ground

displacements based on finite element models. A wide range of models have been established towards different considerations on the element selection for the pipe, e.g., beam or shell elements [9], the constitutive modeling of soil, e.g., soil spring modeling [10] or solid-element soil modeling [11], the representation of pipe-soil interactions, e.g., resistance of soil springs [10] or contact surfaces specification [11], and the management on boundary conditions, e.g., actual or equivalent boundary conditions [12]. The experimental studies, usually conducted by small-scale tests based on the centrifuge machine [13][14], haven been performed to offer the validation data for the above-mentioned models.

In the real word, uncertainties exist in almost all engineering applications. The uncertainties of designing parameters are usually described by random variables characterized by probability distributions, which lead to uncertain mechanical response in pipes that is to be solved by reliability analysis. The pipeline industry has recently shown a keen interest in reliability-based assessment methods. As for the pipeline buried in the geohazard zones, most researchers pay more attention to the risk against ground shaking induced by seismic wave [15][16][17], which can be categorized into the semiology dynamic domain. While the damage due to ground shaking is associated with lower damage rates compared to ground displacements that can be triggered by geohazards. Zhou [18] analyzed the pressurized pipes under the ground displacement induced by slope instability, and the strain demand is estimated based on the model proposed by Yoosef-Ghodsi et al. [19] which unfortunately is only applicable for pipes deforming in the longitudinal direction. Utilizing a probabilistic fault displacement hazard analysis, Zheng et al. [20] assessed the reliability of the pipeline buried across Bo-A fault in China where the strain demand in the limit state function was represented by the trained BP neural network as developed by Liu et al. [21]. Nevertheless, the collection of strain demand dataset was time-consuming based on a large number of calculations by Abaqus.

This paper presents reliability assessment of pipes subjected to ground displacements due to geohazards. The strain demand, denoted by the maximum tensile and compressive strains along the pipe, is predicted by a novel and simple model proposed based on the finite difference method. The pipe is modelled as an Euler-Bernoulli beam, and a system of finite difference equations is constructed for each assigned node, in which the nonlinearity arising from the pipe material,

geometric deformation, and the pipe-soil contact are considered. The strain demand can be derived by solving the nonlinear system of equations. After validating the accuracy of the proposed method by finite element method using Abaqus, the developed strain demand model is employed as the function for strain demand in the limit state function, which is used in reliability analysis to describe the performance of the pipe. Subsequently, an innovative reliability method, Weighted Monte Carlo Simulation (WMCS) [22], is utilized to facilitate the reliability calculation for its high efficiency. It is worth noting that the code for strain demand prediction is parallelized for the loops in WMCS, which can highly enhance the calculation efficiency. The workability and applicability of the present reliability assessment is assessed based on study cases. The high computational efficiency makes it available for reference in the preliminary design and safety assessment of the pipe subjected to ground displacements.

5.2 Strain demand prediction model based on finite difference

The primary object of the model is to capture the pipes' deformation with ground displacement triggered by geohazards, e.g., landslide, liquefaction-induced lateral spreading, soil settlement and heave, etc. The pipe's deformation can be simply pictured as illustrated in Figure 5-1. For the sake of simplicity, the present paper only discusses the situation that the pipe deforms in the horizontal plane, e.g., the *x*-*y* plane in Figure 5-1. But the methodology proposed can be certainly applicable to ground displacements in the vertical plane, e.g., the *x*-*z* plane in Figure 5-1.

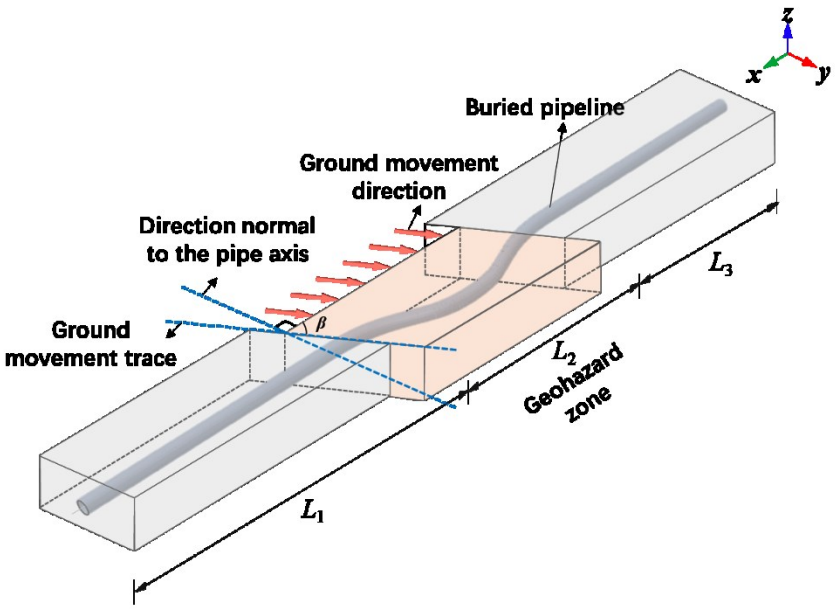

Figure 5-1: Schematic representation of the pipe subjected to the ground displacement

The finite difference method is widely used to solve (partial) differential equations. In the finite difference method, the continuum instance is replaced by the discrete nodes in the space of the instance, and a set of discrete equations, named finite difference equations, can be established towards those nodes to represent the status of the instance. The finite difference method is typically defined on a regular grid and this fact can be used for very efficient solution methods. In this study, the finite difference method is applied to the pipe which can be seen as a regular shaped instance in one dimension, and the finite difference equations are developed as functions of pipe displacements (the axial displacement u and lateral displacement v) of each node.

5.2.1 Governing equations

In the present paper, the pipeline is simulated as an Euler-Bernoulli beam considering large deformation. The governing equations are shown in Eq. (5-1) based on the sign conventions in Figure 5-2.

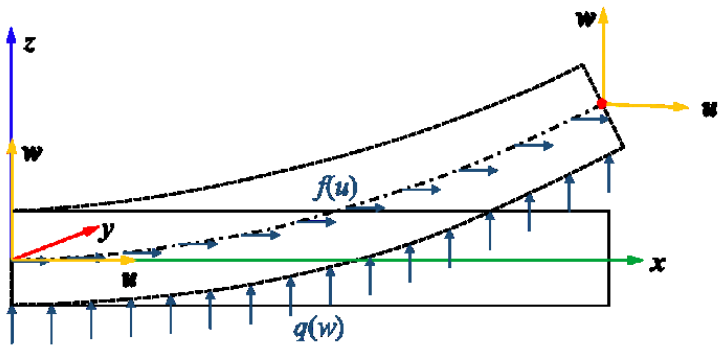

Figure 5-2: Euler-Bernoulli beam under deformation

$$\begin{cases} \dfrac{dN}{dx} + f(u) = 0 \\ \dfrac{d^2M}{dx^2} - \dfrac{d}{dx}(N\dfrac{dw}{dx}) - q(w) = 0 \end{cases} \tag{5-1}$$

where N and M are the axial internal force and internal bending moment on the cross section of the pipe respectively; u and w represent the axial and lateral deformation of the pipe respectively; $f(u)$ and $q(w)$ are externally distributed loads in the longitudinal and lateral directions.

5.2.2 Representations of axial force N and bending moment M

According to the assumption that "plane sections remain plane" in Euler-Bernoulli beam theory, the stress and strain distributions in the cross section can be depicted as shown in Figure 5-3.

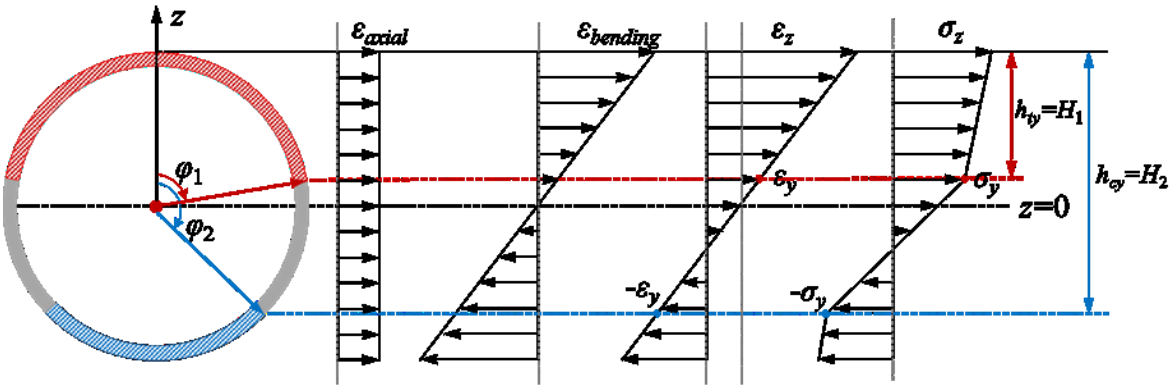

Figure 5-3: Strain and stress distribution on the cross section of the pipe

The axial strain ε_{axial} is uniformly distributed on the pipe cross section, while the bending strain only accounts for the behavior induced by pure bending moment (Figure 5-3). The longitudinal strain ε_z is the summation of the axial and bending strain, and the stress distribution is given based on the stress-strain curve of the pipe material. In the present paper, the stress-strain curve is assumed to follow a bilinear relationship for pipe steel with the yielding stress σ_y corresponding to the yielding strain ε_y. The distance from the pipe top to the tensile yielding position is denoted as h_{ty}, and the distance to the compressive yielding position is h_{cy}.

The expression of the longitudinal strain ε_z can be written as Eq. (5-2) based on the definition of the Lagrangian Green strain the large deformation theory ("Euler-Bernoulli beam theory", 2021).

$$\varepsilon_z = \varepsilon_{axial} + \varepsilon_{bending} = u' + \frac{1}{2}w'^2 + zw'' \tag{5-2}$$

where z denotes the position along the pipe cross section; $(X)'$ and $(X)''$ represent the first and second derivatives of X to the pipe axial direction.

Hence, the strain in the extreme fibers, the strain at the top of the pipe ε_{top} and the strain at the bottom of the pipe ε_{bot} can be written as Eqs. (5-3) and (5-4) respectively.

$$\varepsilon_{top} = u' + \frac{1}{2}w'^2 + \left(\frac{OD}{2}\right)w'' \tag{5-3}$$

$$\varepsilon_{bot} = u' + \frac{1}{2}w'^2 - \left(\frac{OD}{2}\right)w'' \tag{5-4}$$

where *OD* is the outer diameter. h_{ty} and h_{cy} can be geometrically derived as Eqs. (5-5) and (5-6), respectively.

$$h_{ty} = \frac{\varepsilon_{top} - \varepsilon_y}{\varepsilon_{top} - \varepsilon_{bot}} OD = \frac{2u' + w'^2 + w''\bullet}{2w''} \tag{5-5}$$

$$h_{cy} = \frac{\varepsilon_{top} + \varepsilon_y}{\varepsilon_{top} - \varepsilon_{bot}} OD = \frac{2u' + w'^2 + w''\bullet}{2w''} \tag{5-6}$$

It is worth noting that Figure 5-3 only shows the situation that the pipe top is in tension and the pipe bottom is in compression. To generally include all the potential schemes, two auxiliary variables H_1 and H_2 are used to represent the relative position of h_{ty} and h_{cy}, which $H_1 = \max\left(h_{ty}, h_{cy}\right)$ and $H_2 = \min\left(h_{ty}, h_{cy}\right)$. The corresponding intersection angles to ϕ_1 and ϕ_2 can be defined as Eq. (5-7).

$$\phi_{1,2} = \begin{cases} 0 & , \quad H_{1,2} \le 0 \\ \arccos\left(\dfrac{OD - 2H_{1,2}}{OD}\right) & , \quad 0 < H_{1,2} < OD \\ \pi & , \quad H_{1,2} \ge OD \end{cases} \tag{5-7}$$

Rewriting the equations of the strains in the cylinder coordinate, the strain ε_θ can be written as Eq. (5-8), and the corresponding stress σ_θ can be expressed as Eq. (5-9) considering the bilinear stress-strain relationship.

$$\varepsilon_\theta = u' + \frac{w'^2}{2} + w''\bullet \left(\frac{OD}{2}\right) \cos\theta \tag{5-8}$$

$$\sigma_\theta = \begin{cases} IE\varepsilon_y + E_h\left(\varepsilon_\theta - I\varepsilon_y\right) & , \quad 0 \le \theta \le \phi_1 \\ E\varepsilon_\theta & , \quad \phi_1 < \theta < \phi_2 \\ -IE\varepsilon_y + E_h\left(\varepsilon_\theta + I\varepsilon_y\right) & , \quad \phi_2 \le \theta \le \pi \end{cases} \tag{5-9}$$

where E is the Young's modulus; E_h is the hardening modulus; I is the sign function indicating that the relative position between tensile yield point and compressive yield point, which is defined as $I = sign\left(h_{cy} - h_{ty}\right)$.

Based on the definition of internal force N and bending moment M, N and M can be derived as piecewise functions as Eqs. (5-10) to (5-13).

When $w'' = 0$,

$$N = \int_A \sigma_z dA = \begin{cases} \left(E\varepsilon_y + E_h\left(\varepsilon_{axial} - \varepsilon_y\right)\right)A & , \quad \varepsilon_{axial} > \varepsilon_y \\ E\varepsilon_{axial}A & , \quad -\varepsilon_y \le \varepsilon_{axial} \le \varepsilon_y \\ \left(-E\varepsilon_y + E_h\left(\varepsilon_{axial} + \varepsilon_y\right)\right)A & , \quad \varepsilon_{axial} < -\varepsilon_y \end{cases} \tag{5-10}$$

$$M = 0 \tag{5-11}$$

When $w'' \neq 0$,

$$\begin{aligned} N &= 2\int_0^\pi \sigma_\theta \left(\frac{OD - WT}{2}\right) WT d\theta \\ &= \left(OD - WT\right)WT \begin{pmatrix} \varepsilon_{axial}\left(E_h\left(\pi + \phi_1 - \phi_2\right) - E\left(\phi_1 - \phi_2\right)\right) + I\varepsilon_y\left(E - E_h\right) \\ \left(\phi_1 + \phi_2 - \pi\right) - \varepsilon_{b\max}\left(E - E_h\right)\left(\sin\phi_1 - \sin\phi_2\right) \end{pmatrix} \end{aligned} \tag{5-12}$$

$$\begin{aligned} M &= 2\int_0^\pi \sigma_\theta \left(\frac{OD - WT}{2}\right)^2 WT\cos\theta d\theta \\ &= \frac{1}{4}\left(OD - WT\right)^2 WT \begin{pmatrix} \varepsilon_{b\max}\left(E_h\left(\pi + \phi_1 - \phi_2\right) - E\left(\phi_1 - \phi_2\right)\right) + \\ \left(E - E_h\right)\begin{pmatrix} -\left(2\left(\varepsilon_{axial} - I\varepsilon_y\right) + \varepsilon_{b\max}\cos\phi_1\right)\sin\phi_1 \\ +\left(2\left(\varepsilon_{axial} + I\varepsilon_y\right) + \varepsilon_{b\max}\cos\phi_2\right)\sin\phi_2 \end{pmatrix} \end{pmatrix} \end{aligned} \tag{5-13}$$

where WT is the wall thickness of the pipe.

5.2.3 Interaction between pipe and soil

This study adopts the soil springs recommended by ALA-2001 Guidelines [23] where the pipe-soil interactions are modeled as bilinear curves as shown in Figure 5-4. T_u, P_u, Q_u and Q_d respectively represent the soil spring resistances in the axial direction, the lateral direction, the vertical upward and the vertical downward directions in N/m, and Δt, Δp, Δq_u and Δq_d are the corresponding displacements to T_u, P_u, Q_u and Q_d, in m. Those parameters can be calculated by the formulations given in ALA-2001 Guidelines based on the soil properties and burial information of the pipe.

(a) Axial (b) Lateral (c) Vertical

Figure 5-4: Soil spring properties in (a) axial, (b) lateral, and (c) vertical directions

5.2.4 Calculation procedure for strain demand

To solve the problem based on the finite difference method, the terms of derivatives in the governing equations, e.g., $\frac{dN}{dx}$, $\frac{d^2M}{dx^2}$, and $\frac{d}{dx}(N\frac{dw}{dx})$, should be written using finite differences. Since the internal force N and bending moment M are functions of u and w, the finite difference equations are composed of unknown of u and w of each node. The calculation flow is elaborated as follows:

Step 1: meshing the pipe by defining nodes in the axial direction.

Step 2: assigning the initial guess (usually set as 0) of the pipe's deformation at each node (u_i and w_i).

Step 3: calculating derivatives of u and w based on finite difference method at each node (u'_i, w'_i and w''_i).

Step 4: calculating the axial force N and bending moment M at each node (N_i and M_i).

Step 5: representing the derivative items in the governing equation based on finite difference strategy at each node (N'_i, M''_i and $(N_i w'_i)'$).

Step 6: replacing the derivative items in the governing equation by those obtained in ***Step 4***.

Step 7: constructing the finite difference equations based on the formulations obtained in ***Step 6*** together with boundary conditions at each node (Eq_i).

Step 8: using a solver to get the convergent solutions of u_i and w_i.

Step 9: calculating the longitudinal strain along the pipe based on Eq. (5-2), and recording the tensile strain demand ε_t (the maximum positive strain value) and the compressive strain demand ε_c (the minimum negative strain value).

5.3 Reliability assessment

5.3.1 Limit state functions

As the basic format of the safety margin represented by the difference between the structural resistance and demand, the limit state function is established based on the strain as shown in Eq. (5-14).

$$\begin{cases} g_t(x) = \varepsilon_{rt} - \varepsilon_t(x) \\ g_c(x) = \varepsilon_{rc} - \left|\varepsilon_c(x)\right| \end{cases} \tag{5-14}$$

where g_t is the safety margin regarding tension; ε_{rt} and ε_t respectively denote the tensile strain capacity and demand. The formulation for the situation with respect to compression is in the same format, and the subscript "*c*" denotes the compressive strain. It should be mentioned that since the strain demands, ε_t and ε_c, are calculated based on the model presented in section 5.2, so the ε_t is always positive and ε_c is negative. In that case, the absolute sign is applied for the compressive

strain demand ε_c because strain capacity is employed as positive numbers in this study. Moreover, the pipe is considered to be in the safe domain when both g_t and g_c are simultaneously higher than 0, which defines a series-system reliability problem. Otherwise, the pipe is in the failure domain.

5.3.2 Weighted Monte Carlo Simulation

Monte Carlo Simulation is acknowledged as the most applicable method for reliability calculation, and it can give sufficiently reliable results by sampling the design space based on the full stochastic characterization of random variables. However, the Monte Carlo Simulation method requires a large number of samples to achieve an accurate result especially when the probability of failure (PoF) very small and therefore, in these situations the calculation will be inefficient.

In this study, the Weighted Monte Carlo simulation is employed to overcome the inefficiency related to Monte Carlo Simulation. In this method, the weight indices of each sample are introduced and the expression of PoF is expressed as Eq. (5-15). Its accuracy and efficiency have been well validated through different benchmark problems [22], and it has been well practiced in Zheng et al. [24] to achieve PoFs of pipes in different limit states.

$$\mathrm{PoF} = \frac{\sum_{i=1}^{m} I(\boldsymbol{x_i})\bullet}{\sum_{i=1}^{m} W_i(\boldsymbol{x_i})} \tag{5-15}$$

where $I(x_i)$ is the indicator function of the sample set $\boldsymbol{x_i}$; $W_i(\boldsymbol{x_i})$ denotes the weight of the *i*th sample set, which is defined as the product of probabilities density function evaluated as the sampled value for each random variable; *m* represents the sample size. The background theory and computational scheme for this method are elaborated in Rashki et al. [22] and thus skipped in this paper.

5.3.3 Computational optimization

Generally, implementing stochastic simulation using random samples within loops is supposed to be avoided as this will make the computation time-consuming. However, since the strain demand model developed in section 5.2 can only pass the result for one sample case at a time, it is inevitable to utilize loops for implementing the code of Monte Carlo simulation or Weighted Monte Carlo simulation. Solving a large size of nonlinear equations in the strain demand model is not a fast process compared with over-simplified analytical models, and therefore the reliability calculation will be prohibitively expensive for situations requiring a large number of samples.

In this study, a computational optimization is employed to obtain the best performance from code. The code is parallelized based on the function of ***jit*** and ***njit*** in the Numba library for Python, which enables a Numba transformation pass that attempts to automatically parallelize and perform other optimizations on a function. This scheme can be well supported for explicit parallel loops, and thus is used for implementing the reliability calculation in this paper with highly improved efficiency.

5.4 Case study

This study concerns a 508-mm-diameter pipeline with wall thickness equal to 7.14 mm, subjected to the ground displacements in horizontal plane, with cohesionless soil conditions (see Figure 5-1). The middle span involved in the geohazard is set as L_2 = 10 m with 11 nodes, and the two segments connected to the middle span are determined as $L_1 = L_3$ = 100 m with 51 nodes. The fixed boundary condition is applied to pipe ends. The pipe is made with X65 steel with a yield stress of σ_y = 450 MPa and the Young's Modulus is E = 199 GPa. The ultimate strain and stress are respectively adopted as ε_t = 3% and σ_t = 663 MPa based on Vazouras et al. [25]. Since the pipe is under the load in the horizontal plane, the pipe-soil interaction in the vertical direction can be ignored. The axial soil spring resistance is set as T_u = 14 kN/m with a Δt = 0.265 m, and the lateral soil spring is P_u = 204 kN/m with a Δp = 0.029 m. A parametric study on the reliability is

performed with respect to different combinations of ground displacement d and pipe-ground intersection angle β (30°, 60° and 90°, see Figure 5-1). The tensile and compressive strain capacity are set as 2% and 1% respectively [26]. The statistical data of the random variables considered is tabulated in Table 5-1.

Table 5-1: Stochastic properties of basic random variables

Random Variable	Distribution	Unit	Mean	COV	Source
Pipe diameter	Normal	mm	D_n	0.0006	Zimmerman et al. [27]
Wall thickness	Normal	mm	$1.01t_n$	0.01	Zimmerman et al. [27]
Yield strength	Normal	MPa	1.10 SMYS	0.036	Jiao et al. [28]
Tensile strength	Normal	MPa	1.12 SMTS	0.035	Jiao et al. [28]
Young's Modulus	Normal	MPa	2.10×10^5	0.04	Sotberg et al. [29]

Note: D_n is the nominal diameter; t_n is the nominal wall thickness; SMYS denotes the specified minimum yield strength; SMTS represents the specified minimum tensile strength.

Figure 5-5 shows the comparison of the PoFs obtained based on the Monte Carlo simulation and the Weighted Monte Carlo simulation. It can be seen that the pipe is in the most vulnerable situation when the ground moves perpendicularly to its axis. The critical ground displacements at intersection angles 30°, 60°, and 90° are 1.19 m, 0.67 m, and 0.59m respectively. When the ground displacement approaches the critical value, the PoF increases abruptly. In addition, the results from Weighted Monte Carlo simulation are accurate compared with those obtained from the Monte Carlo simulation. Furthermore, the Weighted Monte Carlo can reach a lower level of PoF, e.g., 10^{-6}, 10^{-7}, 10^{-8}, based on its sample size 10,000. In that case, users can reach the precision with a smaller number of samples, which is supposed to use more samples based on the Monte Carlo simulation. Each case takes about 15 mins in a computer configurated by an Intel® Core™ i7-8750H CPU @2.20GHz and a memory of 8 GB.

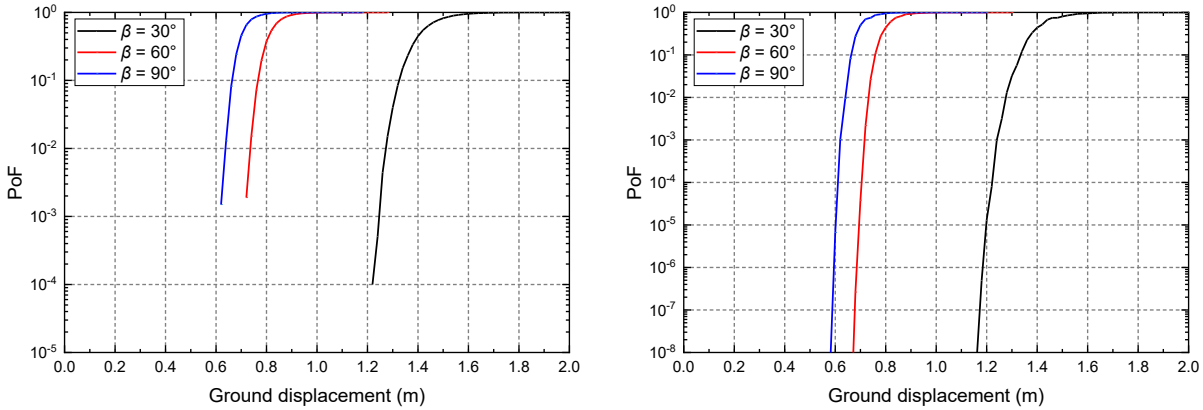

(a) Monte Carlo simulation (b) Weighted Monte Carlo simulation

Figure 5-5: PoF versus ground displacements based on (a) Monte Carlo simulation and (b) Weighted Monte Carlo simulation

5.5 Chapter conclusions

This paper proposed a methodology to evaluate the reliability of pipes subjected to ground displacements where the strain demand is estimated based on a novel model developed based on finite difference method. Considering the nonlinearities arising from geometry due to large deformation, pipe material, and soil stiffness, the strain demand is obtained by solving a large set of nonlinear equations. An effective reliability analysis method, named Weighted Monte Carlo simulation, is utilized to facilitate the calculation of probabilities of failure (PoFs). The proposed approach is applied to an assumed study case where the parameters are given based on an example case study. For the studied case, the results show that the pipe is more vulnerable with the increase of the angle of intersection between the moving ground and the pipe longitudinal axis. The probability of failure rises sharply at the onset of the critical ground displacement. Moreover, the accuracy of the Weighted Monte Carlo simulation is validated in comparison with the Monte Carlo simulation, and a lower level of probability of failure can be reached with a smaller sample size, which demonstrates a higher efficiency of the strategy. The proposed method in the present paper is suitable for reliability estimation used for preliminary design and safety pre-screening.

Reference

[1] N.M. Newmark, W.J. Hall, Pipeline design to resist large fault displacement, in: Proceedings of U.S. National Conference on Earthquake Engineering, Earthquake Engineering Research Institute, Michigan, 1975, pp. 416-25.

[2] R.P. Kennedy, A.W. Chow, R.A. Williamson, Fault movement effects on buried oil pipeline, ASCE J. Transport. Eng. 103 (1977) 617-33.

[3] L.R.L. Wang, Y.A. Yeh, A refined seismic analysis and design of buried pipeline for fault movement, Earthq. Eng. Struct. Dyn. 13 (1985) 75-96.

[4] D.K. Karamitros, G.D. Bouckovalas, G.P. Kouretzis, Stress analysis of buried steel pipelines at strike-slip fault crossings, Soil. Dyn. Earthq. Eng. 27 (2007) 200-11.

[5] D.K. Karamitros, G.D. Bouckovalas, G.P. Kouretzis, V. Gkesouli, An analytical method for strength verification of buried steel pipelines at normal fault crossings, Soil Dyn. Earthq. Eng. 31 (2011) 1452-1464.

[6] O.V. Trifonov, V.P. Cherniy, Elastoplastic stress strain analysis of buried steel pipelines subjected to fault displacements with account for service loads, Soil. Dyn. Earthq. Eng. 33 (2012) 54-62.

[7] G.C. Sarvanis, S.A. Karamanos, Analytical model for the strain analysis of continuous buried pipelines in geohazard areas, Eng. Struct. 152 (2017) 57-69.

[8] X. Liu, H. Zhang, M. Xia, J. Liu, Q. Zheng, An improved analytical strain analysis method for buried steel pipelines subjected to abrupt permanent ground displacement, in: International Pipeline Conference (IPC2020), American Society of Mechanical Engineers (ASME), Calgary, 2021, pp. V002T06A012.

[9] S. Takada, N. Hassani, K. Fukuda, A new proposal for simplified design of buried steel pipes crossing active faults, Earthquake Eng. Struct. Dyn. 30 (2001) 1243-1257.

[10] X. Liu, H. Zhang, Y. Han, M. Xia, W. Zheng. A semi-empirical model for peak strain prediction of buried X80 steel pipelines under compression and bending at strike-slip fault crossings, J. Nat. Gas Eng. 32 (2016) 465-475.

[11] K. Gawande, R. Kiran, H.P. Cherukuri, A numerical study of the response of buried steel pipelines undergoing strike-slip fault, Eng. Fail. Anal. 102 (2019) 203-218.

[12] A. Liu, Y. Hu, F. Zhao, X. Li, S. Takada, L. Zhao, An equivalent-boundary method for the shell analysis of buried pipelines under fault movement, Acta. Seismol. Sin. 1 (2004) 150-156.

[13] M.J. O'Rourke, V. Gadicherla, T.H. Abdoun, Centrifuge modeling of PGD response of buried pipe, Earthq. Eng. 4 (2005) 69-73.

[14] D. Ha, T.H Abdoun, M.J. O'Rourke, M.D. Symans, T.D. O'Rourke, M.C. Palmer, H.E. Stewart, Buried high-density polyethylene pipelines subjected to normal and strike-slip faulting-a centrifuge investigation, Can. Geotech. J. 45 (2008) 1733-1742.

[15] A.U. Ebenuwa, K.F. Tee, 2019. Reliability estimation of buried steel pipes subjected to seismic effect, Transp. Geotech. 20, 100242.

[16] V. Jahangiri, H. Shakib, Reliability-based seismic evaluation of buried pipelines subjected to earthquake-induced transient ground motions, Bull. Earthq. Eng. 18 (2020) 3603-3627.

[17] S. Fan, X. Yan, Strain design of long pipeline crossing fault under seismic loading, China Pet. Mach. 43 (2015) 114-118.

[18] W. Zhou, Reliability of pressurised pipelines subjected to longitudinal ground movement, Struct. Infrastruct. Eng. 8 (2012) 1123-1135.

[19] N. Yoosef-Ghodsi, J. Zhou, D.W. Murray, A simplified model for evaluating strain demand in a pipeline subjected to longitudinal ground movement, in: International Pipeline Conference (IPC2008), American Society of Mechanical Engineers (ASME), Calgary, 2008, pp. 657-664.

[20] Q. Zheng, X. Liu, H. Zhang, X. Gu, M. Fang, L. Wang, S. Adeeb, 2021. Reliability evaluation method for pipes buried in fault areas based on the probabilistic fault displacement hazard analysis, J. Nat. Gas Eng. 85, 103698.

[21] X. Liu, H. Zhang, M. Xia, J. Liu, Q. Zheng, An improved analytical strain analysis method for buried steel pipelines subjected to abrupt permanent ground displacement, in: International Pipeline Conference (IPC2020), American Society of Mechanical Engineers (ASME), Calgary, 2020, pp. V002T06A012.

[22] M. Rashki, M. Miri, M.A. Moghaddam, A new efficient simulation method to approximate the probability of failure and most probable point, Struct. Saf. 39 (2012) 22-29.

[23] American Lifelines Alliance (ALA), Guidelines for the Design of Buried Steel Pipe, American Society of Civil Engineers, 2001.

[24] Q. Zheng, A. K. Abdelmoety, Y. Li, M. Kainat, N. Yoosef-Ghodsi, S. Adeeb, 2021. Reliability analysis of intact and defected pipes for internal pressure related limit states specified in CSA Z622: 19, Int. J. Press. Vessels Pip. 192, 104411.

[25] P. Vazouras, S.A. Karamanos, P. Dakoulas, Finite element analysis of buried steel pipelines under strike-slip fault displacements, Soil Dyn. Earthq. Eng. 30 (2010) 1361-1376.

[26] Q. Zheng, X. Liu, H. Zhang, S. Adeeb, Reliability-Based Assessment Method of Buried Pipeline at Fault Crossings, in: International Pipeline Conference (IPC2020), American Society of Mechanical Engineers (ASME), Calgary, 2020, pp. V002T07A019.

[27] T.J.E. Zimmerman, A. Cosham, P. Hopkins, N. Sanderson, Can limit states design be used to design a pipeline above 80% SMYS?, in: 17th International Conference on Offshore Mechanics and Arctic Engineering (OMAE 1998), Lisbon, 1998.

[28] G. Jiao, T. Sotberg, R. Igland, SUPERB 2M statistical data-basic uncertainty measures for reliability analysis of offshore pipelines, SUPERB project report, No. STF70 F95212, 1995.

[29] T. Sotberg, B.J. Leira, Reliability-based pipeline design and code calibration, in: Proceedings of the 13th International Conference on Offshore Mechanics and Arctic Engineering, OMAE, Houston, 1994, pp. 940230.

CHAPTER 6: DEVELOPMENT OF AN ONLINE CALCULATION TOOL FOR SAFETY EVALUATION OF PIPES SUBJECTED TO GROUND MOVEMENTS

This chapter is derived from the paper presented in a conference:

Q. Zheng, W. Qiu, N. Ergezinger, Y. Li, N. Yoosef-Ghodsi, M. Fowler, S. Adeeb, Development of an online calculation tool for safety evaluation of pipes subjected to ground movements, in: International Pipeline Conference (IPC2022), American Society of Mechanical Engineers (ASME), Calgary, 2022, pp. V001T06A004.

Abstract

Underground pipelines are inevitably installed in unstable geohazard areas associated with the possible development of significant ground deformations. Under ground movement, excessive strains can be generated in the pipe wall, which poses a threat to pipeline integrity. This study aims to develop an industry-oriented calculation tool for safety evaluation of pipes subjected to ground movements induced by a variety of nature and construction-related hazards. The tool, comprised of deterministic and reliability-based analyses, is designed within MecSimCalc which is an innovative online platform for creating and sharing web-based Apps for individuals and groups. Calculation flow behind the tool is developed according to a novel method proposed based upon the finite difference method (FDM). Given grid nodes along the pipe, a large set of simultaneous finite-difference equations are constructed based on nonlinear governing differential equations of the Euler-Bernoulli beam under large deflections. The nonlinearities arising from pipe material, pipe-soil interaction, and geometry of the pipe are considered within the model. As unknowns of the finite-difference equations, the axial and lateral displacement of the pipe at each grid node can

be obtained using nonlinear equation solvers. This method is utilized to predict the strain demand in the limit state function for reliability-based assessment. Applying stochastic properties for each basic parameter, the probability of failure can be calculated using Monte Carlo Simulation. Meanwhile, the program is compiled using Numba in Python and then optimized by the parallelization technique to enhance computational efficiency.

Keywords: pipeline; finite element method; finite difference method; geohazard; strain demand; reliability

List of Symbols

A = Cross-sectional area of pipes
D = Outer diameter of pipes
E = Young's modulus
E_p = Strain hardening slope
I = Area moment of inertia
I_s = Signum function of h_{cy} - h_{ty}
M = Internal bending moment
N = Internal axial force
O = Imperfection of ovality
P_{int} = Internal pressure
P_u = Lateral soil resistance
Q_d = Vertical upward soil resistance
Q_u = Vertical downward soil resistance
T_u = Axial soil resistance
H_1 = Lower value between h_{cy} and h_{ty}
H_2 = Higher value between h_{cy} and h_{ty}
U = Axial ground movement
V = Lateral ground movement

a = Flaw height

c = Half of the flaw length

e = Additional global strain

$f(\cdot)$ = External longitudinal load per unit length of pipe

g = Limit state function

$q(\cdot)$ = External lateral load per unit length of pipe

h_{cy} = Vertical coordinate from the pipe top to the compressive yielding point

h_m = Girth weld high-low misalignment

h_{ty} = Vertical coordinate from the pipe top to the tensile yielding point

i = Identity of grid points

n = Total number of grid points

t = Wall thickness of pipes

u = Axial displacement of pipes

uEL = Pipe uniform elongation

v = Lateral displacement of pipes

z = Vertical position in the z-coordinate

Δp = Yield displacement corresponding to P_u

Δq_d = Yield displacement corresponding to Q_d

Δq_u = Yield displacement corresponding to Q_u

Δt = Yield displacement corresponding to T_u

δ_A = Girth weld apparent CTOD toughness

ε_{axial} = Axial strain

$\varepsilon_{bending}$ = Component of longitudinal strain due to bending

ε_{bottom} = Membrane longitudinal strain on the pipe bottom

ε_l = Longitudinal strain

ε_{top} = Membrane longitudinal strain on the pipe top

ε_y = Pipe yield strain

ε_c^C = Compressive strain capacity

ε_c^D = Compressive strain demand

ε_t^C = Tensile strain capacity

ε_t^D = Tensile strain demand

ε_c^{buckle} = Buckling strain capacity

θ = Polar angle in the polar coordinate system

σ_h = Hoop stress on the pipe

σ_l = Longitudinal stress

σ_u = Pipe ultimate tensile strength

σ_y = Pipe yield stress

σ_u^W = Weld metal tensile strength

φ_1 = Angle from the polar axis to tensile yield point

φ_2 = Angle from the polar axis to compressive yield point

λ_{seg} = Interval distance between two adjacent grid points within a specific pipe

Glossary of Terms

CoV = Coefficient of Variation

CVN = Charpy V-Notch Toughness

FDM = Finite Difference Method

FEM = Finite Element Method

LB = Lower Bound

PoF = Probability of Failure

SD = Standard Deviation

UP = Upper Bound

6.1 Introduction

As a critical member of infrastructural lifelines, pipelines fulfill a vital role in energy delivery; networks of large transmission pipelines are akin to energy highways. Pipelines are generally constructed underground and extend over vast distances transporting great amounts of crude oil and natural gas from often-remote locations to the populated areas where the products are needed. Due to natural restrictions, long-distance pipelines are inevitably buried across unstable geohazard areas. In Canada, pipelines are exposed to a wide range of geotechnical hazards (ground movement hazards), e.g., landslide, creep slope, frost heave, and thaw settlement [1].

Under ground movement, the pipe material is potentially subjected to excessive strains that could precipitate failure, which may cause catastrophic consequences including environmental effects and disruptions to essential services for human needs. It is therefore imperative to conduct the safety evaluation on pipelines undergoing ground movements.

To assess the pipeline fitness for service under the ground-induced displacement, the most commonly-used approach is to compare the resulting strain demand with the allowable strain capacity, which is a traditionally deterministic method. Two types of strain capacity, i.e., tensile and compressive strain capacity, are respectively investigated regarding tensile rupture at girth welds and local buckling. To date, multiple models have been developed and widely recognized by the pipeline industry, such as PRCI-CRES [2] and ExxonMobil [3] equations for estimating tensile strain capacities; UoA [4], C-FER [5], and CRES [6] equations for predicting compressive strain capacities.

To obtain the strain demand induced by ground movements, generally, a sophisticated calculation based on analytical studies or numerical modeling is required with various considerations on the pipeline modelling, material nonlinearity, and characterization of pipe-soil interaction. Newmark and Hall [7] pioneered this study by introducing an analytical model where the pipe was simplified as a cable under a tectonic fault. This study has been further developed with various modifications, e.g., consideration of transverse soil loads [8], elaborate modelling of the pipe in different locations [9][10], and refinement of the pipe's behavior near the fault trace [11], which aim to improve robustness and expand the applicable range of analytical models. Some published models, such as Karamitros et al. [12], Trifonov and Vladimir [13], Sarvanis [14], and Liu et al. [15], are capable of predicting strain demands with high accuracy against FEA. However, most of analytical models are implemented with complexity of algorithm programming especially for those where multiple enhancements are required for achieving more reliable results. Numerical simulations gradually become the alternative to analyze structural reactions to exerting loads with rapid development of computer engineering. Numerous models have been established based on finite element method (FEM). The existing models, typically, were constructed with three critical concerns: element selection for pipe, constitutive modeling of soil, and management of boundary conditions. Takada et al. [16] developed a hybrid model of pipes withstanding fault displacement

where shell and beam elements were respectively utilized to simulate pipe segments near and far from the fault trace, which was an inventive strategy to balance predictive resolution and computational efficiency. Gawande et al. [17] simulated the soil as solid blocks, and the force was transferred to the pipe through the surface contact between pipe and soil. To enhance computational efficiency, it is recommended to employ soil springs to represent the pipe-soil interaction [18]. Additionally, the model proposed by Liu et al. [19] considers equivalent boundary conditions for decreasing computational cost. For the same purpose, Liu et al. [19] reduced the length of pipe by proposing equivalent boundary conditions to replace the effect from the two pipe segments at the far ends.

Reliability-based assessment recognizes explicitly the variability of both loads and resistances. It is an embodiment of probabilistic method. Provided that sufficient statistical data are available (usually provided by the industry-related codes or field inspections), structural adequacy can be quantified by reliability index or probability of failure (PoF), which is compared to the specific reliability target or allowable probability of failure. Reports of reliability-based assessment on pipes subjected to ground movements are scarce in the literature. Zhou [20] analyzed pressurized pipes under ground movement due to slope instability where the soil force was only applied to the longitudinal direction, and the strain demand was estimated based on the model proposed by Yoosef-Ghodsi et al. [21]. Utilizing a probabilistic fault displacement hazard analysis, Zheng et al. [22] assessed the reliability of the pipeline buried across Bo-A fault in China where the strain demand in the limit state function was described by a surrogate based on the trained back propagation neural network as developed by Liu et al. [23]. Nevertheless, the collection of strain demand datasets was time-consuming based on a large number of calculations by ABAQUS®.

With its potentially wide range of applications, an integrated calculation tool would be highly welcomed by the pipeline industry. To the best of the authors' knowledge, such tools or Apps specifically used for safety assessment of pipes buried across geohazard zones rarely exist in Canadian pipeline industry. To this end, this paper aims to bridge the gap by establishing the calculator-like tool to assess the safety of pipes subjected to ground movement incorporating both the deterministic and probabilistic analysis. Firstly, a novel strain demand prediction model is

developed using the finite difference method (FDM), which extends the research conducted by Zheng et al. [24] with further investigation on the pipe material nonlinearity. In the module of reliability-based assessment, the developed strain demand model is employed as the term of strain demand in the limit state function. Subsequently, the probability of failure is calculated using Monte Carlo Simulation. It is worth noting that computational techniques including parallelization and compiling are employed to optimize the calculation speed of developed programs. Finally, the developed programs are deployed on the platform of MecSimCalc [26] which is a website for creating and sharing online python Apps.

6.2 FDM-based strain demand prediction model

The general idea of the model development stems from the prior work performed by Zheng et al. [24] where the FDM is initially used to analyze pipes' behavior under displacement-based loads. The primary function of this model is to predict the pipe's response under ground movement. The generic layout of the deformed pipe is depicted in Figure 6-1 where the pipeline is buried across a geohazard where the middle segment is within moving ground such as a moving slope, landslide, or liquefaction-induced lateral spreading in which the induced ground movement is shown in the horizontal plane. But one should bear in mind that the proposed method is applicable to a wide range of geohazards, such as geotechnical activities of general soil settlement, frost heave and thaw settlement in which the displacement happens in the vertical plane, and tectonic faults where only one ground discontinuity is considered.

FDM is widely used for approximating solutions to differential equations. Specifically, it finds a function (or some discrete approximation to this function) that satisfies a given relationship between derivatives on some given region of space and/or time, along with boundary conditions at the edges of this domain [25]. Generally, when there is a complicated problem and an analytic formula cannot be found for the solution, FDM can proceed by replacing the derivatives in the differential equations with finite difference approximations. This generates a large system of algebraic equations to be solved in lieu of the differential equation. The algebraic system of equations can be solved by programming on a computer. For the application in engineering, FDM

is usually used in the problem with regular-shaped objects where node assignment and governing equations should not be too complex.

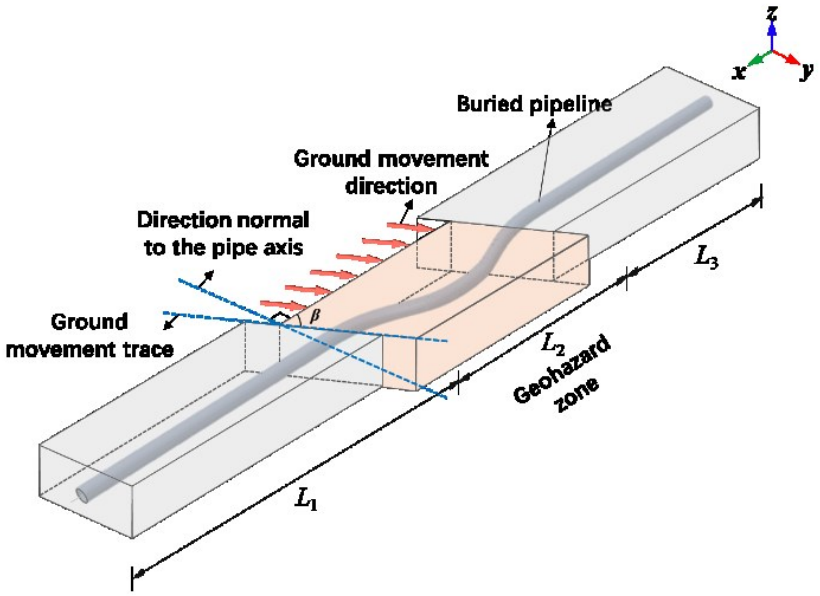

Figure 6-1: Schematic representation of the pipe subjected to ground displacement

6.2.1 Overview of the model in Zheng et al. [24]

This paper carries on the methodology developed by Zheng et al. [24] with further studying steel pipes subject to inelastic strains. To facilitate readers' understanding, a brief outline of the method in Zheng et al. [24] is described below.

(1) Governing equation

The pipe under consideration in the study is simplified as an Euler-Bernoulli Beam under the distributed load exerted by the surrounding soil. Assuming the pipe is deformed in a two-dimensional plane, the governing equation can be written as Eq. (6-1) considering the sign conventions in Figure 6-2.

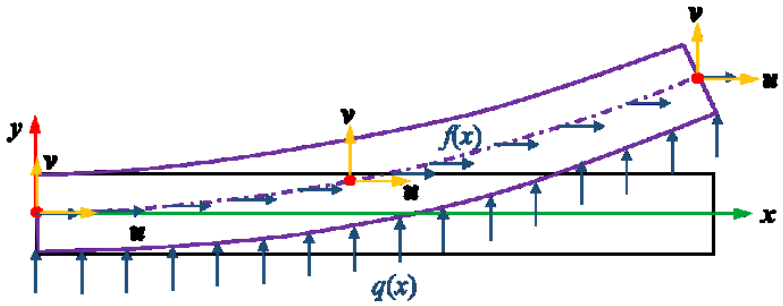

Figure 6-2: Euler-Bernoulli beam under deformation

$$\begin{cases} \dfrac{dN}{dx} + f(x) = 0 \\ \dfrac{d^2M}{dx^2} - \dfrac{d}{dx}\left(N\dfrac{dv}{dx}\right) - q(x) = 0 \end{cases} \tag{6-1}$$

(2) Pipe-Soil Interaction

The pipe-soil interaction, i.e., $f(x)$ and $q(x)$ in Eq. (6-1) representing external forces, are modelled by soil springs. The soil force per unit length and the relative displacement between the pipe and soil follow an elastic-perfectly plastic relationship (see Figure 6-3) where the soil resistance (T_u, P_u, Q_u, and Q_d) and corresponding yield displacement (Δt, Δp, Δq_u, and Δq_d) can be calculated based on the recommended equations in a guideline released by PRCI [18].

(a) Axial (b) Lateral (c) Vertical

Figure 6-3: Soil spring properties in three principal directions

(3) Application of FDM

To solve the problem based on FDM, the derivative terms in the governing equations, i.e., $\frac{dN}{dx}$, $\frac{d^2M}{dx^2}$, and $\frac{d}{dx}(N\frac{dv}{dx})$, should be rewritten as functions of u and v using finite differences. Since only the elastic stage is focused, the internal axial force N and bending moment M can be derived as Eqs. (6-2) and (6-3) respectively.

$$N = EA\left(u' + \frac{1}{2}v'^2\right) \tag{6-2}$$

$$M = EIv'' \tag{6-3}$$

Substituting Eqs. (6-2) and (6-3) into the governing equation (Eq. (6-1)), and surrogating the pipe-soil interaction ($f(x)$ and $q(x)$) by soil force properties, a finite-difference equation set can be obtained as Eq. (6-4) with boundary conditions of two fixed ends.

$$\begin{cases} EA\left(u_i'' + v_i'v_i''\right) + f(U_i - u_i) = 0 \\ EIv_i'''' - EA\left[\left(u_i'' + v_i'v_i''\right)v' + (u_i' + \frac{1}{2}v_i'^2)v_i''\right] - q\left(V_i - v_i\right) = 0 \\ u_1 = u_n = v_1 = v_n = v_1' = v_n' = 0 \end{cases} \quad (i = 1, 2, \cdots) \tag{6-4}$$

Assigning grid points along the pipe and applying the central finite difference for derivatives, i.e., u', u'', v', v'', and v'''' in Eq. (6-4), a large set of simultaneous finite-difference equations can be established with unknowns of axial and lateral pipe displacement (u and v) at predefined gird points along the pipe. Essentially, the problem of solving the differential equations is transformed into a problem of solving a set of nonlinear equations, which can be carried out using a nonlinear equation solver. Subsequently, the strain demand at extreme fibers can be calculated based on the obtained nodal values of u and v, thus the strain demand (the maximum strain along the pipe) can be attained.

6.2.2 Consideration of Material Nonlinearity

The above-mentioned procedure focuses on elastic behavior. However, under large ground movements, the stresses in steel pipes frequently exceed the yielding point and experience material nonlinearity. This study addresses the major limitation in Zheng et al. [24] by introducing the explicit expressions of axial force N and bending moment M. The stress-strain relationship is described as a bilinear curve. Considering whether the bending effect exists, the strain and stress distribution along the pipe cross-section can be generalized into two scenarios indicated in Figure 6-4 according to the basic assumption of "plane sections remain plane". Hence, the longitudinal strain ε_l can be written as the summation of the axial strain ε_{axial} and component of longitudinal strain caused by bending $\varepsilon_{bending}$ (see Eq. (6-5)).

$$\varepsilon_l = \varepsilon_{axial} + \varepsilon_{bending} = \left(u' + \frac{v'^2}{2} \right) - v'' \bullet \tag{6-5}$$

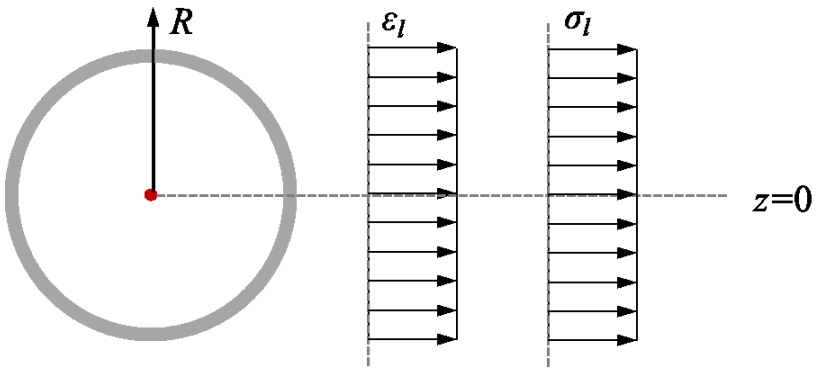

(a) Strain and stress distribution without bending effect

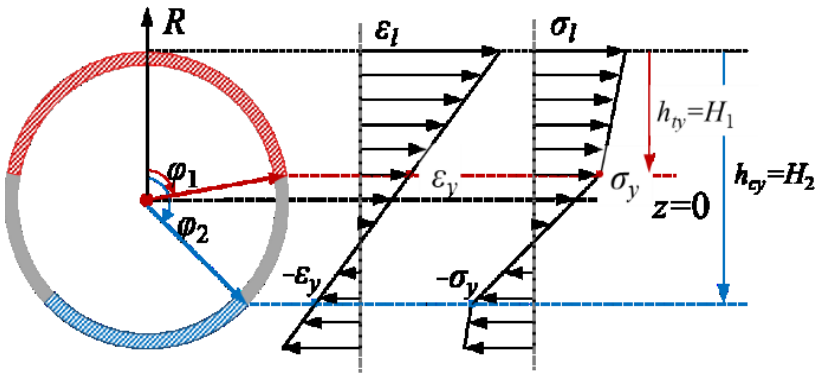

(b) Strain and stress distribution with bending effect

Figure 6-4: Longitudinal strain and stress distribution on the pipe cross-section

It is noteworthy that, in the study, the pipe is in uniaxial stress state in the longitudinal direction under ground displacement. In case of pressurized pipes where hoop stress should be considered, the plasticity framework should be applied to describe the mechanical behavior. This is beyond the scope of this paper and will be addressed in a future publication.

(1) Scenario 1

The bending action does not exist in Scenario 1, which indicates that $v''=0$ and $M = 0$. According to the definition of axial force, the expression of axial force N can be derived as Eq. (6-6).

$$N=\int_A \sigma_l dA=\begin{cases}\left(E\varepsilon_y+E_p\left(u'+\dfrac{v'^2}{2}-\varepsilon_y\right)\right)A & \varepsilon_l>\varepsilon_y \\ EA\left(u'+\dfrac{v'^2}{2}\right) & -\varepsilon_y\le\varepsilon_l\le\varepsilon_y \\ \left(-E\varepsilon_y+E_p\left(u'+\dfrac{v'^2}{2}+\varepsilon_y\right)\right)A & \varepsilon_l<-\varepsilon_y\end{cases} \tag{6-6}$$

(2) Scenario 2

When bending effect exists, the stress cannot be evenly distributed like in Scenario 1 especially when the pipe material plastifies. In Figure 6-4 (b), plastic areas in the pipe cross-section due to tension and compression are respectively shaded in red and blue. In addition, two variables,

h_{ty} and h_{cy}, are introduced to distinguish the elastic area and plastic areas of tension and compression. It is noteworthy that Figure 6-4 (b) only shows a unique pattern of strain and stress distribution when plasticity happens in both tensile and compressive areas. Therefore, to generalize all possible cases, two auxiliary variables H_1 and H_2 (see Eqs. (6-11) and (6-12)) are employed to denote the lower and higher values between h_{ty} and h_{cy} with two corresponding angles φ_1 and φ_2 depicted on the pipe cross-section ($\varphi_1 < \varphi_2$ because $H_1 < H_2$), respectively. Using the membrane strain on the pipe top ε_{top} and bottom ε_{bottom} defined in Eqs. (6-7) and (6-8), the above-mentioned variables can be derived as Eqs. (6-9) to (6-13) in accordance with the geometric relationship.

$$\varepsilon_{top} = u' + \frac{v'^2}{2} - v''\bullet \left(\frac{D}{2}\right) \tag{6-7}$$

$$\varepsilon_{bottom} = u' + \frac{v'^2}{2} + v''\bullet \left(\frac{D}{2}\right) \tag{6-8}$$

$$h_{ty} = \frac{\varepsilon_{top} - \varepsilon_y}{\varepsilon_{top} - \varepsilon_{bot}} D = \frac{2u' + v'^2 + v''\bullet}{-2v''} \tag{6-9}$$

$$h_{cy} = \frac{\varepsilon_{top} + \varepsilon_y}{\varepsilon_{top} - \varepsilon_{bot}} D = \frac{2u' + v'^2 + v''\bullet}{-2v''} \tag{6-10}$$

$$H_1 = \min\left(h_{ty}, h_{cy}\right) \tag{6-11}$$

$$H_2 = \max\left(h_{ty}, h_{cy}\right) \tag{6-12}$$

$$\varphi_i = \begin{cases} 0 & H_i \le 0 \\ \arccos\left(\dfrac{D - 2H_i}{D}\right) & 0 < H_i < D \ \ (i = 1, 2) \\ \pi & H_i \ge D \end{cases} \tag{6-13}$$

Transformed into the polar coordinate system, the longitudinal strain ε_l (in the rectangular coordinate system) can be rearranged as ε_θ shown in Eq. (6-14). The stress distribution can be therefore written as Eq. (6-15) based on the bilinear property of the stress-strain relationship where I_s is the signum function (see Eq. (6-16)) to indicate the relative position between tensile yield point and the compressive yield point.

$$\varepsilon_\theta = u' + \frac{v'^2}{2} - v''\bullet \qquad \vdots [0,\pi] \tag{6-14}$$

$$\sigma_\theta = \begin{cases} I_s E\varepsilon_y + E_p\left(\varepsilon_\theta - I_s\varepsilon_y\right) & 0 \le \theta \le \varphi_1 \\ E\varepsilon_\theta & \varphi_1 < \theta < \varphi_2 \\ -I_s E\varepsilon_y + E_p\left(\varepsilon_\theta + I_s\varepsilon_y\right) & \varphi_2 \le \theta \le \pi \end{cases} \tag{6-15}$$

$$I_s = sign\left(h_{cy} - h_{ty}\right) \tag{6-16}$$

According to the definition of internal axial force and bending moment, the expressions of N and M are respectively derived as Eqs. (6-17) and (6-18).

$$\begin{aligned} N &= 2\int_0^\pi \sigma_\theta \left(\frac{D-t}{2}\right) t d\theta \\ &= (D-t)t \begin{pmatrix} \left(u' + \frac{w'^2}{2}\right)\left(E_p\left(\pi + \varphi_1 - \varphi_2\right) - E\left(\varphi_1 - \varphi_2\right)\right) \\ + I\varepsilon_y\left(E - E_p\right)\left(\varphi_1 + \varphi_2 - \pi\right) \\ + \frac{D}{2}v''\left(E - E_p\right)\left(\sin\varphi_1 - \sin\varphi_2\right) \end{pmatrix} \end{aligned} \tag{6-17}$$

$$\begin{aligned} M &= 2\int_0^\pi \sigma_\theta \left(\frac{D-t}{2}\right)^2 t\cos\theta d\theta \\ &= \frac{1}{4}(D-t)^2 t \begin{pmatrix} -\frac{D}{2}v''\left(E_p\left(\pi + \varphi_1 - \varphi_2\right) - E\left(\varphi_1 - \varphi_2\right)\right) + \left(E - E_p\right) \\ \left(-\left(2\left(u' + \frac{w'^2}{2} - I\varepsilon_y\right) - \frac{D}{2}v''\cos\varphi_1\right)\sin\varphi_1 \right. \\ \left. + \left(2\left(u' + \frac{w'^2}{2} + I\varepsilon_y\right) - \frac{D}{2}v''\cos\varphi_2\right)\sin\varphi_2 \right) \end{pmatrix} \end{aligned} \tag{6-18}$$

Assigning n grid points in total and assuming they are equally-spaced in each concerned span, the finite-difference equation set can be rearranged as functions of the unknown nodal values of u and v with respect to each grid point as shown in Eq. (6-19) where N and M can be calculated by Eqs. (6-17) and (6-18) respectively. Subsequently, this simultaneous finite-difference equation set can be solved according to the procedure in Zheng et al. [24].

$$\begin{cases} \dfrac{1}{2\lambda_{seg}}\left(N_{i+1}-N_{i-1}\right)+f\left(U_i-u_i\right)=0 \\ \dfrac{1}{\lambda_{seg}{}^2}\begin{bmatrix}\left(M_{i+1}-2M_i+M_{i-1}\right) \\ -\dfrac{1}{4}\left(N_{i+1}-N_{i-1}\right)\bullet \\ -N_i\left(v_{i+1}-2v_i+v_{i-1}\right)\end{bmatrix}-q\left(V_i-v_i\right)=0 \end{cases} \quad (6\text{-}19)$$
$$\left(i=1,2,\cdots\right)$$

6.3 Reliability-based assessment

6.3.1 Limit state function

In this study, failures of pipes due to tension and compression are considered individually, and the final limit state function is governed by the lower safety margin induced by the tensile strain and compressive strain. The formula of limit state function is given as Eq. (6-20) where the superscript "*C*" and "*D*" respectively denote the strain capacity and strain demand, and the subscript "*t*" and "*c*" are used to differentiate tensile strain and compressive strain. The pipe is in the safe domain when $g(x)$ is higher than 0; otherwise, the pipe is in the failure domain.

$$g\left(x\right)=\min\left(\varepsilon_t^C\left(x\right)-\varepsilon_t^D\left(x\right),\ \varepsilon_c^C\left(x\right)-\varepsilon_c^D\left(x\right)\right) \quad (6\text{-}20)$$

6.3.2 Strain capacity

In the limit state function, the strain demand is calculated using the established prediction model in section 6.2. Generally, it is considered that the tensile strain capacity is much lower at girth welds than that of the pipe body. In addition, given the high ductility at the pipe body, tensile overload at the pipe body is not expected. Hence, the tensile failure is expected to occur at a girth weld. In this paper, the tensile strain capacity is estimated by the model developed by PRCI-CRES with the coefficients related to the flux-cored arc welding [2].

Local wall buckle can be potentially induced under sufficient compressive strain. When the buckle occurs and ground movement continues, the pipe may crack at the buckle location resulting

in a leak. The buckle strain capacity of the pipe at each crossing is calculated using UoA equation [4]. However, the formation of buckle is a serviceability limit state. The ultimate limit state is considered that the circumferential crack is formed at the buckle. In this paper, the ultimate compressive strain capacity is assumed as the summation of the buckle strain capacity and an additional global compressive strain which is uniformly distributed between 2% to 3%. The basic concept here is that the loss of containment occurs as a result of excessive local pipe wall deformation following the local buckling initiation. The compressive strain causing loss of containment is not well characterized in the industry and is an area of active research. The above scheme is considered to be conservative and is based on the authors' experience with experimental and field buckles.

(1) Tensile strain capacity: PRCI-CRES model

The PRCI-CRES equation is given as the function of normalized geometric and material parameters which are listed in Table 6-1.

Table 6-1: Normalized parameters in PRCI-CRES model

Parameter	**Definition**
$f_p = \sigma_h / \sigma_y$	Pressure factor
$\beta = 2c/t$	Normalized flaw length
$\varphi = \sigma_u^W / \sigma_u$	Weld metal strength mismatch ratio
$\eta = a/t$	Normalized flaw depth
$\psi = h_m/t$	Normalized weld high-low misalignment
$\xi = \sigma_y / \sigma_u$	Base metal Y/T ratio

The tensile strain capacity is calculated based on the empirical equation given as Eq. (6-21).

$$\varepsilon_t^C = \min\left(uEL, P(f_p)G(t)\varepsilon_p\right) \tag{6-21}$$

$P(f_p)$ and $G(t)$ respectively characterize the effect of internal pressure and wall thickness which are calculated according to Eqs. (6-22) and (6-23).

$$P\left(f_p\right)=\begin{cases}2.25-2\eta-\dfrac{5}{3}f_p\left(1.25-2\eta\right) & 0\le f_p<0.6\\ 1 & 0.6\le f_p\le 0.8\end{cases} \tag{6-22}$$

$$G\left(t\right)=\left(\frac{15.9}{t}\right)^{0.8096\left(1+1.503\psi^{1.229}\right)} \tag{6-23}$$

Function of ε_p in Eq. (6-21) is shown in Eq. (6-24) where the equation of $F(\delta_A)$ is shown in Eq. (6-25).

$$\varepsilon_p = A\frac{F\left(\delta_A\right)}{1+F\left(\delta_A\right)}=A\frac{\left(C\delta_A\right)^{B\delta_A^D}}{1+\left(C\delta_A\right)^{B\delta_A^D}} \tag{6-24}$$

$$F\left(\delta_A\right)=\left(C\delta_A\right)^{B\delta_A^D} \tag{6-25}$$

For flux-cored arc welding, the parameters A, B, C, and D in Eqs. (6-24) and (6-25) should be computed according to Eqs. (6-26) to (6-29) where the coefficients are organized in

Table 6-2.

$$A=a_1e^{a_2/\beta}e^{\alpha_3\eta\beta e^{a_4/\beta}}\left[1+a_5\psi^{a_6}+a_7\psi^{a_8}\left(\eta\beta\right)^{a_9}\right]\left(1+a_{10}\xi^{a_{11}}\varphi^{a_{12}}\right) \tag{6-26}$$

$$B=\beta^{b_1}\eta^{b_2\beta^{b_3}/\eta}\left[b_4\varphi^{b_5}\left(b_6\varphi^{b_7}\right)^{\xi}+b_8\psi^{b_9}\right] \tag{6-27}$$

$$C=e^{c_1/\beta}e^{\frac{c_2\beta}{(1+c_3\beta)\eta}}\left(1+c_4\psi^{c_5}+c_6\psi e^{-\eta}+c_7\psi e^{-\beta}\right)\left(c_8+c_9\varphi^{c_{10}}+c_{11}\xi^{c_{12}}\varphi\right) \tag{6-28}$$

$$D=d_1\beta^{d_2}\eta^{d_3}\left(1+d_4\psi^{d_5}+d_6\eta\beta\psi\right)\left(1+d_7\xi^{d_8}+d_9\varphi^{d_{10}}\right) \tag{6-29}$$

Table 6-2: Coefficients in Eqs. (6-26) to (6-29)

Parameter	**Value**	**Parameters**	**Value**
a_1	9.281×10^{-1}	b_1	-5.578×10^{-2}
a_2	9.573×10^{-2}	b_2	1.112×10^{-2}
a_3	-5.053×10^{-1}	b_3	-1.735×10^{-1}
a_4	3.718×10^{-1}	b_4	1.675
a_5	-2.023	b_5	2.603×10^{-1}

a_6	7.585×10^{-1}	b_6	1.106
a_7	6.299×10^{-1}	b_7	-1.073
a_8	5.168×10^{-1}	b_8	-1.519
a_9	7.168×10^{-1}	b_9	1.965
a_{10}	-9.815×10^{-1}		
a_{11}	2.909×10^{-1}		
a_{12}	-3.141×10^{-1}		
c_1	1.609	d_1	6.822×10^{-3}
c_2	1.138×10^{-1}	d_2	1.014
c_3	6.729×10^{-1}	d_3	1.746
c_4	2.357	d_4	2.378
c_5	1.057	d_5	9.434×10^{-1}
c_6	-4.444	d_6	-1.243
c_7	1.727×10^{-2}	d_7	3.579×10^{1}
c_8	-1.354×10^{-2}	d_8	7.500
c_9	-1.224×10^{-2}	d_9	6.294×10^{1}
c_{10}	8.128	d_{10}	-6.930
c_{11}	2.007×10^{-1}		
c_{12}	-1.594		

(2) Compressive strain capacity: UoA model

UoA model was reported by PRCI to be the most representative of actual compressive strain capacity based on full-scale buckling tests [6]. The equation of buckle strain capacity is described in Eq. (6-30).

$$\varepsilon_c^{buckle} = \left(\frac{2.94}{D/t}\right)^{1.59} \cdot \left(1 - 0.808\frac{0.01}{\left(P_{\text{int}}\left(D-2t\right)/\left(2t\sigma_y\right)\right)}\right) \cdot \left(\frac{\sigma_y}{\quad}\right)^{0.854} \cdot \left[\quad\left(\frac{\quad}{100}\right)^{0.150}\right] \tag{6-30}$$

As defined before, the strain capacity for ultimate limit state used in this study can be expressed as Eq. (6-31) where *e* is an additive error yielding uniform distribution with bounds of [0.02, 0.03].

$$\varepsilon_c^C = \varepsilon_c^{buckle} + e \tag{6-31}$$

6.3.3 Computational optimization

Monte Carlo Simulation is recognized as the most applicable method for reliability calculation when limit state function evaluations are not computationally intensive, and it can give sufficiently reliable results by sampling the design space based on the full stochastic characterization of random variables.

Generally, implementing stochastic simulation using random samples within loops is expected to be avoided as this will make the computation time-consuming. However, since the strain demand prediction model developed in section 6.2 can only pass results of one sample case at a time, it is inevitable to utilize loops for implementing the code of Monte Carlo Simulation. In addition, solving a large size of nonlinear equations in the strain demand model is not a fast practice, and therefore the reliability calculation will be prohibitively expensive for situations requiring a large number of samples.

In this study, computational optimization is employed to achieve the best performance of the code implemented in Python. Firstly, the code is compiled based on the function of ***jit*** and ***njit*** in the Numba library for Python, which enables the functions in Python to optimize machine code at runtime to accelerate the running speed. Secondly, parallel programming is utilized for each loop calculation, which means multiple sample cases generated by the stochastic simulation can be computed at the same time. This scheme can be well supported for explicit parallel loops, and thus is used for implementing the reliability calculation in this research with highly improved efficiency.

6.4 Establishment of calculation tool

Based upon the established methodology of this study, the tool for estimating safety of pipes subjected to geohazard-induced ground movements is created under the platform of MecSimCalc [26]. MecSimCalc is a website that enables building and sharing computational tools or Apps using Python on the web.

6.4.1 Tool for strain demand evaluation

To evaluate safety of pipes in a deterministic way, the pipe capacity is seen as a threshold under the allowable load. However, that is not included in the tool established in MecSimCalc at present since safety inspectors or pipeline operators would have different determinations on the strain capacity. For a deterministic evaluation, a tool is designed for strain demand prediction under MecSimCalc [27]. Three segments of pipes are considered in the model where only the middle section is subjected to ground movement as pictured in Figure 6-1. Two ends of the pipeline are fixed. Length of the middle segment is the span of the pipeline buried across the geohazard zone, which is usually determined by geotechnical investigators. Length of the two side pipe segments should be properly decided to balance computational efficiency and result accuracy. Based on the proposed model in section 6.2, the tool is developed for predicting the response of the straight pipe under uniformly distributed ground movement where the spatial variability of soil is not considered. Effects of internal pressure and temperature change are not accounted for in the study. It is acceptable to use this tool for quick and crude estimation. But one should keep in mind that a detailed finite element analysis is necessary for rigorous investigations.

For instance, given the necessary inputs listed in Table 6-3, the output of the case is shown in Figure 6-5 including the basic information of the calculation, e.g., strain demand and the corresponding location, and the displacement of the pipe after deformation and the strain along the pipe. The convergence condition is also reported to users to identify if the results are acceptable.

Table 6-3: Inputs of the study case in section 6.4.1

Parameter	Value	Unit
Outer diameter	508	mm
Wall thickness	7.14	mm
Young's modulus	210000	MPa
Yield strength	450	MPa
Ultimate strength	663	MPa
Ultimate strain	0.03	-
Ground displacement	0.1	m
Intersection angle	60	°
Axial soil spring resistance	14	kN/m
Yield displacement of axial soil spring	5	mm
Lateral soil spring resistance	204	kN/m
Yield displacement of lateral soil spring	46	mm
Length of the left pipe segment	100	m
Length of the middle pipe segment	10	m
Length of the right pipe segment	100	m
Number of nodes in left pipe segment	51	-
Number of nodes in middle pipe segment	21	-
Number of nodes in left pipe segment	51	-

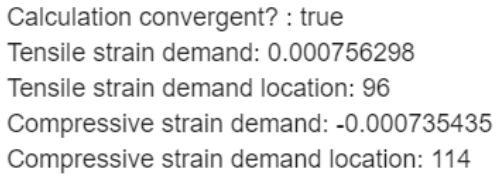

(a) Strain demands and corresponding locations

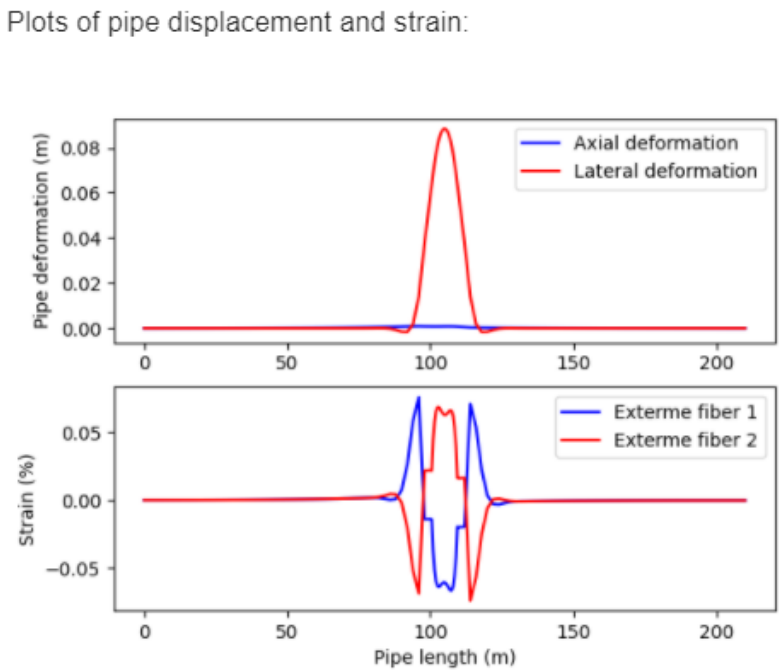

(b) Figures of pipe displacement and strain distribution

Figure 6-5: Outputs of the tool for strain demand prediction

6.4.2 Tool for reliability-based assessment

Two types of geohazards, i.e., steady-state creep and sudden mass landslide, are specifically considered in the reliability-based assessment as they are of great concern to the pipeline industry in Canada. Steady-state creep movement (hereafter referred to as slope creep) is what most commonly occurs at pipeline slope crossings whereby slope movements occur at relatively slow rates; sudden mass landslide (hereafter referred to as landslide) is the condition whereby the ground suddenly moves by a large magnitude. Therefore, in the calculation, ground movement is the summation of initial movement and the accumulated movement in the re-inspection interval.

Monte Carlo Simulation is employed for the reliability calculation where uncertainties of both strain capacity and demand are incorporated. The random properties of pipe geometries are given in Table 6-4 according to Annex O of CSA Z662. For the convenience of users, some parameters are set as choices according to industrial codes or experimental data. To be specific, the pipe material-related variables, such as yield strength, ultimate strength, uniform strain, and

CTOD toughness, are all credited to the input of pipe grade and vintage, which can be seen in Table 6-5. The yield and tensile strength distributions are mainly based on the distributions proposed in the Annex O of CSA Z662 as well. Toughness distributions for different pipe grades and vintages are not well characterized in the industry at this point, and this remains an area of active research. The CTOD distributions in Table 6-5 are example distributions based on tentative CVN values and conversion to CTOD relationships. Young's modulus is set as a constant, and the ratio of strain hardening slope to young's modulus is 0.03, 0.02, and 0.01 for pipes manufactured before 1980, during 1980 to 1990, and after 1990, respectively.

The soil spring resistances are inputs by users, but the yielding displacements are summarized in the soil class including six types, which are categorized into sand and clay in the background calculation. The definition of each soil class and category are tabulated in Table 6-6. Based on the geotechnical observations on the slope sites in Canada, the stochastic data for slope creep and mass landslide can be determined as Table 6-7, which shows the threshold of ground movements. The distributions in the table were established based on the input provided by geotechnical experts. The material flaws and imperfection distributions (see Table 6-8), which are used in the strain capacity models, are tentative distributions used here as a reasonable example based on field experience.

Table 6-4: Stochastic properties of pipe geometries

Parameter	**Distribution**	**Mean**	**CoV**	**Unit**
Diameter	Normal	Nominal	0.0017	mm
Wall thickness	Normal	Nominal	0.0235	mm

Table 6-5: Stochastic properties of material tensile properties

(a) Yield strength

Grade	**Yield strength**				**Ultimate strength**			
	Distribution	**Mean**	**SD**	**Unit**	**Distribution**	**Mean**	**SD**	**Unit**
X42	Normal	319	11	MPa	Normal	463	6	MPa
X46	Normal	352	12	MPa	Normal	483	6	MPa

X48	Normal	364	13	MPa	Normal	487	6	MPa
X52 > 1980[1]	Normal	393	19	MPa	Normal	555	4	MPa
X52 <= 1980[2]	Normal	387	22	MPa	Normal	548	14	MPa
X56	Normal	425	15	MPa	Normal	548	7	MPa
X60	Normal	459	16	MPa	Normal	582	8	MPa
X65	Normal	483	16	MPa	Normal	599	8	MPa
X70	Normal	531	19	MPa	Normal	638	8	MPa

Note: [1] X52 pipe manufactured after the year 1980; [2] X52 pipe manufactured before or in the year 1980.

(b) CTOD toughness

Year	**Grade**	**Distribution**	**Mean**	**SD**	**Unit**
> 1980	X42	Normal	0.12	11	mm
	X46	Normal	0.15	12	mm
	X48	Normal	0.16	13	mm
	X52	Normal	0.17	19	mm
	X56	Normal	0.16	15	mm
	X60	Normal	0.16	16	mm
	X65	Normal	0.18	16	mm
	X70	Normal	0.18	19	mm
<= 1980	X42	Lognormal	0.08	0.05	mm
	X46	Lognormal	0.10	0.06	mm
	X48	Lognormal	0.10	0.06	mm
	X52	Lognormal	0.11	0.07	mm
	X56	Lognormal	0.10	0.06	mm
	X60	Lognormal	0.10	0.06	mm
	X65	Lognormal	0.11	0.07	mm
	X70	Lognormal	0.12	0.07	mm

Table 6-6: Description of soil class

Soil class	Soil description	Soil category
CL	Clay till	Clay
CL-CI	Fine sand, silt, clay	Clay
CH	Inorganic clay	Clay
CI	Lean clay	Clay
ML	Silt, and fine sand	Sand
SM	Fine sand, and silt	Sand

Table 6-7: Stochastic properties of ground movement

Parameter	Distribution	Mean/Mode	SD	LB	UB	Unit
Initial movement for creep	Uniform	-	-	200	400	mm
Slope creep rate	Lognormal	12.50	6.25	-	-	mm/yr
Landslide movement	Triangular	800	-	300	4000	mm

Table 6-8: Stochastic properties of girth weld flaws

Parameter	Distribution	Mean/Mode	SD	LB	UB	Unit
Flaw length	Lognormal	15	6.00	-	-	mm
Flaw height	Lognormal	1.00	0.40	-	-	mm
Misalignment	Triangular	0.1	-	0	1.43	mm
Overmatch ratio	Uniform	-		1.00	1.30	-
Ovality	Triangular	0.08	-	0.07	1.07	%t

A study case is implemented based on the established tool in MecSimCalc [28] which allows users to input the variables in Table 6-9. The length of the pipe segment in the two ends is two times the length of the middle segment. To demonstrate, a reliability calculation is implemented based on small number of runs (100 simulations) due to the limited memory in MecSimCalc currently. The output of reliability-based assessment is shown in Figure 6-6 which indicates that the PoF of this study case is 0.02.

Table 6-9: The study case in section 6.4.2

Parameter	Value	Unit
Outer diameter	559	mm
Wall thickness	7.14	mm
Pipe grade	X46	-
Young's modulus	210000	MPa
Year of mill run	1952	
Re-inspection interval	9	yrs
Length of slope	34	m
Pipe crossing angle	70	°
Soil class	ML	-
Axial soil spring resistance	14	kN/m
Lateral soil spring resistance	170	kN/m
Type of geohazard	Slope creep	-

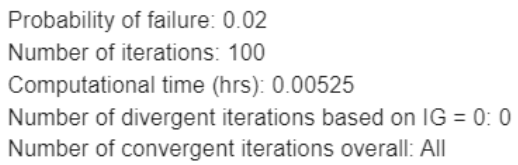

Figure 6-6: Output of reliability calculation

6.5 Chapter conclusions

This study proposes calculator-like tools for safety evaluation of pipelines subjected to ground movements based on the finite difference method. Compared with implementing through the finite element method, the tools are more convenient as the process of modelling is eliminated. Furthermore, the efficiency of Monte Carlo Simulation is highly improved by employing the proposed FDM-based strain demand prediction method within the loops for reliability calculation.

This is a good alternative for crude estimations and appropriate to be used in industry for preliminary design and safety pre-screening.

Reference

[1] M. Porter, M. Leir, A. Baumgard, G. Ferris, Integrating terrain and geohazard knowledge into the pipeline lifecycle, in: Proceedings of 6th Canadian Geohazards Conference, Kingston. 2014.

[2] M. Liu, Y.Y. Wang, Y. Song, D. Horsley, S. Nanney, Multi-tier tensile strain models for strain-based design: Part 2-Development and formulation of tensile strain capacity models, in: International Pipeline Conference (IPC2012), American Society of Mechanical Engineers (ASME), Calgary, 2012, pp. 415-425.

[3] D.P. Fairchild, M.L. Macia, S. Kibey, X. Wang, V.R. Krishnan, F. Bardi, H. Tang, W. Cheng, A multi-tiered procedure for engineering critical assessment of strain-based pipelines, in: The 21st International Offshore and Polar Engineering Conference, OnePetro, Cupertino, 2011, pp. ISOPE-I-11-144.

[4] A.B. Dorey, D.W. Murray, J.R. Cheng, Critical buckling strain equations for energy pipelines-A parametric study, ASME. J. Offshore Mech. Arct. Eng. 128 (2006) 248-255.

[5] C.M. Timms, D.D. DeGeer, M.R. Chebaro, Y. Tsuru, Compressive strain limits of large diameter X80 UOE linepipe, in: The 19th International Offshore and Polar Engineering Conference, OnePetro, Cupertino, 2009, pp. ISOPE-I-09-332.

[6] M. Liu, Y.Y. Wang, F. Zhang, K. Kotian, Realistic Strain Capacity Models for Pipeline Construction and Maintenance, Center for Reliable Energy Systems (CRES), Dublin, 2013.

[7] N.M. Newmark, W.J. Hall, Pipeline design to resist large fault displacement, in: Proceedings of U.S. National Conference on Earthquake Engineering, Earthquake Engineering Research Institute, Michigan, 1975, pp. 416-425.

[8] R.P. Kennedy, A.W. Chow, R.A. Williamson, Fault movement effects on buried oil pipeline, ASCE J. Transport. Eng. 103 (1977) 617-633.

[9] L.R.L. Wang, Y.A. Yeh, A refined seismic analysis and design of buried pipeline for fault movement, Earthq. Eng. Struct. Dyn. 13 (1985) 75-96.

[10] L.R.L. Wang, Y.A. Yeh, Seismic design of buried pipeline for fault movement effects, J. Press. Vessel. Technol. 108 (1986) 202-208.

[11] Y.J. Chiou, S.Y. Chi, H.Y. Chang, A study of buried pipeline response to fault movement, J. Press. Vessel Technol. Trans. ASME 116 (1994).

[12] D.K. Karamitros, G.D. Bouckovalas, G.P. Kouretzis, Stress analysis of buried steel pipelines at strike-slip fault crossings, Soil. Dyn. Earthq. Eng. 27 (2007) 200-211.

[13] O.V. Trifonov, V.P. Cherniy, Elastoplastic stress strain analysis of buried steel pipelines subjected to fault displacements with account for service loads, Soil. Dyn. Earthq. Eng. 33 (2012) 54-62.

[14] G.C. Sarvanis, S.A. Karamanos, Analytical model for the strain analysis of continuous buried pipelines in geohazard areas, Eng. Struct. 152 (2017) 57-69.

[15] X. Liu, H. Zhang, M. Xia, J. Liu, Q. Zheng, An improved analytical strain analysis method for buried steel pipelines subjected to abrupt permanent ground displacement, in: International Pipeline Conference (IPC2020), American Society of Mechanical Engineers (ASME), Calgary, 2020, pp. V002T06A012.

[16] S. Takada, N. Hassani, K. Fukuda, A new proposal for simplified design of buried steel pipes crossing active faults, Earthquake Eng. Struct. Dyn. 30 (2001) 1243-1257.

[17] K. Gawande, R. Kiran, H.P. Cherukuri, A numerical study of the response of buried steel pipelines undergoing strike-slip fault, Eng. Fail. Anal. 102 (2019) 203-218.

[18] Pipeline Research Council International (PRCI). Guidelines for Constructing Natural Gas and Liquid Hydrocarbon Pipelines Through Areas Prone to Landslide and Subsidence Hazards, Technical Toolboxes, Inc., 2009.

[19] A. Liu, Y. Hu, F. Zhao, X. Li, S. Takada, L. Zhao. An equivalent-boundary method for the shell analysis of buried pipelines under fault movement, Acta. Seismol. Sin. 17 (2004) 150-156.

[20] W. Zhou, Reliability of pressurised pipelines subjected to longitudinal ground movement, Struct. Infrastruct. Eng. 12 (2012) 1123-1135.

[21] N. Yoosef-Ghodsi, J. Zhou, D.W. Murray, A simplified model for evaluating strain demand in a pipeline subjected to longitudinal ground movement, in: International Pipeline

Conference (IPC2008), American Society of Mechanical Engineers (ASME), Calgary, 2008, pp. 657-664.

[22] Q. Zheng, X. Liu, H. Zhang, X. Gu, M. Fang, L. Wang, S. Adeeb, 2021. Reliability evaluation method for pipes buried in fault areas based on the probabilistic fault displacement hazard analysis, J. Nat. Gas Eng. 85, 103698.

[23] X. Liu, Q. Zheng, K. Wu, Y. Yang, Z. Zhao, H. Zhang, 2020. Development of a novel approach for strain demand prediction of pipes at fault crossings on the basis of multi-layer neural network driven by strain data, Eng. Struct. 214, 110685.

[24] Q. Zheng, L. Graf-Alexiou, Y. Li, N. Yoosef-Ghodsi, M. Fowler, M. Kainat, S. Adeeb, Strain demand of elastic pipes subjected to permanent ground displacements using the finite difference method, J. Pipeline. Sci. Eng. 1 (2021) 176-186.

[25] R.J. LeVeque, Finite difference methods for differential equations, Draft version for use in AMath, 1998.

[26] W. Qiu, S. Adeeb, The simplest way to share computational tools, MecSimCalc, March, 7, 2022, https://mecsimcalc.com/.

[27] Q. Zheng, Strain Demand in Pipes Subjected to Ground Movement, MecSimCalc, March, 7, 2022, https://mecsimcalc.com/app/5339494/strain_demand_in_pipes_subjected_to_ground_movement.

[28] Q. Zheng, Reliability of Pipes Subjected to Ground Movement, MecSimCalc, March, 7, 2022, https://mecsimcalc.com/app/6934977/reliability_of_pipes_subjected_to_ground_movement.

CHAPTER 7: PROBABILISTIC ANALYSIS OF PIPELINES BURIED THROUGH GEOHAZARD-PRONE ZONES BASED ON A NOVEL APPROACH

This chapter is derived from the paper in preparation:

Q. Zheng, I. Allouche, W. Qiu, Y. Li, N. Yoosef-Ghodsi, M. Fowler, S. Adeeb, Probabilistic Analysis of Pipelines Buried Through Geohazard-Prone Zones based on a Novel Approach, Journal of Pipeline Systems Engineering and Practice.

Abstract

This paper presents a novel approach for probabilistic analysis of pipelines buried through geohazard-prone areas which induce permanent ground movements potentially. In this approach, an easy-to-implement response prediction tool based on the finite difference method is integrated with simple but robust Monte Carlo simulation methods. The probability of strain capacity exceedance is calculated when a pipeline is subjected to the ground movement of different magnitudes. In the strain-based limit state function, the strain capacity is determined using existing equations in the literature, and the strain demand is calculated using an accurate and efficient tool based on the finite difference method. After obtaining the conditional probabilities of failure of pipes at given magnitudes of ground movement, the probability of failure of pipes as a function of time is also calculated considering the probability of ground movement initiation. The proposed approach is demonstrated through a case study of pipelines subjected to landslides

Keywords: reliability; pipeline; strain demand; ground movement; finite difference method; Monte Carlo method

7.1 Introduction

As an essential part of the lifeline infrastructure systems, pipelines play a vital role in the transmission of various gas and fluid substances. Generally, pipes are constructed underground to avoid severe weather conditions, natural disasters, and several other loads that pipes may be exposed to when installed above ground. However, geohazard-related pipeline failures, which are dominated by landslides, are one of the major concerns in North America [1]. In general, the pipe is deformed due to the force exerted by the surrounding soils induced by ground displacements in geohazards. Therefore, integrity and safety of pipelines buried in geohazard zones have witnessed a growing interest among pipeline researchers and operators.

Geohazard-related pipeline failures are typically associated with higher consequences. Increasingly, risk-based assessment is employed for proactive management by prudent operators to optimize the maintenance strategies of the pipes under geohazard-prone zones. For a pipe buried across geohazard-prone areas, the risk can be expressed quantitatively as the product of the annual probability of hazard occurrence, vulnerability of the pipe which determines the effect of the ground movement on the pipeline integrity, and the consequence associated with the ground movement occurrence. The vulnerability, recognized as the probability of failure (PoF), is frequently estimated in a simplified manner based on expert judgement supported by historical data and empirical relations [2][3][4][5]. However, the results are subjected to substantial uncertainties. Rigorous probabilistic analysis is more recognized for higher accuracy. To calculate the PoF, e.g., the probability of capacity exceedance by the strain demand imposed by geohazard, a computationally efficient and reliable model is required to calculate the strain demand.

To date, a variety of models have been developed to analyze pipes' behavior and strain demand underground movements. The analytical works pioneered by Newmark and Hall [6] and Kennedy et al. [7] respectively focused on the pipe response in longitudinal and lateral directions under fault displacements. However, the ignorance of lateral soil force in [6] and exaggerated curvature of deformed pipe in [7] sacrificed the accuracy of resultant strain demands. This model was further refined by Wang and Yeh [8][9] in which the pipe segments near the fault behaved like circular arcs, and the segments far from the fault were modeled as beams-on-elastic foundations. In recent decades, analytical models were devoted to improving the accuracy of

models mentioned above. Some representative studies, such as Karamitros et al. [10], Trifonov and Cherniy [11], and Liu et al. [12], had developed models, which are capable of predicting the pipes' response to fault displacement with relatively high accuracy when only one ground discontinuity is required for analyzing pipeline subjected to tectonic faults

As for some other geohazards, such as landslides, subsidence, and liquefaction-induced lateral spreading, where the pipes' behavior is significantly influenced by the length of geohazard zone, two ground discontinuities at either side of the geohazard interface should be concerned. Typically for landslides, the pipes' response to transverse and longitudinal ground displacements was examined in an approximate manner by O'Rourke et al. [13][14]. In the scenario of transverse ground movements (ground movement perpendicular to the pipeline axis), the pipeline was characterized as either a flexure pipe (modeled as a cable) closely following the ground movement or a stiff pipe (modeled as a fixed-fixed beam) which allowed the soil to flow over and around the pipeline [13]. The critical length of landslide span between the flexible pipe and stiff pipe was estimated based upon local buckling stress capacity. Similarly, pipes subjected to longitudinal displacement were classified as the "compliant pipe" and the "noncompliant pipe" based on the pipe's response to the landslide [14]. The "compliant pipe" literally denoted the pipes conforming to the imposed soil deformation, so the pipe displacement was essentially identical to the magnitude of ground movement which was, on the contrary, substantially higher than the displacement of "noncompliant pipe". In the analytical models developed by O'Rourke et al. [13][14], the length of landslide zones and the magnitude of ground movements were crucial factors for determining the performance of the pipe. In view of this, Liu et al. [15] proposed an analytical model to examine the elastic pipe response to transverse displacement at any arbitrary length of landslide by considering the combined effects of flexure (beam-like behavior) and axial tension (cable-like behavior). The aforementioned analytical methods provided simplified design approaches. However, the assumptions led to the lack of prediction accuracy and applicability. Although the recent analytical model proposed by Zahid et al. [16] refined this study by considering more physical factors, i.e., temperature change, internal pressure, and pipe self-weight, it only focused on the elastic pipe undergoing the longitudinal ground movement in the landslide.

In addition to the above-mentioned analytical models, current state of practice for assessing inelastic pipelines' response to ground movements heavily relies on finite element modeling where the pipe and surrounding soil are simulated either by a rigorous continuum model or a shell/beam-on-spring model recommended by pipeline design codes [17][18]. In addition, Liu et al. [19] proposed the hybrid model integrating shell and beam (pipe) elements, appropriately leveraging computational efficiency and accuracy. Furthermore, to reduce the computational cost, Liu et al. [20] proposed the equivalent boundary conditions applied to the ends of the pipeline represented by shell elements near fault crossings, which can highly reduce the computational cost, and this idea was adopted in [21] for generating the database of strain demand. Overall, finite element modeling serves as a reliable tool for analyzing pipes' response subjected to ground movements.

However, using finite element models in probabilistic analysis (e.g., PoF calculation) has been limited due to high computational costs. Moreover, the source code of commercial finite element software is generally not available, which prevents its use in the computing cloud due to license constraints. Thus, it is challenging for users of commercial software to take advantage of readily available computational resources for prohibitively expensive calculation tasks when Monte Carlo simulation (MCS) is used for probabilistic analysis. For this reason, simplified analytical models are preferred, which has been demonstrated by related publications. Zhou [22] analyzed the reliability of pressurized pipes under the ground displacement induced by slope instability, and the strain demand was estimated based on the model proposed by Yoosef-Ghodsi et al. [23]. Sen et al. [24] developed probabilistic approaches with different levels, i.e., qualitative, semi-quantitative, and full quantitative, to analyze the risk of pipes crossing potential moving slopes; the strain demand in [23] was also adopted in the strain-based limit state function for the semi-quantitative analysis. It is worth noting that the analytical method in [23] was only applicable to pipes deforming in the longitudinal direction. Alternatively, cheap-to-evaluate surrogate models for strain demand calculation, like the neural network developed by Liu et al. [19] and used by Zheng et al. [25] to assess the reliability of the pipeline buried across an active fault area, can be used in probabilistic analysis. Nevertheless, the collection of strain demand datasets for model training was time-consuming due to a large number of calculations based on the finite element method (e.g., using ABAQUS).

In contrast, analytical models are preferred for MCS-based probabilistic analysis for their efficiency and availability, but existing analytical approaches to estimate pipes' behavior are either limited in their accuracy and/or applicability range. For instance, the approaches with reasonable accuracy are mainly for pipelines under fault displacements, which cannot be applied to other geohazards, such as landslides and subsidence. The use of simplified analytical models can raise issues about the relatively large model uncertainty arising from the prediction error and their negative impact on probabilistic analysis. All of these explain the fact that research works related to reliability-based assessment of pipelines buried under geohazard-prone zones are scarce in literature.

To facilitate studies on probabilistic analysis or reliability-based assessment of pipes buried through geohazard-prone zones considering permanent ground movements, this paper presents a novel approach by integrating an easy-to-implement response prediction tool with simple but robust MCS methods. The probability of strain capacity exceedance is calculated when a pipeline is subjected to the ground movement of different magnitudes. The limit state function is defined based on the criterion of strain. The strain capacity is determined based on existing formulas in the literature; the strain demand, denoted by the maximum tensile and compressive strains along the pipe, is predicted by a new approach using the finite difference method developed by Zheng et al. [27][28]. The method is slightly modified to account for the effects due to internal pressure and temperature change according to the treatment in [23]. The conditional PoF of pipes at a given magnitude of ground movement is assessed using Monte Carlo Simulation. Meanwhile, the code is equipped with computational optimization methods to enhance the calculation efficiency. For a comprehensive evaluation, this study makes use of the landslide as an example, and the probability of the ground movement initiation is considered based on the published guideline [29]. The probability of failure over time is also derived. The proposed probabilistic assessment method is demonstrated based on a study case in this paper.

7.2 Probabilistic analysis approach for pipelines subjected to ground movement

For the pipeline design and assessment, two criteria including stress- and strain- based methods can be employed according to the load types. Stress-based method is a conventional

approach where the applied stress should be kept below the specified minimum yield stress (SMYS) by an amount controlled by a safety factor. Typically, since the SMYS for line pipe is defined as the stress measured at 0.5% total strain, the longitudinal strain is limited to a value less than 0.5%. Recognizing that a pipe retains its integrity even after being deformed plastically to some degree, the strain-based method is proposed in which the strain that would lead to failures such as rupture and buckling (termed the strain capacity) is not expected to be excessed by the amount of strain induced by external loads (termed the strain demand). Hence, the strain-based criterion is appropriate for situations in which the pipe's resistance is governed by deformation capacity, e.g., the pipe is under the displacement-controlled load such as ground movements [30].

7.2.1 Strain capacity models

Since most pipe ruptures induced by ground movements occur as the result of tension at girth welds rather than within the pipe body, the primary concern on the tensile strain capacity focuses on the highest tensile strain or weld can sustain without a leak or rupture. Existing models, such as PRCI-CRES [31], CSA Z552-07 equations [32], and ExxonMobil [33], show that the tensile strain capacity is significantly influenced by factors including pipe dimension, mechanical properties of pipe and welding consumables, girth weld profile, and welding imperfections. Some factors are generally known to pipeline operators; however, most other factors like weld flaws are acquired through further examination and testing. Experimental data have revealed that the tensile strain capacity can be as low as 0.2% to well over 2% even under the same normalized weld flaw dimension [34], which indicates that the tensile strain capacity can vary significantly. As such, determination of the tensile strain capacity requires careful consideration in selecting the model and detailed case-specific information for the best accuracy.

The compressive strain capacity is usually defined as the strain corresponding to the point of the maximum bending moment in a lateral bending test where pipes have a minimal amount of bulging or wrinkle in most cases [29], which corresponds to the serviceability limit state. Several models, such as CSA Z662-07 equations [32], UoA model [35], C-FER [36], and CRES formulas [37], are most commonly used for predicting the compressive strain capacity. On the other hand, the immediate consequence of the formation of a wrinkle or buckle can vary from a benign

serviceability concern (no breach of the pipe wall occurs) to leaks due to the local high strain in the vicinity of the severe wrinkle or buckle. Specifically, further increase of strain in the vicinity of severe wrinkles and buckles may cause loss of contaminate in seam welds. However, this ultimate compressive strain causing loss of containment has been well-characterized in neither academic publication nor industrial practice.

Responding to the complexity mentioned above, ALA Guideline [17] suggests the acceptance criteria of deformation and strain of pipelines under different ground-induced loads. For the condition of ground movement due to earthquakes, landslides, or mine subsidence, combined with thermal effects, the longitudinal strain capacity is given under the operable limit (serviceability limit state) and pressure integrity limits (ultimate limit state). The tensile strain capacities (ε_c^T) corresponding to the two limit states are respectively 2% and 4%; the compressive strain capacities (ε_c^C) corresponding to the two limit states are given as Eqs. (7-1) and (7-2), respectively.

Operable limit:
$$\varepsilon_c^C = 0.5\frac{t}{D} - 0.0025 + 3000\left(\frac{PD}{2Et}\right)^2 \tag{7-1}$$

Pressure integrity limit:
$$\varepsilon_c^C = 1.76\frac{t}{D} \tag{7-2}$$

Where D (mm) is the outer diameter of the pipeline; t (mm) is the pipe wall thickness; E (MPa) is Young's modulus of pipe steel; P (MPa) is the internal pressure of the pipeline.

7.2.2 Strain demand prediction model

7.2.2.1 Recap of the model based on the finite difference method

The finite difference-based model was initially developed by Zheng et al. [27][28] in which the effects of temperature change and internal pressure were ignored. The primary object of the model was to capture the pipes' deformation with ground movements triggered by geohazards. The general layout of a pipe bearing the ground movement can be simply pictured as shown in Figure 7-1. This method takes advantage of the fact that the finite difference method is typically

defined on a regular grid. The pipe can be treated as a regular-shaped instance in one dimension, and the finite difference equations are developed as functions of pipe displacements (the axial displacement *u* and lateral displacement *v*) of each node.

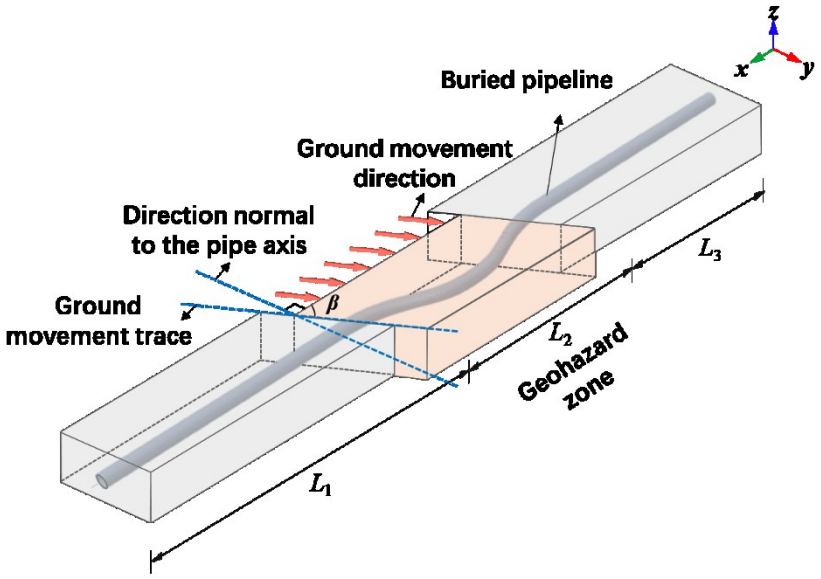

Figure 7-1: Schematic representation of the pipe subjected to the ground displacement

The pipeline is modeled following the Euler-Bernoulli beam theory under large deformation. The governing equations are shown in Eq. (7-3) based on the sign conventions in Figure 7-2.

$$\begin{cases} \dfrac{dN}{dx} + f\left(U-u\right) = 0 \\ \dfrac{dM}{dx^2} - \dfrac{d}{dx}\left(N\dfrac{dv}{dx}\right) - q\left(V-v\right) = 0 \end{cases} \tag{7-3}$$

where *N* and *M* are the axial internal force and bending moment on the cross-section of the pipe respectively; *u* and *v* represent the axial and lateral deformation of the pipe respectively; *U* and V are respectively the axial and lateral ground displacements; *f* and *q* are externally distributed loads in the longitudinal and lateral directions, which are represented by soil springs as recommend by PRCI guidelines [18].

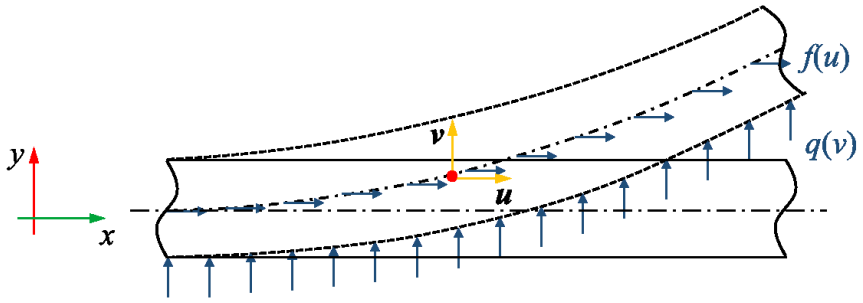

Figure 7-2: Euler-Bernoulli beam under deformation

To solve the problem based on the finite difference method, the terms of derivatives in the governing equations, e.g., $\frac{dN}{dx}$, $\frac{d^2M}{dx^2}$, and $\frac{d}{dx}(N\frac{dv}{dx})$, should be written using finite differences. The internal force N and bending moment M are functions of u and v, the finite difference equations are composed of unknowns of u and v of each node. Readers of interest about the details of this method are referred to [27][28], but for the sake of completeness here, the calculation flow is summarized as follows:

Step 1: mesh the pipe by defining nodes (grid points) in the longitudinal direction.

Step 2: assign the initial guess (usually set as 0) of the pipe's deformation at each node i (u_i and v_i).

Step 3: calculate derivatives of u and w based on finite difference method at each node (u'_i, v'_i and v''_i).

Step 4: calculate the axial force N and bending moment M at each node (N_i and M_i).

Step 5: represent the derivative items in the governing equation based on finite difference strategy at each node (N'_i, M''_i and $(N_iv'_i)'$).

Step 6: replace the derivative items in the governing equation by those obtained in step 4.

Step 7: construct the finite difference equations based on the formulations obtained in ***Step 6*** together with boundary conditions at each node (Eq_i).

Step 8: use a solver to get the convergent solutions of u_i and v_i.

compute the longitudinal strain along the pipe based on the obtained solutions, and calculating the tensile strain demand ε_d^T (the maximum positive strain value) and the compressive strain demand ε_d^C (the minimum negative strain value).

7.2.2.2 Consideration of effects due to operational loads

The formulations of internal force *N* and bending moment *M* in Zheng et al. [28] are derived based on bilinear stress-strain relationship under uniaxial stress state (see Figure 7-3 (a)). To incorporate the effects of internal pressure and temperature differential, formulas of *N* and *M* should be updated based on the data of stress-strain curve considering the biaxial stress state as detailed below. This is necessitated when the effect of internal pressure on pipelines is taken into account, because the internal pressure causes stress in the hoop direction so that pipe is under the biaxial stress-strain state as shown in Figure 7-3 (b).

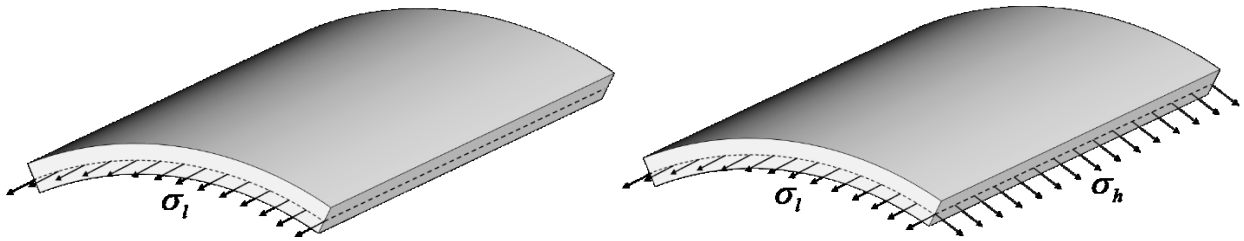

(a) Uniaxial stress state (b) Biaxial stress state

Figure 7-3: Stress state of pipe with and without internal pressure

The stress-strain relationship used in Zheng et al. [27][28] is bilinear based on a uniaxial test in the longitudinal direction as shown in the black solid curve in Figure 7-4. The presence of internal pressure leads to a biaxial state of stress, requiring a more rigorous treatment of the material behavior than the direct use of the stress-strain relationship obtained based on uniaxial tests. Hence, a plasticity formulation should be developed based on a biaxial yield criterion and isotropic strain hardening for the pipeline material. This paper follows the work in Yoosef-Ghodsi

et al. [23] for attaining the longitudinal stress-strain relationship at specific hoop stress induced by internal pressure.

According to the von Mises yield criterion, the effective stress σ_{vM} in the biaxial state of stress with the longitudinal stress σ_l and hoop stress σ_h shown in Figure 7-3 (b) can be expressed as Eq. (7-4). Hence, the equivalent longitudinal tensile and compressive stress upon the onset of yielding, respectively denoted by σ_y^T and σ_y^C, can be obtained as Eqs. (7-5) and (7-6) by solving Eq. (7-4) for σ_l in which the effective stress σ_{vM} equals the yield stress σ_y in the uniaxial test. When the longitudinal stress is in the range of $\left[\sigma_y^C,\ \sigma_y^T\right]$, the pipe material is elastic, and the longitudinal stress-strain relationship can be obtained according to Hooke's constitutive law.

$$\sigma_{vM} = \sqrt{\sigma_l^2 + \sigma_h^2 - \sigma_l \bullet \ _h} \tag{7-4}$$

$$\sigma_y^T = \frac{1}{2}\left(\sigma_h + \sqrt{4\left(\sigma_y\right)^2 - 3\sigma_h{}^2}\right) \tag{7-5}$$

$$\sigma_y^C = \frac{1}{2}\left(\sigma_h - \sqrt{4\left(\sigma_y\right)^2 - 3\sigma_h{}^2}\right) \tag{7-6}$$

Response of the pipe material after the onset of yielding is calculated based on the flow rule of plasticity. The infinitesimal increment of longitudinal strain within the plastic deformation can be derived as Eq. (7-7) [23]. Strain in the inelastic range can be obtained after integrating the two sides of Eq. (7-7). Therefore, longitudinal strain in the biaxial stress state can be summarized as Eq. (7-8).

$$d\varepsilon_l = \left(\frac{1}{E} + \frac{\left(2\sigma_l - \sigma_h\right)^2}{4H_p\left(\sigma_l{}^2 + \sigma_h{}^2 - \sigma_l\sigma_h\right)}\right)d\sigma_l \tag{7-7}$$

$$\varepsilon_l = \begin{cases} \dfrac{\sigma_l}{E} + \dfrac{1}{4H_p}\displaystyle\int_{\sigma_y^T}^{\sigma_l} \frac{\left(2\sigma_x - \sigma_h\right)^2}{\sigma_x{}^2 + \sigma_h{}^2 - \sigma_x\sigma_h} d\sigma_x & , \quad \sigma_l > \sigma_y^T \\ \dfrac{\sigma_l - \nu\sigma_h}{E} & , \quad \sigma_y^C \le \sigma_l \le \sigma_y^T \\ \dfrac{\sigma_l}{E} + \dfrac{1}{4H_p}\displaystyle\int_{\sigma_y^C}^{\sigma_l} \frac{\left(2\sigma_x - \sigma_h\right)^2}{\sigma_x{}^2 + \sigma_h{}^2 - \sigma_x\sigma_h} d\sigma_x & , \quad \sigma_l < \sigma_y^C \end{cases} \tag{7-8}$$

where H_p is the plastic modulus equaling to $\dfrac{EE_h}{E - E_h}$.

Figure 7-4 illustrates the longitudinal stress-strain relationships in the uniaxial and biaxial based on the same pipe material with properties next to the figure. It can be seen that stress in the plastic range in the biaxial stress state is approximately linear with the strain, which indicates that the hardening slopes in tension and compression, represented by E_h^T and E_h^C respectively, can be approximated as constant values.

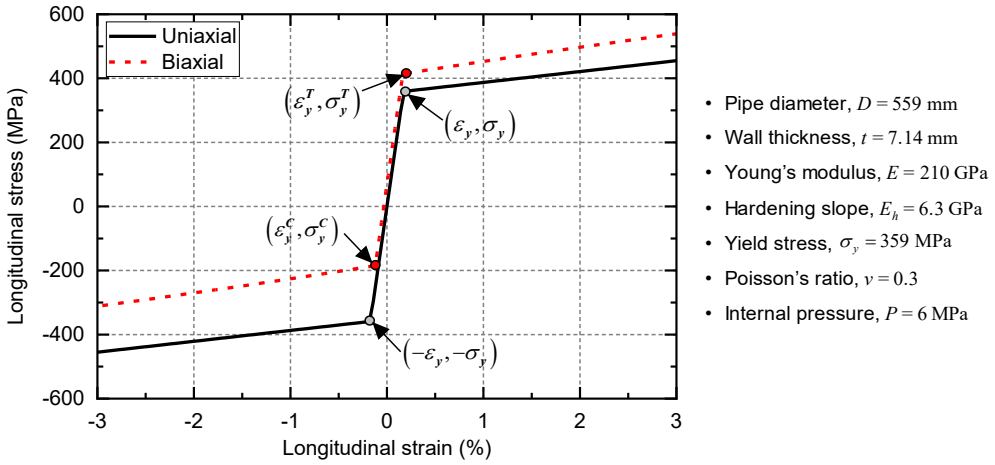

Figure 7-4: Longitudinal stress-strain relationships in uniaxial and biaxial tests

The hoop stress σ_h due to internal pressure can be calculated using Barlow's formula, and the resultant longitudinal stress can be obtained according to the Poisson effect. The longitudinal

stress due to temperature change can be estimated based on the thermal effect. Hence, the initial longitudinal stress $\sigma_{initial}$, applied prior to the ground movement, can be written as Eq. (7-9).

$$\sigma_{initial} = \nu\sigma_h - E\alpha\Delta T = \frac{\nu P(D-2t)}{2t} - E\alpha\Delta T \tag{7-9}$$

where ν is Poisson's ratio; σ_h is the hoop stress induced by internal pressure; P is the internal pressure; D and t are respectively the outer diameter and wall thickness of the pipe; α denotes the thermal expansion coefficient of pipe material; ΔT represents the difference in temperature between the time when the ground movement is concerned and the time of pipeline tie-in.

It is assumed that the pipe has no displacement or actual strain under the two operational loads due to the soil constraint. Nevertheless, from the perspective of material response, a pseudo initial strain $\varepsilon_{initial}$ is supposed to be generated corresponding to the initial longitudinal stress as shown in Eq. (7-10). Therefore, the total longitudinal strain ε_l can be written as Eq. (7-11).

$$\varepsilon_{initial} = \frac{\sigma_{initial}}{E} = \frac{\nu P(D-2t)}{2Et} - \alpha\Delta T \tag{7-10}$$

$$\begin{aligned}\varepsilon_l &= \varepsilon_{initial} + \varepsilon_{axial} + \varepsilon_{bending} \\ &= \left(\frac{\nu P(D-2t)}{2Et} - \alpha\Delta T\right) + \left(u' + \frac{1}{2}v'^2\right) - zv''\end{aligned} \tag{7-11}$$

where $(x)'$ and $(x)''$ are respectively the first and second derivative of x; z represents the radial location in the pipe cross-section, e.g., $\varepsilon_{bending}$ would represent the bending strain on the pipe extreme fiber when z equals the pipe radius of $\frac{D}{2}$. With updated formulation of the longitudinal strain, the internal axial force and bending moment can be reformulated, compared with those in [27][28], to consider the biaxial stress state in the following two scenarios.

(1) Longitudinal strain pattern without bending effect

Absence of bending action indicates that $v'' = 0$ thus $M = 0$, and the stress is uniformly distributed on the pipe cross-section. The formulation of axial force N and M can be respectively expressed as Eqs. (7-12) and (7-13).

$$N=\begin{cases}\left(\sigma_y^T+E_h^T\left(\varepsilon_l-\varepsilon_y^T\right)\right)A & , \quad \varepsilon_l>\varepsilon_y^T \\ E\varepsilon_l A & , \quad \varepsilon_y^C\le\varepsilon_l\le\varepsilon_y^T \\ \left(\sigma_y^C+E_h^C\left(\varepsilon_l-\varepsilon_y^C\right)\right)A & , \quad \varepsilon_l<\varepsilon_y^C\end{cases} \tag{7-12}$$

$$M=0 \tag{7-13}$$

(2) Longitudinal strain pattern with bending effect

The distributions of longitudinal strain and stress distribution on the pipe cross-section are generalized as the two scenarios in Figure 7-5 when the bending effect exists. According to the geometric relationship, the vertical coordinate (the origin is the pipe top, and the positive side points to the downside) from the pipe top to the tensile yielding position h_{ty} and compressive yielding position h_{cy} can be expressed as Eqs. (7-14) and (7-15).

$$h_{ty}=\frac{\nu P\left(D-2t\right)-Et\left(2\alpha\Delta T-2u'-v'^2+Dv''+2\varepsilon_y^T\right)}{-2Etv''} \tag{7-14}$$

$$h_{cy}=\frac{\nu P\left(D-2t\right)-Et\left(2\alpha\Delta T-2u'-v'^2+Dv''+2\varepsilon_y^C\right)}{-2Etv''} \tag{7-15}$$

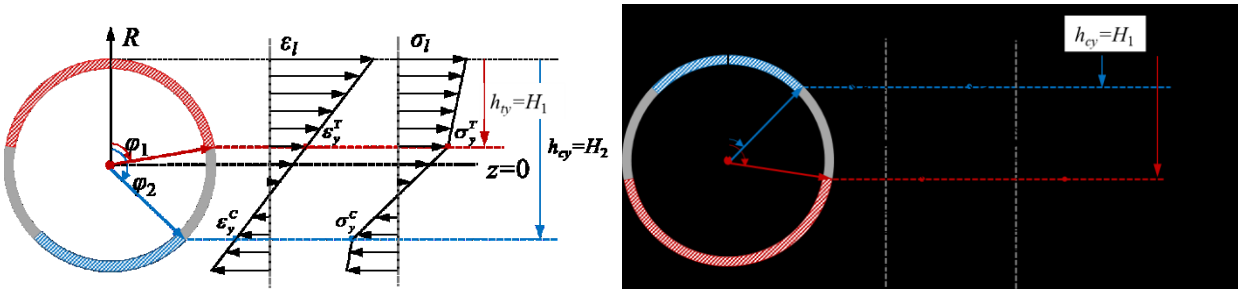

(a) Scenario 1 (b) Scenario 2

Figure 7-5: Longitudinal strain and stress distribution on pipe cross-section

The two auxiliary variables H_1 and H_2, utilized to distinguish the two scenarios in Figure 7-5, can be obtained based on Eqs. (7-16) and (7-17) respectively. In addition, the angle corresponding to H_1 and H_2 on the pipe cross-section can be subsequently derived as Eq. (7-18).

$$H_1 = \min\left(h_{ty}\ ,\ h_{cy}\right) \tag{7-16}$$

$$H_2 = \max\left(h_{ty}\ ,\ h_{cy}\right) \tag{7-17}$$

$$\varphi_i = \begin{cases} 0 & H_i \le 0 \\ \arccos\left(\dfrac{D-2H_i}{D}\right) & 0 < H_i < D \ \ (i=1,2) \\ \pi & H_i \ge D \end{cases} \tag{7-18}$$

Formulations of axial force N and bending moment M can be derived based on their definitions as shown in Eqs. (7-19) and (7-20) respectively.

$$N = (D-t)t \cdot \begin{cases} \left(E_h^C\pi + \left(E-E_h^C\right)\phi_2\right)\left(\dfrac{\nu P(D-2t)}{2Et} - \alpha\Delta T + u' + \dfrac{1}{2}v'^2\right) \\ -\dfrac{D}{2}\left(\left(E-E_h^T\right)\sin\phi_1 - \left(E-E_h^C\right)\sin\phi_2\right)v'' \\ -\left(E-E_h^T\right)\left(\dfrac{\nu P(D-2t)}{2Et} - \alpha\Delta T + u' + \dfrac{1}{2}v'^2 - \varepsilon_y^T\right)\phi_1 \\ +\left(E-E_h^C\right)(\pi-\phi_2)\varepsilon_y^C \end{cases} , \quad h_{cy} > h_{ty}$$

$$\begin{cases} \left(E_h^T\pi + \left(E-E_h^T\right)\phi_2\right)\left(\dfrac{\nu P(D-2t)}{2Et} - \alpha\Delta T + u' + \dfrac{1}{2}v'^2\right) \\ -\dfrac{D}{2}\left(\left(E-E_h^C\right)\sin\phi_1 - \left(E-E_h^T\right)\sin\phi_2\right)v'' \\ -\left(E-E_h^C\right)\left(\dfrac{\nu P(D-2t)}{2Et} - \alpha\Delta T + u' + \dfrac{1}{2}v'^2 - \varepsilon_y^C\right)\phi_1 \\ +\left(E-E_h^T\right)(\pi-\phi_2)\varepsilon_y^T \end{cases} , \quad h_{cy} < h_{ty} \tag{7-19}$$

$$M=\frac{1}{4}(D-t)^2 t\bullet\begin{cases}\left(\begin{array}{l}\frac{D}{2}\left(\begin{array}{l}E_h^C\pi-\left(E-E_h^T\right)\left(\phi_1+\sin\phi_1\cos\phi_1\right)+\\ \left(E-E_h^C\right)\left(\phi_2+\sin\phi_2\cos\phi_2\right)\end{array}\right)v''\\ -2\left(\begin{array}{l}\left(E-E_h^T\right)\sin\phi_1\\ -\left(E-E_h^C\right)\sin\phi_2\end{array}\right)\left(\frac{\nu P(D-2t)}{2Et}-\alpha\Delta T+u'+\frac{1}{2}v'^2\right)\\ +2\left(E-E_h^T\right)\sin\phi_1\varepsilon_y^T\\ -2\left(E-E_h^C\right)\sin\phi_2\varepsilon_y^C\end{array}\right) & ,\quad h_{cy}>h_{ty}\\ \left(\begin{array}{l}\frac{D}{2}\left(\begin{array}{l}E_h^C\pi-\left(E-E_h^C\right)\left(\phi_1+\sin\phi_1\cos\phi_1\right)+\\ \left(E-E_h^T\right)\left(\phi_2+\sin\phi_2\cos\phi_2\right)\end{array}\right)v''\\ -2\left(\begin{array}{l}\left(E-E_h^C\right)\sin\phi_1\\ -\left(E-E_h^T\right)\sin\phi_2\end{array}\right)\left(\frac{\nu P(D-2t)}{2Et}-\alpha\Delta T+u'+\frac{1}{2}v'^2\right)\\ +2\left(E-E_h^C\right)\sin\phi_1\varepsilon_y^C\\ -2\left(E-E_h^T\right)\sin\phi_2\varepsilon_y^T\end{array}\right) & ,\quad h_{cy}<h_{ty}\end{cases} \tag{7-20}$$

The above formulations allow the strain demand calculation considering ground movement, internal pressure, and temperature effect simultaneously by extending the finite difference method developed earlier by the authors [27][28].

7.2.3 Probability estimation for strain capacity exceedance

Aiming at estimating the probability of strain capacity exceeding strain demand in pipelines subjected to permanent ground movement, this study defines the following limit state function as Eq. (7-21).

$$g(\boldsymbol{x})=\min\left[g_T(\boldsymbol{x}),\ g_C(\boldsymbol{x})\right]=\min\left[\varepsilon_c^T(\boldsymbol{x})-\varepsilon_d^T(\boldsymbol{x}),\ \varepsilon_c^C(\boldsymbol{x})-\left|\varepsilon_d^C(\boldsymbol{x})\right|\right] \tag{7-21}$$

where g is the safety margin, which is governed by the lower safety margin due to tension g_T and compression g_C, meaning that pipe is considered to be in the safe domain when both g_T and g_C are simultaneously higher than 0, and otherwise in the failure domain; $\boldsymbol{x}$ represents the random vector comprised of basic random variables that influence strain capacities and strain demands.

Thus, the event $g(\boldsymbol{x}) < 0$ is deemed as failure and the probability of failure PoF = P[$g(\boldsymbol{x}) < 0$] in this context. It should be mentioned that the strain demands are calculated based on the model presented in section 7.2.1, so ε_d^T is always positive and ε_d^C is negative. In that case, the absolute sign is applied for the compressive strain demand ε_d^C in Eq. (7-21) because strain capacity is employed as positive number in this study.

Considering the fact that MCS is acknowledged as the most robust method for reliability calculation, the PoF can be calculated based on Eq. (7-22).

$$p_f = \frac{n\left(g\left(\boldsymbol{x}_i\right) \le 0\right)}{N} \tag{7-22}$$

where $n\left(g\left(\boldsymbol{x}_i\right) \le 0\right)$ means the number of failure cases; N is the sample size, namely the total number of sampling cases in the design space according to the full stochastic characterization of random variables using MCS.

Probabilistic analysis is computationally extensive, because solving a large size of nonlinear equations in the strain demand calculation is still a time-consuming process. To improve the efficiency further, the implementation is optimized in this study. The python code is compiled based on the Numba library, which translates the functions in Python to optimized machine code at runtime so that the speed of computation can be improved. In addition, calculation of strain demand is parallelized for each loop. The schemes can be well supported for explicit parallel loops, and thus are used for implementing the probability of failure calculation in this paper with highly improved efficiency.

7.3 Probability of ground movement initiation

Long-distance transmission pipelines unavoidably transverse over a number of land unstable zones along the right-of-way. From the geotechnical perspective, every piece of land exhibits the potential to initiate a ground movement under certain conditions. The induced ground movement can pose serious threats to the integrity of pipelines from the structural viewpoint. Knowledge of the two different engineering areas is required for a comprehensive failure rate calculation of pipes buried across geohazard zones.

As for landslides, the movement velocity is classified into different levels. Accordingly, the geohazard of landslides is generalized into steady-state creep movement and sudden mass landslides. Steady-state creep movement, customarily termed slope creep, has extremely slow movement such as a few millimeters per year. Sudden mass landslide (named landslide hereafter) is the case whereby the slope suddenly moves by a large magnitude within a short period of time. The velocity difference between slope creep and landslide should be identified by the pipeline operators based on the case-specific hazard analysis.

Estimation of the probability of ground movement initiation is extremely difficult given the complexity of the land characteristics, limited information available from field observations, and uncertainty in future environmental conditions. PRCI Guideline [18] published the characteristics of slope creep and the associated probabilities depending on the relative likelihood (see Table 7-1). According to Sen et al. [24], landslides refer to ground movement with a larger magnitude than 300 mm within one year, and the annual probabilities of landslide initiation are assumed to be less than (e.g., 1/50) that of the probability of slope creep, as considered in Table 7-1.

Table 7-1: Probability of initiation of creep slope and landslide

Classification of likelihood	**Probability of creep slope initiation (per year)**	**Probability of landslide initiation (per year)**
Certain	$> 2 \times 10^{-1}$	$> 4 \times 10^{-3}$
Probable	$1 \times 10^{-1} \sim 2 \times 10^{-1}$	$2 \times 10^{-3} \sim 4 \times 10^{-3}$
Possible	$1 \times 10^{-2} \sim 1 \times 10^{-1}$	$2 \times 10^{-4} \sim 2 \times 10^{-3}$
Unlikely	$1 \times 10^{-3} \sim 1 \times 10^{-2}$	$2 \times 10^{-5} \sim 2 \times 10^{-4}$
Remote	$1 \times 10^{-4} \sim 1 \times 10^{-3}$	$2 \times 10^{-6} \sim 2 \times 10^{-5}$
Negligible	$< 1 \times 10^{-4}$	$< 2 \times 10^{-6}$

7.3.1 PoF calculation of pipes buried across slope zones

7.3.1.1 Calculation of PoF due to creep slope

Regarding the situation with slope creep, the ground movement moves slowly so that the strain is accumulated in the pipe over years. As per instructions in CSA Z662:19 [38], the limit state of pipe undergoing slope creep is time-dependent where the strain demand increases with growing ground movement over elapsed time and the strain capacity is assumed to be constant. Provided that the ground movement initiation in each year is an independent event, and if it occurs, the PoF of the pipe subjected to slope creep at a specific site can be calculated using Eqs. (7-23) and (7-24).

$$p_f^{creep}\left(\tau = n\right) = \sum_{i=1}^{n} p_{f|creep}\left(\tau = i\right) \times p_{creep}\left(i, n\right) \tag{7-23}$$

$$p_{creep}\left(i, n\right) = \alpha^i \left(1-\alpha\right)^{n-i} C_i^n = \alpha^i \left(1-\alpha\right)^{n-i} \times \frac{n!}{i!\left(n-i\right)!} \tag{7-24}$$

where τ is the elapsed time in years; $p_f^{creep}\left(\tau = n\right)$ is the PoF of pipes subjected to slope creep at a specific site after n year(s); $p_{f|creep}\left(\tau = i\right)$ is the PoF given the magnitude of slope creep accumulated after being initiated in i years, namely i times ; $p_{creep}\left(i, n\right)$denotes the probability of i occurrences of slope creep initiation over the n year(s), which can be calculated using Eq. (7-24) where α is the annual probability of creep slope initiation depending the site categorization in terms of likelihood as specified in Table 7-1.

7.3.1.2 Calculation of PoF due to landslide

Contrary to the situation in slope creep, pipes subjected to landslides can be treated as time-independent events as the occurrence of ground movement is instantaneous and immediate action should be taken to avoid or alleviate pipeline failure. As such, failures of pipes due to each landslide occurrence in different years are independent. Likewise, the PoF of pipes subjected to landslide per year can be calculated using Eq. (7-25).

$$p_f^{landslide} = p_{landslide} \bullet \tag{7-25}$$

where $p_f^{landslide}$ is the PoF of pipes due to the landslide; $p_{landslide}$ is the probability of landslide initiation per year; $p_{f|landslide}$ represents the conditional probability of pipe failure under ground movements given landslide initiation. Within *n* years, the pipeline can fail due to landslides can be therefore written as Eq. (7-26). It should be noted that the distribution of landslides for each year is assumed to be the same.

$$p_f^{landslide}(\tau = n) = 1 - \left(1 - p_f^{landslide}\right)^n \tag{7-26}$$

Assuming that the initiations of slope creep and landslide are independent, the total PoF of pipes buried across at a slope crossing can be calculated using Eq. (7-27) assuming the pipeline fails due to slope creep or landslide.

$$p_f(\tau) = 1 - \left[1 - p_f^{creep}(\tau)\right] \bullet \qquad {}^{lide}(\tau)\Big] \tag{7-27}$$

In Eq. (7-27), the two terms $p_f^{creep}(\tau)$ and $p_f^{landslide}(\tau)$ can be estimated using the method introduced in section 7.2 based on the information related to slope creep and landslide provided in section 7.3.

7.4 Application of the method to transmission pipelines in service

7.4.1 Problem statement

This study considers a 559-mm-diameter pipeline with a wall thickness equal to 7.14 mm, buried across a geohazard-prone zone where slope creep or landslide may happen. The length of span involved in the geohazard is 10 m. The vintage pipe is made with X52 steel with a nominal yield stress of σ_y = 359 MPa and nominal Young's Modulus is E = 210 GPa. The strain hardening slope is E_h = 2.1 GPa (i.e., 1% of Young's modulus). The properties of backfill are attributed to soil springs which have axial resistance T_u = 14 kN/m (yield displacement Δt = 0.265 m) and lateral resistance P_u = 204 kN/m (yield displacement Δp = 0.029 m), which are assumed to be deterministic due to the lack of stochastic data. The pipe is operated under the maximum operating

pressure of 7.3 MPa. For the strain demand calculation, the number of nodes for the span across geohazard is set as 21. The two segments connected to the geohazard-involved span are determined as 100 m with 51 nodes for each. The fixed boundary condition is applied to pipe ends.

The tensile and compressive strains are considered simultaneously in the limit state function stated in Eq. (7-21). However, most existing tensile and compressive strain capacity models, as stated in section 7.2.1, correspond to different levels of limit states, which cannot be adopted together in the limit state function. In addition, the specified applicable parameter ranges of those models restrain their practice in MCS since the generated random data would be out of the range. For the above two reasons, the strain capacities specified in ALA Guideline [17], including the operable limit and integrity limit, are determined to be employed in the following calculation.

The parametric calculation on the PoFs of the pipe is performed with respect to pipe-ground intersection angle β (30°, 60° and 90°) based on Monte Carlo Simulation with a sample size of 10,000. Parameters considered as random variables are tabulated in Table 7-2 in which the stochastic properties are reasonably assumed based on CSA Z662:19 [38] and the relevant industry publication [24].

Table 7-2: Stochastic properties of pipe geometries

Parameter	**Distribution**	**Mean**	**Standard deviation**	**Mode**	**Lower bound**	**Upper bound**	**Unit**
Diameter, D	Normal	559	0.9503	-	-	-	mm
Wall thickness, t	Normal	7.14	0.1678	-	-	-	mm
Yield strength, σ_y	Normal	387	22	-	-		MPa
Temperature, ΔT	Uniform	-	-	-	-25	45	℃
Creep slope rate	Lognormal	12.4	6.24	-	-	-	mm/yr
Landslide movement	Triangular	-	-	796	298	3,980	mm

7.4.2 Results and discussions

Results of PoF of pipes underground movements due to slope creep and sudden landslide are shown in Figure 7-6, in which the operable limit and integrity limit are referred to as SLS and ULS respectively. It can be seen that the PoFs for integrity limit (ULS) are lower than those for operable limit (SLS) since the ULS has greater strain capacity so a larger safety margin is induced. PoFs of the pipe under the ground movements due to slope creep are calculated over time (in years). Since the slope magnitude grows with the elapsed time, the cumulative strain on the pipe gradually increases. Hence, PoFs increase with time as shown in Figure 7-6 (a). Comparing the PoFs under different intersection angles, it can be observed that the higher the intersection angle is, the greater the PoF will be, which implies that the pipe is more vulnerable when undergoing a greater intersection angle. In addition, the effect of intersection angle on PoFs becomes weaker with the increase of the intersection angle as the PoFs with 60° are closer to those with 90° . This phenomenon can also be observed in Figure 7-6 (b), which describes the PoFs of the pipe subjected to ground movements induced by sudden landslides.

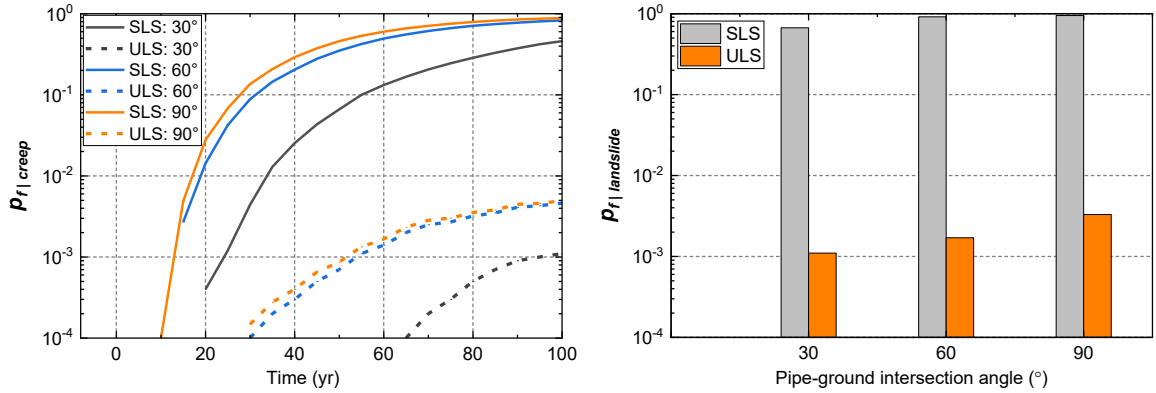

(a) PoF of pipes under creep slope (b) PoF of pipes under landslide

Figure 7-6: PoF of the pipe subjected to two different geohazard scenarios

A period of 40 years is considered to investigate the PoF of the pipe buried across the unstable ground zone considering different likelihoods of ground movement initiation. The calculated results are reported in Figure 7-7, including the permissible PoF of 10^{-1}/year for

operable limits and 10^{-3}/year for integrity limits (assuming population density is 0), which are transferred into the cumulative format with elapsed time as indicated by the red dashed line. The PoF corresponding to different likelihoods of ground movement initiation is highlighted by different colors. As observed, the higher the probability of ground movement initiation, the higher the resultant PoF is. The difference in PoF diminishes with the increase of the probability of ground movement initiation.

The comparison between the resultant PoFs and the permissible PoF can be used for determining the re-inspection time and making the maintenance plan. Taking the results for SLS as an example, PoFs with a certain likelihood of ground movement initiation are higher than the permissible PoF over 40 years for all three pipe-ground intersection angle cases, which means that the pipe should be re-checked within a shorter period, e.g., less than one year. When the likelihood of ground movement initiation is probable, the permissible PoF is between the upper and lower bound of PoF when the pipe-ground intersection angle is 30°, and it approaches the lower bound of PoF with the increase of pipe-ground intersection angle. Hence, careful consideration of the exact probability of ground movement initiation is required for making a relatively comprehensive re-inspection plan. As for the lower likelihood of ground movement initiation, i.e., possible, unlikely, remote, and negligible, the PoFs are always below the permissible PoF, which indicates that the pipe is safe since the probability of ground movement occurrence is very low. In contrast, the PoFs for ULS are all within the permissible range for the likelihood of geohazard initiation is not certain, which indicates that the re-inspection period could be longer if ULS is used for decision-making.

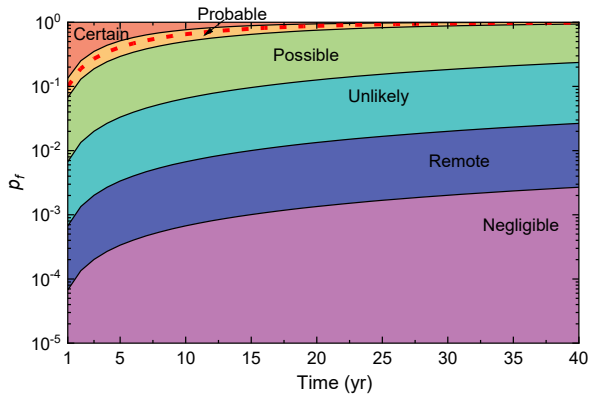

(a) PoF of pipes for SLS ($\beta = 30°$)

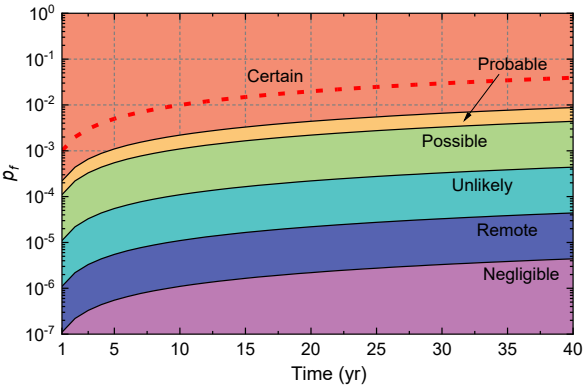

(b) PoF of pipes for ULS ($\beta = 30°$)

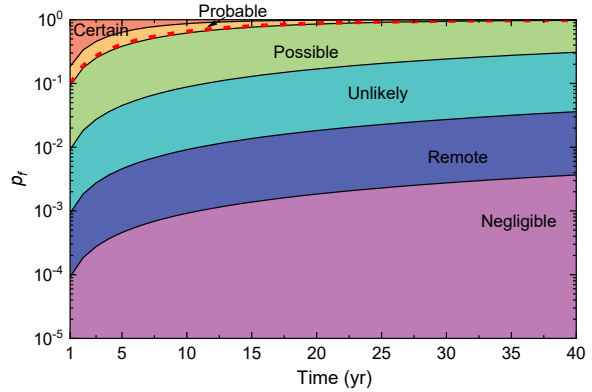

(c) PoF of pipes for SLS ($\beta = 60°$)

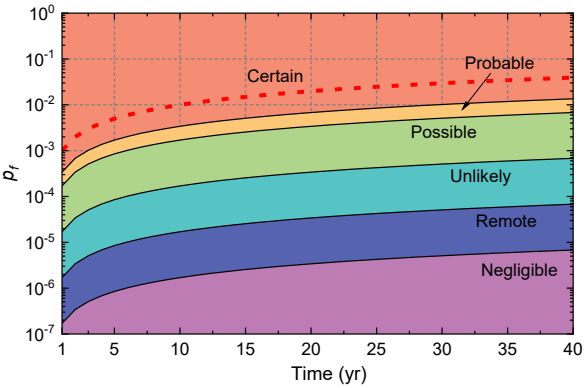

(d) PoF of pipes for ULS ($\beta = 60°$)

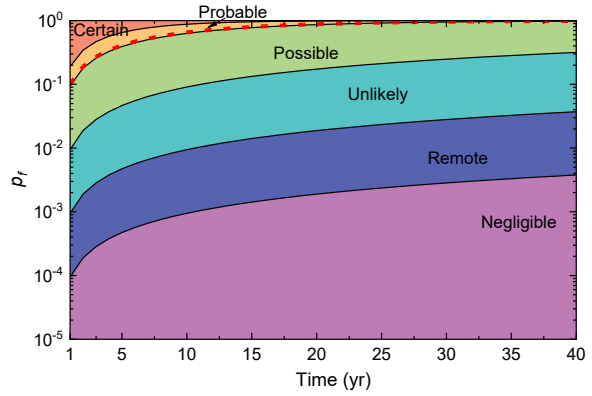

(e) PoF of pipes for SLS ($\beta = 90°$)

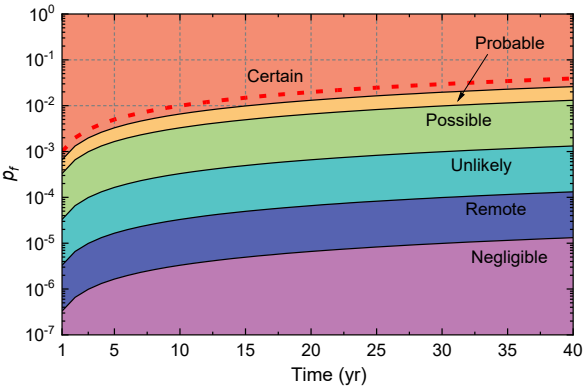

(f) PoF of pipes for ULS ($\beta = 90°$)

Figure 7-7: PoF of pipes buried across geohazard zone over time

7.5 Chapter conclusions

This paper presents a general procedure for an engineering practice of reliability-based assessment of pipes buried across geohazard-prone areas. The assessment is based on the criterion of strain: the strain capacity can be calculated using the published models, and the strain demand is estimated based on the finite difference method initially proposed by Zheng et al. [27][28]. To account for the effects of internal pressure and temperature change, the flow rule of plasticity is employed to investigate the response of the pipe material after the onset of yielding. The probability of failure (PoF) at a given magnitude of ground movement is calculated based on Monte Carlo Simulation. The total PoF is obtained by considering the probability of ground movement initiation. This study takes landslides as an example and the related stochastic properties are reasonably assumed based on published data.

The proposed finite difference-based method for strain demand prediction is developed based upon the one-dimension beam model, which cannot account for complex spatial behavior like local buckling. Hence, this method is more suitable for preliminary design and safety pre-screening where rigorous analysis is unnecessary. In addition, the probabilistic data related to geohazard used in the study case is assumed based on guidelines and publications, which involves a large amount of uncertainties and affects accuracy of the results. For better accuracy, a case with adequate site-specific information is required, and it is a better practice of the proposed method.

Reference

[1] M. Porter, G. Ferris, M. Leir, M. Leach, M. Haderspock, Updated estimates of frequencies of pipeline failures caused by geohazards, in: International Pipeline Conference, American Society of Mechanical Engineers (ASME), Calgary, 2016, pp. V002T07A003.

[2] R.R. Read, M. Rizkalla, Bridging the gap between qualitative, semi-quantitative and quantitative risk assessment of pipeline geohazards: the role of engineering judgment, in: 24 ASME International Pipeline Geotechnical Conference (IPG2015), American Society of Mechanical Engineers (ASME), Bogota, 2015, pp. V001T02A004.

[3] A. Baumgard, M. Beaupre, M. Leir, Implementing a quantitative geohazard frequency analysis framework as a component of risk assessment of new pipelines, in: 2016 11th International Pipeline Conference (IPC2016), American Society of Mechanical Engineers (ASME), Calgary, 2016, pp. V002T07A020.

[4] R. Guthrie, E. Reid, Estimating landslide induced probability of failure to pipelines using a structured reductionist approach, in: 2018 12th International Pipeline Conference (IPC2018), American Society of Mechanical Engineers (ASME), Calgary, 2018, pp. V002T07A004.

[5] M. Porter, J. Van Hove, P. Barlow, Analysis of dynamic system risks where pipelines cross slow-moving landslides, in: 2022 14th International Pipeline Conference (IPC2022), American Society of Mechanical Engineers (ASME), Calgary, 2022, pp. V001T07A007.

[6] N.M. Newmark, W.J. Hall, Pipeline design to resist large fault displacement, in: Proceedings of U.S. National Conference on Earthquake Engineering, Earthquake Engineering Research Institute, Michigan, 1975, pp. 416-425.

[7] R.P. Kennedy, A.W. Chow, R.A. Williamson, Fault movement effects on buried oil pipeline, ASCE J. Transport. Eng. 103 (1977) 617-633.

[8] L.R.L. Wang, Y.A. Yeh, A refined seismic analysis and design of buried pipeline for fault movement, Earthq. Eng. Struct. Dyn. 13 (1985) 75-96.

[9] L.R.L. Wang, Y.A. Yeh, Seismic design of buried pipeline for fault movement effects, J. Press. Vessel. Technol. 108 (1986) 202-208.

[10] D.K. Karamitros, G.D. Bouckovalas, G.P. Kouretzis, Stress analysis of buried steel pipelines at strike-slip fault crossings, Soil. Dyn. Earthq. Eng. 27 (2007) 200-211.

[11] O.V. Trifonov, V.P. Cherniy, Elastoplastic stress strain analysis of buried steel pipelines subjected to fault displacements with account for service loads, Soil. Dyn. Earthq. Eng. 33 (2012) 54-62.

[12] X. Liu, H. Zhang, M. Xia, J. Liu, Q. Zheng, An improved analytical strain analysis method for buried steel pipelines subjected to abrupt permanent ground displacement, in: International Pipeline Conference (IPC2020), American Society of Mechanical Engineers (ASME), Calgary, 2020, pp. V002T06A012.

[13] M.J. O'Rourke, Approximate analysis procedures for permanent ground deformation effects on buried pipelines, in: Proceedings from the Second U.S.-Japan workshop on liquefaction,

large ground deformation and their effects on lifelines, National Center for Earthquake Engineering Research, New York, 1989, pp. 336-347.

[14] M.J. O'Rourke, X. Liu, R. Flores-Berrones, Steel pipe wrinkling due to longitudinal permanent ground deformation, J. Civ. Eng. 121 (1995) 443-451.

[15] X. Liu, M.J. O'Rourke, Behaviour of continuous pipeline subject to transverse PGD, Earthq. Eng. Struct. Dyn. 26 (1998) 989-1003.

[16] U. Zahid, A. Godio, S. Mauro, 2020. An analytical procedure for modelling pipeline-landslide interaction in gas pipelines, J. Nat. Gas. Sci. Eng. 81, 103474.

[17] American Lifelines Alliance (ALA), Guidelines for the Design of Buried Steel Pipe, American Society of Civil Engineers, 2001.

[18] Pipeline Research Council International (PRCI). Guidelines for Constructing Natural Gas and Liquid Hydrocarbon Pipelines Through Areas Prone to Landslide and Subsidence Hazards, Technical Toolboxes, Inc., 2009.

[19] X. Liu, Q. Zheng, K. Wu, Y. Yang, Z. Zhao, H. Zhang, 2020. Development of a novel approach for strain demand prediction of pipes at fault crossings on the basis of multi-layer neural network driven by strain data, Eng. Struct. 214, 110685.

[20] A. Liu, Y. Hu, F. Zhao, X. Li, S. Takada, L. Zhao. An equivalent-boundary method for the shell analysis of buried pipelines under fault movement, Acta. Seismol. Sin. 17 (2004) 150-156.

[21] J. Xie, L. Zhang, Q. Zheng, X. Liu, S. Dubljevic, H. Zhang. Strain demand prediction of buried steel pipeline at strike-slip fault crossings: a surrogate model approach, Earthq. Struct. 20 (2021) 109-122.

[22] W. Zhou, Reliability of pressurised pipelines subjected to longitudinal ground movement, Struct. Infrastruct. Eng. 12 (2012) 1123-1135.

[23] N. Yoosef-Ghodsi, J. Zhou, D.W. Murray, A simplified model for evaluating strain demand in a pipeline subjected to longitudinal ground movement, in: International Pipeline Conference (IPC2008), American Society of Mechanical Engineers (ASME), Calgary, 2008, pp. 657-664.

[24] M. Sen, S. Hassanien, On estimating pipelines reliability at slope crossings, in: Proceedings of The Asset Integrity Management-Pipeline Integrity Management Under Geohazard

Conditions, American Society of Mechanical Engineers (ASME), New York, 2019, pp. 81-92.

[25] Q. Zheng, X. Liu, H. Zhang, X. Gu, M. Fang, L. Wang, S. Adeeb, 2021. Reliability evaluation method for pipes buried in fault areas based on the probabilistic fault displacement hazard analysis, J. Nat. Gas Eng. 85, 103698.

[26] X. Liu, H. Zhang, Y. Han, M. Xia, W. Zheng. A semi-empirical model for peak strain prediction of buried X80 steel pipelines under compression and bending at strike-slip fault crossings, J. Nat. Gas Eng. 32 (2016) 465-475.

[27] Q. Zheng, L. Graf-Alexiou, Y. Li, N. Yoosef-Ghodsi, M. Fowler, M. Kainat, S. Adeeb, Strain demand of elastic pipes subjected to permanent ground displacements using the finite difference method, J. Pipeline. Sci. Eng. 1 (2021) 176-186.

[28] Q. Zheng, Y. Li, N. Yoosef-Ghodsi, M. Fowler, M. Kainat, S. Adeeb, 2022. A finite difference-based approach for strain demand prediction of inelastic pipes subjected to permanent ground displacements, Eng. Struct. 273, 115072.

[29] Interstate Natural Gas Association of America (INGAA), Guidelines for Management of Landslide Hazards for Pipelines, first ed., Geosyntec Consultants, Inc., Golder Associates, Inc., Center for Reliable Energy Systems (CRES), 2020.

[30] N. Yoosef-Ghodsi, Strain-based design of pipelines, in: Oil and Gas Pipelines Integrity and Safety Handbook, 2015, pp. 37-48.

[31] M. Liu, Y.Y. Wang, Y. Song, D. Horsley, S. Nanney, Multi-tier tensile strain models for strain-based design: Part 2-Development and formulation of tensile strain capacity models, in: International Pipeline Conference (IPC2012), American Society of Mechanical Engineers (ASME), Calgary, 2012, pp. 415-425.

[32] CSA Z662-07, Oil and Gas Pipeline Systems, Canadian Standard Association, Mississauga, Ontario, 2007.

[33] D.P. Fairchild, M.L. Macia, S. Kibey, X. Wang, V.R. Krishnan, F. Bardi, H. Tang, W. Cheng, A multi-tiered procedure for engineering critical assessment of strain-based pipelines, in: The 21st International Offshore and Polar Engineering Conference, OnePetro, Cupertino, 2011, pp. ISOPE-I-11-144.

[34] Y.Y Wang, D. Rudland, R. Denys, D. Horsley, A preliminary strain-based design criterion for pipeline girth welds, in: International Pipeline Conference (IPC2002), American Society of Mechanical Engineers (ASME), Calgary, 2002, pp. 415-427.

[35] A.B. Dorey, D.W. Murray, J.R. Cheng, Critical buckling strain equations for energy pipelines-A parametric study, ASME. J. Offshore Mech. Arct. Eng. 128 (2006) 248-255.

[36] C.M. Timms, D.D. DeGeer, M.R. Chebaro, Y. Tsuru, Compressive strain limits of large diameter X80 UOE linepipe, in: The 19th International Offshore and Polar Engineering Conference, OnePetro, Cupertino, 2009, pp. ISOPE-I-09-332.

[37] M. Liu, Y.Y. Wang, F. Zhang, K. Kotian, Realistic Strain Capacity Models for Pipeline Construction and Maintenance, Center for Reliable Energy Systems (CRES), Dublin, 2013.

[38] CSA Z662:19, Oil and Gas Pipeline Systems, Canadian Standard Association, Toronto, Ontario, 2019.

CHAPTER 8: CONCLUSIONS

8.1 Summary of research work

Pipelines are systems of connected pipes used to transport liquids and gases, namely oil and natural gas, across long distances from source to market. Since the middle of the last century, pipelines have been extensively used to transmit water, natural gas, and liquid fuels that are necessary for daily life. Internal pressure and ground movements are two typical loads that pipes encounter in service. Internal pressure is from the pumping stations and is the main drive to the flowing of the media in the pipeline. Ground movements are usually caused by geohazards, which become a significant threat to long-distance transmission pipelines. This research carries on the reliability-based analysis of pipes subjected to internal pressure and ground movements regarding the respective industry concerns.

For pipes subjected to internal pressure, the relationship between the probabilities of failure (PoFs) of pipes and the factors indicating safety is investigated for intact pipes and defected pipes. For intact pipes, PoFs for yielding and burst are calculated with respect to design factors which are used for the designing stage; PoFs for burst are also reported for intact pipes considering different hydrostatic test pressure factors utilized for hydrostatic tests before the pipe commission. For defected pipes with cracks or corrosions, PoFs for burst are studied with respect to safety factors to provide guidance in pressure control in the operation of defected pipes.

Given the limitations that existing models are not applicable for reliability calculation, a novel model (referred to as the FDM-based model), is developed to predict the pipe response to ground movements using the finite difference method. The pipeline is assumed as an Euler-Bernoulli beam with large deformations, and the governing differential equations of the elastic response of the pipe are formulated as functions of displacements of the deformed pipe in the axial and lateral directions at each node. The pipe-soil interaction is represented by soil springs whose properties are calculated based on the published guideline. A large set of nonlinear finite difference equations can be therefore established together with boundary conditions and the solution can be achieved based on the nonlinear equation solver built in the programming language.

To account for the inelastic behavior of the pipe, the axial force and the bending moment in a pipe, as required in the finite difference equations, are derived as explicit functions of the deformations at each node after considering the stress distribution of the pipe cross-section based on the bilinear property of the stress-strain behavior. Two indicative case studies including ground movement in the horizontal and vertical planes are utilized to validate the proposed method against the finite element method (FEM). Furthermore, this FDM-based model is also adopted to predict the tensile strain demand of pipes subjected to strike-slip fault displacements. The results are compared with those derived from four existing analytical methods as well as the FEM.

Substantially, the FDM-based model is incorporated into the limit state function for reliability-based assessment. The PoFs of pipes at the given magnitude of ground movements are calculated using MCS and the code is implemented through Python. To enhance the computational efficiency, the code is firstly compiled so that functions in the code can be transferred into machine code; in the meantime, the loop calculation in MCS is paralleled, which enables multiple sample cases generated by the stochastic simulation to be computed at the same time. In addition, an effective reliability analysis method, named Weighted Monte Carlo simulation (WMCS), is applied to calculate the PoFs using a smaller sample size compared with MCS. Efficiency and accuracy of WMCS are tested via comparison with MCS. Finally, based upon the developed codes in the research, two calculator-like tools are established respectively for deterministic analysis and reliability-based assessment of the integrity of pipelines subjected to ground movements.

Moreover, a general procedure is presented for comprehensive probabilistic evaluation of pipes buried across geohazard-prone areas. To do this, the FDM-based model is further developed by taking into account the effects of internal pressure and temperature change based on the flow rule in plasticity. The probability of ground movement initiation is employed to obtain the total cumulative PoF. Besides, the formula of cumulative PoF over elapsed time is derived, which can be useful for making the maintenance plan and determining the re-inspection time. An indicative case is proposed to illustrate the application of the procedure.

8.2 Conclusions of research work

Research on pipes subjected to internal pressure reveals the interrelationship between the design (and safety) factors in deterministic analysis and PoFs in probabilistic analysis, which provides a useful reference for safety control from the perspective of reliability-based assessment. The main conclusions about pipes subjected to internal pressure are summarized as follows.

(1) For intact pipes, PoFs for yielding increase with the growth of design factors. Specifically, for design factors 0.80 (division 1) and 0.72 (division 2) used in class location 1, probabilities of failure for yielding limit state are 2.81×10^{-7} and 1.13×10^{-11} respectively. However, PoFs for yielding limit state are independent of yield strength, internal pressure, pipe diameter, and wall thickness based on the stochastic properties recommended by CSA Z662: 19.

(2) PoFs of intact pipes for burst (ultimate limit state) are generally lower than those for yielding (serviceability limit state). Additionally, higher-grade pipes are more vulnerable to burst since their higher yield-to-tensile ratios decrease the capacities in the limit state function.

(3) As for defected pipes, a higher safety factor corresponds to a higher reliability level (lower PoF), and pipe grade shows little impact on the relationship between PoFs and safety factors. Pipe dimensions (i.e., diameter and wall thickness), and flaw sizes (i.e., flaw length and depth) have negligible influence on PoFs of cracked pipes but show significant impact on PoFs of corroded pipes. Corroded pipes with larger diameter-to-wall thickness ratios and deeper and longer defects show higher PoFs under internal pressure.

(4) The published model error of CorLAS is large, which leads to a considerable increase in the associated PoFs. Hence, reliable burst pressure prediction models are needed for cracked pipes.

(5) Compared with MCS, WMCS has a fairly good capability to calculate the PoFs in terms of accuracy and efficiency.

On the other hand, this research implements the reliability-based assessment on pipes buried across geohazard-prone zones by developing the FDM-based model, which fills the gap in the

pipeline industry. The general conclusions about the FDM-based model and its application in the reliability-based assessment are summarized below:

(1) The FDM-based model is of good accuracy for both elastic and inelastic behaviors of pipes under ground movements. It is a good alternative to one-dimensional beam finite element models for preliminary design and safety pre-screening.
(2) The FDM-based model is applicable to predict pipes' response to a wide range of geohazards, including landslides, ground heave and subsidence in which two ground discontinuities should be considered in analysis, as well as tectonic faults where one ground discontinuity is required.
(3) Using the computational optimization methods, i.e., compiling and parallelization, it is practical to incorporate the FDM-based model into the limit state function for reliability calculation. The efficiency is acceptable based on the sample size of 10,000 in MCS.

8.3 Research contributions and highlights

The main contributions and highlights of this research work, which focuses on reliability-based assessment on pipes subject to internal pressure and ground movements, are summarized as follows.

(1) This research provides the quantitative design/safety factors-PoFs interrelationship for intact pipes which are used before the commission for design and hydrostatic test, as well as the defected pipes (cracked pipes and corroded pipes) which are concerned in service. The obtained results can be employed in engineering for safety control for a higher level of confidence.
(2) This research proposed the FDM-based model to calculate the strain demand of pipes under ground movement, which contributes a brand-new method to the field of integrity analysis of pipes under ground-induced displacements. In particular, the FDM-based model provides a unified approach to evaluate the pipe's response to ground movements triggered by geohazards, such as landslides, ground heave and subsidence, tectonic fault,

etc. In addition, the FDM-based model is feasible to be used for reliability-based assessment on pipes subject to ground movements.

(3) The tools established for deterministic analysis and reliability-based assessment on pipes under ground movements provide the direct application of the methods proposed in this research. Especially, the formula for calculating the annual PoF of pipes buried through landslide-prone zones is presented, which provides an important reference to the decision on the maintenance plan.

(4) This research brings the established reliability method, named Weighted Monte Carlo Simulation (WMCS), to the attention of the pipeline industry. The advantages on accuracy and efficiency of this method are demonstrated through extensive practice on case studies. It is an appropriate alternative to Monte Carlo Simulation (MCS) for the sake of efficiency.

8.4 Limitations and recommendations

Although this research work provides a number of contributions and significant enhancements to the objectives of the project, there are some limitations and challenges that need to be solved in order to establish a thorough methodology that could bring more realistic results to engineering practice. The limitations and recommendations are listed as follows.

(1) The defected pipes under internal pressure only consider a single flaw, i.e., a crack or corrosion on the pipe. Multiple flaws and mixed flaws, which are common in the field, are not accounted for in the reliability calculation. Therefore, further reliability-based study can be conducted on pipes with multiple or mixed flaws.

(2) The proposed FDM-based model is established on the basis of the one-dimension beam model, which cannot be applicable to solve the complex spatial behavior of the pipe cross-section like local buckling. Detailed finite element analysis, i.e., full 3D models, is still necessary to investigate the pipe strength required for comprehensive analysis.

(3) Algorithm of the FDM-based model doesn't always output the true results due to convergence issues. The effect becomes more pronounced with the increase of deformation in pipes. Besides, it is more appropriate to be used for the analysis on

relatively short pipe length. The longer the pipe length is, the more grid nodes are required, which caused a larger non-linear finite difference equation set. This is also a major reason leading to convergence issues. To minimize the problem, more robust solvers are demanded for solving large nonlinear finite difference equation sets.

(4) There are some limitations which are not the main focuses but significant to the reliability-based assessment on pipes under geohazard-prone zones. Firstly, the existing predictive models of strain capacity have tight applicable ranges of input parameters, which restrains their practice in reliability calculation. Additionally, getting the probability of ground movement initiation is full of challenges from the perspective of geotechnical engineering. Collaborative efforts from a diverse array of industry expertise and experience are required. Currently, for higher accuracy, the reliability calculation can be implemented on case-specific analysis to reduce the uncertainties arising from the strain capacity and ground movements.

BIBLIOGRAPHY

Amendment 10 R6, revision 4, Assessment of the integrity of the structures containing defects, Gloucester: EDF Energy, 2013.

American Lifelines Alliance (ALA), Guidelines for the Design of Buried Steel Pipe, American Society of Civil Engineers, 2001.

API, API Specification 5L: Line pipe, American Petroleum Institute, 2018.

API 579, Fitness for Service Assessments, American Society of Mechanical Engineers, New York, 2007.

ASME, ASME B31.8S-2001: Managing System Integrity of Gas Pipelines, American Society of Mechanical Engineers, 2001.

ASME B31.8, Gas transmission and distribution piping systems, American Society of Mechanical Engineers, New York, 2018.

A.W. Al-Khafaji, R. Jacobs, Excel Based Settlement of beams on elastic foundations with free-ends and arbitrary loading, in: E. Pellicer, J.M. Adam, V. Yepes, and S. Yazdani, editors, Resilient Structures and Sustainable Construction, Fargo: ISEC Press, 2017.

A. Baumgard, M. Beaupre, M. Leir, Implementing a quantitative geohazard frequency analysis framework as a component of risk assessment of new pipelines, in: 2016 11th International Pipeline Conference (IPC2016), American Society of Mechanical Engineers (ASME), Calgary, 2016, pp. V002T07A020.

A.B. Dorey, D.W. Murray, J.R. Cheng, Critical buckling strain equations for energy pipelines-A parametric study, ASME. J. Offshore Mech. Arct. Eng. 128 (2006) 248-255.

A.U. Ebenuwa, K.F. Tee, 2019. Reliability estimation of buried steel pipes subjected to seismic effect, Transp. Geotech. 20, 100242.

A. Ghali, A.M. Neville, T.G. Brown, Structural Analysis: A unified classical and matrix approach, sixth ed., Spon Press, London and New York, 2009.

A. Guillal, N. Abdelbaki, M.E.A. Bensghier, M. Betayeb, Effect of shape factor on structural reliability analysis of a surface cracked pipeline-parametric study, Frat. ed Integrita. Strutt. 13 (2019): 341-349.

A. Liu, S. Takada, Y. Hu, A shell model with an equivalent boundary for buried pipelines under the fault movement, in: 13th World Conference on Earthquake Engineering, Vancouver, 2004, pp. 613.

A. Liu, Y. Hu, F. Zhao, X. Li, S. Takada, L. Zhao, An equivalent-boundary method for the shell analysis of buried pipelines under fault movement, Acta. Seismol. Sin. 1 (2004) 150-156.

A.P. Teixeira, C. Guedes Soares, T.A. Netto, S.F. Estefen, Reliability of pipelines with corrosion defects, Int. J. Press. Vessel. Pip. 85.4 (2008) 228-237.

A. Vasseghi, E. Haghshenas, A. Soroushian, A., M. Rakhshandeh, M., 2021. Failure analysis of a natural gas pipeline subjected to landslide, Eng. Fail. Anal. 119, 105009.

B. Liu, X.J. Liu, H. Zhang, Strain-based design criteria of pipelines, J. Loss Prev. Process Ind., 22 (2009) 884-888.

BS 7910, Guide to methods for assessing the acceptability of flaws in metallic structures. London, UK: British Standards Institution, 2005.

Canadian Energy Pipeline Association, Pipeline Industry Performance Report. https://cepa.com/en/performance-report/, 2016 (accessed 20 September 2021).

CSA. Oil and gas pipeline system, CSA standard Z662:19. Mississauga, Ontario, Canada: Canadian Standard Association; 2019.

CSA Z662-07, Oil and Gas Pipeline Systems, Canadian Standard Association, Mississauga, Ontario, 2007.

C.E. Jaske, J.A. Beavers, Development and evaluation of improved model for engineering critical assessment of pipelines, in: International Pipeline Conference (IPC2002), American Society of Mechanical Engineers (ASME), Calgary, 2002, pp. 1459-1466.

C.M. Timms, D.D. DeGeer, M.R. Chebaro, Y. Tsuru, Compressive strain limits of large diameter X80 UOE linepipe, in: The 19th International Offshore and Polar Engineering Conference, OnePetro, Cupertino, 2009, pp. ISOPE-I-09-332.

Dassault Systems Simulia Corporation, Abaqus, 2017.

D.P. Fairchild, M.L. Macia, S. Kibey, X. Wang, V.R. Krishnan, F. Bardi, H. Tang, W. Cheng, A multi-tiered procedure for engineering critical assessment of strain-based pipelines, in: The 21st International Offshore and Polar Engineering Conference, OnePetro, Cupertino, 2011, pp. ISOPE-I-11-144.

D. Ha, T.H Abdoun, M.J. O'Rourke, M.D. Symans, T.D. O'Rourke, M.C. Palmer, H.E. Stewart, Buried high-density polyethylene pipelines subjected to normal and strike-slip faulting-a centrifuge investigation, Can. Geotech. J. 45 (2008) 1733-1742.

D. Ha, T.H. Abdoun, M.J. O'Rourke, M.D. Symans, T.D. O'Rourke, M.C. Palmer, H.E. Stewart, Centrifuge modeling of earthquake effects on buried high-density polyethylene (HDPE) pipelines crossing fault zones, J. Geotech. 134 (2008) 1501-1515.

D.K. Karamitros, G.D. Bouckovalas, G.P. Kouretzis, Stress analysis of buried steel pipelines at strike-slip fault crossings, Soil. Dyn. Earthq. Eng. 27 (2007) 200-211.

D.K. Karamitros, G.D. Bouckovalas, G.P. Kouretzis, An analytical method for strength verification of buried steel pipelines at normal fault crossings, Soil Dyn. Earthq. Eng. 31 (2011) 1452-1464.

D.S. Cronin, R.J. Pick, Prediction of the failure pressure for complex corrosion defects, Int. J. Press. Vessels Pip. 79 (2002), 279-287.

F.R. Rofooei, H.H. Jalali, N.K. Attari, M. Alavi, Full-scale laboratory testing of buried pipelines subjected to permanent ground displacement caused by reverse faulting, in: Proceedings of the 15th World Conference on Earthquake Engineering, Lisboa, 2012, pp. 24-28.

F. Talebi, J. Kiyono, 2020. Introduction of the axial force terms to governing equation for buried pipeline subjected to strike-slip fault movements, Soil Dyn. Earthq. Eng. 133 106125.

F. Talebi, J. Kiyono, A refined nonlinear analytical method for buried pipelines crossing strike‐slip faults. Earthquake Eng. Struct. Dyn. 50 (2021) 2915-2938.

G. Demofonti, J. Ferino, S.A. Karamanos, P. Vazouras, P. Dakoulas, An integrated experimental-numerical approach to predict strain demand for buried steel pipelines in geo-hazardous areas, in: Rio Pipeline Conference and Exposition, 2013.

G. Jiao, T. Sotberg, R. Igland, SUPERB 2M statistical data-basic uncertainty measures for reliability analysis of offshore pipelines, SUPERB project report, No. STF70 F95212, 1995.

G. Jiao, T. Sotberg, R. Igland, SUPERB 2M Project: Wall Thickness Sizing: Limit-States Based Design for Offshore Pipelines, SUPERB project report, 1995.

G.C. Sarvanis, S.A. Karamanos, Analytical model for the strain analysis of continuous buried pipelines in geohazard areas, Eng. Struct. 152 (2017) 57-69.

G.C. Sarvanis, S.A. Karamanos, P. Vazouras, E. Mecozzi, A. Lucci, P. Dakoulas, Permanent earthquake‐induced actions in buried pipelines: Numerical modeling and experimental verification, Earthq. Eng. Struct. Dyn., 47.4 (2018) 966-987.

Interstate Natural Gas Association of America (INGAA), Guidelines for Management of Landslide Hazards for Pipelines, first ed., Geosyntec Consultants, Inc., Golder Associates, Inc., Center for Reliable Energy Systems (CRES), 2020.

J.F. Kiefner, P.H. Vieth, A modified criterion for evaluating the remaining strength of corroded pipe (No. PR-3-805), Battelle Columbus Div., Ohio, 1989.

J.F. Kiefner, W. Maxey, R. Eiber, A. Duffy, Failure stress levels of flaws in pressurized cylinders, in: Progress in flaw growth and fracture toughness testing, ASTM International, 1973.

J.A. Mason, T.D. O'Rourke, Compressive behavior of steel pipelines with welded slip joints, in: Proceedings of the 2009 TCLEE Conference, Lifeline Earthquake Engineering in a Multihazard Environment, American Society of Civil Engineers (ASCE), Reston, 2009, pp. 811-822.

J.A. Mason, T.D. O'Rourke, Tensile behavior of steel pipelines with welded slip joints, in: Proceedings of the 2009 TCLEE Conference, Lifeline Earthquake Engineering in a Multihazard Environment, American Society of Civil Engineers (ASCE), Reston, 2009, pp. 831-841.

J.J. Muhammed, Deterministic and probabilistic approaches in the analysis of the bearing capacity of a bridge foundation on undrained clay soil, Slovak J. Civ. Eng. 27 (2019) 44-51.

J.M. Oswell, Pipelines in permafrost: geotechnical issues and lessons, Can. Geotech. J. 48 (2011), 1412-1431.

J. Xie, L. Zhang, Q. Zheng, X. Liu, S. Dubljevic, H. Zhang. Strain demand prediction of buried steel pipeline at strike-slip fault crossings: a surrogate model approach, Earthq. Struct. 20 (2021) 109-122.

K. Gawande, R. Kiran, H.P. Cherukuri, A numerical study of the response of buried steel pipelines undergoing strike-slip fault, Eng. Fail. Anal. 102 (2019) 203-218.

L.R.L. Wang, Y.A. Yeh, A refined seismic analysis and design of buried pipeline for fault movement, Earthq. Eng. Struct. Dyn. 13 (1985) 75-96.

L.R.L. Wang, Y.A. Yeh, Seismic design of buried pipeline for fault movement effects, J. Press. Vessel. Technol. 108 (1986) 202-208.

M. Brown, M. Nessim, H. Greaves, Pipeline defect assessment: deterministic and probabilistic considerations, Second International Conference on Pipeline Technology, Ostend, Belgium, September. 1995.

M. Hasan, F. Khan, S. Kenny, Identification of the cause of variability of probability of failure for burst models recommended by Codes/Standards, J. Press. Vessel Technol. 133 (2011) 041101.

M.S. Okyere, Stress-based design of pipelines, in: R.W. Revie (Eds.), Oil and Gas Pipelines, John Wiley & Sons Inc., Hoboken, 2015, pp. 49-66.

M.J. O'Rourke, Approximate analysis procedures for permanent ground deformation effects on buried pipelines, in: Proceedings from the Second U.S.-Japan workshop on liquefaction, large ground deformation and their effects on lifelines, National Center for Earthquake Engineering Research, New York, 1989, pp. 336-347.

M.J. O'Rourke, X. Liu, Seismic design of buried and offshore pipelines, Buffalo, MCEER; 2012.

M.J. O'Rourke, X. Liu, R. Flores-Berrones, Steel pipe wrinkling due to longitudinal permanent ground deformation, J. Civ. Eng. 121 (1995) 443-451.

M.J. O'Rourke, V. Gadicherla, T.H. Abdoun, Centrifuge modeling of PGD response of buried pipe, Earthq. Eng. 4 (2005) 69-73.

M. Liu, Y.Y. Wang, F. Zhang, K. Kotian, Realistic Strain Capacity Models for Pipeline Construction and Maintenance, Center for Reliable Energy Systems (CRES), Dublin, 2013.

M. Liu, Y.Y. Wang, Y. Song, D. Horsley, S. Nanney, Multi-tier tensile strain models for strain-based design: Part 2-Development and formulation of tensile strain capacity models, in: International Pipeline Conference (IPC2012), American Society of Mechanical Engineers (ASME), Calgary, 2012, pp. 415-425.

M. Porter, G. Ferris, M. Leir, M. Leach, M. Haderspock, Updated estimates of frequencies of pipeline failures caused by geohazards, in: International Pipeline Conference, American Society of Mechanical Engineers (ASME), Calgary, 2016, pp. V002T07A003.

M. Porter, J. Van Hove, P. Barlow, Analysis of dynamic system risks where pipelines cross slow-moving landslides, in: 2022 14th International Pipeline Conference (IPC2022), American Society of Mechanical Engineers (ASME), Calgary, 2022, pp. V001T07A007.

M. Porter, M. Leir, A. Baumgard, G. Ferris, Integrating terrain and geohazard knowledge into the pipeline lifecycle, in: Proceedings of 6th Canadian Geohazards Conference, Kingston. 2014.

M. Rashki, M. Miri, M.A. Moghaddam, A new efficient simulation method to approximate the probability of failure and most probable point, Struct. Saf. 39 (2012) 22-29.

M. Sen, S. Hassanien, On estimating pipelines reliability at slope crossings, in: Proceedings of The Asset Integrity Management-Pipeline Integrity Management Under Geohazard Conditions, American Society of Mechanical Engineers (ASME), New York, 2019, pp. 81-92.

N.M. Newmark, W.J. Hall, Pipeline design to resist large fault displacement, in: Proceedings of U.S. National Conference on Earthquake Engineering, Earthquake Engineering Research Institute, Michigan, 1975, pp. 416-425.

N. Wang, M.S. Zarghamee, Evaluating Fitness-for-Service of Corroded Metal Pipelines: Structural Reliability Bases, J. Pipeline Syst. Eng. 5 (1) (2014) 04013012.

N. Yoosef-Ghodsi, Strain-based design of pipelines, in: R.W. Revie (Eds.), Oil and Gas Pipelines, John Wiley & Sons Inc., Hoboken, 2015, pp. 37-48

N. Yoosef-Ghodsi, J. Zhou, D.W. Murray, A simplified model for evaluating strain demand in a pipeline subjected to longitudinal ground movement, in: 2008 7th International Pipeline Conference (IPC2008), American Society of Mechanical Engineers (ASME), Calgary, 2009, pp. 657-664.

O.S. Lee, H.M. Kim, D.H. Kim, H.B. Choi, Reliability Estimation of a Natural Gas Pipeline with Surface Crack, in: Proceedings of the ASME 2009 Pressure Vessels and Piping Conference (PVP2009), New York, 2009, pp. 459-466.

O.V. Trifonov, 2015. Numerical stress-strain analysis of buried steel pipelines crossing active strike-slip faults with an emphasis on fault modeling aspects, J. Pipeline Syst. Eng. 6, 04014008.

O.V. Trifonov, The effect of variation of soil conditions along the pipeline in the fault crossing zone, Soil Dyn. Earthq. Eng. 104 (2018) 437-448

O.V. Trifonov, V.P. Cherniy, A semi-analytical approach to a nonlinear stress–strain analysis of buried steel pipelines crossing active faults, Soil Dyn. Earthq. Eng. 30 (2010) 1298-1308.

O.V. Trifonov, V.P. Cherniy, Elastoplastic stress strain analysis of buried steel pipelines subjected to fault displacements with account for service loads, Soil Dyn. Earthq. Eng. 33 (2012) 54-62.

Pipeline Research Council International (PRCI). Guidelines for Constructing Natural Gas and Liquid Hydrocarbon Pipelines Through Areas Prone to Landslide and Subsidence Hazards, Technical Toolboxes, Inc., 2009.

P. Liu, J. Zheng, B. Zhang, P. Shi, Failure analysis of natural gas buried X65 steel pipeline under deflection load using finite element method, Mater. Des. 31 (2010) 1384-1391.

P. Vazouras, P. Dakoulas, S.A. Karamanos, Pipe–soil interaction and pipeline performance under strike-slip fault movements, Soil Dyn. Earthq. Eng. 72 (2015) 48-65.

P. Vazouras, S.A. Karamanos, P. Dakoulas, Finite element analysis of buried steel pipelines under strike-slip fault displacements, Soil Dyn. Earthq. Eng. 30 (2010) 1361-1376.

Q. Zheng, Reliability of Pipes Subjected to Ground Movement, MecSimCalc, March, 7, 2022, https://mecsimcalc.com/app/6934977/reliability_of_pipes_subjected_to_ground_movement.

Q. Zheng, Strain Demand in Pipes Subjected to Ground Movement, MecSimCalc, March, 7, 2022, https://mecsimcalc.com/app/5339494/strain_demand_in_pipes_subjected_to_ground_movement.

Q. Zheng, A. K. Abdelmoety, Y. Li, M. Kainat, N. Yoosef-Ghodsi, S. Adeeb, 2021. Reliability analysis of intact and defected pipes for internal pressure related limit states specified in CSA Z622: 19, Int. J. Press. Vessels Pip. 192, 104411.

Q. Zheng, L. Graf-Alexiou, Y. Li, N. Yoosef-Ghodsi, M. Fowler, M. Kainat, S. Adeeb, Strain demand of elastic pipes subjected to permanent ground displacements using the finite difference method, J. Pipeline. Sci. Eng. 1 (2021) 176-186.

Q. Zheng, X. Liu, H. Zhang, S. Adeeb, Reliability-Based Assessment Method of Buried Pipeline at Fault Crossings, in: International Pipeline Conference (IPC2020), American Society of Mechanical Engineers (ASME), Calgary, 2020, pp. V002T07A019.

Q. Zheng, X. Liu, H. Zhang, X. Gu, M. Fang, L. Wang, S. Adeeb, 2021. Reliability evaluation method for pipes buried in fault areas based on the probabilistic fault displacement hazard analysis, J. Nat. Gas Eng. 85, 103698.

Q. Zheng, Y. Li, N. Yoosef-Ghodsi, M. Fowler, M. Kainat, S. Adeeb, 2022. A finite difference-based approach for strain demand prediction of inelastic pipes subjected to permanent ground displacements, Eng. Struct. 273, 115072.

R. Amaya-Gómez, M. Sánchez-Silva, E. Bastidas-Arteaga, F. Schoefs, F. Munoz, Reliability assessments of corroded pipelines based on internal pressure–A review, Eng. Fail. Anal. 98 (2019) 190-214.

R. Guthrie, E. Reid, Estimating landslide induced probability of failure to pipelines using a structured reductionist approach, in: 2018 12th International Pipeline Conference (IPC2018), American Society of Mechanical Engineers (ASME), Calgary, 2018, pp. V002T07A004.

R.J. LeVeque, Finite difference methods for differential equations, Draft version for use in AMath, 1998.

R.P. Kennedy, A.W. Chow, R.A. Williamson, Fault movement effects on buried oil pipeline, ASCE J. Transport. Eng. 103 (1977) 617-633.

R.R. Read, M. Rizkalla, Bridging the gap between qualitative, semi-quantitative and quantitative risk assessment of pipeline geohazards: the role of engineering judgment, in: ASME International Pipeline Geotechnical Conference (IPG2015), American Society of Mechanical Engineers (ASME), Bogota, 2015, pp. V001T02A004.

S. Fan, X. Yan, Strain design of long pipeline crossing fault under seismic loading, China Pet. Mach. 43 (2015) 114-118.

S. Hasan, F. Khan, S. Kenny, Probability assessment of burst limit state due to internal corrosion, Int. J. Press. Vessel. Pip. 89 (2012) 48–58.

S. A. Karamanos, B. Keil, R. J. Card, (2014). Seismic design of buried steel water pipelines, in: Pipelines 2014: From Underground to the Forefront of Innovation and Sustainability, ASCE, pp. 1005-1019.

S.R. Dash, S.K. Jain, Guidelines for seismic design of buried pipelines, IITK-GSDMA Codes. 2007.

S.J. Polasik, C.E. Jaske, T.A. Bubenik, Review of Engineering Fracture Mechanics Model for Pipeline Applications, in: International Pipeline Conference (IPC2016), American Society of Mechanical Engineers (ASME), Calgary, 2016, pp. V001T03A038.

S.K.S Shokouhi, A. Dolatshah, E. Ghobakhloo, Seismic strain analysis of buried pipelines in a fault zone using hybrid FEM-ANN approach, Earthq. Struct. 5 (2013) 417-438.

S. Takada, N. Hassani, K. Fukuda, A new proposal for simplified design of buried steel pipes crossing active faults, Earthquake Eng. Struct. Dyn. 30 (2001) 1243-1257.

SY/T 0450, 2004. Code for seismic design of oil and gas steel pipeline. The National Development and Reform Commission, Beijing, China.

T.A. Netto, U.S. Ferraz, S.F. Estefen, The effect of corrosion defects on the burst pressure of pipelines, J. Constr. Steel Res. 61 (2005) 1185–204.

T. Sotberg, B.J. Leira, Reliability-based pipeline design and code calibration, Proceedings of the 13th International Conference on Offshore Mechanics and Arctic Engineering, New York, Unit State, 1994 (No. 940230).

T.J.E. Zimmerman, A. Cosham, P. Hopkins, N. Sanderson, Can limit states design be used to design a pipeline above 80% SMYS?, in: 17th International Conference on Offshore Mechanics and Arctic Engineering (OMAE 1998), Lisbon, 1998.

U. Zahid, A. Godio, S. Mauro, 2020. An analytical procedure for modelling pipeline-landslide interaction in gas pipelines, J. Nat. Gas. Sci. Eng. 81, 103474.

V. Jahangiri, H. Shakib, Reliability-based seismic evaluation of buried pipelines subjected to earthquake-induced transient ground motions, Bull. Earthq. Eng. 18 (2020) 3603-3627.

W. Feng, R. Huang, J. Liu, X. Xu, M. Luo, Large-scale field trial to explore landslide and pipeline interaction, Soils Found. 55 (2015) 1466-1473.

W. Qiu, S. Adeeb, The simplest way to share computational tools, MecSimCalc, March, 7, 2022, https://mecsimcalc.com/.

W. Zheng, H. Zhang, X. Liu, J. Chen, Comparative study on the FEM models of buried pipeline under fault movement, China Pet. Mach. 43.12 (2015) 109-113.

W. Zhou, Reliability of pressurised pipelines subjected to longitudinal ground movement, Struct. Infrastruct. Eng. 12 (2012) 1123-1135.

W. Zhou, G.X. Huang, Model error assessments of burst capacity models for corroded pipelines, Int. J. Press. Vessel. Pip. 99 (2012) 1–8.

X. Gu, H. Zhang, Research on aseismatic measures of gas pipeline crossing a fault for strain-based design, in: ASME Pressure Vessels and Piping Conference (PVP2009), American Society of Mechanical Engineers (ASME), New York, 2009, pp. 571-580.

X. Liu, H. Zhang, M. Li, M. Xia, W. Zheng, K. Wu, Y. Han, Effects of steel properties on the local buckling response of high strength pipelines subjected to reverse faulting, J. Nat. Gas Eng. 33 (2016) 378-387.

X. Liu, H. Zhang, M. Xia, J. Liu, Q. Zheng, An improved analytical strain analysis method for buried steel pipelines subjected to abrupt permanent ground displacement, in: International Pipeline Conference (IPC2020), American Society of Mechanical Engineers (ASME), Calgary, 2020, pp. V002T06A012.

X. Liu, H. Zhang, X. Gu, Y. Chen, M. Xia, K. Wu, Strain demand prediction method for buried X80 steel pipelines crossing oblique-reverse faults, Earthq. Struct. 12 (2017) 321-332.

X. Liu, H. Zhang, Y. Han, M. Xia, W. Zheng. A semi-empirical model for peak strain prediction of buried X80 steel pipelines under compression and bending at strike-slip fault crossings, J. Nat. Gas Eng. 32 (2016) 465-475.

X. Liu, M.J. O'Rourke, Behaviour of continuous pipeline subject to transverse PGD, Earthq. Eng. Struct. Dyn. 26 (1998) 989-1003.

X. Liu, Q. Zheng, K. Wu, Y. Yang, Z. Zhao, H. Zhang, 2020. Development of a novel approach for strain demand prediction of pipes at fault crossings on the basis of multi-layer neural network driven by strain data, Eng. Struct. 214, 110685.

X. Liu, S.P. Sun, Strain based design of buried pipelines crossing faults, Spec. Struct. 22.2 (2005) 81-85.

Y. Bai, R. Song, Fracture assessment of dented pipes with cracks and reliability-based calibration of safety factor, Int. J. Press. Vessel. Pip. 74.3 (1997) 221-229.

Y.J. Chiou, S.Y. Chi, H.Y. Chang, A study of buried pipeline response to fault movement, J. Press. Vessel Technol. Trans. ASME 116 (1994).

Y.Y. Wang, D., West, D. Dewar, J. Hart, A. McKenzie-Johnson, D. Gray, Management of Ground Movement Hazards for Pipelines, CRES project No. CRES-2012-M03-01, 2016.

Y.Y Wang, D. Rudland, R. Denys, D. Horsley, A preliminary strain-based design criterion for pipeline girth welds, in: International Pipeline Conference (IPC2002), American Society of Mechanical Engineers (ASME), Calgary, 2002, pp. 415-427.

Z. Hu, X. Ren, Q. Wang, R. Wang, R. Pan, Analytical method for the mechanical response of buried pipeline under the action of strike-slip faulting, Undergr. Space 7 (2022) 268-277.

Z. Yan, S. Zhang, W. Zhou, Model error assessment of burst capacity models for energy pipelines containing surface cracks, Int. J. Press. Vessel. Pip. 120 (2014) 80-92.

APPENDIX A: SUMMARY OF PREDICTIVE MODELS OF BURST PRESSURE

Table A-1: Models for assessing failure pressure following the NG-18 equation

Model	**Defect shape**	$f_{geometry}$	σ_{flow} **(MPa)**	f_{shape}	**Folias factor** M
ASME B31G [1]	Parabolic	$\frac{2t}{D}$	$1.1\sigma_y$	$\begin{cases} 2/3, & d_{\max}/t \le 0.8 \text{ and } L^2/Dt \le 20 \\ 1, & d_{\max}/t \le 0.8 \text{ and } L^2/Dt > 20 \end{cases}$	$\begin{cases} \sqrt{1+0.8\left(\frac{L^2}{Dt}\right)}, & d_{\max}/t \le 0.8 \text{ and } L^2/Dt \le 20 \\ \infty, & d_{\max}/t \le 0.8 \text{ and } L^2/Dt > 20 \end{cases}$
Modified B31G-0.85L [2]	Mixed	$\frac{2t}{D}$	$\sigma_y + 69$	0.85	$\begin{cases} \sqrt{1+0.6275\left(\frac{L^2}{Dt}\right)-0.003375\left(\frac{L^2}{Dt}\right)^2}, & d_{\max}/t \le 0.8 \cap \quad 50 \\ 3.3+0.032\left(\frac{L^2}{Dt}\right), & d_{\max}/t \le 0.8 \cap \quad 50 \end{cases}$
Modified B31G-RSTRENG [3]	Effective area	$\frac{2t}{D}$	$\sigma_y + 69$	$d_{eff}/d_{\max Aeff}$	$\begin{cases} \sqrt{1+0.6275\left(\frac{L^2}{Dt}\right)-0.003375\left(\frac{L^2}{Dt}\right)^2}, & d_{\max}/t \le 0.8 \cap \quad 50 \\ 3.3+0.032\left(\frac{L^2}{Dt}\right), & d_{\max}/t \le 0.8 \cap \quad 50 \end{cases}$
RPA model [4]	Rectangular/ Parabolic	$\frac{2t}{D}$	$\sigma_y + 69$	$\begin{cases} 0.85, & L^2/Dt \le 20 \\ 1-\frac{0.15\left(64\times10^6\right)}{\left(L^2/Dt\right)^6}, & L^2/Dt > 20 \end{cases}$	$\begin{cases} \sqrt{1+0.6275\left(\frac{L^2}{Dt}\right)-0.003375\left(\frac{L^2}{Dt}\right)^2}, & L^2/Dt \le 20 \\ 2.1+0.07\left(\frac{L^2}{Dt}\right), & L^2/Dt > 20 \end{cases}$

SHELL92 [5]	Rectangular	$\frac{2t}{D}$	$0.9\sigma_t$	1	$\sqrt{1+0.8\left(\frac{L^2}{Dt}\right)}$
DNV RP-F101 [6]	Rectangular	$\frac{2t}{D-t}$	σ_t	1	$\sqrt{1+0.31\left(\frac{L^2}{Dt}\right)}$
FITNET FFS [7]	Rectangular	$\frac{2t}{D-t}$	$\sigma_t\left(\frac{1}{2}\right)^{\frac{65}{\sigma_y}}$	1	$\sqrt{1+0.8\left(\frac{L^2}{Dt}\right)}$

Table A-2: Semi-regression models for assessing burst pressure for corroded pipes

Model	**Defect shape**	$f_{geometry}$	σ_{flow} **(MPa)**	$f_{regression}$
PCORRC [8]	Rectangular	$\frac{2t}{D}$	σ_t	$1-\frac{d_{\max}}{t}\left(1-\exp\left(\frac{-0.157L}{\sqrt{\frac{D}{2}(t-d_{\max})}}\right)\right),\ d_{\max}/t \le 0.8 \cap$
Yeom et al. [9]	Rectangular	$\frac{2t}{D}$	$0.9\sigma_t$	$1-\frac{d_{\max}}{t}\left(1-\exp\left(\frac{-0.224L}{\sqrt{\frac{D}{2}(t-d_{\max})}}\right)\right)$
Choi [10]	Elliptical	$\frac{2t}{D}$	$\begin{cases}0.9\sigma_t, & L/\sqrt{Dt/2}<6\\ \sigma_t, & L/\sqrt{Dt/2}\ge 6\end{cases}$	$\begin{cases}C_0+C_1\left(\frac{L}{\sqrt{Dt/2}}\right)+C_2\left(\frac{L}{\sqrt{Dt/2}}\right)^2, & L/\sqrt{Dt/2}<6\\ C_3+C_4\left(\frac{L}{\sqrt{Dt/2}}\right), & L/\sqrt{Dt/2}\ge 6\end{cases}$ * C_0, C_1, C_2, C_3, and C_4 are fitted parameters as a quadratic equation of $d_{\max}/t$
CUP [11]	Parabolic	$\frac{2t}{D}$	σ_t	$1-\frac{d_{\max}}{t}\left(1-\left(\begin{array}{l}0.1075\left(1-\left(\frac{w}{\pi D}\right)^2\right)^6+\\ (1-0.1075)\exp\left(\frac{-0.4103L}{\sqrt{Dt}}\right)\end{array}\right)\left(1-\frac{d_{\max}}{t}\right)^{0.2504}\right)$
Netto [12]	Elliptical	$\frac{2t}{D}$	$1.1\sigma_y$	$1-0.9435\left(\frac{d_{\max}}{t}\right)^{1.6}\left(\frac{L}{D}\right)^{0.4}$

Burst pressure models for corroded pressure

1. CSA Z662 [13]

$$P_b = \begin{cases} e_1 P_c + (1-e_1) P_i - e_2 \sigma_t, & \text{SMYS} > 241 \text{ MPa} \\ e_3 P_c + (1-e_3) P_i - e_4 \sigma_y, & \text{SMYS} \le 241 \text{ MPa} \end{cases}$$

*e_1, e_2, e_3, e_4 are model error factors, e_1 = 1.04, $e_2 \sim N$(-0.00056, 0.001469); e_3 = 1.17, $e_4 \sim N$(-0.007655, 0.006506)

$$P_c = P_i \left(\frac{1 - \frac{d_{\max}}{t}}{1 - \frac{d_{\max}}{tM}} \right)$$

$$P_i = \begin{cases} \dfrac{2t\bullet}{D}, & \text{SMYS} > 241 \text{ MPa} \\ \dfrac{2t\bullet}{D}, & \text{SMYS} \le 241 \text{ MPa} \end{cases}$$

$$M = \begin{cases} \sqrt{1 + 0.6275\left(\frac{L^2}{Dt}\right) - 0.003375\left(\frac{L^2}{Dt}\right)^2}, & L^2/Dt \le 50 \\ 3.3 + 0.032\left(\frac{L^2}{Dt}\right), & L^2/Dt > 50 \end{cases}$$

2. CPS [14]

$$P_b = P_{LG} + g\left(P_{PP} - P_{LG}\right)$$

$$P_{PP} = 0.9\left(\frac{E\sigma_y^{n_{ro}-1}}{\sqrt{3}\alpha_{RO} n_{RO}}\right)^{1/n_{RO}} \frac{2}{\sqrt{3}} \frac{t}{R_i\left[\exp\left(\frac{1}{2n_{RO}}\right)\right]^2}$$

$$P_{LG} = \frac{2\sigma_{crit}}{(D-2t)\sqrt{\frac{3}{4}}}(t - d_{\max}) \exp\left(-\sqrt{\frac{3}{4}}\varepsilon_{crit}\right), \frac{d_{\max}}{t} \ge 0.2$$

$$g = \frac{4\tan^{-1}\left[\exp\left(-\frac{L}{2\sqrt{D(t-d_{\max})}}\right)\right]}{\pi}$$

Burst pressure models for cracked pipes

1. NG-18 [15]

$$P_b = \min\left\{ \begin{array}{l} \dfrac{2t\sigma_{flow}}{D}\dfrac{1-d_{\max}/t}{1-d_{\max}/Mt}, \\ \dfrac{4t\sigma_{flow}}{\pi D}\dfrac{1-d_{\max}/t}{1-d_{\max}/Mt}\arccos\left(\exp\left(-\dfrac{\pi K_{mat}^2}{4L\sigma_{flow}^2}\right)\right) \end{array} \right\}$$

$$\sigma_{flow} = \sigma_y + 69\text{MPa}$$

$$M = \begin{cases} \sqrt{1+0.6275\left(\dfrac{L^2}{Dt}\right)-0.003375\left(\dfrac{L^2}{Dt}\right)^2}, & L^2/Dt \le 50 \\ 3.3+0.032\left(\dfrac{L^2}{Dt}\right), & L^2/Dt > 50 \end{cases}$$

$$K_{mat} = \sqrt{\frac{C_v E}{A_c}}$$

2. CorLAS [16]

$$P_b = \min\left(P_{b(flow)},\ P_{b(toughness)}\right)$$

- Calculation of $P_{b(flow)}$

$$P_{b(flow)} = \frac{\sigma_f}{\dfrac{D}{2t}-y}$$

$$y = \begin{cases} 0.4, & D/2t \le 10 \\ 0, & D/2t > 10 \end{cases}$$

$$\sigma_f = \sigma_{flow}\left(\frac{1-\dfrac{A_{eff}}{A_0}}{1-\dfrac{A_{eff}}{MA_0}}\right)$$

$A_0 = L\bullet$

$$\sigma_{flow} = \begin{cases} \sigma_y + 10{,}000, & \text{pipe grade} < \text{X70} \\ \dfrac{\sigma_y+\sigma_t}{2}, & \text{pipe grade} \ge \text{X70} \end{cases}$$

$$A_{eff} = \begin{cases} Ld, & \text{rectangular flaw} \\ \dfrac{\pi Ld}{4}, & \text{semi-elliptical flaw} \end{cases}$$

$$M = \begin{cases} \sqrt{1 + 0.6275\left(\dfrac{L^2}{Dt}\right) - 0.003375\left(\dfrac{L^2}{Dt}\right)^2}, & L^2/Dt \le 50 \\ 3.3 + 0.032\left(\dfrac{L^2}{Dt}\right), & L^2/Dt > 50 \end{cases}$$

- Calculation of $P_{b(flow)}$

$$P_{b(toughness)} = \begin{cases} \dfrac{\sigma_n t}{\pi A/4 + 0.5D}, & \text{internal flaw} \\ 2\sigma_n t/D, & \text{external flaw} \end{cases}$$

$$A = \begin{cases} d, & \text{rectangualr flaw} \\ \dfrac{4A_{eff}}{\pi L}, & \text{elliptical flaw} \end{cases}$$

$$\sigma_n = \sigma \frac{1 - A_{eff}/A_0}{1 - A_{eff}/(M\bullet}$$

$$\sigma \Leftarrow \begin{cases} J_c = Q_f F_{sf} A \left[\dfrac{\sigma^2 \pi}{E} + F_3 \left(\dfrac{0.005 - \dfrac{\sigma_y}{E}}{\sigma_y^{\frac{1}{n}}} \right) \sigma^{\frac{1+n}{n}} \right] \\ J_c = \dfrac{12 C_v}{0.124} \end{cases}$$

$$Q_f = 1.2581 - 0.20589z - 11.493z^2 + 29.586z^3 - 23.584z^4$$

$$z = \begin{cases} 0.5, & \dfrac{A}{L} > 0.5 \\ \dfrac{A}{L}, & 0 < \dfrac{A}{L} \le 0.5 \end{cases}$$

$$F_{sf} = \begin{cases} \dfrac{2t}{\pi A}\tan\left(\dfrac{\pi A}{2t}\right)(1-2z) + 2z, & \dfrac{A}{t} \le 0.95 \\ \left(8.515 + \left(\dfrac{A}{t} - 0.95\right)\dfrac{162}{t}\right)(1-2z) + 2z, & \dfrac{A}{t} > 0.95 \end{cases}$$

$$n = -0.00546 + 0.556\frac{\sigma_y}{\sigma_t} - 0.547\left(\frac{\sigma_y}{\sigma_t}\right)^2$$

$$F_3 = \left[3.85(1-n)\sqrt{\frac{1}{n}} + \pi n \right](1+n)$$

Reference

[1] ASME B31G, Manual for determining the remaining strength of corroded pipelines. The American Society of Mechanical Engineers, New York, 1991.

[2] J.F. Kiefner, P.H. Vieth, A modified criterion for evaluating the remaining strength of corroded pipe (No. PR-3-805), Battelle Columbus Div., Ohio, 1989.

[3] ASME B31G, Manual for determining the remaining strength of corroded pipelines. The American Society of Mechanical Engineers, New York, 2009.

[4] A.C. Benjamin, E.Q.D. Andrade, Modified method for the assessment of the remaining strength of corroded pipelines, in: Rio Pipeline Conference 2003 (RPC 2003), 2003, pp. IBP413-03.

[5] D. Ritchie, S. Last, Burst criteria of corroded pipelines-defect acceptance criteria, in: Proceedings of the EPRG/PRC 10th biennial joint technical meeting on line pipe research, Cambridge, 1995, pp. 1-11.

[6] DNV RP-F101, Corroded pipelines, Det Norske Veritas, Høvik, 2010.

[7] G. Qian, M. Niffenegger, S. Li, Probabilistic analysis of pipelines with corrosion defects by using FITNET FFS procedure, Corros. Sci. 53 (2011), 855-861.

[8] D.R. Stephens, B.N. Leis, Development of an alternative criterion for residual strength of corrosion defects in moderate-to high-toughness pipe, in: International Pipeline Conference (IPC2020), American Society of Mechanical Engineers (ASME), Calgary, 2020, pp. V002T06A012.

[9] K.J. Yeom, W.S. Kim, K.H. Oh, Integrity assessment of API X70 pipe with corroded girth and seam welds via numerical simulation and burst test experiments, Eng. Fail. Anal. 70 (2016) 375-386.

[10] J.B. Choi, B.K. Goo, J.C. Kim, Y.J. Kim, W.S. Kim, Development of limit load solutions for corroded gas pipelines. Int. J. Press. Vessels Pip. 80 (2003) 121-128.

[11] Y. Shuai, J. Shuai, K. Xu, Probabilistic analysis of corroded pipelines based on a new failure pressure model, Eng. Fail. Anal. 81 (2017) 216-233.

[12] T.A. Netto, U.S. Ferraz, S.F. Estefen, The effect of corrosion defects on the burst pressure of pipelines, J. Constr. Steel Res. 61 (2005) 1185–204.

[13] CSA. Oil and gas pipeline system, CSA standard Z662:19. Mississauga, Ontario, Canada: Canadian Standard Association; 2019.

[14] D.S. Cronin, R.J. Pick, Prediction of the failure pressure for complex corrosion defects, Int. J. Press. Vessels Pip. 79 (2002), 279-287.

[15] J. Kiefner, W. Maxey, R. Eiber, A. Duffy, Failure stress levels of flaws in pressurized cylinders, in: Progress in flaw growth and fracture toughness testing, ASTM International, 1973.

[16] C.E. Jaske, J.A. Beavers, Development and evaluation of improved model for engineering critical assessment of pipelines, in: International Pipeline Conference (IPC2002), American Society of Mechanical Engineers (ASME), Calgary, 2002, pp. 1459-1466.

APPENDIX B: CODE OF RELIABILITY CALCULATION USING MONTE CARLO SIMULATION

The following code is to calculate the reliability of pipes under ground movements in Chapter 7.

1. Appendix_B_main

```
# Title: Reliability calculation in Chapter 7
# Author: Qian Zheng
# Date: 20220715


# # Clear Console
try:
    from IPython import get_ipython
    get_ipython().magic('clear')
    get_ipython().magic('reset -f')
except:
    pass


# import os

import numpy as np
import time
import concurrent.futures
import pandas as pd
from scipy.stats import truncnorm
```

```
from colorama import Fore
import Appendix_B_fun_FDM_PT
import os
import warnings
warnings.filterwarnings('ignore')


if __name__ == "__main__":
    timeStart = time.time()
    #%% Independent variables (the same for all cases)
    # Material property
    Ee = 210.0e3  # Young's modulus, MPa
    # Ground displacement
    # Geohazard = 'Landslide'  # Slope or Landslide
    Geohazard = 'Slope'  # Slope or Landslide
    if Geohazard == 'Slope':
        delta_mean, delta_SD = 12.5e-3, 6.25e-3  # Mean of creep rate, m/yr
        InitialCreep_min, InitialCreep_max = 200.0e-3, 400.0e-3  # Initil creep, m
        sto_InitialCreep = [InitialCreep_min, InitialCreep_max, 'Uniform']
        sto_delta = [delta_mean, delta_SD, 'Lognormal']
    elif Geohazard == 'Landslide':
        delta_left, delta_mode, delta_right = 300.e-3, 800.e-3, 4000.e-3  # Lower bound of
landslide, m/yr
        InitialCreep_min, InitialCreep_max = 0, 0  # Initil creep, m
```

```
    sto_InitialCreep = [InitialCreep_min, InitialCreep_max, 'Uniform']
    sto_delta = [delta_left, delta_mode, delta_right, 'Triangular']

### Operation parameters
Delta_T_min = -25   # Unit: degree
Delta_T_max = 45   # Unit: degree
sto_Delta_T = [Delta_T_min, Delta_T_max, 'Uniform']

# Soil type
Sand = ['ML', 'SM']
Clay = ['CL', 'CL-CI', 'CH', 'CI']

### Pipe geometry
OD_nominal = 559  # Diameter, mm
WT_nominal = 7.14 # Wall thickness, mm

### Material properties dependent on date of birth of the pipe
PipeGrade = 'X52'
DoB = 1952
if PipeGrade == 'X52' and DoB > 1980:
    SMYS = 359.0  # Yield strength, MPa
    sY_mean, sY_SD = 393.0, 19.  # Mean of yield strength, MPa
    SMTS = 455.0  # Ultimate strength, MPa
```

```
    sU_mean, sU_SD = 555.0, 4.  # Mean of tensile strength, MPa
    uEL_left, uEL_mode, uEL_right = 0.072, 0.101, 0.13  # Lower bound of uniform strain
    CTOD_mean, CTOD_SD = 0.16, 0.02  # Mean of CTOD, mm
    sto_CTOD = [CTOD_mean, CTOD_SD, 'Normal']
elif PipeGrade == 'X52' and DoB <=1980:
    SMYS = 359.0  # Yield strength, MPa
    sY_mean, sY_SD = 387.0, 22.  # Mean of yield strength, MPa
    SMTS = 455.0  # Ultimate strength, MPa
    sU_mean, sU_SD = 548.0, 14.  # Mean of tensile strength, MPa
    uEL_left, uEL_mode, uEL_right = 0.072, 0.101, 0.13  # Lower bound of uniform strain
    CTOD_mean, CTOD_SD = 0.1, 0.06  # Mean of CTOD, mm
    sto_CTOD = [CTOD_mean, CTOD_SD, 'Lognormal']
elif PipeGrade == 'X70':
    SMYS = 485.0  # Yield strength, MPa
    sY_mean, sY_SD = 531., 19.  # Yield strength, MPa
    SMTS = 570.0  # Ultimate strength, MPa
    sU_mean, sU_SD = 638., 8.  # Ultimate strength, MPa
    uEL_left, uEL_mode, uEL_right = 0.051, 0.07, 0.09  # Lower bound of uniform strain
    if DoB > 1980:
        CTOD_mean, CTOD_SD = 0.19, 0.03  # Mean of CTOD, mm
        sto_CTOD = [CTOD_mean, CTOD_SD, 'Normal']
    elif DoB <= 1980:
        CTOD_mean, CTOD_SD = 0.12, 0.07  # Mean of CTOD, mm
```

```
        sto_CTOD = [CTOD_mean, CTOD_SD, 'Lognormal']
    elif PipeGrade == 'X46':
        sY_mean, sY_SD = 352., 12.  # Yield strength, MPa
        sU_mean, sU_SD = 483., 6.  # Ultimate strength, MPa
        uEL_left, uEL_mode, uEL_right = 0.072, 0.101, 0.13  # Lower bound of uniform strain
        if DoB > 1980:
            CTOD_mean, CTOD_SD = 0.16, 0.02  # Mean of CTOD, mm
            sto_CTOD = [CTOD_mean, CTOD_SD, 'Normal']
        elif DoB <= 1980:
            CTOD_mean, CTOD_SD = 0.10, 0.06  # Mean of CTOD, mm
            sto_CTOD = [CTOD_mean, CTOD_SD, 'Lognormal']
    elif PipeGrade == 'X65':
        sY_mean, sY_SD = 483., 16.  # Yield strength, MPa
        sU_mean, sU_SD = 599., 8.  # Ultimate strength, MPa
        uEL_left, uEL_mode, uEL_right = 0.054, 0.075, 0.09  # Lower bound of uniform strain
        if DoB > 1980:
            CTOD_mean, CTOD_SD = 0.19, 0.03  # Mean of CTOD, mm
            sto_CTOD = [CTOD_mean, CTOD_SD, 'Normal']
        elif DoB <= 1980:
            CTOD_mean, CTOD_SD = 0.12, 0.07  # Mean of CTOD, mm
            sto_CTOD = [CTOD_mean, CTOD_SD, 'Lognormal']
    if DoB > 1990:
        Ep = 0.03*Ee
```

```
    elif DoB >= 1980 and DoB < 1990:
        Ep = 0.02*Ee
    elif DoB < 1980:
        Ep = 0.01*Ee

    ### Geometry of pipe-ground movement data
    InspectionInterval = 9  # Year
    Beta = 70  # Intersection angle, degree

    ### Pressure
    MOP = np.minimum(round(0.8 * 2 * SMYS * WT_nominal/OD_nominal, 4), 12.)  # MOP,
MPa

    ### Pipe section length
    soilM = 34  # Length of middle segment, m
    soilL = 70  # Length of left segment, m
    soilR = 70  # Length of right segment, m

    ### Horizontal & vertical bi-linear force
    SoilType = 'ML'
    Tu = 14  # Axial soil spring resistance, N/mm
    if SoilType in Sand:
        dTu = 5 # Axial soil spring resistance, mm
```

```
    elif SoilType in Clay:
        dTu = 10 # Axial soil spring resistance, mm
    Qu = Qd = 170  # Lateral soil spring resistance, N/mm (symmetric soil force)
    dQu = dQd = round(0.15 * OD_nominal, 1) # Lateral soil spring resistance, mm (symmetric soil force)

    #%% Number of node on each segment
    EleSize = 1
    nodeL = int(soilL/EleSize) + 1
    nodeM = int(soilM/EleSize) + 1
    nodeR = int(soilR/EleSize) + 1
    node = []
    for i in [nodeL, nodeM, nodeR]:
        if i%2 == 0:
            node.append(i+1)
        else:
            node.append(i)
    [nodeL, nodeM, nodeR] = node
    nodes = nodeL + nodeM + nodeR

    #%% Stocastic properties of all variables (non random variables: mean = varaible, sd = 0)
    sto_CSC_ALA = {'OD': [OD_nominal, 0.0017 * OD_nominal, 'Normal'],
                   'WT': [WT_nominal, 0.0235 * WT_nominal, 'Normal'],}
```

```
    sto_FDM = {'OD': [OD_nominal, 0.0017 * OD_nominal, 'Normal'],
               'WT': [WT_nominal, 0.0235 * WT_nominal, 'Normal'],
               'sY': [sY_mean, sY_SD, 'Normal'],
               'sU': [sU_mean, sU_SD, 'Normal'],
               'InitialCreep': sto_InitialCreep,
               'delta': sto_delta,  # Stochastic delta in Squash
               'Delta_T': sto_Delta_T,}
    #%% Generate random data
    def data_generation(n_size, sto):
        data_variables = []
        for item in sto.keys():
            if sto[item][-1] == 'Normal':
                data_variables.append(np.random.normal(sto[item][0], sto[item][1], size = n_size))
            elif sto[item][-1] == 'Lognormal':
                COV_item = sto[item][1]/sto[item][0]
                lambda_item = np.log(sto[item][0])-0.5*np.log(1+COV_item**2)
                xi_item = np.sqrt(np.log(1+COV_item**2))
                data_variables.append(np.random.lognormal(lambda_item, xi_item, size = n_size))
            elif sto[item][-1] == 'Uniform':
                data_variables.append(np.random.uniform(sto[item][0], sto[item][1], size = n_size))
            elif sto[item][-1] == 'Triangular':
                data_variables.append(np.random.triangular(sto[item][0], sto[item][1], sto[item][2],
size = n_size))
```

```
        elif sto[item][-1] == 'Truncated_Normal':
            mu, sigma = sto[item][0], sto[item][1]
            lower_bound, upper_bound = sto[item][2], sto[item][3]
            a, b = (lower_bound-mu)/sigma, (upper_bound-mu)/sigma
            data_truncnorm = truncnorm.rvs(a, b, loc = mu, scale = sigma, size = n_size)
            data_variables.append(data_truncnorm)
    data_variables = np.array(data_variables).T
    return data_variables


### Strain demand calculation data
def get_parameters_FDM(sto_data, Geohazard):
    deterministic_data = [Geohazard, InspectionInterval, MOP, Ee, Ep, Beta, Tu, dTu, Qu, dQu,
Qd, dQd,
                          soilL, soilM, soilR, nodeL, nodeM, nodeR]
    basic_data = list(sto_data) + deterministic_data
    IG = np.zeros(2*nodes, dtype=np.float64)
    basic_data.append(IG)
    parameters = tuple(basic_data)
    return parameters


#%% Monte Carlo Simulation
N_mc = 10000  # Data property: int
chunk_size_mc = 200
```

```
    data_CSC_ALA = data_generation(N_mc, sto_CSC_ALA)
    data_FDM = data_generation(N_mc, sto_FDM)

    ########### Compressive strain capacity - CSA_ALA
    CSC_ALA = []
    for i in range(N_mc):
        D = data_CSC_ALA[i, 0]
        t = data_CSC_ALA[i, 1]
        P = MOP
        CSC_params = (D, t, Ee, P,)
        CSC_ALA.append(Appendix_B_fun_FDM_PT.fun_CSC_ALA(CSC_params))
    CSC_ALA = np.array(CSC_ALA)
    CSC_ALA1 = CSC_ALA[:, 0]
    # CSC_ALA2 = CSC_ALA[:, 1]

    #%% Strain demand calulation
    ## Strain demand calculation: 1st round, using IG = 0
    time1 = time.time()
    conver_diver_collect_mc = []
    with concurrent.futures.ProcessPoolExecutor() as executor:
        executor_outputs = executor.map(Appendix_B_fun_FDM_PT.fun_SD,
[get_parameters_FDM(data_FDM[i, :], Geohazard) for i in range(N_mc)], chunksize =
chunk_size_mc)  # Get the results of limit state function: convergence, safety margin, strain data
along the pipe
```

```
    outputs_FDM = np.array(list(executor_outputs))
    if np.sum(outputs_FDM[:, 0]) == N_mc:
        conver_num = N_mc
        diver_num = 0
        conver_diver_collect_mc.append(['FDM IG0', conver_num, diver_num])
        outputs_final = outputs_FDM  # root_success, eTmax, eCmin, TSC, CSC, data
        print(Fore.BLUE + '\nAll cases are convergent based on FDM (IG = 0)')
    else:
        ## Strain demand calculation: 2nd round, using IG = incremental for divergent cases
        conver_num = np.sum(outputs_FDM[:, 0] == 1)
        diver_num = np.sum(outputs_FDM[:, 0] == 0)
        conver_diver_collect_mc.append(['FDM IG0', conver_num, diver_num])
        index_diver = np.argwhere(outputs_FDM[:, 0] == 0)
        index_diver = index_diver.reshape((len(index_diver), ))
        with concurrent.futures.ProcessPoolExecutor() as executor:
            output_diver = executor.map(Appendix_B_fun_FDM_PT.fun_SD_backup,
[get_parameters_FDM(data_FDM[index, ], Geohazard) for index in index_diver], chunksize =
10)
        outputs_FDM[index_diver] = np.array(list(output_diver))
        if np.sum(outputs_FDM[:, 0]) == N_mc:
            conver_num = N_mc
            diver_num = 0
            conver_diver_collect_mc.append(['FDM incre', conver_num, diver_num])
            print(Fore.BLUE + '\nAll cases are convergent based on FDM (Incremental)')
```

```
            outputs_final = outputs_FDM
        else:
            conver_num = np.sum(outputs_FDM[:, 0] == 1)
            diver_num = np.sum(outputs_FDM[:, 0] == 0)
            conver_diver_collect_mc.append(['FDM incre', conver_num, diver_num])
            pass
    outputs_final = outputs_FDM


    ########### Safety margin and PoF by MC
    PoF_mc = []
    SafetyMargin_collect = {}
    SafetyMargin_case_data = []
    # Include_divergent_case = True  # Including divergent case means using the divergent value as true value
    Include_divergent_case = False
    if Include_divergent_case:
        ### Case TSC_ALA + Tension: Using 2% strain capacity to calculate safety margin, only tensile strain is considered
        g_T1_mc = 0.02 - outputs_final[:, 1]
        SafetyMargin_case_data.append(g_T1_mc)
        failure_num = np.sum(g_T1_mc <= 0)
        PoF_mc_T1 = failure_num/N_mc  # Use the total number
        PoF_mc.append(PoF_mc_T1)
```

```
        ### Case CSC_ALA + Compression: Using CSC_ALA strain capacity to calculate safety margin, only compressive strain is considered
        g_C1_mc = CSC_ALA1 - np.abs(outputs_final[:, 2])
        SafetyMargin_case_data.append(g_C1_mc)
        failure_num = np.sum(g_C1_mc <= 0)
        PoF_mc_C1 = failure_num/N_mc  # Use the total number
        PoF_mc.append(PoF_mc_C1)

        ### Case 2% Tension and Compression: tension and compressive strain are considered
        g_TC1_mc = np.minimum(g_T1_mc, g_C1_mc)
        SafetyMargin_case_data.append(g_TC1_mc)
        failure_num = np.sum(g_TC1_mc <= 0)
        PoF_mc_TC1 = failure_num/N_mc  # Use the total number
        PoF_mc.append(PoF_mc_TC1)

    #%% Excluding divergent cases
    else:
        N_mc_conver = np.sum(outputs_final[:, 0])
        index_conver = np.where(outputs_final[:, 0] == 1)[0]
        ##### ALA
        ### Case 2% + Tension: Using 2% strain capacity to calculate safety margin, only tensile strain is considered
        g_T1_mc = 0.02 - outputs_final[index_conver, 1]
        SafetyMargin_case_data.append(g_T1_mc)
```

```
        failure_num = np.sum(g_T1_mc <= 0)
        PoF_mc_T1 = failure_num/N_mc_conver  # Use the convergent number
        PoF_mc.append(PoF_mc_T1)

        ### Case 1% + Compression: Using 1% strain capacity to calculate safety margin, only compressive strain is considered
        g_C1_mc = CSC_ALA1[index_conver] - np.abs(outputs_final[index_conver, 2])
        SafetyMargin_case_data.append(g_C1_mc)
        failure_num = np.sum(g_C1_mc <= 0)
        PoF_mc_C1 = failure_num/N_mc_conver  # Use the convergent number
        PoF_mc.append(PoF_mc_C1)

        ### Case 2% Tension and 1% Compression: tension and compressive strain are considered
        g_TC1_mc = np.minimum(g_T1_mc, g_C1_mc)
        SafetyMargin_case_data.append(g_TC1_mc)
        failure_num = np.sum(g_TC1_mc <= 0)
        PoF_mc_TC1 = failure_num/N_mc_conver  # Use the convergent number
        PoF_mc.append(PoF_mc_TC1)

    durT_mc = time.time() - time1
    print("\nMonte Carlo Simulation",
          "\n2% Tension (ALA): PoF = ", round(PoF_mc_T1, 7),
          "\nCompression (ALA1): PoF = ", round(PoF_mc_C1, 7),
```

```
        "\n2% Tension + Compression: PoF = ", round(PoF_mc_TC1, 7),
        "\nTotal time = ", round(durT_mc / 3600, 5), " hrs")

    #%% Calculation time
    timeEnd = time.time()
    duration = round((timeEnd - timeStart) / 3600, 3)
    print("\n Program finished!  Duration = ", duration, " hrs")
```

2. Appendix_B_fun_FDM_PT

```
import math
import numpy as np
from scipy import optimize

import warnings
warnings.filterwarnings('ignore')

# Optimazation libraries
from numba import njit, jit
#%% Soil resistance
warnings.filterwarnings('ignore')
@njit
def Tu0(x, Tu, dTu):
    if x <= -dTu:
```

```
        y = -Tu
    elif x >= dTu:
        y = Tu
    else:
        y = Tu/dTu*x
    return y


@njit
def Pu0(x, Qu, dQu, Qd, dQd):
    if x <= -dQd:
        y = -Qd
    elif (x > -dQd) * (x <= 0):
        y = Qd/dQd*x
    elif (x > 0) * (x < dQu):
        y = Qu/dQu*x
    else:
        y = Qu
    return y


#%% Finite difference equation
warnings.filterwarnings('ignore')
@njit
def firstD(a, c, h):  # a: the a(i-1); aii: a(i+1)
```

```
    p = (c - a) / (2 * h)  # ai: the a(i)
    return p


@njit
def secondD(a, b, c, h):
    pp = (c - 2 * b + a) / (h ** 2)
    return pp


#%% Equation for N and M
warnings.filterwarnings('ignore')
@njit
def NMnon(du,dw,d2w, basic_params):
    D, t, A, Ee, EpT, EpC, s_YT, s_YC, e_YT, e_YC, e_initial = basic_params
    eA=du + 1/2*(dw)**2 + e_initial
    eBmax=D/2*(d2w)
    if np.abs(d2w)<= 1e-15:
        M = 0.
        if eA > e_YT:
            N=A*(s_YT + EpT*(eA-e_YT))
        elif eA < e_YC:
            N=A*(s_YC + EpC*(eA-e_YC))
        else:
            N=A*Ee*eA
```

```
else:
    hty=D/2-(e_YT-eA)/(2*eBmax)*D
    hcy=D/2+(-e_YC+eA)/(2*eBmax)*D
    H1=min(hty,hcy)
    H2=max(hty,hcy)
    if H1>=D:
        phi1=np.pi
    elif H1<=0:
        phi1=0
    else:
        phi1=np.arccos((D-2*H1)/D)
    if H2>=D:
        phi2=np.pi
    elif H2<=0:
        phi2=0
    else:
        phi2=np.arccos((D-2*H2)/D)
    if hcy > hty: # Ii = 1
        N = (D - t)*t*(
            (EpC*np.pi + (Ee - EpC)*phi2)*eA
            - ((Ee - EpT)*np.sin(phi1) - (Ee - EpC)*np.sin(phi2))*eBmax
            - (Ee - EpT)*(eA - e_YT)*phi1
            + (Ee - EpC)*(np.pi - phi2)*e_YC
```

```
            )
        M = 0.25*(D - t)**2*t*(
            (EpC*np.pi - (Ee - EpT)*(phi1 + np.sin(phi1)*np.cos(phi1)) + (Ee -
EpC)*(phi2+np.sin(phi2)*np.cos(phi2)))*eBmax
            - 2*((Ee - EpT)*np.sin(phi1) - (Ee - EpC)*np.sin(phi2))*eA
            + 2*np.sin(phi1)*e_YT*(Ee - EpT) - 2*np.sin(phi2)*e_YC*(Ee - EpC)
            )
    else:
        N = (D - t)*t*(
            (EpT*np.pi + (Ee - EpT)*phi2)*eA
            - ((Ee - EpC)*np.sin(phi1) - (Ee - EpT)*np.sin(phi2))*eBmax
            - (Ee - EpC)*(eA - e_YC)*phi1
            + (Ee - EpT)*(np.pi - phi2)*e_YT
            )
        M = 0.25*(D - t)**2*t*(
            (EpT*np.pi - (Ee - EpC)*(phi1 + np.sin(phi1)*np.cos(phi1)) + (Ee -
EpT)*(phi2+np.sin(phi2)*np.cos(phi2)))*eBmax
            - 2*((Ee - EpC)*np.sin(phi1) - (Ee - EpT)*np.sin(phi2))*eA
            + 2*np.sin(phi1)*e_YC*(Ee - EpC) - 2*np.sin(phi2)*e_YT*(Ee - EpT)
            )
  return [N,M]

#%% Equation construction
warnings.filterwarnings('ignore')
```

```
@njit
def Equations(x, zero_arrays, Equations_params, soil_params, MNnon_params):    # Finite difference z is an array containing us followed by ws with length nodes.
    (upL, wpL, wppL, NL, NwpL, ML, NpL, MpL, MppL,
     upM, wpM, wppM, NM, MM, NpM, MpM, NwpM, MppM,
     upR, wpR, wppR, NR, MR, NpR, MpR, NwpR, MppR) = zero_arrays
    hL, hM, hR, nodeL, nodeM, nodeR, coordinate = Equations_params
    Tu, dTu, U, Qu, dQu, Qd, dQd, W = soil_params
    D, t, A, Ee, EpT, EpC, s_YT, s_YC, e_YT, e_YC, e_initial = MNnon_params

    l=int(len(x)/2)
    u=x[:l]
    w=x[l:]
    # Range function doesn't consider last value
    # Forward
    upL[0]=(u[1]-u[0])/hL
    wpL[0]=(w[1]-w[0])/hL
    wppL[0]=(w[2]-2*w[1]+w[0])/hL**2
    [NL[0],ML[0]]=NMnon(upL[0],wpL[0],wppL[0], MNnon_params)
    # Backward
    upL[nodeL-1]=(u[nodeL-2]-u[nodeL-1])/(-hL)
    wpL[nodeL-1]=(w[nodeL-2]-w[nodeL-1])/(-hL)
    wppL[nodeL-1]=(w[nodeL-1]-2*w[nodeL-2]+w[nodeL-3])/hL**2
```

```
    [NL[nodeL-1],ML[nodeL-1]]=NMnon(upL[nodeL-1], wpL[nodeL-1], wppL[nodeL-1],
MNnon_params)
    for i in range(1, nodeL-1): #First derivatives and second derivatives start from second node to
one before last
        upL[i]=firstD(u[i-1],u[i+1],hL)
        wpL[i]=firstD(w[i-1],w[i+1],hL)
        wppL[i]=secondD(w[i-1],w[i],w[i+1],hL)
        [NL[i],ML[i]]=NMnon(upL[i],wpL[i],wppL[i], MNnon_params)
    for i in range(1, nodeL-1): #First derivatives and second derivatives start from second node to
one before last
        NpL[i]=firstD(NL[i-1],NL[i+1],hL)
        MppL[i]=secondD(ML[i-1],ML[i],ML[i+1],hL)
        NwpL[i]=firstD(NL[i-1]*wpL[i-1],NL[i+1]*wpL[i+1],hL)


    # Forward
    upM[0]=(u[nodeL+1]-u[nodeL+0])/hM
    wpM[0]=(w[nodeL+1]-w[nodeL+0])/hM
    wppM[0]=(w[nodeL+2]-2*w[nodeL+1]+w[nodeL+0])/hM**2
    [NM[0],MM[0]]=NMnon(upM[0],wpM[0],wppM[0], MNnon_params)
    # Backward
    upM[nodeM-1]=(u[nodeL+nodeM-2]-u[nodeL+nodeM-1])/(-hM)
    wpM[nodeM-1]=(w[nodeL+nodeM-2]-w[nodeL+nodeM-1])/(-hM)
    wppM[nodeM-1]=(w[nodeL+nodeM-1]-2*w[nodeL+nodeM-2]+w[nodeL+nodeM-3])/hM**2
```

```
    [NM[nodeM-1],MM[nodeM-1]]=NMnon(upM[nodeM-1],wpM[nodeM-1],wppM[nodeM-1],
MNnon_params)
    for i in range(1, nodeM-1):
        upM[i]=firstD(u[i-1+nodeL],u[i+1+nodeL],hM)
        wpM[i]=firstD(w[i-1+nodeL],w[i+1+nodeL],hM)
        wppM[i]=secondD(w[i-1+nodeL],w[i+nodeL],w[i+1+nodeL],hM)
        [NM[i],MM[i]]=NMnon(upM[i],wpM[i],wppM[i], MNnon_params)
    for i in range(1, nodeM-1): #First derivatives and second derivatives start from second node to
one before last
        NpM[i]=firstD(NM[i-1],NM[i+1],hM)
        MppM[i]=secondD(MM[i-1],MM[i],MM[i+1],hM)
        NwpM[i]=firstD(NM[i-1]*wpM[i-1],NM[i+1]*wpM[i+1],hM)


    # Forward
    upR[0]=(u[nodeL+nodeM+1]-u[nodeL+nodeM+0])/hR
    wpR[0]=(w[nodeL+nodeM+1]-w[nodeL+nodeM+0])/hR
    wppR[0]=(w[nodeL+nodeM+2]-2*w[nodeL+nodeM+1]+w[nodeL+nodeM+0])/hR**2
    [NR[0],MR[0]]=NMnon(upR[0],wpR[0],wppR[0], MNnon_params)
    # Backward
    upR[nodeR-1]=(u[nodeL+nodeM+nodeR-1]-u[nodeL+nodeM+nodeR-2])/hR
    wpR[nodeR-1]=(w[nodeL+nodeM+nodeR-1]-w[nodeL+nodeM+nodeR-2])/hR
    wppR[nodeR-1]=(w[nodeL+nodeM+nodeR-1]-2*w[nodeL+nodeM+nodeR-
2]+w[nodeL+nodeM+nodeR-3])/hM**2
```

```
    [NR[nodeR-1],MR[nodeR-1]]=NMnon(upR[nodeR-1],wpR[nodeR-1],wppR[nodeR-1],
MNnon_params)
    for i in range(1, nodeR-1):
        upR[i]=firstD(u[i-1+nodeL+nodeM],u[i+1+nodeL+nodeM],hR)
        wpR[i]=firstD(w[i-1+nodeL+nodeM],w[i+1+nodeL+nodeM],hR)
        wppR[i]=secondD(w[i-1+nodeL+nodeM],w[i+nodeL+nodeM],w[i+1+nodeL+nodeM],hR)
        [NR[i],MR[i]]=NMnon(upR[i],wpR[i],wppR[i], MNnon_params)
    for i in range(1, nodeR-1): #First derivatives and second derivatives start from second node to
one before last
        NpR[i]=firstD(NR[i-1],NR[i+1],hR)
        MppR[i]=secondD(MR[i-1],MR[i],MR[i+1],hR)
        NwpR[i]=firstD(NR[i-1]*wpR[i-1],NR[i+1]*wpR[i+1],hR)
    # Establishing equations
    ### New equations (change on soil springs)
    EqsLu = np.array([NpL[i] + Tu0(0 - u[i], Tu, dTu) for i in range(1, nodeL - 1)])
    EqsLw = np.array([MppL[i] - NwpL[i] - Pu0(0- w[i], Qu, dQu, Qd, dQd) for i in range(2,
nodeL - 2)])
    EqsMu = np.array([NpM[i] + Tu0(U - u[i + nodeL], Tu, dTu) for i in range(1, nodeM - 1)])
    EqsMw = np.array([MppM[i] - NwpM[i] - Pu0(W - w[i + nodeL], Qu, dQu, Qd, dQd) for i in
range(2, nodeM - 2)])
    EqsRu = np.array([NpR[i] + Tu0(0 - u[i + nodeL + nodeM], Tu, dTu) for i in range(1, nodeR -
1)])
    EqsRw = np.array([MppR[i] - NwpR[i] - Pu0(0 - w[i + nodeL + nodeM], Qu, dQu, Qd, dQd)
for i in range(2, nodeR - 2)])
```

```
    BCs=[]
    BCs.append(u[0])#Fixed horizontal displacement end 1
    BCs.append(u[nodeL+nodeM+nodeR-1])#Fixed horizontal displacement far end
    BCs.append(w[0])#Fixed vertical displacement end 1
    BCs.append(w[nodeL+nodeM+nodeR-1])#Fixed vertical displacement far end
    BCs.append((w[1]-w[0])/hL)#Fixed rotation near end
    BCs.append((w[nodeL+nodeM+nodeR-1]-w[nodeL+nodeM+nodeR-2])/hR)#Fixed rotation
far end
    # First connection
    BCs.append(u[nodeL-1]-u[nodeL]) #connectivity of u
    BCs.append(w[nodeL-1]-w[nodeL]) #connectivity of w
    BCs.append((u[nodeL-1]-u[nodeL-2])/(coordinate[nodeL-1]-coordinate[nodeL-2])-
(u[nodeL+1]-u[nodeL])/(coordinate[nodeL+1]-coordinate[nodeL])) #connectivity of first slope
of u
    BCs.append((w[nodeL-1]-w[nodeL-2])/(coordinate[nodeL-1]-coordinate[nodeL-2])-
(w[nodeL+1]-w[nodeL])/(coordinate[nodeL+1]-coordinate[nodeL])) #next is connectivity of
first slope of w
    BCs.append((w[nodeL-3]-2*w[nodeL-2]+w[nodeL-1])/(hL**2)-(w[nodeL+2]-
2*w[nodeL+1]+w[nodeL])/(hM**2)) #connectivity of second derivative of w
    BCs.append((w[nodeL-1]-3*w[nodeL-2]+3*w[nodeL-3]-w[nodeL-4])/(hL**3)-(w[nodeL+3]-
3*w[nodeL+2]+3*w[nodeL+1]-w[nodeL])/(hM**3)) #connectivity of third derivative of w
    # Second connection
    BCs.append(u[nodeM+nodeL-1]-u[nodeM+nodeL]) #connectivity of u
    BCs.append(w[nodeM+nodeL-1]-w[nodeM+nodeL]) #connectivity of w
```

```
    BCs.append((u[nodeM+nodeL-1]-u[nodeM+nodeL-2])/(coordinate[nodeM+nodeL-1]-coordinate[nodeM+nodeL-2])-(u[nodeM+nodeL+1]-u[nodeM+nodeL])/(coordinate[nodeM+nodeL+1]-coordinate[nodeM+nodeL])) #connectivitify of first slope of u

    BCs.append((w[nodeM+nodeL-1]-w[nodeM+nodeL-2])/(coordinate[nodeM+nodeL-1]-coordinate[nodeM+nodeL-2])-(w[nodeM+nodeL+1]-w[nodeM+nodeL])/(coordinate[nodeM+nodeL+1]-coordinate[nodeM+nodeL])) #next is connectivity of first slope of w

    BCs.append((w[nodeM+nodeL-3]-2*w[nodeM+nodeL-2]+w[nodeM+nodeL-1])/(hM**2)-(w[nodeM+nodeL+2]-2*w[nodeM+nodeL+1]+w[nodeM+nodeL])/(hR**2)) #connectivity of second derivative of w

    BCs.append((w[nodeM+nodeL-1]-3*w[nodeM+nodeL-2]+3*w[nodeM+nodeL-3]-w[nodeM+nodeL-4])/(hM**3)-(w[nodeM+nodeL+3]-3*w[nodeM+nodeL+2]+3*w[nodeM+nodeL+1]-w[nodeM+nodeL])/(hR**3)) #connectivity of third derivative of w


    BCs = np.array(BCs)

    Eqs = np.concatenate((EqsLu, EqsLw, EqsMu, EqsMw, EqsRu, EqsRw, BCs))

    return Eqs


#%% Calculate the compressive strain capacity

warnings.filterwarnings('ignore')

@njit

def fun_CSC_ALA(CSC_params):

    (D, t, Ee, P,) = CSC_params

    epsilon_operate = 0.5*(t/D) - 0.0025 + 3000*(P*D/(2*Ee*t))**2
```

```
    epsilon_integrity = 1.76*t/D
    return epsilon_operate, epsilon_integrity


#%% Reliability calculation based on IG = 0
warnings.filterwarnings('ignore')
@njit
def piecewise_material(x, Ee, Ep, eY, nv, s_2):
    if np.abs(x) <= eY:
        y = nv*s_2 - Ee*x
    else:
        y = nv*s_2 - (Ee*eY + Ep*(x-eY))
    return y


warnings.filterwarnings('ignore')
@jit
def fun_SD(params):
    (D, t, sY, sU,
     InitialCreep,
     delta_or_rate,
     Delta_T,
     Geohazard, year,
     MOP, Ee, Ep, Beta, Tu, dTu, Qu, dQu, Qd, dQd,
     soilL, soilM, soilR, nodeL, nodeM, nodeR,
```

```
 IG) = params
eY = sY / Ee

########## Calculation of EpT and EpC
nv = 0.3  # Possion's ratio
alpha = 1.2e-5  # Coef. thermal expansion
s_2 = MOP*(D-2*t)/(2*t)  # hoop stress, MPa
x = alpha*Delta_T # Thermal strain
s_initial = piecewise_material(x, Ee, Ep, eY, nv, s_2)
e_initial = s_initial/Ee
if 4*sY**2 - 3*s_2**2 >= 0:
    s_YT = 0.5 * (s_2 + np.sqrt(4*sY**2 - 3*s_2**2))
    s_YC = 0.5 * (s_2 - np.sqrt(4*sY**2 - 3*s_2**2))
else:
    s_YT = 0.5 * s_2
    s_YC = 0.5 * s_2
e_YT = (s_YT-nv*s_2)/Ee
e_YC = (s_YC-nv*s_2)/Ee
h = (Ee*Ep)/(Ee-Ep)

### Plastic stress-strain
## Tensile state
n = 50
```

```
    incr = (1000 - s_YT)/(n-1)
    s_p1T = np.arange(s_YT, 900 + incr, incr)
    # e_p1T = np.zeros(len(s_p1T))
    inte = (-2*(-2*s_p1T+s_2)+2*np.sqrt(3)*s_2*np.arctan((-2*s_p1T+s_2)/(np.sqrt(3)*s_2))) - (-2*(-2*s_YT+s_2)+2*np.sqrt(3)*s_2*np.arctan((-2*s_YT+s_2)/(np.sqrt(3)*s_2)))
    e_p1T = e_YT + 1/Ee*(s_p1T - s_YT) + 1/(4*h) * inte
    ## Compressive state
    incr = (-1000 - s_YC)/(n-1)
    s_p1C = np.arange(s_YC, -800 + incr, incr)
    # e_p1C = np.zeros(len(s_p1C))
    inte = (-2*(-2*s_p1C+s_2)+2*np.sqrt(3)*s_2*np.arctan((-2*s_p1C+s_2)/(np.sqrt(3)*s_2))) - (-2*(-2*s_YC+s_2)+2*np.sqrt(3)*s_2*np.arctan((-2*s_YC+s_2)/(np.sqrt(3)*s_2)))
    e_p1C = e_YC + 1/Ee*(s_p1C - s_YC) + 1/(4*h) * inte
    ### Plastic slope
    EpT = (s_p1T[-1]-s_p1T[0])/(e_p1T[-1]-e_p1T[0])
    EpC = (s_p1C[-1]-s_p1C[0])/(e_p1C[-1]-e_p1C[0])

    # Fixed variables
    soilL = 1000 * soilL
    soilM = 1000 * soilM
    soilR = 1000 * soilL
    hL = soilL / (nodeL - 1)
    hM = soilM / (nodeM - 1)
    hR = soilR / (nodeR - 1)
```

```
coordinateL = np.array([i * hL for i in range(nodeL)])
coordinateM = np.array([soilL + i * hM for i in range(nodeM)])
coordinateR = np.array([soilL + soilM + i * hR for i in range(nodeR)])
coordinate = np.concatenate((coordinateL, coordinateM, coordinateR))

A = 1 / 4 * np.pi * (D ** 2 - (D - 2 * t) ** 2)  # Section area, mm^2
if Geohazard == 'Slope':
    DeltaTotal = (InitialCreep + delta_or_rate*year) * 1000  # Total ground displacement, mm
elif Geohazard == 'Landslide':
    DeltaTotal = (InitialCreep + delta_or_rate)* 1000  # Total ground displacement, mm
elif Geohazard == 'None':
    DeltaTotal = delta_or_rate * 1000  # Total ground displacement, mm
U = round(DeltaTotal * math.cos(Beta * math.pi / 180), 5)  # Horizontal displacement, mm
W = round(DeltaTotal * math.sin(Beta * math.pi / 180), 5)  # Vertical displacement, mm

# Assign room for deformations and derivatives
upL = np.zeros(nodeL, dtype=np.float64)
wpL = np.zeros(nodeL, dtype=np.float64)
wppL = np.zeros(nodeL, dtype=np.float64)
NL = np.zeros(nodeL, dtype=np.float64)
NwpL = np.zeros(nodeL, dtype=np.float64)
ML = np.zeros(nodeL, dtype=np.float64)
NpL = np.zeros(nodeL, dtype=np.float64)
```

```
MpL = np.zeros(nodeL, dtype=np.float64)
MppL = np.zeros(nodeL, dtype=np.float64)

upM = np.zeros(nodeM, dtype=np.float64)
wpM = np.zeros(nodeM, dtype=np.float64)
wppM = np.zeros(nodeM, dtype=np.float64)
NM = np.zeros(nodeM, dtype=np.float64)
MM = np.zeros(nodeM, dtype=np.float64)
NpM = np.zeros(nodeM, dtype=np.float64)
MpM = np.zeros(nodeM, dtype=np.float64)
NwpM = np.zeros(nodeM, dtype=np.float64)
MppM = np.zeros(nodeM, dtype=np.float64)

upR = np.zeros(nodeR, dtype=np.float64)
wpR = np.zeros(nodeR, dtype=np.float64)
wppR = np.zeros(nodeR, dtype=np.float64)
NR = np.zeros(nodeR, dtype=np.float64)
MR = np.zeros(nodeR, dtype=np.float64)
NpR = np.zeros(nodeR, dtype=np.float64)
MpR = np.zeros(nodeR, dtype=np.float64)
NwpR = np.zeros(nodeR, dtype=np.float64)
MppR = np.zeros(nodeR, dtype=np.float64)
```

```
zero_arrays = (upL, wpL, wppL, NL, NwpL, ML, NpL, MpL, MppL,
 upM, wpM, wppM, NM, MM, NpM, MpM, NwpM, MppM,
 upR, wpR, wppR, NR, MR, NpR, MpR, NwpR, MppR)


# Equation params: x, zero_arrays, Equations_params, NMnon_params, other_params
root = optimize.root(Equations,
    IG,
    jac=False,
    tol=1e-10,
    args=(zero_arrays,
        (hL, hM, hR, nodeL, nodeM, nodeR, coordinate),
        (Tu, dTu, U, Qu, dQu, Qd, dQd, W),
        (D, t, A, Ee, EpT, EpC, s_YT, s_YC, e_YT, e_YC, e_initial)))  # Be careful of the tol


root_success = root.success
loc = [round(i/1000., 2) for i in coordinate]
u = root.x[:nodeL+nodeM+nodeR]/1000.
w = root.x[nodeL+nodeM+nodeR:]/1000.
dudx = np.concatenate((upL, upM, upR))
dwdx = np.concatenate((wpL, wpM, wpR))
d2wdx2 = np.concatenate((wppL, wppM, wppR))
eTop = dudx + 1 / 2 * dwdx ** 2 + D / 2 * d2wdx2
eBot = dudx + 1 / 2 * dwdx ** 2 - D / 2 * d2wdx2
```

```
    eL = np.concatenate((eTop, eBot))
    eTmax = np.max(eL)
    eCmin = np.min(eL)
    data = np.transpose(np.vstack((loc, u, w, eTop, eBot)))
    return (root_success, eTmax, eCmin, data)

#%% Backup reliability calculation based on IG = 0
warnings.filterwarnings('ignore')
@jit
def fun_SD_backup(params):
    (D, t, sY, sU, InitialCreep, delta_or_rate, Delta_T, Geohazard, year,
     MOP, Ee, Ep, Beta, Tu, dTu, Qu, dQu, Qd, dQd, soilL, soilM, soilR, nodeL, nodeM, nodeR,
IG) = params

    root_success = 0
    IncreNum = 5
    while root_success == 0 and IncreNum <= 20:
        InitialCreep_step = [round(i, 2) for i in np.linspace(InitialCreep/IncreNum, InitialCreep,
IncreNum)]
        delta_or_rate_step = [round(i, 2) for i in np.linspace(delta_or_rate/IncreNum, delta_or_rate,
IncreNum)]

        for i in range(IncreNum):
            if i == 0:
```

```
            parameters = (D, t, sY, sU, InitialCreep_step[i], delta_or_rate_step[i], Delta_T,
Geohazard, year, MOP, Ee, Ep, Beta, Tu, dTu, Qu, dQu, Qd, dQd, soilL, soilM, soilR, nodeL,
nodeM, nodeR, IG)
            ans = fun_SD(parameters)
            root_success = ans[0]
            if root_success:  # Calculate the first step and its results are used as IG for the next step
               last_ans = ans
            else:
               last_ans = ans  # Using the divergent results as initial guess
         else:
            Factor = [1.0, 10., 100.,1000., 500., 2000., 10000.]
            MaxCal = len(Factor)
            sino = 0
            root_success = 0
            while root_success == 0 and sino < MaxCal:
               factor = Factor[sino]
               IG_u = last_ans[-1][:, 1]
               IG_v = last_ans[-1][:, 2]
               IG = np.concatenate((IG_u, IG_v)) * factor # Should *1000 to unit of mm
               parameters = (D, t, sY, sU, InitialCreep_step[i], delta_or_rate_step[i], Delta_T,
Geohazard, year, MOP, Ee, Ep, Beta, Tu, dTu, Qu, dQu, Qd, dQd, soilL, soilM, soilR, nodeL,
nodeM, nodeR, IG)
               ans = fun_SD(parameters)
               root_success = ans[0]
```

```
            sino = sino + 1
            if root_success:
                last_ans = ans
    IncreNum = IncreNum + 1

eTmax = last_ans[1]
eCmin = last_ans[2]
data = last_ans[3]
return (root_success, eTmax, eCmin, data)
```